GREASE FLOW BEHAVIORS IN ELASTOHYDRODYNAMIC POINT CONTACTS

陈, 婧

https://doi.org/10.15017/1654878

出版情報：九州大学, 2015, 博士（工学）, 課程博士
バージョン：

GREASE FLOW BEHAVIORS IN ELASTOHYDRODYNAMIC POINT CONTACTS

JING CHEN

ABSTRACT

The flow behaviors is probably the dominate factor to judge the performance of the grease-lubricated machine elements. Because its complexity and abstract, there is no research mainly related to the issue of grease flow pattern at present. Due to the semi-solid composition and the complex rheological properties, the features of grease flow are different for different grease types and different conditions. This unique flow pattern contains a lot of important information: the interaction between the thickener and the base oil, the lubricating conditions, the rheological properties and the mechanisms of redistribution and transportation, etc.

The purpose of this work is to find the information behind the flow pattern as mentioned above through systematic observation on the features of grease flow. The focus is on the grease flow behaviors in point contact. It includes the features of flow pattern surround the contact point and the lubricating conditions of the contact point.

The experimental arrangements are: Firstly, through optical interferometry measurements on a ball-on-disk test rig, the features of grease flow are observed under different entrainment speed, test duration and slide-to-roll ratio, respectively. Then, the artificial replenishment setup is adopted. The change characters of the track pattern and the film thickness with test conditions are observed in the series tests with artificial replenishment and without artificial replenishment, respectively. Finally, the fluorescence technique is used to know the in-situ flow behaviors.

In addition, covariance analysis is used to find out whether there exists correlation among all these factors such as characteristic parameters, test conditions, rheological properties and lubricating conditions. Principal component analysis is used to select the most appropriate parameters which can represent the change of track morphology when the entrainment speed, test duration and slide to roll ratio change, respectively.

The main conclusions are summarized: The features of track pattern are different for different grease types and different test conditions. Lithium-12-hydroxy stearate grease shows clear track pattern, Di-urea grease shows obscure track pattern and heavy thickener deposition in the center of track. The thickener type and base oil viscosity are more important than base

oil among the factors that may affect the area of grease finger. The features of track pattern are not only related to the constituents of grease, the changes in rheological properties also produce alterations in them. For example: The grease with smaller yield stress and higher viscosity tends to have larger finger area. The grease with better flow ability tends to have a clearer finger pattern.

Moreover, the relationships between track pattern and lubrication mechanisms are also found. The variation of the parameterized track pattern can represent the grease flow behaviors, regardless of the type of grease. The formation and maintenance of grease finger in track pattern are dependent on the state of lubricating contact.

The features of track pattern are different for different lubricating conditions. In high speed，starvation and finger-loss will occur. The apparent viscosity of the grease at low shear rate in the inlet zone has a great impact on the resupply of the greases and the starvation speed. The starvation speeds are always lower than the finger-loss speeds. It is proposed that the grease finger provides supply to the contact area and the side reservoir. And one part of grease finger which lies near the center of track plays the main role. In addition, the thickener deposition in the center of track plays a positive role in the film formation.

In summary, this study develops a new method to describe visual characteristics of flow and tracks around the contact in rolling/sliding point contact EHL with greases, finds dependence of the flow characteristics parameters on various factors including operating conditions, rheological properties of greases and the state of fluid film formation, and proposes mechanisms of grease supply to the contact which depend on these factors.

TABLE OF CONTENTS

CHAPTER 1

Introduction

1.1 Lubricating requirement in mechanical industries

Machinery is closely linked with daily life and work; industry, agriculture transportation and national defense are all inseparable from machines. A machine is a combination of individual machine elements or parts. There are relative motions between parts and machine elements, which are utilized or converted into mechanical energy; but some part of this energy is consumed by friction. According to statistics, about 1/3 to 1/2 of the world's energy is consumed by friction [1]. Therefore, if we can reduce energy loss due to friction as far as possible, a lot of energy will be saved.

Using lubricants is the primary method to reduce friction. Grease is one type of lubricant and is defined as 'a solid to semi-fluid product or dispersion of a thickening agent in a liquid lubricant. Other ingredients imparting special properties may also be included' [2]. Thickeners, base oil and additives are three major components of greases. These constituents and their manufacturing processes are the key factors to determine and influence the properties of greases.

Greases have rather complex rheological properties. At normal temperature and under stationary state, a grease is in a solid state. It remains unchanged and can be attached to the surface of metals without sliding down. However, at high temperature or when the applied force exceeds a certain limit, the grease will easily flow like a fluid. When a grease is subjected to shear in a machine component, it produces a flow.

This flow of grease lubricates surfaces and reduces the friction between the relatively moving surfaces. When the shear action is stopped, the grease can be recovered to a certain extent. These distinctive properties allow greases to be used in situations which are not suitable for oil lubrication. Furthermore, the sealing and protective effects of greases are better than oils. The main functions of greases are lubrication, protection and sealing.

Greases and oils are all used to reduce friction. However, it is necessary to use greases rather than oil in some cases. Grease is favored, for instance, when the mechanical component requires a lubricant that has good sealing effect, such that it can avoid contamination, or when

the mechanical component requires a lubricant that can keep attached to the relatively moving surfaces. In the machine industry, rolling bearings are the most commonly used typical machine elements. According to statistics, for over 80% of rolling bearings and 20% of sliding bearings grease is the preferred lubricant [1]. Although oil is commonly used in gear boxes, a grease may achieve better results in some cases. It not only solves the problems of oil leakage and environmental pollution, but lubricant consumption can also be effectively reduced.

Experience shows that about 80% of premature bearing failures are due to lubrication problems. Thus, the correct understanding of grease lubrication mechanisms is very important. Nevertheless, the understanding of grease lubrication is far inferior to oil lubrication. One of the reasons may be related with the output, *i.e*. the market share of greases is much smaller than oil, but other important reasons are that the composition, structure, and rheological properties of greases are more complex than oils.

1.2 Grease composition

1.2.1 Base oil

The base oil is trapped in the network of thickener, and therefore it cannot easily flow out. Mineral oils and synthetic oils have been used as the main types of base oil of grease lubricants. Different kinds of oils are also often used for the base oil. In the composition of grease, the content of base oil is 70% to 90%, and might even be as high as 95% [3]. Therefore, the base oil often has an important influence on the main properties of the grease.

For instance, the evaporation and the compatibility for the rubber sealing material almost entirely depend on the base oil. The low temperature performance of greases is largely determined by the viscosity, the freezing point and viscosity-temperature characteristics of the base oil. The high temperature performance of greases is influenced by the oxidation stability, decomposition temperature and the evaporation of the base oil. The colloidal stability of greases is related to the viscosity and type of base oil; the grease is more likely to bleed when the viscosity of the base oil is smaller.

1.2.2 Thickener

The grease thickener is an indispensable solid part in the grease, and the content of

thickener is about 5% to 30% [3]. It can be dispersed in the base oil and forms a structure skeleton; the base oil is absorbed and trapped in this structure skeleton. The thickener particles or fibers make a dispersed phase in the colloidal dispersion system.

The naming of greases is classified according to the kind of thickener used in grease. There are many thickeners used, and they are classified into four types: soap base, alkyl, organic and inorganic. All the properties of greases including chemical and physical properties, bleeding rate, rheology, mechanical stability etc. depend on the type of thickening material. For the same grease, the different manufacturing processes have a great effect on the structure of the thickener. The type of thickener determines the basic properties of the grease.

1.2.3 Additives

Additives usually are chemicals added to grease to improve the lubricating performance in the application. They improve the properties of the grease or add some new properties to the grease. The most commonly used additives are: antioxidants, stabilizers, metal passivators, antirust, anti-wear and extreme pressure additives and so on.

1.3 Grease lubrication

As described in section 1.1, greases have widespread application. The issues of grease lubrication are complicated, because the lubrication process is different for different running conditions and machine element types. Taking bearings for example, usually temperature and speed are the main factors which influence the lubrication process. In this section, the mechanisms of grease lubrication under different conditions are discussed in detail.

1.3.1 Temperature influence

The high viscosity and consistency of a grease can cause excessive initial bearing torque under low temperatures. At high temperatures, oxidation and loss of consistency play a major role. As shown in Figure 1.1, the lower function limit is the lowest temperature at which the grease will enable the bearing to be started up without difficulty. The upper function limit is determined by the dropping point of the grease. If the operating temperature is outside the low and high temperature limits, the bearing is easily damaged.

1.3.1.1 Low temperature

In the temperature domain between the lower function limit and lower operating temperature limit, excessive initial bearing torques may lead to startup failure. The startup is often regarded as a research topic [5–7]. Many authors [6–10] try to find the relations between the rheological properties of greases and bearing torque, the viscosity of greases is acknowledged as a major factor. In this case, the grease which has a low base oil viscosity is suggested for use [11]. Besides, other factors such as penetration are also relevant to the start torque [12].

The tendency of a grease to bleed decreases and the consistency of the grease increases with decreasing temperature. The lubricated conjunction is likely to be starved as a result of lack of timely and effective supplement. This has a negative impact on the lubricating effects.

However, the friction heat generated during the startup and partly increased as a result of slip results in a very rapid increase in the temperature of the bearing, so that it quickly reaches a range where the lubricant can function without problems. Therefore, the bearing which works at low temperature for a long time does not bring as much harmful effects as that at high temperature.

1.3.1.2 High temperature

A bearing that works for a long duration of time in a tough high temperature environment will undoubtedly have a shorter life. It also can bring a series of problems such as oxidation [13] or the evaporation of the base oil [14]. The process in which the properties of greases change along with time in a running bearing is known as aging. Aging can be classified into mechanical aging and chemical aging. Mechanical aging is embodied in the change of consistency and the separation of the base oil due to the deterioration of thickener structure. Chemical aging is mainly caused by oxidation.

Ito *et al.* [15] proposed that mechanical aging is dominant in low temperature and high speed applications, and chemical aging is the determinant factor at high temperature and low speed. As a rule, mechanical aging and chemical aging exist simultaneously. In the temperature domain between the upper operating temperature limit and upper function limit, greases not only suffer the shear motion on the mechanical deterioration of the thickener

structure, but also some irreversible chemical changes to the grease structure.

Currently, research on the oxidation process of greases under high temperature is not as abundent as that of oil, especially on the effects of the thickener on it. It is generally accepted that the thickener plays a major role on the oxidation process. For instance, oxidation may prohibit further bleeding of the grease and thus reduce the interaction between the base oils and thickeners [16].

Compared to oil lubricated bearings, oxidation in grease lubricated bearings is more pronounced. This is due to the larger exposure area and thinner thickness of the films that are formed in the bearing during operation. Moreover, the sludge produced during the oxidation process can also affect the lubricated condition.

1.3.2 Speed influence

Besides temperature, speed is another main factor that influences the lubrication process. All the speed issues discussed in this section are in the temperature regime between the lower operating temperature limit and the upper operating temperature limit. This range is called the green zone, where the grease will function reliably.

1.3.2.1 Low speed

Lubricating conditions

The slowly rotating rolling bearings are usually large-scale and used in fields such as mining, marine, etc. The interacting surfaces are separated by a layer of lubricant film, which results in the reduction of friction and wear. In oil lubrication, the film thickness will be thin at low speeds according to the Elastohydrodynamic lubrication (EHL) theory.

On the contrary, the film thickness with grease lubrication is greatly higher than that of the corresponding base oil under identical conditions [17–22]. In addition to this, the film thickness and the flow behavior of the grease around the contact conjunction are much more complex and unpredictable at low speeds.

Grease lubrication in bearings is generally divided into ‘churning phase’ and ‘channeling phase’ for grease lubrication in bearings running under constant conditions. The ‘churning phase’ typically takes from a few hours up to 24 hours of operation, and it is often accompanied by a high temperature. There will be sufficient lubricant available in the inlets

of the contacts in the churning state. As the high film thickness can always be preserved, starvation can be negligible in this state.

The 'channeling phase' is the main phase in the long running process of grease lubricated bearings. Starvation often occur during this phase, the rupture and rebuild of the film thickness frequently take place [23]. Mechanisms of starved grease lubrication will be discussed in detail in next section. In the churning phase, the grease flow behaviors are determined by the internal design of the bearing, the design of the housing, the rheological properties of the grease, etc.

As the bearings rotate, the initial packs of greases are distributed to places such as the adjacent area of the contacts, cage bars and in the cage pocket, thus gradually forming the initial grease reservoirs. Therefore, the churning phase has important influences on the long-term reliable operation of bearings.

The churning and channeling phases as mentioned above are not directly related to the operating speed of bearings. In fact they are two different lubrication processes which are experienced by most bearings under constant conditions. However, the effects of speed on the time allocation of churning and channeling during the whole period of operation should not be disregarded.

The high film thickness generated by greases at low speeds will promote a longer churning phase. Continuous churning will consume excess energy and maintain a high temperature in the bearing, and may even cause failure. For these reasons, the choice of grease to be used and the understanding of the lubrication mechanisms under low speeds are particularly important.

As early as 1972, Poon [24] measured the thickness by means of a magnetic reluctance technique, and he found that the film thickness of the grease was higher than that of the corresponding base oil at low speeds. As shown in Figure 1.2, many authors [17,18,20,25] have observed that the grease film thickness decreases first and then increases with increasing speed, and forms a V-curve.

Hurley and Cann *et al*. [26] proposed that the accumulation of thickeners plays a decisive role on this phenomenon, especially in the speed range from the starting speed to the speed corresponding of the lowest point of the V-curve, *i.e*., the transition speed. Subsequently,

Kimura *et al*. [20] used the Carreau-Yasuda viscosity equation to successfully simulate the V-curve at low speeds. Through the results obtained from a mass of experiments based on a ball-on-disk test rig, Hui cen *et al*. [18] have proved that the transition speed is a function of temperature, which is independent of load and slip.

Moreover, the V-curve which is observed in a ball-on-disk rig also occurring in a real full rolling bearing has been confirmed, supported by using the electrical capacitance method in a real bearing at ultralow speed. Furthermore, G.E Morales *et al*. [25] established a relation between apparent viscosity and the bearing lubrication parameter kappa. The mechanical aging process decreases the grease film thickness at very low speeds with aging time, but no significant difference is found at higher speeds [17]. On the whole, research on grease lubrication mechanisms under low speeds is still needed.

1.3.2.2 Medium speed

Lubrication mechanisms

At present, there is no consensus on the mechanisms of the film formation process in the starved regime, nor the influence of the constituents of greases on lubrication performance. One of the early models is the 'Sponge model' [33], the function of the thickener is only deemed as a storage place for base oil. Booser and Wilcock [34] postulated that rolling bearings are lubricated by the base oil released by the grease during operation.

Afterwards, Wikstrom and Hoglund [6] show that the grease and base oil have similar bearing friction torques, by using these two constituents in full rolling bearing tests respectively. However, recent research [8,35] demonstrated that there are large differences between the bearing friction torque when it is lubricated by grease or base oil. This contradicts the previous hypothesis. Perhaps this is due to the extension of the speed range and temperature range in the latest tests.

The other viewpoint is that the bleeding oil lubricates the contact zone. Cousseau *et al*. [36] have found that the rheological properties of the bleeding oil are very different from that of the base oil. In addition, the viscosity and pressure-viscosity coefficient of the bleeding oil can be used to predict the grease film thickness under full flooded condition [35]. Baart *et al*. [37] developed a flow model based on Darcy's law, and the relation between the pressure

gradient, oil viscosity, thickener structure deformation and permeability to the volumetric oil flow out of the thickener skeleton is illustrated. Based on the results of experiments, Gonçalves *et al*. [19] show that the rheological properties of the grease and that of the bleeding oil are quite similar to each other under typical EHL shear.

A model proposed by Cann *et al*. [38] is that the grease-lubricated contacts are layered by a shear degraded residual thickener layer and an oil layer formed by hydrodynamic action. Cann and Spikes [39] used FTIR and IR to show that the thickeners are detected in the regime of inlet and outlet which are fairly close to the conjunction. This means that the thickeners can move across the contacts.

Furthermore, many authors [40–42] have confirmed the thickeners enter and pass the contacts through optical interferometry measurements. On the whole, it is generally believed that both the thickeners and base oils participated in the process of building the film thickness.

Booser and Wilcock [34], Baker [43] suggest that the rate at which lubricant is entrained and lost around the contact, i.e. the feed and loss rates, have been deemed as the determining factors for the degree of starvation in grease lubrication [23]. When the loss rate is larger than the feed rate, starvation occurs.

As shown in Figure 1.3, Wikstrom *et al*. [23] summarize a model to describe the balance of feed and loss rates for the contact. The main loss mechanisms are lubricant passing through the contact, oxidation, polymerization, surface spreading and evaporation. The main feed mechanisms include bleeding due to shear and replenishment induced by centrifugal and capillary forces. These show that the various factors that we need to consider in a real bearing are complex and mutually connected. The lubricating condition is affected by various factors.

As shown in Figure 1.4, Williamson [44] summarizes the film formation process based on his research results. At a relatively long distance from the Hertzian loaded region, the bulk grease begins to break down into smaller clumps of tangled thickener fibers and associated base oil in the areas closest to the moving surfaces. In this circumstance, if the force exerted on it does not exceed the yield stress of the bulk grease, core formation can occur.

Bordenet *et al*. [45] also suggest that two layers can exist in the inlet regime. Mahncke and Tabor [46] have observed the core formation in a glass tube. As the Hertzian loaded region is

approached, the clumps experience increasingly higher shear rates resulting in disentanglement and alignment of individual thickener fibers in the direction of the shear field and subsequent breakage. The core will disappear gradually. The film in the Hertzian loaded region presents a glass-like structure. At the outlet regime, a cavitation wake forms. The issues about the film thickness and wake will be discussed in the following part.

Starvation and replenishment

Machine elements such as rolling bearings which run in the medium speed regime are the most common. Most of the time, bearings are running in the starved regime. This is because once the grease is pushed aside by the passage of a rolling element during the initial phase of operation, the low mobility of the grease prevents it from turning back to the contact point easily. It often leads to the depletion of lubricant and the inability to maintain a film separating the interacting surfaces, and may ultimately lead to failure and damage. The hazards of starvation are self-evident.

The relative magnitude of the lubricant film thickness compared to the composite surface roughness of the two surfaces, named the film thickness ratio, is considered as the standard parameter used to describe the lubricated condition [47]. This means the bearings operate in a reliable state only when a certain film thickness can be maintained.

With regard to the measurements of grease film thickness, there are some models which relate to the rheological properties of the grease that can be applied. That is, the numerical simulations and the measurements of film thickness are performed by using the rheological equations which are expressed by the apparent viscosity or shear stress as a function of shear rate in the Grubin theory calculation.

The Herschel-Bulkley model is often used in the calculation of grease film thickness [48–50]. Yang and Qing [51] used the Bingham model to predict the film thickness. They all obtain results which show that the grease film thickness is higher than that of the base oil. Dong and Qian [52] developed a film thickness model using a more complex rheology model, and the fact that the apparent viscosity of the grease under high shear approaches that of the base oil is taken into account.

Aihara and Dowson [53] claimed that the grease film thickness can be simply replaced by a value 70 percentage that of the base oil. Ever since optical interferometry was introduced by

Gohar and Cameron [54], the film thickness could be measured with a resolution of few nanometers by combining the spacer layer coating and image analysis method [55]. Moreover, combining this technique with high speed videos would allow recording of the film thickness change with time. Thus, it has been applied widely in many areas.

Furthermore, it is also possible to observe the flow behaviors around the contact. The grease flow behaviors around the contact directly relate to the lubricating condition. The tracing and observation of the grease flow behaviors around the contact can contribute to elucidating the underlying mechanisms.

To understand the grease starved mechanisms well, one should firstly clarify the reasons for starvation. The film formation depends on the continuous supply of grease to the inlet area. The inlet area is defined as the place from where the pressure starts at the boundary of the Hertzian contact. As previously mentioned, starvation occurs due to the rate of loss overtaking that of feed.

One part of the lubricant passes through the Hertzian regime, while the other part escapes around the Hertzian regime and ruptures into cavitation finger-like patterns. The cavitation may accelerate the loss of lubricant from the contact, but may also play a positive role [56].

In some reciprocating motions, both fretting [57] and the film formation [58,59] will be affected by cavitation with the change of frequency and amplitude. Micro-cavitation occur because the surface roughness of the rubber surfaces can contribute to the decrease in the friction coefficient [60].

Generally, in most bearing applications the cavitation outlet regime is immediately followed by an inlet region due to the periodic rotation of many rolling elements. The influence of the cavitation outlet regime on the lubricant supply condition in the inlet region is an important practical aspect which is often overlooked. Therefore, both the flow behaviors in the inlet and outlet regimes should be considered.

As mentioned above, the amount of lubricant available in the inlet regime determines the film thickness. In 1970, Wedeven *et al*. [61] proposed that the degree of starvation in EHL can be predicted by the length of the inlet meniscus, i.e., inlet distance. The differences between grease and oil lubrication in connection with starvation are related to the mechanisms by which the lubricant is transported and redistributed in the vicinity of the inlet region. This is

due to the differences in rheological properties between them.

Pemberton and Cameron [62] used aerated oil to reveal the 'butterfly' boundary shape of oil in constant conditions. As shown in Figure 1.5, they observed that there are two bands of oil prior to the inlet regime. As the two bands of oil approach, some streams gather in the inlet regime and become one source of replenishment.

The majority of streams bypasses the contact and looks like the spread-open wings of a butterfly, and continues to converge into two side bands again at the exit of contact. The oil that has passed through the contact regime is left both on the ball and race in the outline of banana leaves which consist of finger-like streams.

If there is no additional lubricant supply, the replenishment to the inlet regime becomes determinant of the film thickness. Besides the inlet distance and side bands, many authors [63–65] propose that the efficiency of replenishment is more influenced by the meniscus of the inlet regime.

In addition, Kaneta *et al*. [66] found the adhesion of thickener on the track contributes to the lubrication. The film can be recovered after a long time running. Cann *et al*. [67] believe this is due to the replenishment of bleeding oils which flow from the reservoirs. Nagata *et al*. [68] stated that lateral oscillations have a beneficial influence on grease performance by pushing the grease in the side bands back onto the track.

As shown in Figure 1.6, many authors [69–71] have noticed the finger patterns which are formed in the outlet of contacts both in oil and grease lubrication. Usually the solubility constant of gas in oils is around 10% at standard temperature and pressure [72]. Cavitation occurs in grease due to either gas evolution or vapor evolution.

Gaseous cavitation occurs when the pressure decreases below saturation pressure, whereas vaporous cavitation occurs when the pressure drops below the vapor pressure of the lubricant. Vaporous cavitation requires a much greater pressure drop. Thus the gaseous cavity is more commonly observed.

Otsu *et al*. [56] conducted both lubricated point contact sliding and separate tests in oil lubrication, and showed that the growth of the cavity pattern depended on the rapid evolution of negative pressure at the exit of the conjunction through a numerical analysis. Similarly, accompanied by the development of cavity at the exit of the conjunction, the negative

hydrodynamic pressure gradient triggers the instability [73] and induces the growth of the finger pattern outward from the interface of the cavity and grease. Then the complex finger patterns are formed.

These cavitation fingers grow perpendicular to a line which makes an angle of 35°with the direction of motion [61]. The basic structure is a single finger, which is usually divided into a number of tiny rods that grow like tree branches. The dark parts are grease and the light parts are cavitation [21].

Some researchers [13,61,69,71,74] showed that this shape is related with surface tension, the running conditions and the divergent geometry of the two interacting surfaces in the outlet area etc. Lubricants with large surface tension produce more round fingers [61]. Cann *et al*. [69] suggest that the rheological behavior of greases under low shear is the key for these issues. The quantity and properties of the grease which lies in the inlet regime have a great influence on the capacity of replenishment [61].

The transport and redistribution of the grease near the contact conceals a transfer mechanism, which may contribute to a better understanding of the replenishment mechanisms. Unlike in oil lubrication, the wake can only be observed when the test is kept running. In grease lubrication, the flow behavior around the contact can be preserved to a great extent even after stopping due to the special rheological properties of the grease. All these provide a platform for the further research, since it is usually difficult to get a clear photo in video.

Aström *et al*. [21] added molybdenum disulfide particles to the grease in order to observe the movement and distribution of the grease in the vicinity of the contact. They showed that outlet cavitation occurs and forms the finger pattern. They also observed that the finger pattern can remain unchanged several days after test.

Merieux *et al*. [74] observed that the angle of the grease fingers towards the rolling track becomes smaller after a period of operation. They also pointed out that the tiny rod fingers lead the bleeding oil to replenish into the track. In addition, the grease finger relates directly to the amount of reservoirs. The change in slide-to-roll ratios can cause a change in the shape of the fingers, and this will have an impact on the replenishing of the contact [75]. Further research is needed on the features of grease finger changes with running

conditions and the relationship between the rheological properties of the grease, the lubricated conditions and the grease wake patterns.

1.3.2.3 High speed

Severe starvation is more likely to occur in high speed rolling bearings. Research on the replenishment of grease has been conducted for a long time. As shown in Figure 1.7, as the rolling elements rotate, they produce a depressed oil layer shape in the center of the track. Two adjacent oil ridges are formed due to the push exerted by the rolling elements.

Chiu [77] is the first to simulate the replenishment process of two side ridges towards the track. He assumes the surface is fed by a uniform layer of oil, and the trigger forces are surface tension and viscosity. Then Jacob *et al*. [63] add Van der Waals forces which may have effects under ultrathin film thickness. Yin *et al*. [78] also made simulations based on the model of Chiu, and a good fit between simulation results and experimental data shows that this model can be applied in real rolling motion.

Gershuni *et al*. [76] consider the influence of centrifugal forces. The conclusion is that the replenishment of side ridges can almost be ignored in a real cylindrical roller bearing. One of the essential reasons for this is that there is not enough time between successive rolling elements for the adjacent oil to get back onto the track. In addition, the centrifugal forces remove the oil from the track. However, it is still important for single contacts or low speed conditions etc.

In severe starvation, grease lubrication can be treated as oil lubrication with high viscosity. Chevalier and Lubrecht *et al*. [65] conducted a numerical simulation based on Elrod's [79,80] starvation model, proving that there is a direct relation between the amount of lubricant and its distribution in the inlet. Later the thin layer flow model was extended under stable and dynamic conditions, and successfully used to explain various aspects of bearings and of grease lubrication [81–83].

1.4 Objectives

Although in the past few decades some research has involved the flow pattern in a contact, there is no research mainly related to the issue of grease flow pattern at present. Due to its semi-solid composition and the complex rheological properties, the features of grease flow

are different for different grease types and different conditions. This unique flow pattern contains a lot of important information: the interaction between the thickener and the base oil, the lubricating conditions, the rheological properties and the mechanisms of redistribution and transportation etc. Due to its complexity, literature studies about this issue are few.

In the work presented in this thesis, the focus is on the grease flow behavior in a point contact. It includes the features of flow pattern surrounding the contact point and the lubricating conditions of the contact point. The purpose of this work is to find the information behind the flow pattern as mentioned above through systematic observation on the features of grease flow.

1.5 Outline

The detailed structure of this thesis is listed as follows:

Chapter 1 introduces the research background and describes the motivation for carrying out the research.

In Chapter 2, the rheological properties of greases are described by testing the yield stress and apparent viscosity.

In Chapter 3, optical interferometry measurements and a ball-on-disk test rig are used. The features of grease flow for different greases under different test conditions are observed. The track pattern is selected as the representatives of grease flow, and eight characteristic parameters are defined to parameterize the track pattern. The variation of these parameters under different test conditions is discussed in detail.

In Chapter 4, a pair of scoops is used as an artificial replenishment setup in a ball-on-disk test rig, thus the contact point is kept in a fully flooded state. The track pattern and the film thickness are observed with artificial replenishment and without artificial replenishment, respectively. Therefore information under different lubricating conditions can be obtained. The replenishment, distribution and lubrication mechanisms are proposed and discussed.

In Chapter 5, on the basis of the previous data presented in Chapter 3 and Chapter 4, covariance analysis is used to discuss the correlations between all these factors, such as the characteristic parameters of grease flow, test conditions, rheological properties, film thickness and lubricating conditions. Principal component analysis is used to select the most appropriate

parameters which can represent the change of the features of flow when the entrainment speed, test duration and slide to roll ratio change, respectively.

In Chapter 6, fluorescence technique is used to observe the in-situ base oil behavior in a wider observation range. The replenishment of side reservoir is verified.

Chapter 7 introduces conclusions and further work.

References

[1] Theo Mang, Wilfried Dresel. Lubricants and Lubrication, John Wiley & Sons, 2007.

[2] NLGI. Lubricanting Grease Guide, second edition, Kansas City, 1987.

[3] G.B. Froishteter, K.K. Trilisky, L. Ishchuk, Y, and P.M. Stupak. Rheological and Thermophysical Properties of Greases. Edited by G.V Vinogradov, Gordon and Breach Science Publishers, New York, USA, English edition, 1989. Translated from Russian by G.E. Miram.

[4] J Gerstenberger, G Poll, Rolling bearing lubrication with grease at low temperatures, Tribology Series, 2001.

[5] D Kim, G Zimbru, Start-Stop Characteristics and Thermal Behavior of a Large Hybrid Airfoil Bearing For Aero-Propulsion Applications, J Eng Gas Turbines Power, 2012.

[6] Wikström V, Höglund E, Starting and Steady-State Friction Torque of Grease-Lubricated Rolling Element Bearings at Low Temperatures — Part II : Correlation with Less-Complex Test Methods, Tribol Trans, 1996; 39: 37–41.

[7] Wikström V, Höglund E, Starting and Steady-State Friction Torque of Grease-Lubricated Rolling Element Bearings at Low Temperatures—Part I: A Parameter Study. Tribol Trans, 1996; 39: 684–90.

[8] Cousseau T, Grac BM, Campos A V, Seabra JHO, Influence of grease rheology on thrust ball bearings friction torque, Tribology International , 2012; 46: 106–13.

[9] Oikawa E, Inami N, Hokao M, Yokouchi A, Sugimura J. Bearing torque characteristics of lithium soap greases with some synthetic base oils, Proceedings of the Institution of Mechanical Engineers, Part J: Journal of Engineering Tribology, 2012; 226: 575-583.

[10] Cousseau T, Graça B, Campos A, Seabra J. Friction torque in grease lubricated thrust ball bearings. Tribology International, 2011; 44: 523–531.

[11] Rolling bearing lubrication, Technical Report Publ. No. WL 81 115/4 EA, FAG, 2002.

[12] Strong, S.B., Grease flow properties and some relationships between them, NLGI Spokesman, 1969; 32: 120-130.

[13] P.M. Cann, Grease degradation in a bearing simulation device, Tribology International, 2006; 39: 1698-1706.

[14] R McClintock, A laboratory study of wheel bearing grease high temperature life, NLGI Spokesman, 1980; 414.

[15] H Ito, M Tomaru, T Suzuki, Physical and chemical aspects of grease deterioration in sealed ball bearings, Lubrication engineering, 1988; 44: 872-879.

[16] Komatsuzakl s, Uematsu t, Kobayashl y, Change of grease characteristics to the end of lubricating life, NLGI spokesman, 2000; 63: 22-29.

[17] Cen H, Lugt PM, Morales-Espejel G, Film Thickness of Mechanically Worked Lubricating Grease at Very Low Speeds, Tribol Trans, 2014: 1066-1071.

[18] Cen H, Lugt PM, Morales-Espejel G, On the film thickness of grease lubricated contacts at low speeds, Tribol Trans, 2014: 668-678.

[19] Gonçalves D, Graça B, Campos A V., Seabra J, Leckner J, Westbroek R. On the film thickness behaviour of polymer greases at low and high speeds. Tribol international, 2015; 90: 435-444.

[20] Yoshitsugu Kimura, Toshiaki Endo, Daming Dong, EHL with Grease at Low Speeds, Advanced Tribology, 2010: 15-19.

[21] Henrik Åström, Jan Ove Östensen and Erik Höglund, Lubricating Grease Replenishment in an Elastohydrodynamic Point Contact, Journal of Tribology, 1993; 115: 501–506.

[22] H. Åström, O. Isaksson, E. Höglund, Video recordings of an EHD point contact lubricated with grease, Tribology International, 1991; 24:179–84.

[23] V Wikström1 B Jacobson, Loss of lubricant from oil-lubricated near-starved spherical roller bearings, Proceedings of the Institution of Mechanical Engineers, Part J: Journal of Engineering Tribology, 1997; 211: 51-66.

[24] Poon SY. An Experimental Study of Grease in Elastohydrodynamic Lubrication, J. of Lubrication Tech, 1972; 94: 27-34.

[25] Morales-espejel GE, Lugt PM, Pasaribu HR, Cen H. Film thickness in grease lubricated slow rotating rolling bearings, Tribology International, 2014; 74: 7–19.

[26] Hurley S., Cann R. M., Grease composition and film thickness in rolling contacts, NLGI spokesman, 1999, 63; 12-22.

[27] Howard A. Barnes, A review of the slip (wall depletion) of polymer solutions, emulsions and particle suspensions in viscometers: its cause, character, and cure, Journal of Non-Newtonian Fluid Mechanics, 1995; 56: 221-251.

[28] Magnin A., Piau JM, Application of freeze-fracture technique for analyzing the structure of lubricant greases, Journal of Materials Research, 1989; 4: 990–995.

[29] Meng Yonggang, Zheng Jie, A rheological model for lithium lubricating grease, Tribology International, 1999; 31: 619–625.

[30] H.A. Barnes, Thixotropy - A review, Journal of Non-Newtonian Fluid Mechanics, 1997; 70: 1-33.

[31] A.D. Bramhall and J.F.Hutton, Wall effect in the flow of lubricating grease in plunger viscosimeters. British Journal of Applied Physics, 1960; 11: 363-369.

[32] R. Czarny, The influence of surface material and topography on the wall effect of grease, Lubrication Science, 2004; 14: 255-274.

[33] NA Scarlett, Use of grease in rolling bearings, Proc. Instn. Mech. Engrs., 1967; 182: 585-624.

[34] E.R., Booser and D.F. Wilcock, Minimum Oil Requirements of Ball Bearings, Lub Eng.,1953.

[35] Grac B, Campos A, Seabra J, Larsson R, Film thickness in a ball-on-disc contact lubricated with greases, bleed oils and base oils, Tribology International, 2012; 53: 53–60.

[36] Cousseau T, Graca B, Campos A, Seabra J, Experimental measuring procedure for the friction torque in rolling bearings, Lubrication Science, 2010; 22: 133-147.

[37] Baart P, Vorst B Van Der, Lugt PM, Ostayen RAJ Van. Oil-Bleeding Model for Lubricating Grease Based on Viscous Flow Through a Porous Microstructure, Tribology Transactions, 2010; 53: 340-348.

[38] Cann PM, Starvation and Reflow in a Grease-Lubricated Elastohydrodynamic Contact, Tribology Transactions, 1996; 39: 698-704.

[39] P.M. Cann, H.A. Spikes, In-contact IR spectroscopy of hydrocarbon lubricants, Tribology Letters, 2005; 19:289–297.

[40] Larsson R, Eriksson P, Wikstro V, Grease soap particles passing through an elastohydrodynamic contact under side slip conditions, Proceedings of the Institution of Mechanical Engineers, Part J: Journal of Engineering Tribology, 2000; 214: 317–325.

[41] Larsson PO, Larsson R, Jolkin A, Marklund O, Pressure fluctuations as grease soaps pass through an EHL contact, Tribology International, 2000; 33: 211–216.

[42] Larsson R, Eriksson P, Wikstro V. Grease passing through an elastohydrodynamic contact under pure rolling conditions, Proceedings of the Institution of Mechanical Engineers, Part J: Journal of Engineering Tribology, 2000; 214: 309–316.

[43] Baker, A.E., Grease Bleeding-A Factor in Ball Bearing Performance, NLGI Spokesman, 1958; 22: 271-279.

[44] B P Williamson, An optical study of grease rheology in an elastohydrodynamic point contact under fully flooded and starvation conditions, Proceedings of the Institution of Mechanical Engineers, Part J: Journal of Engineering Tribology March, 1995; 209: 63-74.

[45] L. Bordenet, G. Dalmaz, J-P Chaomleffel and F. Vergne, A study of grease film thicknesses in elastorheodynamic rolling point contacts, Lubrication Science, 1990; 2: 273–284.

[46] Mahncke, H.E. and Tabor, W, A Simple Demonstration of Flow Type inGreases, Lubr. Eng., 1955: 22-28.

[47] T. E. Tallian, On Competing Failure Modes in Rolling Contact, ASLE Transactions, 1967; 10: 418-439.

[48] Kauzlarich, J.J., Greenwood, J.A., Elastohydrodynamic Lubrication with Herschel-Bulkley Model Greases, ASLE Trans., 1972; 15: 269-277.

[49] JA Greenwood and JJ Kauzlarich, EHD lubrication with Herschel-Bulkley model greases, ASLE Trans., 1972: 269-277.

[50] W. Jonkisz and H. Krzeminski-Freda, Pressure distribution and shape of elastohydrodynamic grease film, Wear, 1979; 55: 81-89.

[51] L. Bordenet et al., A study of grease film thicknesses in elastohydrodynamic rolling point contacts, Vol.4, EUROTRIB'89, Helsinki,133-138.

[52] Dong D, Qian X. A theory of elastohydrodynamic grease-lubricated line contact based on a refined rheological model, Tribology International, 1988; 21: 261–267.

[53] Aihara,S., and Dowson, D., A Study of Film Thickness in Grease Lubricated Elastohydrodynamic Contacts, Proc. of the 5th Leeds Lyon Symposium on Tribology, 1978; Paper III (v): 104-115.

[54] R.Gohar, A.Cameron, The Mapping of Elastohydrodynamic Contacts, A S L E Transactions,2008;10: 37–41.

[55] Cann PM, Spikes HA, Hutchinson J. The Development of a Spacer Layer Imaging Method (SLIM) for Mapping Elastohydrodynamic Contacts, Tribology Transactions, 2008; 19: 915-921.

[56] Otsu T, Tanaka H, Sugimura J. Initiation and growth of gaseous cavity in concentrated contact in various surrounding gases, Tribiology Int, 2012; 53: 68–75.

[57] Leonard B, Sadeghi F, Cipra R, Leonard BEN. Gaseous Cavitation and Wear in Lubricated Fretting Contacts Gaseous Cavitation and Wear in Lubricated Fretting Contacts, Tribology Transactions, 2008; 51: 351–360.

[58] Jakeman RW. A numerical analysis method based on flow continuity for hydrodynamic journal bearings, Tribology International, 1984; 17: 325–33.

[59] Gasni D, Ibrahim MKW, Measurements of lubricant film thickness in the iso-viscous elastohydrodynamic regime, Tribiology Int, 2011; 44: 933–944.

[60] Kazuyuki Yagi, Wataru Takedomi, Hiroyoshi Tanaka, Joichi Sugimura, Improvement of Lubrication Performance by Micro Pit Surfaces, Tribology Online, 2008; 3: 285-288.

[61] Wedeven LD, Evans D, Cameron A, Optical Analysis of Ball Bearing Starvation, Journal of Lubrication Technology, 1970; 3: 349-361.

[62] Pemberton J, Cameron A. A mechanism of fluid replenishment in elastohydrodynamic contacts, Wear, 1976; 37: 185-190.

[63] B. Jacod, F. Pubilier, P.M.E. Cann, A.A. Lubrecht, An Analysis of Track Replenishment Mechanisms in the Starved Regime, Tribology Series, 1999; 36: 483-492.

[64] B. Damiens, C. H. Venner, P. M. E. Cann and A. A. Lubrecht, Starved Lubrication of Elliptical EHD Contacts, Journal of Tribology, 2004; 126: 105-111.

[65] F. Chevalier, A.A. Lubrecht, P.M.E. Cann, F. Colin and G. Dalmaz, Film Thickness in Starved EHL Point Contacts, Journal of Tribology, 1998; 120: 126-133.

[66] Kaneta M, Ogata T, Takubo Y, Naka M. Effects of a thickener structure on grease elastohydrodynamic lubrication films, Proceedings of the Institution of Mechanical Engineers, Part J: Journal of Engineering Tribology, 2000; 214: 327-336.

[67] Philippa Cann, A. A. Lubrecht, An analysis of the mechanisms of grease lubrication in rolling element bearings, Lubrication Science,1999; 11: 227-245.

[68] Nagata Y, Kalogiannis K, Glovnea R, Track Replenishment by Lateral Vibrations in Grease- Lubricated EHD Contacts, Tribology Transactions, 2012: 37–41.

[69] P.M.E. Cann, Thin-film grease lubrication, Proceedings of the Institution of Mechanical Engineers, Part J: Journal of Engineering Tribology, 1999;213:405-416.

[70] R.T.P. Chan, R.F. Martinez-Botas, R. Gohar, Isoviscous flow past a rigid sphere partially immersed in a thin oil film, Lubrication Science, 2007; 19: 197-212.

[71] P.M. Cann, Grease lubrication of rolling element bearings—role of the grease thickener, Lubrication Science, 2007; 19: 183-196.

[72] P.H. Schweitzer, V.G. Szebehely, Gas Evolution in Liquids and Cavitation, Journal of Applied Physics, 1950; 21.

[73] Saffman PG, Taylor G. The Penetration of a Fluid into a Porous Medium or Hele-Shaw Cell Containing a More Viscous Liquid, Proc. R. Soc. London A, 1958: 312.

[74] J-S. Mérieux, S. Hurley, A.A. Lubrecht, P.M. Cann, Shear-degradation of grease and base oil availability in starved EHL lubrication, Tribology Series, 2000; 38: 581-588.

[75] Huang L, Guo D, Wen S, Wan GTY. Effects of slide/roll ratio on the behaviours of grease reservoir and film thickness of point contact. Tribol Lett, 2014; 54: 263–271.

[76] Leonid Gershuni, Mats G. Larson, Piet M. Lugt, Lubricant Replenishment in Rolling Bearing Contacts, Tribology Transactions, 2008; 51: 643-651.

[77] Chiu YP. An Analysis and Prediction of Lubricant Film Starvation in Rolling Contact Systems, ASLE Transactions, 1974; 17: 22-35.

[78] J.Yin, K.I. Eissa, R.Gohar, P.M.E. Cann, Rebounding lubricant layers, Lubrication Science, 1999; 12: 1-30.

[79] H.G. Elrod, A Cavitation Algorithm,Journal of Lubrication Technology, 1981; 103: 350-354.

[80] Elrod, H.G., and Adams, M.L., A Computer Program for Cavitation and Starvation Problems, Proceedings of the 1st Leeds-Lyon Symposium on Tribology, 1974.

[81] Marco T. Van Zoelena, Cornelis H. Vennera, Piet M. Lugtb, Free Surface Thin Layer Flow in Bearings Induced by Centrifugal Effects,Tribology Transactions, 2010; 53: 297-307.

[82] Venner CH, Zoelen MT Van, Lugt PM, Thin layer flow and film decay modeling for grease lubricated rolling bearings, Tribiology Int, 2012; 47: 175–187.

[83] M.T. van Zoelen, C.H. Venner, P. M. Lugt, Free Surface Thin Layer Flow on Bearing Raceways, Journal of Tribology, 2008; 130.

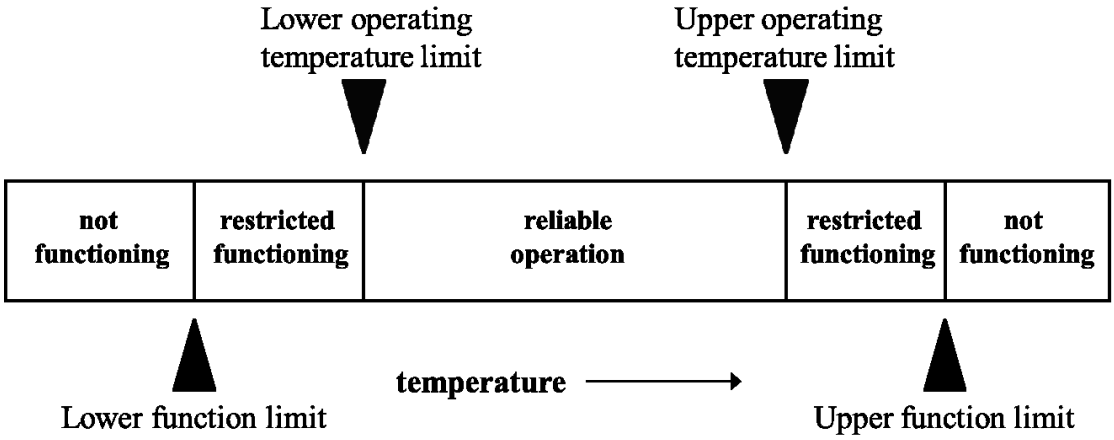

Figure 1.1 Operating temperature range of lubricating greases [4]

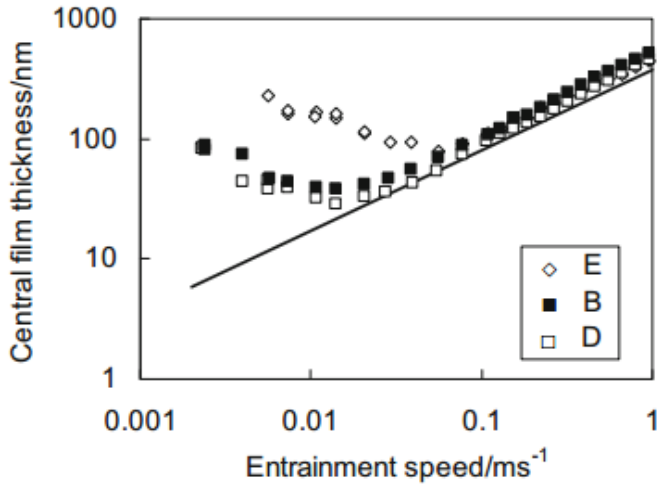

Figure 1.2 Film thickness of grease under low speed [20]

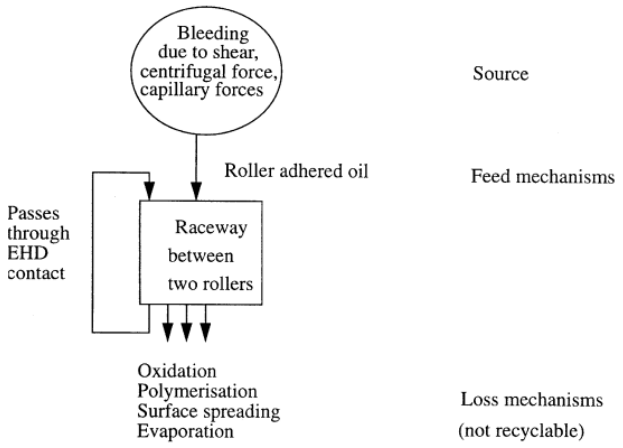

Figure 1.3 Model for feed-loss balance [23]

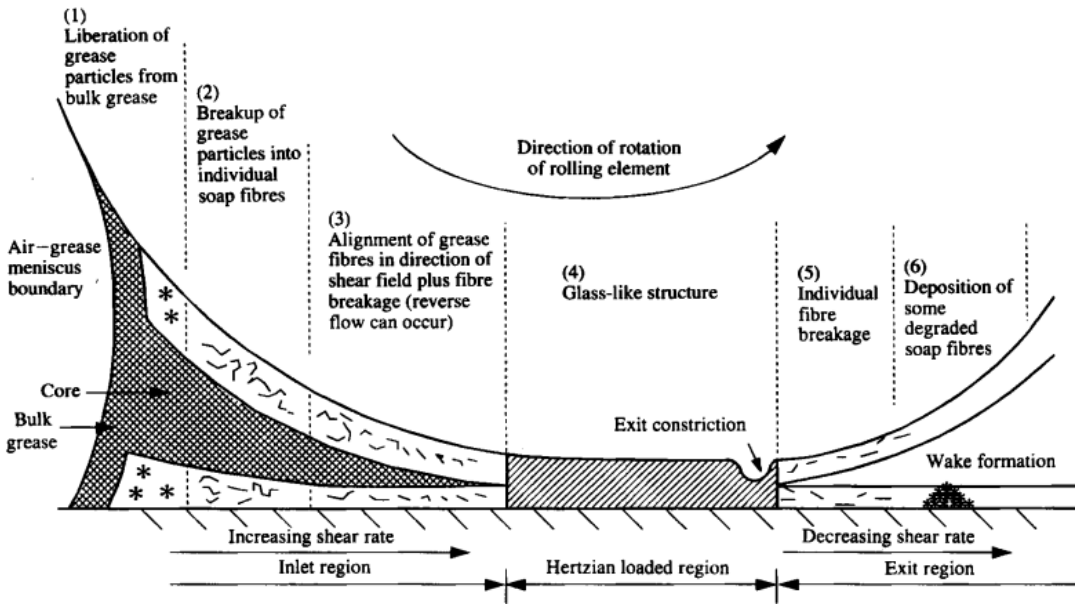

Figure 1.4 Schematic diagram of an operating EHD contact showing main elements of the proposed grease model [44]

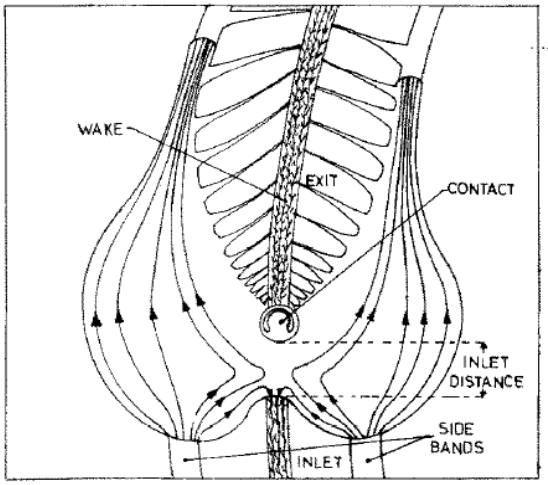

Figure 1.5 Schematic representation of the wake flow around contact in oil lubrication [62]

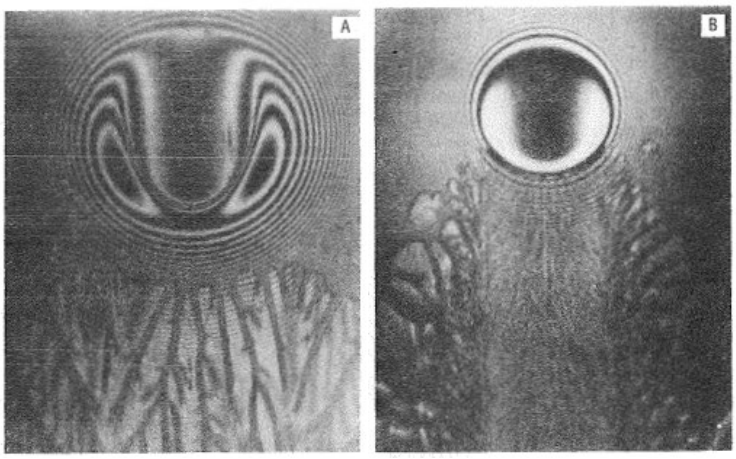

Figure 1.6 Cavitation pattern in rolling contact [61]

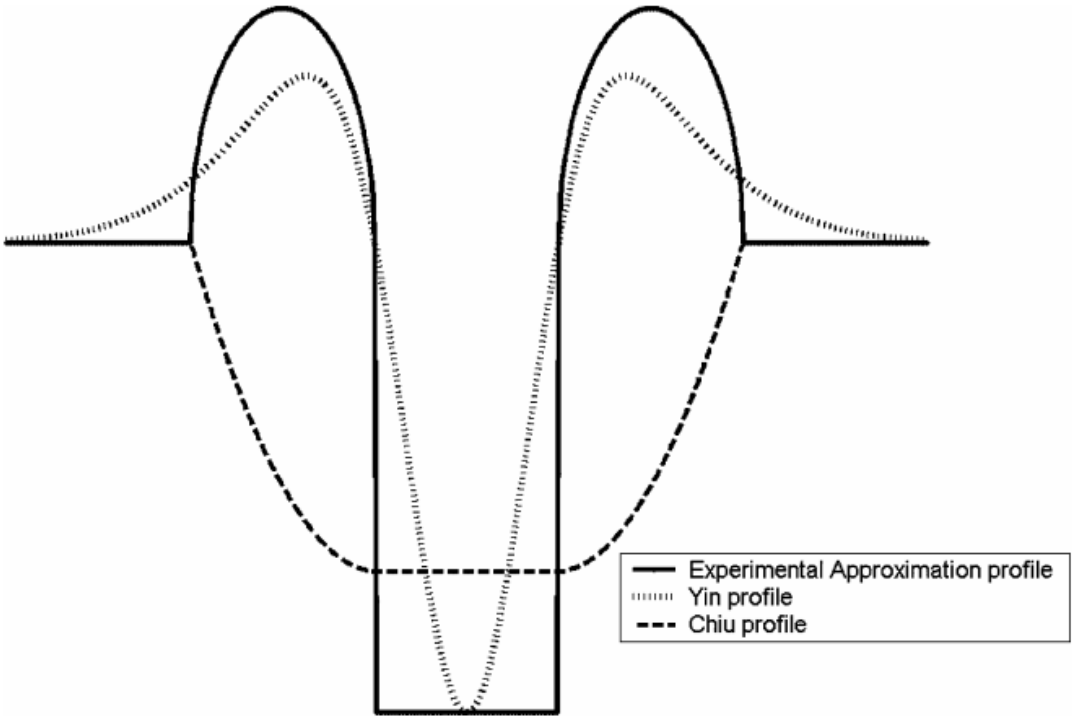

Figure 1.7 Different approximations of initial profiles [76]

CHAPTER 2

Grease rheology

Greases contain a thickener, base oil and additives. This makes the grease a complex semi-solid fluid. In this chapter, the rheological properties of greases are described by the yield stress and the apparent viscosity. The model parameters obtained from rheometer tests can help us understand the properties of test greases.

2.1 The properties of greases

The dispersed-phase thickeners combine with each other and build a three-dimensional skeleton. Base oil is trapped in the thickener skeleton as dispersion medium by a combination of Van der Waals and capillary forces. The strength of the structure skeleton is not only dependent on the thickener size but also the thickener shape and arrangement state.

If the external force on the grease is not greater than the limit strength of the grease structure, at which the grease begins to flow, the grease will experience only elastic deformation and will not flow. On the contrary, if the external force on the grease exceeds that limit, the structure skeleton of the grease will be destroyed. A part of the base oil bleeds from the broken structure and the grease flows. This limit is called the yield stress.

The value of the yield stress has an influence on the starting torque, and channeling and churning conditions of rolling element bearings [1]. The flow properties of the lubricating grease close to the wall are different from those of the bulk grease. This is knowns as the 'wall effect'. Anomalies in the testing of the yield stress under low shear are often ascribed to these wall effects.

Grease is a type of viscoelastic material. Its viscosity is a function of temperature and shear stress, and is not the same as those of lubricating oils. The flow behavior of greases does not conform to the Newtonian fluid law. The viscosity of a grease is not a constant at a certain temperature, but a variable that changes with the shear rate. With the increase of the shear rate, the viscosity of grease decreases.

However, the extent of the viscosity decrease gradually weakens and the value of viscosity approaches the viscosity of the base oil at high shear rate. To distinguish between the viscosity of the oil and grease, the viscosity of the grease is referred to as apparent viscosity. It is calculated by the ratio of shear stress to shear rate. The apparent viscosity is the viscosity of a grease that holds only for the shear rate and temperature at which the viscosity is determined.

In summary, the rheological properties of a grease are determined by the interaction between the thickener and the base oil, shear rate, temperature and running time in practical applications.

2.2 Rheology models

The measurement of the yield stress has not been standardized. The value of the yield stress depends on the test method and the tester. Many models are available to describe the rheological properties of complex fluids. Some specific models find their application in grease lubrication and can be used to describe the apparent viscosity as a function of shear rate.

2.2.1 Yield stress

The examples of yield stress measurement can be found in these papers [2-5]. Figure 2.1 shows the storage modulus G' and the loss modulus G'' for the grease Liohst.pao400. As shown, the definition of the yield stress is the 'crossover stress' at which the storage modulus and loss modulus dramatically change. The storage modulus represents the elastic portion. The loss modulus represents the viscous portion.

2.2.2 Apparent viscosity

Table 2.1 shows some frequently used models of grease rheology. In these equations, τ and $\dot{\gamma}$ are shear stress and shear rate, respectively, and the constants K, n, τ_y and η_b are the consistency factor (consistency index), the shear-thinning index (flow index), the yield stress and the base oil viscosity. They are used to describe the viscosity of the grease or the shear stress as a function of shear rate. Although there is no model that accurately describes the full regime from extremely low to extremely high shear rate, the most widely used model is Herschel-Bulkley [6].

However, it is only suitable for a particular shear rate regime. For example, S.K. Yeong *et al*. [2] set the range of the shear rate from 10^{-3} s^{-1} to 10^{3} s^{-1}. Once the shear rate extends to higher regime, errors may occur. In this case, the Palacios equation [7], which considers the viscosity of the base oil, may be a better choice. The two equations described above both consider the yield stress of the grease which emerges under low shear.

When the start shear rate is high, Power law [8] and Sisko [9] equations are more suitable. The Power law equation has a smaller shear rate regime as compared with the Sisko equation, and it is used when the viscosity of the grease decreases dramatically with the increase of shear rate. The Sisko equation can describe the behavior of the viscosity to approach to the viscosity of the base oil under high shear rate. The Power law model is used in this study.

Table 2.1 Various rheological models for lubricating grease

Power law	$\tau = \mathrm{K} * \dot{\gamma}^n$
Sisko	$\tau = \mathrm{K} * \dot{\gamma}^n + \eta_b * \dot{\gamma}$
Palacios	$\tau = \tau_y + \mathrm{K} * \dot{\gamma}^n + \eta_b * \dot{\gamma}$
Herschel-Bulkley	$\tau = \tau_y + \mathrm{K} * \dot{\gamma}^n$

2.3 Rheometer

Both the yield stress and apparent viscosity can be obtained through testing the grease with rheometers. The most commonly used are rotational rheometers: concentric cylinder and cone-plate rheometers. For the cone-plate rheometer, the cone is sometimes replaced by a plate. In this thesis, the cone-plate rheometer is used. Figure 2.2 is the schematic diagram of the cone-plate rheometer.

In the test, the grease is put between the cone and the plate, and a torque T or rotation w is applied to the cone part while the plate is fixed to shear the grease. Angular velocity or torque data are acquired by sensors and translated into shear stress and shear rate data. When the cone angle is constant, the shear rate is independent of the radius. The advantages of using a cone-plate rheometer are that the shear rate is constant at a certain condition, and it provides better heat transfer and good temperature control. However, the grease may easily leak due to the influence of inertia under high rotational speed. This can cause data distortion.

This study used a Paar Physica MCR 301 rheometer, which controls both stress and shear. The rotating part was supported by air bearings. A cone-on-plate (2° cone angle, 25 mm cone diameter) and a gap size of 0.1 mm were used for this study. Ten greases with different composition and three corresponding base oils are chosen for this study. In this thesis, the test greases are identified by the type of thickener followed by the type of base oil, and the viscosity of base oil.

All samples are laboratory greases and consist of only base oil and thickener, without any additives. They were chosen to provide a range of grease thickener types, base oils types and viscosity. Their composition is given in Table 2.2. The tests were performed at least twice for each pre-shearing samples at 298 K and the results presented here are the average values. For simplicity, only the results of tests for the representative four greases are shown in this chapter.

Table 2.2 Test lubricants

Samples	Thickener type	Base oil properties (mm^2/s)	Penetration
Grease	12%wt lithium 12-hydroxystearate	Poly-alpha-olefin (PAO) viscosity 30	291
	12%wt lithium 12-hydroxystearate	Poly-alpha-olefin (PAO) viscosity 60	291
	12%wt lithium 12-hydroxystearate	Poly-alpha-olefin (PAO) viscosity 400	386
	20%wt lithium 12-hydroxystearate	Polyol ester (POE) viscosity 30	221
	20%wt lithium stearate	Polyol ester (POE) viscosity 30	220
	12%wt lithium stearate	Poly-alpha-olefin (PAO) viscosity 20	336
	12%wt lithium stearate	Poly-alpha-olefin (PAO) viscosity 400	339
	Di-urea	Polyol ester (POE) viscosity 30	280
	13%wt Di-urea	Poly-alpha-olefin (PAO) viscosity 30	280
	Polytetrafluoropolyethers	Perfluoropolyethers (PFPE) viscosity 30	280
Base oil		Poly-alpha-olefin (PAO) viscosity 60	
		Poly-alpha-olefin (PAO) viscosity 400	
		Polyol ester (POE) viscosity 30	

All viscosity values are shown for 313K

2.4 Experimental flow curve

2.4.1 Yield stress

In this thesis, the yield stress test is performed in oscillatory mode. The advantage of this mode is that the grease leakage and the crack formation between the cone and the plate can be avoided. The frequency is 10 Hz, and the range of the shear stress is from 10 Pa to 5000 Pa. Table 2.3 lists the results of the yield stress for the test greases.

The order of the yield stress from maximum to minimum is Urea.poe30, Liohst.poe30, Liohst.pao60 and Liohst.pao400. The yield stress and the penetration depth of the grease are all related to the consistency of grease. The results of the yield stress for the four greases are proportional to the penetration depth listed in Table 2.2, except that the penetration depth of Liohst.poe30 is lower than that of Urea.poe30.

Table 2.3 Values of the yield stress for the test greases

Urea.poe30	Liohst.poe30	Liohst.pao400	Liohst.pao60
2900 Pa	1003 Pa	73 Pa	182 Pa

2.4.2 Apparent viscosity

A shear rate range of 10^{-3} to 10^{3} s^{-1} was selected for measuring the apparent viscosity as a function of the shear rate. Figure 2.3 shows the results of apparent viscosity as a function of shear rate. As the figure shows, the apparent viscosity of all test greases declines with the increase of shear rate. The viscosity of the base oil is constant along this shear rate regime. As shown, 10^{2} s^{-1} is the split shear rate for the apparent viscosity in our test. Lower than this shear rate, the sequence of the relative apparent viscosity for test greases has no change. When the shear rate closes to 10^{2} s^{-1}, the relatively high apparent viscosity for Urea.poe30 and that of Liohst.poe30 have been gradually decreasing. When the shear rate is higher than 10^{2} s^{-1}, the sequence of the relative apparent viscosity for test greases has changed.

Figure 2.4 shows shear-rate-dependence of the apparent viscosities in the lower shear rate range from 10^{-3} to 10^{2} s^{-1}. Compared with the Table 2.6, the sequence of the relative apparent viscosity for test greases is different from that of their corresponding base oils. The apparent viscosity for POE30 is the lowest. However, their corresponding greases Urea.poe30 and Liohst.poe30 have high apparent viscosity. When the grease is under low shear, the main flow resistance is determined by the force required to break the thickener structure and to move the disordered broken fibers. Thus the apparent viscosity of the grease is high. The apparent viscosity in this case is determined by the thickener.

Figure 2.5 shows shear-rate-dependence of the apparent viscosities in the higher shear rate range from 10^{2} to 10^{3} s^{-1}. As it shows, the apparent viscosity of urea.poe30 and liohst.poe30 decreases faster than for liohst.pao60 and liohst.pao400, and all of them decrease and eventually approach that of its corresponding base oil. Moreover, the downward trends of them slow down after the shear rate 400 s^{-1}. The changes in the apparent viscosity within 1 Pa.s with the increasing of shear rate 500 s^{-1}. When the grease is under high shear, the thickener structure may be completely broken, and the broken fibers flow along the oil flow. Therefore the influence of the thickener on the apparent viscosity under high shear diminishes. The base oil determines the apparent viscosity of the grease under high shear.

Table 2.4 lists the consistency factors K and shear-thinning indexes n from the Power law equation under different shear rate range, respectively. As it shows, there are great differences in the value of K and n in different shear ranges. Especially K, two sequences of the relative K for test greases in two shear ranges are opposed to each other. The value of K is related with the apparent viscosity. The reason for this phenomenon is described as earlier: The apparent viscosity is determined by the thickener under low shear, whereas it is determined by the base oil under high shear. The value of n is related with the extent of changes in the apparent viscosity with the shear rate. Only the sequences of the relative n for Urea.poe30 and

Liohst.poe30 in two shear ranges change. From the results in Figure 2.3, their apparent viscosities decrease sharply under high shear, and it is consistent with the results of n.

Table 2.5 shows the consistency factors and shear-thinning indexes from the Power law equation, and the representative apparent viscosity at low and high shear rates for the four greases. Table 2.6 shows the apparent viscosity of the corresponding base oil for the four greases. By comparing the apparent viscosities of greases at a shear rate of 1000 s^{-1} in Table 2.5 and the apparent viscosities of the base oils in Table 2.6, the order of apparent viscosity from high to low is Liohst.pao400, Liohst.pao60, Liohst.poe30 and Urea.poe30, which is the same with the order of apparent viscosity of the corresponding base oil in Table 2.6. These results validate the fact that the viscosity of the grease is determined by the base oil at a high shear rate.

The consistency factor K and shear-thinning index n of Urea.poe32 are highest among all the four greases. This means that Urea.poe30 has the highest consistency and lowest ability to flow. At the low shear rate of 1 s^{-1}, the apparent viscosity of Urea.poe30 is the highest. At the high shear rate of 1000 s^{-1}, the apparent viscosity of Urea.poe30 rapidly decreases and is the closest value to the apparent viscosity of the base oil among the four greases. These mean that the mechanical stability of the thickener structure of Urea.poe30 is poor. Liohst.poe30 and Urea.poe30, which have the same base oil, show very different values of consistency factor and shear-thinning index. It can be inferred that the consistency and flow ability of grease are influenced greatly by the thickener type.

By comparing Liohst.pao60 and Liohst.pao400, it can be seen that the consistency factor K of Liohst.pao60 is much higher than that of Liohst.pao400, but the shear-thinning index of Liohst.pao60 is lower. These indicate that Liohst.pao60 is the grease with the higher consistency and flow ability. The penetration depth of Liohst.pao60 listed in Table 2.2 is much lower than Liohst.pao400. Therefore, the apparent viscosity of Liohst.pao60 is higher than that of Liohst.pao400, probably due to the better mechanical stability and the tight junction between the thickener and base oil of Liohst.pao60.

Table 2.4 Consistency factor, shear-thinning index from the Power law equation in different shear rate regime

Shear region	10^{-3} s^{-1} to 10^{2} s^{-1}		10^{2} s^{-1} to 10^{3} s^{-1}	
Samples	K ($Pa.s^{n}$)	n	K ($Pa.s^{n}$)	n
Urea.poe30	2056	0.017	2214	-0.87
Liohst.poe30	604	-0.03	60	0.29
Liohst.pao60	2302	0.013	203	0.083
Liohst.pao400	1113	0.066	10	0.66

Table 2.5 Consistency factor, shear-thinning index from the Power law equation and the apparent viscosity at different shear rates

Samples	K ($Pa.s^{n}$)	n	1 s^{-1} (Pa.s)	1000 s^{-1} (Pa.s)
Urea.poe30	4085	0.16	3280	0.09
Liohst.poe30	666	0.03	1029	0.27
Liohst.pao60	300	0.02	367	0.33
Liohst.pao400	130	0.07	101	1.03

Table 2.6 Apparent viscosity of the base oils

	PAO60	PAO400	POE30
Apparent viscosity (Pa.s)	0.11	0.88	0.06

2.5 Conclusions

The rheological properties of greases are very complex due to their semi-solid composition. In this chapter, yield stress and apparent viscosity are measured. The parameters used in the Power-law model are determined from fits to measurements on the cone-on-plate rheometer. Based on test results, these parameters can be used to describe the consistency and flow ability of the greases. Understanding the yield stress under low shear may help study the track pattern. Moreover, the apparent viscosity is very important for the lubricating conditions.

References

[1] Oikawa, E., Inami, N., Hokao, M., Yokouchi, A. and Sugimura, J., "Bearing torque characteristics of lithium soap greases with some synthetic base oils," Proc. IMechE, Pt. J., Journal of Engineering Tribology, 226, 6, 2012, 575-583.

[2] S.K. Yeong, P.E. Luckham, and Th.F. Tadros. Steady flow and viscoelastic properties of lubricating grease containing various thickener concentrations. Journal of colloid and interface science, 274: 285-293, 2004.

[3] A.E. Yoesif. Rheological properties of lubricating greases. Wear, 82: 13-25, 1982.

[4] L. Salomonsson, G. Stang and B. Zhmud. Oil/ thickener interactions and rheology of lubricating greases. STLE Tribology Transactions, 50: 302-309, 2007.

[5] G.M. Gow. The CEY to grease rheology. Transaction of Mechanical Engineering, The institution of Engineers, Australia, Special Issue Tribology, ME16(3): 202-205, 1991.

[6] W.H. Herschel and R. Bulkley. Proc. Am. Assoc. Test Mater., 26:621-633, 1926.

[7] J.M. Palacios, M.P. Palacios. Rheological properties of greases in EHD contacts. Tribology International, 17(3):167-171, 1984.

[8] M. A. Delgado, C. Valencia, M. C. Sánchez, J. M. Franco, and C. Gallegos. Influence of Soap Concentration and Oil Viscosity on the Rheology and Microstructure of Lubricating Greases. Ind. Eng. Chem. Res., 45 (6), 1902–1910, 2006.

[9] A.W.Sisko. The flow of lubricating greases. Industrial & Engineering Chemistry, 50(12):1789-1792,1958.

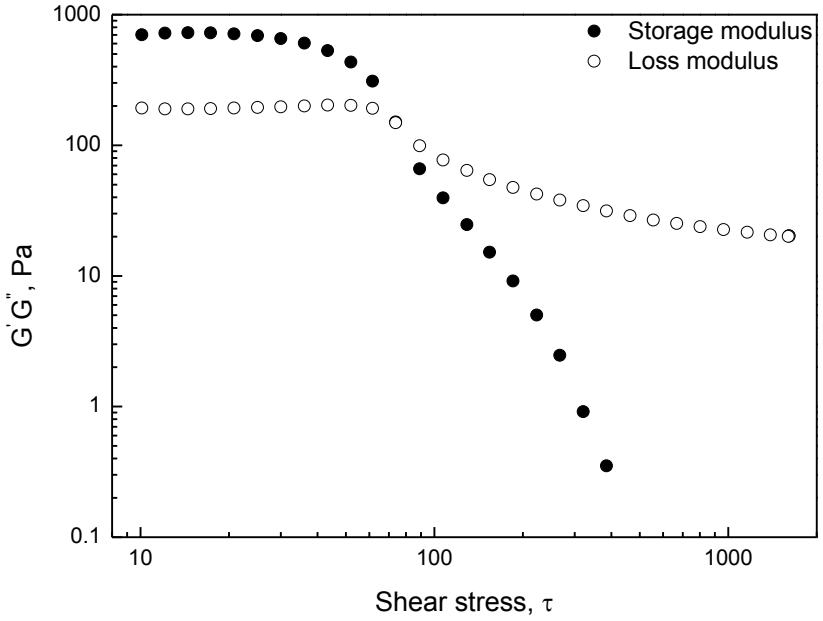

Figure 2.1 Evolution of the storage modulus and the loss modulus of Liohst.pao400 with shear stress at 298 K

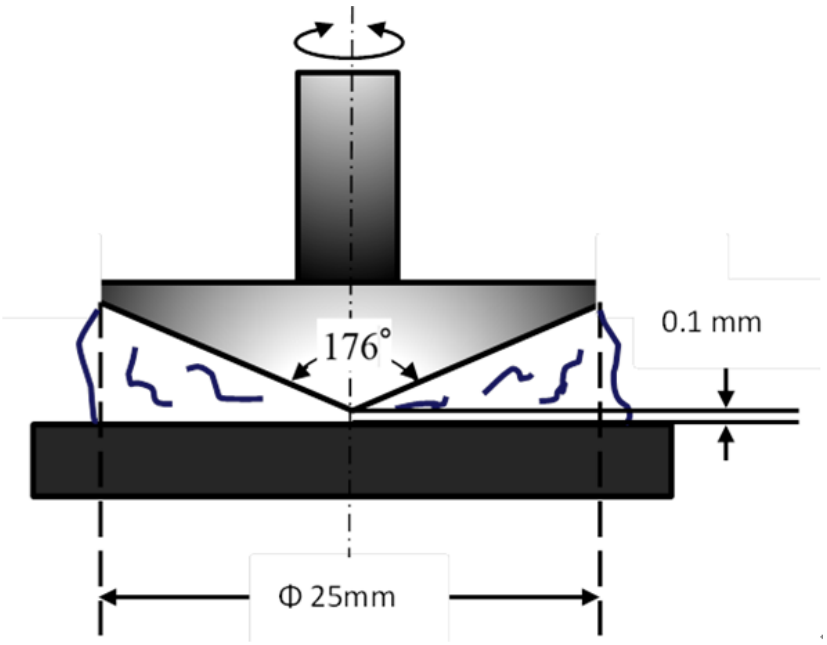

Figure 2.2 Schematic representation of cone-on-plate rheometer

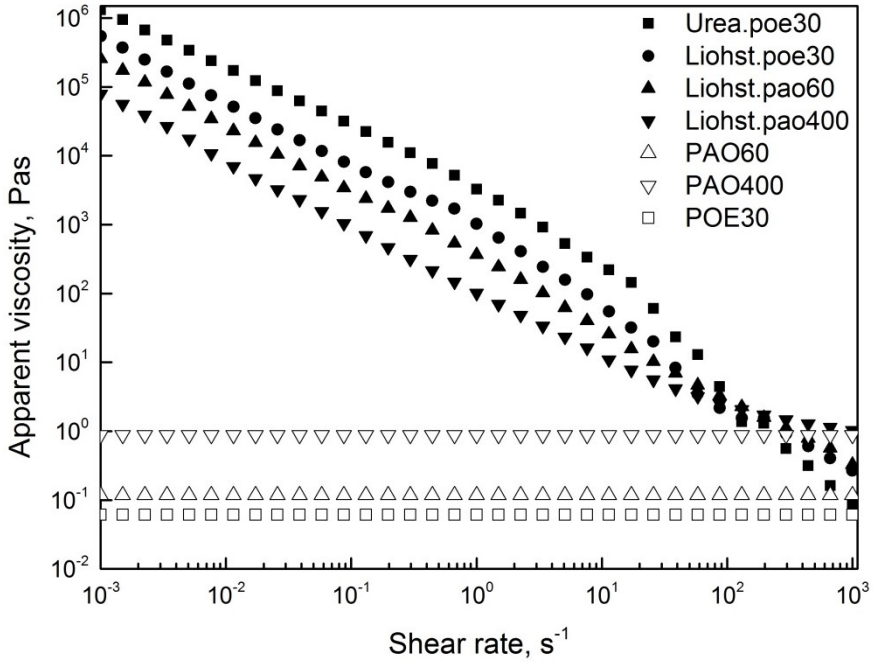

Figure 2.3 Shear-rate-dependence of the apparent viscosities at 298 K

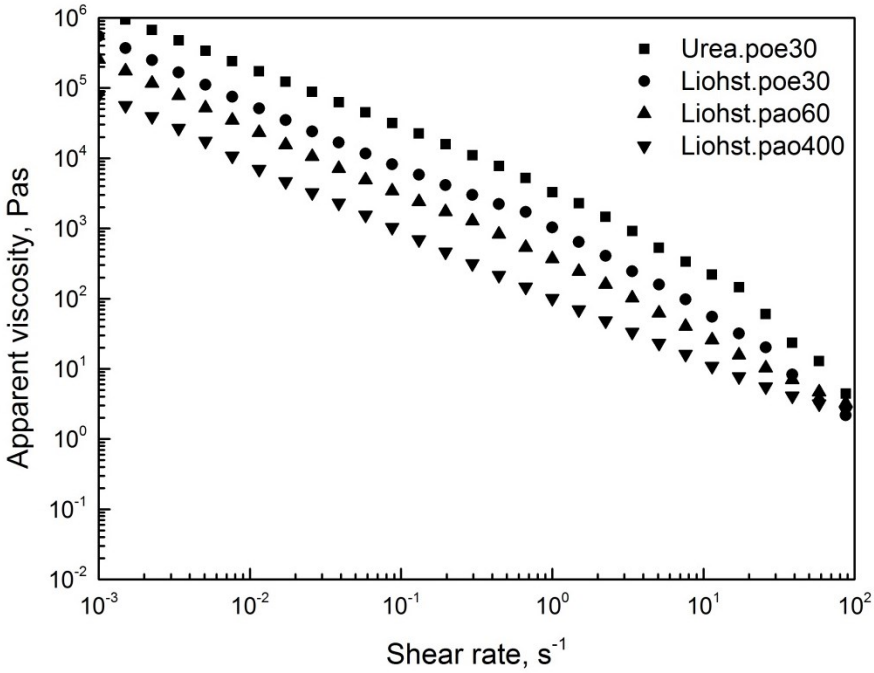

Figure 2.4 Shear-rate-dependence of the apparent viscosities in the lower shear rate range at 298 K

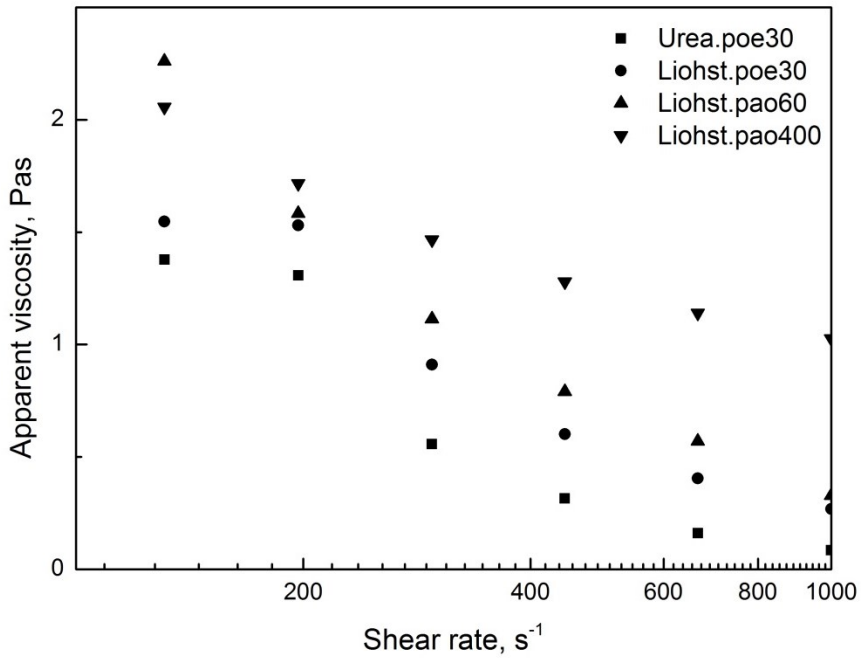

Figure 2.5 Shear-rate-dependence of the apparent viscosities in the higher shear rate range at 298 K

CHAPTER 3

Observation of the grease flow behavior

Abstract

A ball-on-disk test rig equipped with an optical microscope is used to observe grease flow and track patterns through dynamic observation and static observation of the remaining greases on the track on the disk specimens. The features of grease flow and contact tracks for different greases are observed under different entrainment speed, test duration and slide-to-roll ratio. The features of track pattern are different for different grease types and different operating conditions. The track pattern after rolling/sliding tests preserves the most features of grease flow, and eight characteristic parameters are defined to characterize the patterns. The variation of the pattern parameters represents the grease flow behaviors, regardless of the type of grease. It is found that lithium-12-hydroxy stearate grease shows clear track patterns, whereas di-urea grease shows obscure track pattern and heavy thickener deposition in the center of the track. The thickener type and base oil viscosity are more important than base oil among the factors that affect the area of grease fingers at the sides of the tracks. The features of the track patterns are not only related to the constituents of grease, but the changes in rheological properties also produce changes in the patterns. For example, the grease with smaller yield stress and higher viscosity tends to have larger finger area. The grease with better flow ability at low shear rates tends to have a clearer finger pattern. It is proposed that the formation and maintenance of grease fingers in the track pattern are dependent on the state of lubrication.

3.1 Introduction

The flow behavior is probably the dominant factor that influences the performance of grease-lubricated machine elements. However, for a long time researchers have focused on the regime of contact conjunction, rarely studying the trajectory features of flow in grease lubrication. The reason for this is that there appear to be no rules for it, and thus it is a complicated and abstract issue.

Although the number of research reports on flow behavior is still relatively small, many articles have studied it. It is generally held that the flow trajectory around the contact conjunction in a wide area is similar to a butterfly spreading its wings in oil lubrication [1]. A similar flow trajectory is also found in grease lubrication [2].

The difference is that the wake pattern can be conserved relatively complete for long periods in grease lubrication. The track pattern, like tree branches spreading out from the center of track, contains the so called ‘fingers’. Larrson *et al.* [3] report that the appearance of

these fingers changes with grease type and rheology. They suggest that these changes come from a reduction in elastic and viscous properties through loss of thickener structure.

Moreover, some people [3-4] believe that that finger distribution provides a transport mechanism drawing bulk grease close to the contact. These fingers can keep their shape unchanged for weeks. Different testing conditions like the increase of entrainment speed can make the number of fingers increase obviously [5]. These pattern distributions may help to understand the rheological properties of the grease under low shear in an EHL contact.

The direct reason for track pattern formation is the cavitation in the outlet area of the contact conjunction. When the lubricant in the inlet flows and migrates to the contact zone, one part of the lubricant passes through the Hertzian regime, while the other part escapes around the Hertzian regime and ruptures away with the cavitation finger-like patterns. Cavitation may accelerate the loss of lubricant from the contact. With some reciprocating motions, both fretting [6] and film formation [7,8] will be affected by cavitation with the change of frequency and amplitude.

These results illustrated the application of flow behavior on different issues. There is much useful information that can be obtained from the observation of the flow behavior. What is needed now is a systematic observation of the process, which can also provide the foundations of subsequent works. Hopefully, the work in this chapter can help build a system that will lead to the understanding of the mechanisms in grease lubrication from the apparent phenomena.

3.2 Experimental procedure

Table 3.1 Test specimens

Test specimens	
Optical disk	Made of BK7 glass, 80 mm diameter
Steel ball	Made of JIS SUJ2, 15 mm diameter

This chapter mainly contains of two groups of experiments: A series of video observation experiments chiefly on the issue of flow behavior around the lubricated contact conjunction and a series of static observation experiments of the grease distribution on the disk after the experiment. Figure 3.1 is the schematic representation of the ball-on-disk setup used in this study.

Table 3.1 shows information about the test specimens. The disk is made of BK7 glass and with a diameter of 80 mm. In order to obtain a clear picture, the side of the disk in contact with the ball has chromium and silica layers. The ball is made of JIS SUJ2 steel and has a diameter of 15 mm. The disk and the ball are supported by two motors, respectively.

The test materials are listed in Table 2.1. Prior to each test, all specimens are cleaned with acetone in an ultrasonic bath and air dried. Fresh grease is uniformly smeared on the disk to a thickness of 0.1 to 0.2 mm, and no additional lubricant is supplied during the test. The test conditions are summarized in Table 3.2. This chapter focuses on the observation and comparison of the morphological variation of the grease flow around the contact conjunction under different entrainment speeds, test duration and slide to roll ratios.

The entrainment speed varies from 1 to 500 mm/s. The test duration varies from 0 to 40 minutes. The slide to roll ratio varies from -1 to 1. The definitions of slide to roll ratio and entrainment speed are listed on the bottom of Table 3.2. U_{disk} and U_{ball} are the surface velocities of the disk and the ball, respectively. In the interest of brevity, the "slide to roll ratio" will be simply referred to as "SRR" throughout the rest of this thesis.

In practical rolling element bearings, the elements and races experiences various kinds of slip including general gross slip due to speed difference, Heathcoat slip, and other partial slip due to spin. It is assumed that the change of temperature is very small, thus the influence of temperature is ignored. However, the temperature is an important factor in practical situations. The tests are conducted from low to high entrainment speed, short to long test duration and negative to positive SRR. The load is constant as 10 N.

Video observation experiments are conducted using a white light source. A high speed camera is connected to the microscope and records the behavior of grease flow in the vicinity of an EHL contact. The data are recorded as videos. The color pictures used in this chapter are cut from videos.

Static observation experiments are conducted using a green light source. A monochrome CCD camera is connected to the microscope and records the distribution of the grease on the disk after the experiment. The data are recorded as monochrome pictures. Both the ball and the disk display a track pattern. However, only the track pattern on the disk surface can be obtained clearly using the current devices.

These monochrome pictures are taken at different positions of the EHL contact: upstream, inlet, center, outlet and downstream. The upstream and downstream images are taken at 4.5 times the Hertzian contact diameter upstream and downstream from the contact center, respectively. The white arrows in all images used in this chapter show the direction of motion of the specimen surfaces unless otherwise specified.

Table 3.2 Test conditions

Test conditions	
Entrainment speed	1 - 500 mm/s
Temperature	298 K
Normal load	10 N
Maximum Hertzian pressure	0.87 GPa
Hertzian contact radius	98.7 μm
Track radius	37.5 mm
Slide to roll ratio	-1 to 1
Test duration	0 to 40 mins

Slide to roll ratio = $2(U_{disk} - U_{ball})/(U_{disk} + U_{ball})$

Entrainment speed = $(U_{disk} + U_{ball})/2$

3.3 Features of grease pattern

3.3.1 Dynamic observation

Figure 3.2 and Figure 3.3 show the forming process of the wake in oil lubrication and grease lubrication, respectively. The morphological characteristics of the wake in oil lubrication and grease lubrication have both similarities and differences.

The similarities of the wake between oil lubrication and grease lubrication are: after the experiment started, the wake pattern can be observed in all other test samples, as shown in Figure 3.2 by the pictures of PAO20 and PAO60 starting at 10 ms. A common characteristic of the fan shape wake in oil lubrication and grease lubrication is that there are two triangle zones with finger patterns distributed symmetrically to the center of track. These two parts are called fingers. In Figure 3.2, the part of the fingers near the contact conjunction is arranged closely, but other parts of the fingers far away from the contact conjunction look loose.

By contrast, the density of the finger arrangement during grease lubrication seems uniform as shown in Figure 3.3. Using the direction along with the center of the track as a baseline, the angle between the outer edge of the finger zone and the baseline is around 35°. Moreover, there are two side bands which lie between the finger zone and the center of the track with a darker color. These two darker separation barriers are called side ridges.

The differences between the wakes which appear during oil lubrication and grease lubrication are: as shown in Figure 3.2, PAO20 does not form a finger pattern and the outlet

cavity always remains closed. But as the viscosity changes to a higher value, the outlet cavities of PAO60 and PAO400 open faster and the angle of the wakes becomes larger. These suggest that viscosity is an important factor that can influence the morphological characteristics of the wake in oil lubrication.

The criteria of judging whether the cavity is totally open are in terms of meeting the 35° wake angle. However, these phenomena have not been clearly observed in grease lubrication as shown in Figure 3.3. The cavities of all greases totally open rapidly after the experiment started.

Another difference is the connection of the finger to the side ridge. The wake for PAO400 in Figure 3.2 clearly shows that the finger is not directly connected to the side ridge. The finger zones are more like a whole rather than separated by individual fingers, and the fingers emerge at the middle of the finger zone. As opposed to this, the fingers directly connect to the side ridge in grease lubrication as shown in Figure 3.3. The wake of the grease is much clearer than that of oil visually.

The major difference between oil lubrication and grease lubrication is that the wake for the oil can only be observed while the test is running. This is because it will almost disappear simultaneously with the stopping of the test. Nevertheless, the wake pattern can be conserved to a great extent for long periods in grease lubrication.

The above description gives a detailed comparison of the similarities and differences between the oil wake and the grease wake. The reasons are diverse: the cavity of the contact conjunction is triggered by the negative pressure in the outlet area both in oil lubrication and grease lubrication. With many accumulated gases, the cavity changes from the initial closed form into an open form.

The differences of pressure, viscosity etc. between the inside of the cavity and the surrounding lubricant promote the instability of the interface [9]. This leads to the formation of the complicated wake. To simplify, the principles of wake formation for both are the same. Since the rheological properties of the oil and grease are different, the wake for the oil and grease are quite different.

The difference between the grease and the oil is that the former has more complex rheological properties. The grease possesses both the viscous properties of a fluid and the elastic properties of a solid. The rheological properties of a grease vary with the change of entrainment speed, test duration, SRR etc. In conditions of non-extreme temperature or pressure, it can be concluded that the rheological properties of the oil, which are represented by viscosity, are evenly distributed around the contact conjunction.

However, for a grease the consistency drops rapidly around the contact due to the shear action, and this promotes the shredded thickener fibers to be pushed along with the flow. The

properties of the grease, such as viscosity, the concentration of base oil and thickener around the contact conjunction, are not evenly distributed. In other words, the difference of viscosity between the cavity and outer grease is not a constant value as for oil lubrication, but changes along with the boundaries. Therefore, their wakes will show different peculiarities.

Figure 3.4 lists some wake patterns for test greases containing a different thickener, base oil and viscosity of the base oil. It can be seen that the wake patterns in the first row are very different from those the second row. The colors in the center of track for the second row are much darker than those of first row, and with more obscure fingers. In addition to this, the size and orientation of the fingers are not regular. It is even hard to identify a complete finger for Liohst.pao400. By contrast, the wake patterns in the first row have clear characteristics, with light color in center of tracks, distinct side ridges and clear, well organized fingers.

In addition, judging from the color of the contact conjunction, the film thickness for the first row is much lower than that of the second row. This is most likely due to the fact that the film thickness has a direct impact on the appearance of the wake. A possible explanation is as follows: when the film thickness in the contact conjunction is high, the amount of lubricant that comes out from it will increase. A significant amount of lubricant will be pushed to both sides of the track. The boundary between the cavity and outer grease is disturbed by the inner lubricant flow. Thus the appearance of the wake in the second row becomes very different. It is also obvious that the wake patterns in the first row have been less affected by the inner flow, while their film thicknesses are low.

Among the four greases shown in the second row, the film thickness for Liohst.pao400 and Urea.poe30 are the highest. Furthermore, the clarity and the uniformity of their fingers are inferior to those of List.pao400 and PTFE.PFPE. This is consistent with the conjecture as presented above. The high film thickness is not favorable for the formation of fingers. Moreover, the colors in the center of track are darker for Liohst.pao400 and Urea.poe30. This may imply that the deposition in the center of the track also affected the appearance of the fingers.

The advantage of the video observation experiment is that in-situ information can be obtained, and distractions can be eliminated as much as possible, which make the test results more credible. Nonetheless, the pictures cut from videos are unable to give adequate detailed information. For instance, the wakes for the four greases in the first row are not much different from each other. However, the video image may not tell the whole story as whether they are really the same.

In order to investigate the association between the lubricating condition and the wake pattern, further details of the wake pattern need to be explored. The characteristic that the

wake pattern can be conserved relatively complete for long periods of time in grease lubrication provides the basis for obtaining more details.

Although the track pattern that is observed while the test is stopped may not represent the whole process, the morphological change in the wake is small under stable test conditions according to the observation. Hence, the static observation experiments play an important role on the issue of grease flow behavior.

3.3.2 Static observation

Figure 3.5 shows the grease distribution around an EHL contact. With the repeated rolling of the steel ball, the wake forms a relatively stable circle pattern on the disk. The whole circle of grease distribution on the disk is called the track. The track pattern is representative of both the properties of the grease itself and the relative movement between the ball and the disk. In addition to rotation; spin, vibration and squeeze also often occur in real machine elements. To simplify, only rotation is considered in this study.

In static observation experiments we can get monochrome pictures as the one shown in the right top. The monochrome picture is able to emphasize the details of the finger which could not be observed in the video observation experiments. As can be seen from the picture, the finger zone actually looks like a tree branch spread out into the center of track. The color of the fingers is dark. These fingers are separated from each other by black-and-white interference fringes. These fringes are composed of air and grease. Even so, it is generally considered these fringes only consist of air [10]. Greater difficulties will arise when this factor is considered into the research. Thus, the fringe area is seen as air at this stage.

The part of the fingers that is far away from the center of track is regarded as the tree trunk. It is possible that these parts are branched from the trunks outside of the picture frame. The real trunk parts should be connected with further reservoirs. However, it should be noted that the grease remains unchanged and attached to the surface when the shear motion is insufficient.

Whether the grease which lies in the neighboring region of the contact conjunction really participates in lubrication is still a controversial topic. Some believe that the function of the grease which lies far from the contact is merely to seal and to protect when no external force is exerted on it. Hence, our discussion primarily focuses on the track features within the scope of the monochrome pictures.

In the bottom right corner of Figure 3.5 is the schematic representation of the side ridge and the center of the track. As can be seen in Figure 3.4, the color of the side ridge for most greases is darker than those of the center of the track and the finger zone. Thus the amount of grease in the side ridge is larger than the adjacent parts, the raised shape makes them looks like a ridge. These two side ridges are often subjected to shear and squeezing, and the

bleeding oil will flow into the center of the track. Furthermore, the shredded thickener fibers will be easily deposited in the center of the track. Some research shows that most of the deposition in the center of the track after the test is represented by thickeners [11].

Figure 3.6 shows the grease patterns taken at five different positions after the test stops, in static observation experiments. Sequencing from left to right are: upstream, inlet, center, outlet and downstream. The side of the inlet and the outlet close to the contact conjunction has an obvious meniscus. The angles between the finger and the center line are almost the same for all positions.

Although upstream and downstream are not identical; the position of the finger split, the number of fingers near the center of the track etc. have no significant differences. Therefore, it is assumed that the whole circle of the track is distributed evenly except the area from inlet to outlet. In this study, the upstream and the downstream are adopted to represent the distribution state of the remaining parts.

As shown in Figure 3.4, the morphological difference between the wakes of List.pao20 and that of Liohst.poe30 is unapparent, whereas the details of their track patterns are quite different in static observation experiments as shown in Figure 3.7. This supports the suggestion that the static observation experiments can provide further detailed information. In general, the features of the track pattern can be summarized in the following aspects.

Firstly, the degree of finger contrast and visual clarity are different from each other. For instance, all the Liohst base greases reveal a higher degree of contrast and visual clarity. This is expressed by the fact that the intervals between fingers are distinct. But the holistic clarity of the fingers is not only determined by the thickener type. For example, for two greases with a different base oil like Urea.pao30 and Urea.poe30, and two greases with different viscosity of the base oil like List.pao20 and List.400, their degree of contrast and visual clarity show great variations from each other. But usually, Lithium-12-hydroxy stearate grease shows clear track patterns, whereas di-urea grease shows obscure track pattern and heavy thickener deposition in the center of the track. All these suggest that it is actually the result of a comprehensive function of the thickener, the base oil and the viscosity of the base oil.

One characteristic of the side ridges is that there are dense and fine fingers which point to the center of track. It is hard to identify side ridges for Liohst.pao400, List.pao400 and Urea.pao30. This suggests that the junction between the finger zone and the center of the track have barely raised accumulation. For all these three greases which are covered with heavy thickener accumulations in the center of track, the thickness of the accumulations is considerably higher than that of the general cases. Naturally, this is favorable for the film formation in the EHL contact.

Nevertheless, its effect on the degree of ridge contrast and visual clarity is not simply an inverse relationship. For instance, there is neither an obvious side ridge, nor thickener deposition in the center of the track for Urea.poe30. As can be seen in these pictures, the deposition of thickeners is more or less found in other test greases. This is consistent with the observed phenomenon that the thickeners pass through the contact conjunction in the video observation experiments.

The features of the fingers are: the trunks of the finger stretch toward the center of track, the branches from the trunk appear near the center, and they further split into finer fingers. These fingers are distributed symmetrically on the two sides of the center of track. The interval between finger trunks can be deemed as uniform in distribution. The finger split can be observed for almost all test greases, this phenomenon is universal. The number of finger split joints can reflect the intensity of the splitting.

The mean single finger area in the trunk part is usually larger than that of the lower branch part. However, the number of branches is significantly larger than that of the trunk part. In order to know whether the influences of the grease which is located in different positions on the contact conjunction are consistent, the finger pattern is divided into two parts. One part is close to the center of track. Another part is far from it. The first split position for the trunk finger is seen as the separation line in our study.

Figure 3.8 shows the inlet pattern for the test greases. The contact conjunction is on the right of picture. Except for Urea.poe30, the other greases show an obvious meniscus. There is a second side band on the upper side of the center of the track that connects with the grease which lies around the center of the contact conjunction. Although the distance between the top of the meniscus and the contact has some differences with the inlet distance, which is defined in dynamic state [2], it still can offer some information about the state of the inlet area. These observations will provide reference for the dynamic observation of the inlet area in the next chapter.

3.3.3 Characteristic parameters

To explore the changing trend of the track pattern with different test conditions, and also to bring convenience for follow-up work, in accordance with the detailed description of the morphology of the track patterns mentioned above, eight characteristic parameters are selected as typical representatives. Figure 3.9 gives a schematic representation of their definitions.

As shown in Figure 3.9 (a), the wavelength is used to represent the average interval between finger trunks. It indicates the distribution density of the finger trunks. The measurement is conducted perpendicularly to the average tilt angle and generally at a position

4 to 5 times the Hertzian radius apart from the center line of track. The intention is to minimize the influence caused by speed on the direction of the finger.

Based on the research results of instability patterns [12], the fingers are evenly distributed and point to the diverging angle of the contact concave when the two contact surfaces are not in relative motion but only adhesion as shown in Figure 3.10. Under the influence of speed in EHL, the direction of the fingers shifts with the flow.

As shown in Figure 3.9 (b), the number of finger split joints, which represent the finger area near the center of the track and the finger area far from the center of the track are measured as follows: the first step is to get the sum value of these three for both sides of the center of the track, and then to calculate their average values between these three parameters for upstream and downstream. The real width of the monochrome picture is divided by the perimeter of the center of the track to get a proportional value. As previously mentioned, it is assumed that the distribution of the track is even. Thus the average values of these three parameters multiplied by the proportional value respectively can yield the corresponding representative value for the whole track. The measurements for these three parameters adopted in this chapter are these representative values.

The degree of finger contrast and visual clarity, the degree of ridge contrast and visual clarity and the degree of thickener deposition are determined with comprehensive consideration of both upstream and downstream for the same test greases. The bleeding oil will flow back to the area around the contact conjunction after the test stops, and this will determine the meniscus around it, like the inlet meniscus distance as shown in Figure 3.9 (c), to change with time. The inlet meniscus distance used in this chapter is taken just after the test.

Figure 3.11 shows the process of image treatment for the finger area near the center of the track and that far from the center of the track. As mentioned in previous contents, the fringes between fingers are composed by air and grease. In fact, the black part of the fringes which connect with the fingers is also grease like the finger. This makes it harder to select the finger as the object directly. In order to successfully extract the finger pattern from the picture and ignore these fringes, it is necessary to extract the edge of the monochrome image. The Sobel operator [13] is used for edge extraction.

Figure 3.11 (a) and Figure 3.11 (b) show the initial image and the image after Sobel edge extraction and object selection, respectively. After being processed, it can be seen that the finger has been completely extracted to the greatest extent. The finger areas near the center of the track and that far from the center of the track are separated so that these two parameters can be obtained. Table 3.3 lists the characteristic parameters of the grease track pattern and their corresponding simplified code used in this study. The effects of entrainment speed, test

duration and SRR on the features of morphology of track pattern are discussed further in this chapter.

Table 3.3 The characteristic parameters of grease track pattern used in this chapter

Parameters	Simplified code
Wavelength	λ
The number of finger split joints	S-J
The degree of finger contrast and visual clarity	D-F
The degree of ridge contrast and visual clarity	D-R
The degree of thickener deposition	D-T
Finger area-near	A-N
Finger area-far	A-F
Inlet meniscus distance	D

3.4 Flow behavior under different testing conditions

3.4.1 The effects of entrainment speed

Prior to each test, the rotating speed of the ball and the disk are set to appropriate values by the program, respectively. Because the set rotating speeds usually are not immediately reachable at high speed, the film thickness in the first few revolutions of the disk will continue to decline until it reaches a steady thickness at constant speed. The film thickness generally remained stable after 3 or 4 revolutions from the experimental results. Therefore, in order to observe the grease flow behavior in a steady state, the pictures used in this speed section are all after at least 10 revolutions of the disk. Figure 3.12 shows the speed evolution of wake patterns of a group of base oils with different viscosity in pure rolling state. Figure 3.13 shows a group of greases with different base oil viscosity.

In addition to the similarities and differences between the oil wake and the grease wake as described in the section of dynamic observation, the speed factor also brings some new changes. Firstly, the same conclusion is reached that the clarity of the grease wake is generally higher than that of the oil wake. This implies that the clarity of the wake is not influenced by the speed, and is more related to the properties of the lubricant. Based on observation, the length of the outlet cavity in oil lubrication is short and enclosed for a prolonged period at low speeds like 1 mm/s. On the contrary, the outlet cavity in grease lubrication will usually open totally and rapidly at any testing speed.

As the entrainment speed increases, the morphology of the grease wake becomes more complicated, and this is exhibited as a more dense and divided finger pattern. Moreover, the

wake of liohst.pao400 is always more complex than that of liohst.pao60 at the same speed. It is concluded that the high viscosity and fast speed are favorable to form a more complex finger pattern. Although the pictures of the oil wake as shown in Figure 3.12 are not clearly visible, the same phenomena in grease lubrication can also be observed through video observation.

As shown in Figure 3.12 and Figure 3.13, the starvation in grease lubrication at high speed is much more serious than that in oil lubrication, and it is judged by the inlet distance [2]. This is consistent with the properties of oils and greases, i.e., the favorable mobility of the oil allows the adjacent lubricant to return back to the inlet area easily, which is the exact opposite situation in grease lubrication.

Liohst.pao60 and Liohst.pao400 are completely in the starved state at the speed of 500 mm/s. Their center of the track connects the inlet and outlet, which means there is no lubricant available in the inlet area. Whether in oil lubrication or grease lubrication, the wake with the finger pattern is barely seen.

To facilitate the qualitative and quantitative observation, the following content in this chapter is primarily based on the observation of monochrome pictures. Figure 3.14 lists the speed evolution of the upstream pattern. As shown, the fact that the complexity of the finger pattern increases with speed and the random distribution of the grease on the disk at high speeds are in accordance with the previous video observation.

Upstream patterns with different speeds are separated by dotted lines. Being listed in the next row to the original monochrome pictures are the pictures which are processed by the Sobel edge extraction [13]. The shape of the finger pattern can be seen in the images which have been processed. Besides, the black part stands for the grease.

Table 3.4 summarizes the degree of finger contrast and visual clarity, the degree of ridge contrast and visual clarity and the degree of thickener deposition for four test greases as shown in Figure 3.14. The values 1, 2, 3, and 4 represent their extent are from low to high. As shown in Figure 3.14, the clarity of the finger pattern for Liohst.pao60 is always the best among other test greases, whereas the finger zone of Urea.poe30 is always been very blurred.

The same grease under different speeds may also be completely different. For instance, the finger zone of Liohst.poe30 does not form a typical branch finger pattern at the low speed of 1.9 mm/s. However, its clarity instead becomes less varied as compared with that of Liohst.pao60 as the speed increases. The degree of ridge contrast and visual clarity is similar to that of the finger part, only the Liohst.pao400 and Urea.poe30 are in the reversed order. The main reason is that the deposition of Liohst.pao400 in the center of the track is more pronounced.

Table 3.4 Variation of the degree of finger contrast and visual clarity, the degree of ridge contrast and visual clarity and the degree of thickener deposition at 1.9 mm/s, 101.6 mm/s, 500 mm/s entrainment speed as shown in Figure 3.14

	Liohst.pao60	Liohst.poe30	Liohst.pao400	Urea.poe30
D-F	4	3	2	1
D-R	4	3	1	2
D-T	1	2	4	3

Correspondence between D-F, D-R, D-T and the represented values

Low ⟶ High			
1	2	3	4

The deposition in the center of the track is a common occurrence for Urea.poe30 and Liohst.pao400. This kind of deposition is a physical adsorption in general cases, and therefore it is stripped easily under external force. As it can be seen from Figure 3.14, the amount of their deposition in the center of the track is indeed reduced as the shear rate increases (The increase of entrainment speed equals to the increase in the shear rate when SRR is not zero). Although the deposition of thickeners may cause over-high friction coefficients, overheating, noise etc in real machine elements, it is conducive to avoiding the direct contact between the ball and the disk.

Figure 3.15 and Figure 3.16 show the variation of wavelength and finger area far from the center of the track with entrainment speed, respectively. The wavelength values for all test greases decrease with the increase of entrainment speed. This indicates that the number of trunks has increased. This increasing trend is more noticeable when the entrainment speed is lower than 10 mm/s, and then is gradually decreased.

The number of trunks even decreases when the entrainment speed is higher than 100 mm/s. The distribution trends of the wavelength for all test greases are relatively concentrated in the speed range between 10 mm/s and 100 mm/s. No significant difference occurs among various test greases. It suggests that the wavelength is largely determined by the entrainment speed.

Figure 3.16 shows the variation of the finger area far from the center of the track for all test greases with entrainment speed. The far-finger area first increases with increasing entrainment speed, then becomes stable. The data points for some greases show a sharp decline at high speed. The value of wavelength can only reflect the number of trunks, and combines the far-finger area that can get the information about the width of trunks.

In the speed range between 10 mm/s and 100 mm/s, the far-finger areas for test greases are different from each other but their wavelengths are similar. This implies that the growth capability for test greases is different under the same speed. For instance as shown in Figure

3.14, the trunk width for Liohst.poe30 shows an apparent shift from low speed to high speed. It also appears in Figure 3.16 that the far-finger area for Liohst.poe30 increases sharply after 5 mm/s, and exceeds that of Urea.poe30 when previously lower than it within 5 mm/s.

Moreover, the finger pattern for some greases have not been completely destroyed at high speeds of 500 mm/s as shown in Figure 3.14. For example, the upper part of the finger pattern for Liohst.poe30 is completely maintained. It is worth noting that according to the pictures processed by the Sobel edge extraction, there is always some grease that remains in places far from the center of the track. However, the finger-like distribution pattern near the center of the track is almost destroyed. This is the reason why the sharp decline of the far-finger area data for some greases at high speed occurs as shown in Figure 3.16.

The variation of the number of split joints and the finger area near the center of the track with entrainment speed are shown in Figure 3.17 and Figure 3.18, respectively. These are able to provide more information about the finger pattern near the center of the track. The distribution of the finger split joints are complicated, and the data for four test greases gradually show a difference among each other after 4 mm/s as shown in Figure 3.17. Although the data points are scattered, their trend for all greases increases first and then decreases. The increase of the finger split joints equals a higher complexity for the branch part, i.e., the near-finger area.

Nevertheless, the increase of branch does not mean that there will be more grease distributed in the area near the center of track. For example, the number of finger split joints for Urea.poe30 is much more than those of other greases, but it has the lowest near-finger area. This is in line with the fine and intricate finger pattern for Urea.poe30 as observed in Figure 3.14.

With the increasing of entrainment speed, the finger area near the center of the track continuously enlarges first and then reduces. Similarly, the decrease of the near-finger area at high speeds is also because of the affection and damages of the finger grease distribution as observed at high speeds. Unlike the far-finger area, the near-finger area will be totally destroyed when the speed is higher than a certain value.

Figure 3.19 shows the variation of the inlet meniscus distance with entrainment speed. The length of the inlet meniscus distance is proportional to the amount of grease that stays at the inlet area after the test stops. Figure 3.20 shows the concrete data measured from these pictures. Except for Urea.poe30, the other three greases all show the typical meniscus shape. The inlet meniscus distance for all test greases decreases gradually with the increase of the entrainment speed. After the test starts, the amount of grease which stays at the inlet area is easily consumed without additional amounts, thus making the D decrease. This diminution is very obvious before 10 mm/s. However, their variations do not change much after that.

3.4.2 The effects of test duration

Figure 3.21 shows the time evolution of the upstream pattern at the entrainment speed of 47.1 mm/s in pure rolling state. Figure 3.22 shows these patterns at a SRR of 0.6. As shown in Figure 3.21, there are some changes for the finger part of List.pao400 and the track pattern of Liohst.pao60 within 40 minutes under pure rolling state. In addition, no significant changes are found for the other two greases in many respects such as wavelength, the finger and side ridge contrast and visual clarity, the degree of thickener deposition. However the situation changes when the SRR is not zero.

As shown in Figure 3.22, above all, the thickener deposition for the two greases significantly reduces with the increase of test duration. Furthermore, some scratches on the disk are observed both for a test duration of 5 minutes and 10 minutes, and the darkest part is the scratch, which is distinctly different from the track pattern in the pictures. In the 5 minutes test, the number of disk revolutions is around 60, and it is 120 for 10 minutes. So it seems that the disk is easy scratched even the entrainment speed is quite low under slide-roll conditions. According to the video test observations, only a few revolutions are enough to determine the scratch to occur at high speeds. This makes the observation at high speeds very difficult. Thereby, here we only discuss the evolution of the track pattern at the speed of 47.1 mm/s.

The features of the finger pattern vary from each other under different test durations. Figure 3.23 and Figure 3.24 show the variation of the number of finger split joints and near-finger area with test duration, respectively. As shown in these two pictures, the data points at SRR 0.6 are on the left side of a dotted red line, and on the right side of it are the data points at SRR 0. The number of finger spilt joints at SRR 0 is higher than that of SRR 0.6, and the near-finger area at SRR 0 is also larger than that of SRR 0.6.

However, the extent of changes in the number of finger split joints and near-finger area at SRR 0.6 is more severe than those of SRR 0. Even the test duration on the right side is much longer than that on left side. This means that the longer test duration is not the main reason for the variation of the track pattern when other testing conditions change at the same time.

The main difference between SRR 0 and SRR 0.6 is the shear rate. The shear rate is much higher under a slide-roll condition than that under pure rolling condition. As a result, except for the shear-thinning phenomenon, the thickener deposition at the center of the track will gradually flake off because of the lengthy shear action. This is consistent with the gradual change in the thickener deposition for liohst.pao400 as shown in Figure 3.22.

As shown in Figure 3.24, the finger area near the center of the track for test greases decreases over time at SRR 0.6. We are unable to explain exactly why this happened based on current data, but it is very likely related to the continued decline of the film thickness which is due to shear-thinning. The issue of grease lubrication condition will be discussed in the next

chapter. Figure 3.25 shows the variation of the finger area far from the center of the track with test duration. It can be seen that the data points for these different SRRs are scattered without any certain pattern.

Generally speaking, except for the fact that the near-finger area and the thickener deposition continues to drop over time under the slide-roll condition, the extension of the test duration has no steady and consistent effects on morphology parameters.

3.4.3 The effects of slide to roll ratio

Figure 3.26 shows the variation of the upstream pattern with SRRs at an entrainment speed of 47.1 mm/s. One of the most obvious changes is the finger average tilt. This finger average tilt is expressed by the deflection angle as shown in the picture. It is the angle between the finger average tilt line and the center line. The deflection angle decreases gradually when the SRR changes from negative 1 to positive 1 for all test greases. Figure 3.27 shows the deflection angle data which is measured from these pictures. Except at SRR 0.5, the difference between List.pao20 and Liohst.pao60 is not obvious.

As mentioned previously, a similar phenomenon does not occur either in video observation, series speed-change test or series time-change test. Therefore, the relative motion between the geometry of the disk and the ball in the outlet area is considered as the determining factor. In a pure rolling state, the speed of the disk is the same as that of the ball. Under a slide-roll condition, their speeds are different. However, whether the SRR is positive or negative, the relative velocity will exert additional force to promote the deflection of the finger.

Figure 3.28 shows the variation of the finger area with SRR. Although the total finger area for List.pao20 and Liohst.pao60 changes little with the change of SRR, the near-finger areas all present an increasing trend first and then decrease. Their lowest points are all at SRR 0. This situation means that the position of the finger split point has changed under the slide-roll condition.

As a result, the ratio of the near-finger area to the far-finger area also changed. The shear rate continues to increase when the absolute value of SRR changes from 0 to 1. Thus the curve of the shear rate with SRR should also be U shaped with an axis of SRR 0. Certainly, the change of rheological properties of the grease generated by the shearing action is the main reason for the migration of the finger split point.

3.5 The constituents and rheological properties of greases

3.5.1 Track patterns and the constituents of grease

The track pattern changes with different testing conditions, and also changes with the type of grease even under the same testing conditions. In other words, the constituents of greases play an important role in determining the pattern features. We use additive free greases in this study. Their constituents are the thickener and the base oil. The pictures adopted in this

section are from series speed-change test.

3.5.1.1 Thickener

The thickener endows greases with semisolid basic properties, and thus the wake pattern can be conserved for long periods in grease lubrication. The thickener is considered to be an important factor that determines the basic properties of the grease, and it builds a network which entraps the base oil. The wide variety of thickener types and different manufacturing processes can make the physical and the chemical properties of greases vary a lot. Naturally, their track patterns are different.

Table 3.5 lists four types of thickeners and their corresponding greases. To avoid the influence of the base oil as much as possible, Paos are used as the base oils and the difference between their viscosities is small except for PTFE.PFPE. Figure 3.29 shows the chemical structures of the thickeners, Liohst and List being metal soap thickeners, Di-urea and PTFE being non-soap thickeners.

As shown in Figure 3.30, the deposition in the center of the track for Di-urea.pao30 and PTFE.PFPE is much higher than for Liohst.pao30 and List.pao20, their deposition is completely covering the center of the track. The Urea type grease has stronger absorption ability on the metal surface than the metal soap grease. PTFE thickeners are inert. They can work properly in extremely high temperature and low pressure conditions.

Table 3.5 Test greases for different types of thickeners

Thickener type	Samples
Lithium 12-hydroxystearate	Liohst.pao30
Lithium stearate	List.pao20
Di-urea	Di-urea.pao30
Polytetrafluoropolyethers	PTFE.PFPE

Table 3.6 shows the typical morphology parameters for greases with different types of thickeners. The values of S-J, A-N and A-F use the turning points of the data curves, when the entrainment speed changes from low to high as shown in Figure 3.16, Figure 3.17 and Figure 3.18. As shown in this table, the finger split joint S-J for PTFE.PFPE is apparently different from the other three greases, its degree of finger contrast and visual clarity is also the lowest. It can be seen that the finger area of the non-soap thickeners Di-urea and PTFE.PFPE are much smaller than those of the metal soap thickeners Liohst.pao30 and List.pao20.

Table 3.6 Typical morphology parameters for greases with different types of thickeners

Samples	S-J	A-N (mm^2)	A-F (mm^2)
Liohst.pao30	10900	37.03	40.1
List.pao20	5876	24.56	45.15
Di-urea.pao30	9869	28.12	24.61
PTFE.PFPE	25412	17.68	19.24

3.5.1.2 Base oil

The viscous part of the grease is determined by the base oil. It gives greases flow properties and plays an important role in the formation of the track pattern. Table 3.7 shows three types of base oils and their corresponding test greases. To avoid the influence of the thickener as much as possible, List is used as the thickener except for PTFE.PFPE.

Table 3.7 Test greases for different types of base oils

Base oil properties	Samples
Poly-alpha-olefin (PAO)	List.pao20
Poly-alpha-olefin (PAO)	List.pao400
Polyol ester (POE)	List.poe30
Perfluoropolyethers (PFPE)	PTFE.PFPE

Figure 3.31 lists the chemical structures for the base oils. There are three ways that oil molecules are retained inside the thickener structure. There can be attraction between the polar components of the base oil and thickener, there can be capillary effects and there can be mechanical retention in the spaces between adjacent fibers [14]. Generally the increase of the carbon chain for Pao will make the viscosity increase and lower the polarity.

The base oil with a higher viscosity like List.pao400 will change the polar components of the base oil and the thickener, thus the strength of the thickener network and bleeding rate may also be affected. Thereby their features of the track pattern are different. As shown in Figure 3.32, List.pao400 compared to List.pao20, the width of the finger for Liohst.pao400 gets narrower, whereas the intensity of the finger increase. There is a layer of thickener deposition in the center of the track for List.pao400.

Table 3.8 shows the typical morphology parameters for greases with different types of base oils. The method used to get the S-J, A-N and A-F is the same as for the thickener part in the previous part. From this table, the S-J values for List.pao400 and PTFE.PFPE are higher than

those of other greases. Moreover, the difference between the A-N and A-F for List.pao20 and those for List.pao400 is relatively large, whereas the difference between those for List.pao20 and those for List.poe30 is small. Table 3.6 also shows that the changes in the thickener have great effects for the finger area. From this, we can see that the thickener type and base oil viscosity are more important than base oil among the factors that may affect the A-N and A-F.

Table 3.8 Typical morphology parameters for greases with different types of base oils

Samples	S-J	A-N (mm^2)	A-F (mm^2)
List.pao20	5876	24.56	45.15
List.pao400	12458	45.27	39.01
List.poe30	8421	24.15	43.3
PTFE.PFPE	25412	17.68	19.24

3.5.2 Track patterns and the rheological properties of greases

The track pattern, rheological properties of greases and test conditions are closely related to each other. Put simply, the track pattern is decided collaboratively by the rheological properties of the grease and the testing conditions. Under different testing conditions, the inner side of the rheological properties of greases such as viscosity, elasticity etc. and the outer side of the features of the track pattern will produces change subsequently. The basic process of it:

Under force → flow (properties change) → different track patterns

The pictures adopted in this section are from series speed-change test. For the rheological data please refer to Chapter 2. The real rheological information in the EHL contact could not be determined by a rheometer. Even so, we still hope to obtain some useful information.

3.5.2.1 Finger area, apparent viscosity and yield stress

From Figure 3.16 and Figure 3.18 in the entrainment speed series tests, it can be seen that the sequence of the relative finger area for A-N and A-F throughout the whole speed range is listed as follows:

Urea.poe30＜Liohst.poe30＜Liohst.pao60＜Liohst.pao400

The finger area varies independently from the entrainment speed, indicating that it may relate more with the properties of grease itself. Figure 3.33 shows the apparent viscosity at the shear rate of 1000 s^{-1}. The sort order of the finger area for the four test greases on the horizontal axis corresponds from small to large.

For the four test greases, their apparent viscosity changes from 0.09 Pa.s for Urea.poe30 to 1.03 Pa.s for Liohst.pao400. It can be seen that the overall value is relatively low. Figure 3.34 shows the yield stress of the test greases, the sort order of the finger area is the same as the

previous figure. This means that the greases with a smaller yield stress and higher viscosity tends to have a larger finger area.

3.5.2.2 The degree of finger visual clarity and shear-thinning index

Table 3.9 lists the degree of finger contrast and visual clarity order for test greases in the entrainment speed series test. Although this clarity degree sometimes changes for the same grease under different entrainment speeds, overall, however, the clarity sequence between the four test greases barely changes. Figure 3.35 shows the shear-thinning index n for the test greases, its sort order of the finger clarity for the four test greases on the horizontal axis corresponds from low to high. The shear-thinning index stands for the order of difficulty in flowing. It decreases with the increase of finger clarity, and this means that the grease with better flow ability tends to have a clearer finger pattern.

Table 3.9 The degree of finger contrast and visual clarity order for test greases in the entrainment speed series test

	Urea.poe30	Liohst.pao400	Liohst.poe30	Liohst.pao60
D-F	1	2	3	4

The represented values for D-F between test greases throughout the whole speed range

Low ⟶ High			
1	2	3	4

3.6 Summary and discussion

3.6.1 Summary

Figure 3.36 shows the flowchart for this chapter. Firstly a detailed comparison between the oil wake and the grease wake is done. The unique rheological properties of greases make their flow distribution on the disk conserved comparatively intact even after the test is stopped. This can make up for the shortcoming that the details of the flow behavior of greases are hardly observed in video tests. Therefore, dynamic video observation and static picture observation are chosen to provide a relatively comprehensive analysis.

Based on the preliminary observation, eight parameters are selected as typical representatives of morphology features. As the test conditions change, the grease lubrication conditions and flow distribution will change accordingly. The previous content describes the changes in these parameters when entrainment speed, test duration and slide to roll ratio change, respectively. Overall, the features of grease track pattern change with grease type and test conditions. First of all, we need to make a detail summary on these observations.

Table 3.10 Three categories of parameters

Classification	Parameters
Area near the center of track	S-J, A-N, D
Area far from the center of track	λ, A-F
Visual definition	D-F, D-R, D-T

The eight morphology parameters can be divided into three categories according to actual situations. As shown in Table 3.10, the first category contains the parameters which can be used to describe the part near the center of the track, like S-J, A-N and D. The second category contains the parameters which can be used to describe the part far from the center of the track, like λ and A-F. The third category contains the parameters defined visually. Numbers are used to represent the morphology differences in degree, like D-F, D-R and D-T.

The reasons to divide them into three categories are: firstly their physical meanings are different from each other, like the first category and the second category. On the other hand, their evaluation methods are different like the third category and the other two. The values for the third category simply show the sequence, and there is no better way available to evaluate the extent at this stage.

Table 3.11 The change trend of the morphology features under different testing conditions

	Entrainment speed	Test duration	Slide to roll ratio
Entrainment speed	1 mm/s→500 mm/s	47.1 mm/s	47.1 mm/s
SRR	0.4	0 0.6	-1 -0.5 0 0.5 1
Shear rate	S_{min} → S_{max}	0 S_{med}	S_{-1} $S_{-0.5}$ 0 $S_{0.5}$ S_1
Area near the center of track	S-J ↗↘		Total area →
	A-N ↗↘	A-N ↘	A-N ↘↗
	D ↘		Deflection angle ↘
Area far from the center of track	λ ↘		
	A-F ↗→↘		
Visual definition	D-T ↘	D-T ↘	

$$\dot{\gamma} = {}^{U}/_{h} \tag{3.1}$$

$$U = U_d - U_b \tag{3.2}$$

Table 3.11 shows the change trend of the morphology features under different testing conditions. As shown in this table, longitudinal lines correspond to these changes in three series of tests, i.e. entrainment speed part, test duration part and SRR part. The first three lateral lines list the adopted entrainment speed, SRR and their rough estimated shear rate.

The definition of shear rate is shown as equation 3.1. It is the speed difference between the disk and the ball (equation 3.2) divided by the central film thickness. The following three lateral lines for the entrainment speed part and test duration part are the summary of the change trend of the morphology features for the area near the center of the track, the area far from the the center of the track and some visual definitions, respectively.

Certainly, these trends listed are rough; they do not involve precise values. Although the trends of these data have some similarities, such as their increased degrees, the maximum values and turning points are different from each other as their track patterns vary. The last three lateral lines for the SRR part are the summary of the change trend of the morphology features for the total finger area, the area near the center of the track and the deflection angle.

As the table shows, the SRR is set as 0.4 when the entrainment speed changes from 1 mm/s to 500 mm/s. Despite the fact that the shear rate could not be determined without the film thickness value, the range of the shear rate from zero to high on a large scale is well established. The number of the regular change trend of the morphology features in the entrainment speed part has always been the largest.

The distribution of the grease fingers become more complicated, the number of fingers and the intensity of the finger splitting are increased with the increase of speed. They show concretely as follows: both the near-finger area and the number of finger split points increased with speed then decreased. The inlet meniscus distance decreased with the increase in entrainment speed. The wavelength decreased continuously. The far-finger area continues to rise and then remains stable but shows a sharp decline at high speeds.

In addition, grease lubrication is more vulnerable to starvation compared to oil lubrication especially at high speeds. The finger pattern near the center of the track will be totally destroyed when the speed is higher than a certain threshold value, but there is always some residual grease retained far from the center of the track.

The entrainment speed is set as 47.1 mm/s when the test duration gets longer. The change trends of the morphology features for SRR 0 and these for SRR 0.6 are compared. The differences between them are whether the grease in the contact zone would suffer shear action. Under a slide-roll condition, the near-finger area and the thickener deposition continue to drop over time, and the scratches become more serious. Extending the test duration has no steady and consistent effect on morphology parameters under a pure rolling condition.

The entrainment speed is set as 47.1 mm/s when the SRR changes from negative 1 to positive 1. The corresponding shear rate is a U shape, and the SRR 0 is the symmetrical point. Despite the fact that the total finger area almost does not change, the data of the near-finger area with SRR is also a U shape as that of the shear rate, and reveals the trend of first decreasing then increasing. The deflection angle of the finger decreases gradually for all test greases.

Although it is complicated to speculate the flow behaviors from the observations of the track patterns, there are still some phenomena which are worth studying. In addition to the testing conditions, the constituents of the grease and the rheological properties of the grease will affect the track pattern. The non-soap thickener grease has a heavier deposition in the center of the track than that of the metal-soap grease. When the viscosity of the base oil varies greatly, it also causes some changes like the deposition in the center of the track.

Due to the difficulty of using rheometer data in EHL conditions, the analysis of the rheological properties is rough. Even so, on the surface, it can be speculated that the grease with a smaller yield stress and higher viscosity tends to have a larger finger area. The grease with a better flow ability tends to have a clearer finger pattern.

3.6.2 Discussion

Track pattern and the state of lubricating contact

It is proposed that the integrality of the finger pattern is equivalent to whether the lubricating film ruptures. The issues involved as follows: according to the video observation, the finger wake is formed by the outlet cavitation. These finger patterns are a variant of the Saffman-Tylor finger [9], and it is believed that the width of the instability finger can be predicted by the film thickness, velocity, surface tension and the viscous difference between the fluid and the cavity.

According to the previous observation, the decrease of wavelength with increasing entrainment speed is very noticeable indeed. However, if the entrainment speed continues to increase, the finger pattern will be removed. The possible process is:

The lubricating film is built→negative pressure in the outlet→gas accumulation→cavity formation→finger pattern formation

The lubricating film could not be built→negative pressure disappears→cavity disappears→ finger is removed

The lubricating film---negative pressure---finger pattern

It can be seen from these that the formation of the finger pattern and its variation are all related with the lubricating film.

The variation of the track pattern

These observations show that the morphology changes of the track pattern on the disk have a general process, regardless of the type of grease.

When the inlet meniscus distance D gradually decreases, the average interval between finger trunks λ also reduces. The near-finger area A-N will grow. The grease with a lower yield stress and higher viscosity can get a greater finger area.

In addition, for the grease with a lower apparent viscosity under high shear, the increasing of the finger split joints S-J will be more obvious, and the track pattern also becomes more complex. The degree of track pattern contrast and visual clarity such as D-R and D-F tend to rise, and the grease with a better flow ability tends to have a clearer finger pattern. However, the deposition in the center of the track D-T usually decreases.

The above whole process appeared in the series speed-change test. It is also a process by which the amount of grease in the inlet area is gradually being consumed. This is not highlighted for the other two series tests. That may be because the extent of the test duration and the change of the SRR could not induce regular changes on the inlet distance. Although every type of grease has its own characteristics, we can still find some common trends. This illustrates that the track pattern is a subject worthy of further study, since it can represent the common features of grease flow behaviors.

3.7 Conclusions

The main conclusions for this chapter are as follows:

1. The features of the track pattern are different for different grease types and different testing conditions.
2. Lithium-12-hydroxy stearate grease shows clear track patterns, whereas di-urea grease shows obscure track pattern and heavy thickener deposition in the center of the track.
3. The variation of the parameterized track pattern can represent the grease flow behavior, regardless of the type of grease.
4. Among the entrainment spend, test duration and slide-to-roll ratio, the track pattern varies considerably with entrainment spend.
5. The thickener type and base oil viscosity are more important than the base oil among the factors that may affect the area of the grease finger.
6. The grease with a smaller yield stress and higher viscosity tends to have a larger finger area. The grease with a better flow ability tends to have a clearer finger pattern.
7. The formation and maintenance of the grease finger are dependent on the state of the lubricating contact.

References

[1] Pemberton J, Cameron A. A mechanism of fluid replenishment in elastohydrodynamic contacts, Wear, 1976; 37: 185-190.

[2] Wedeven LD, Evans D, Cameron A, Optical Analysis of Ball Bearing Starvation, Journal of Lubrication Technology, 1970; 3: 349-361.

[3] Larrson,P-O. Lubricant replenishment in the vicinity of an EHD contact. PHD thesis, Lulea University of Technology, Sweden, 1996.

[4] Huang L, Guo D, Wen S, Wan GTY. Effects of slide/roll ratio on the behaviours of grease reservoir and film thickness of point contact. Tribol Lett, 2014; 54: 263–271.

[5] Jing Chen, Hiroyoshi Tanaka, Joichi Sugimura. Experimental Study of Starvation and Flow Behavior in Grease-Lubricated EHD Contact. Tribology Online, 2015; 10: 48-55.

[6] Leonard B, Sadeghi F, Cipra R, Leonard BEN. Gaseous Cavitation and Wear in Lubricated Fretting Contacts Gaseous Cavitation and Wear in Lubricated Fretting Contacts, Tribology Transactions, 2008; 51: 351–360.

[7] Jakeman RW. A numerical analysis method based on flow continuity for hydrodynamic journal bearings, Tribology International, 1984; 17: 325–33.

[8] Gasni D, Ibrahim MKW, Measurements of lubricant film thickness in the iso-viscous elastohydrodynamic regime, Tribiology Int, 2011; 44: 933–944.

[9] Saffman PG, Taylor G. The Penetration of a Fluid into a Porous Medium or Hele-Shaw Cell Containing a More Viscous Liquid, Proc. R. Soc. London A, 1958: 312.

[10] Henrik Åström, Jan Ove Östensen and Erik Höglund, Lubricating Grease Replenishment in an Elastohydrodynamic Point Contact, Journal of Tribology, 1993; 115: 501–506.

[11] P.M.Cann, In-Contact Molecular Spectroscopy of Liquid Lubricant Films, MRS Bulletin, Vol: 33, Pages: 1151-1158

[12] Ghatak, A, Chaudhury, M.K. Adhesion induced instability patterns in thin confined elastic film. Langmuir, 2003; 19: 2621–2631.

[13] N. Kanopoulos, N. Vasanthavada, and R. L. Baker, Design of an image edge detection filter using the sobel operator, IEEE Journal of Solid-State Circuits, 1988; 23: 358–367.

[14] R. Czarny. Effect of changes in grease structure on sliding friction. Industrial lubrication and tribology, 1995; 4: 3-7.

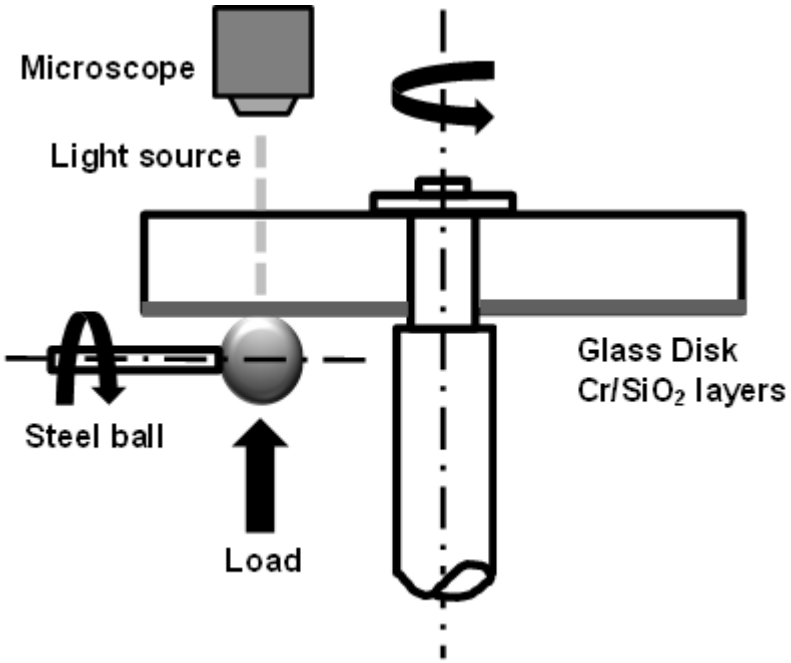

Figure 3.1 Schematic representation of ball-on-disk setup

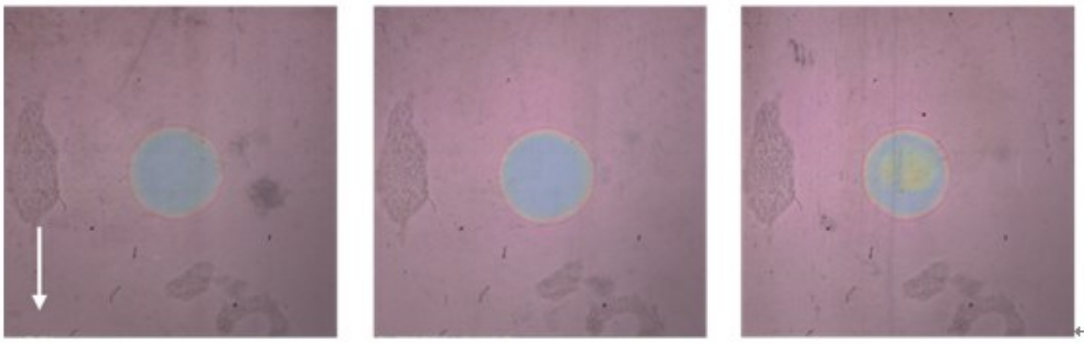

(i) Before test start

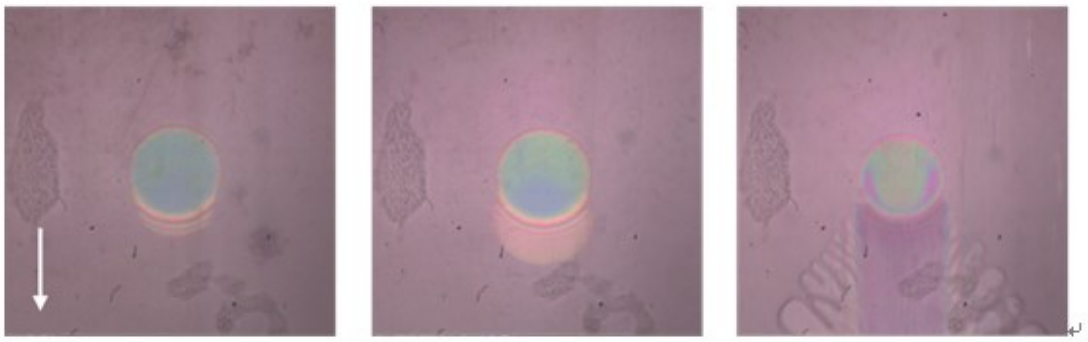

(ii) 10 ms

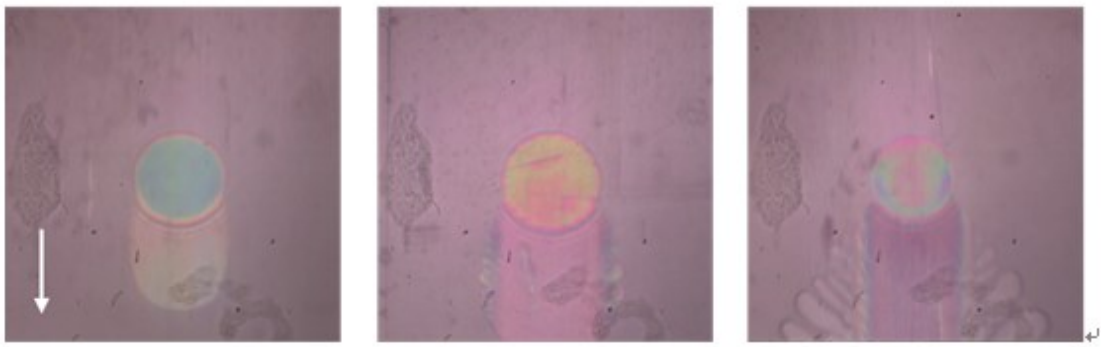

(iii) 60 ms

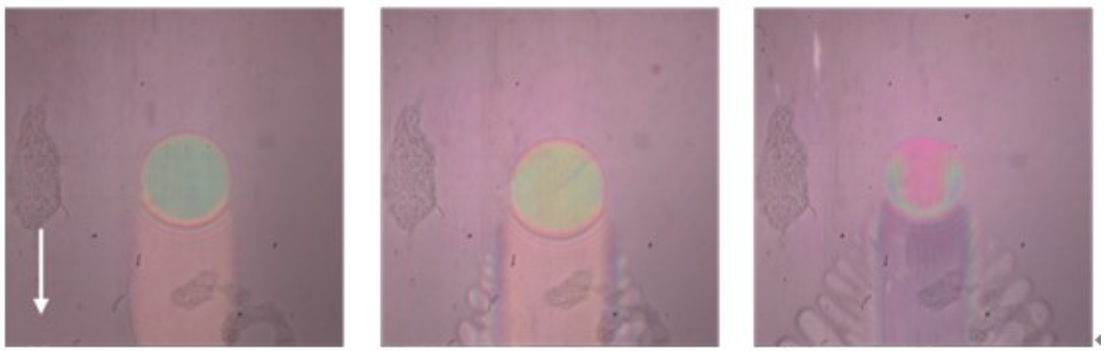

(iv) 200 ms

PAO20 PAO 60 PAO 400

100 µm

Figure 3.2 Wake pattern formations with time for different base oils at entrainment speed of 47.1 mm/s in pure rolling state

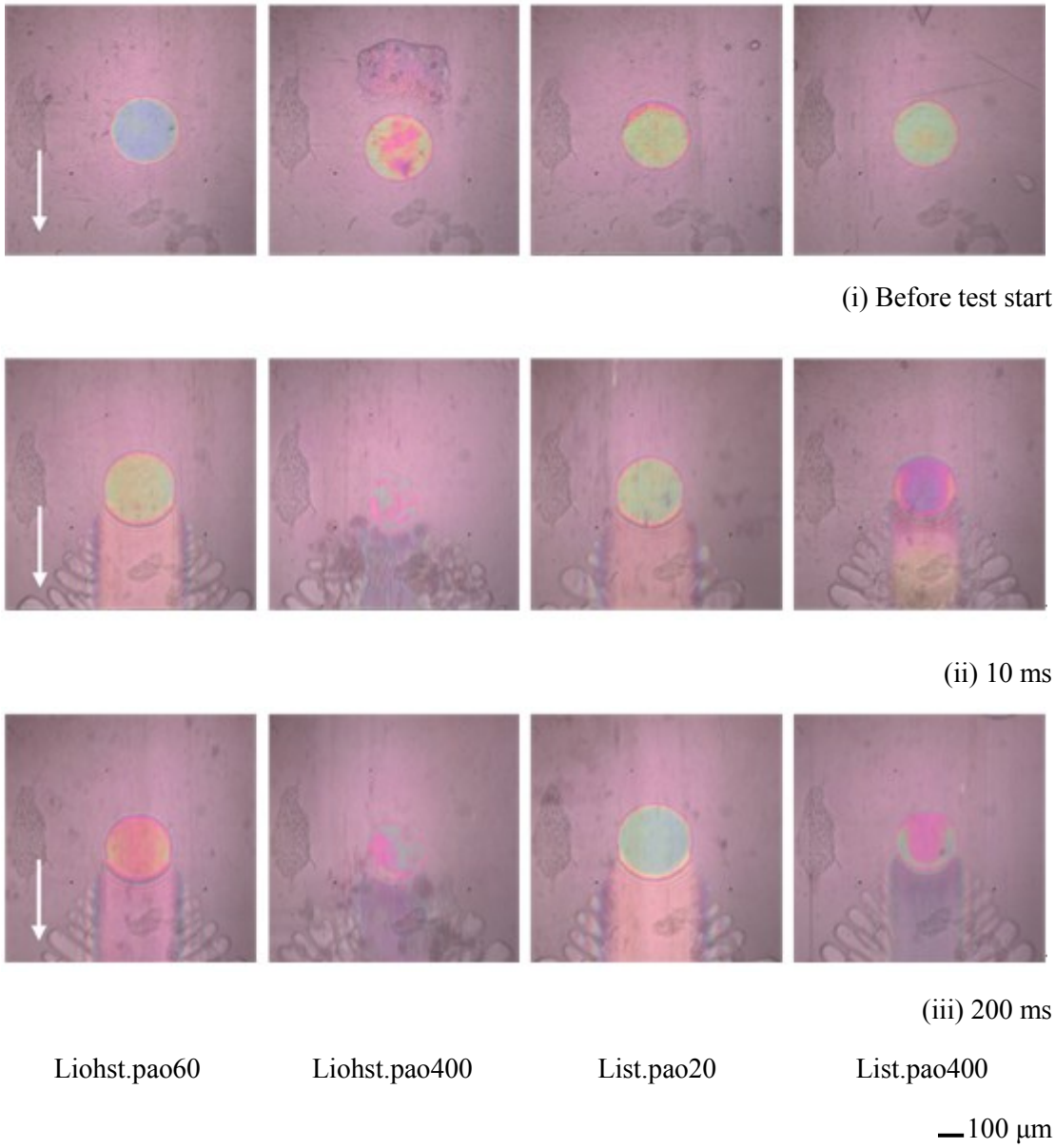

Figure 3.3 Wake pattern formations with time for different greases at entrainment speed of 47.1 mm/s in pure rolling state

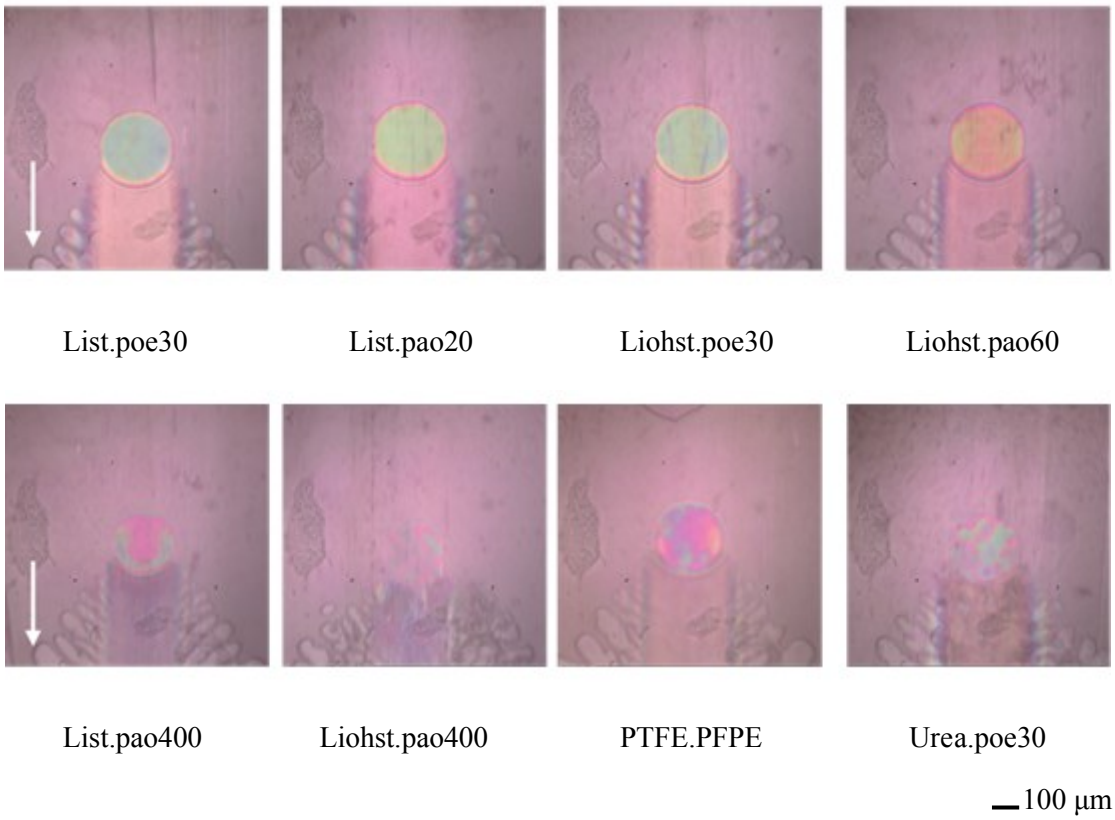

Figure 3.4 Dynamic wake patterns for test greases taken at 100 ms after tests start at entrainment speed of 47.1 mm/s in pure rolling state

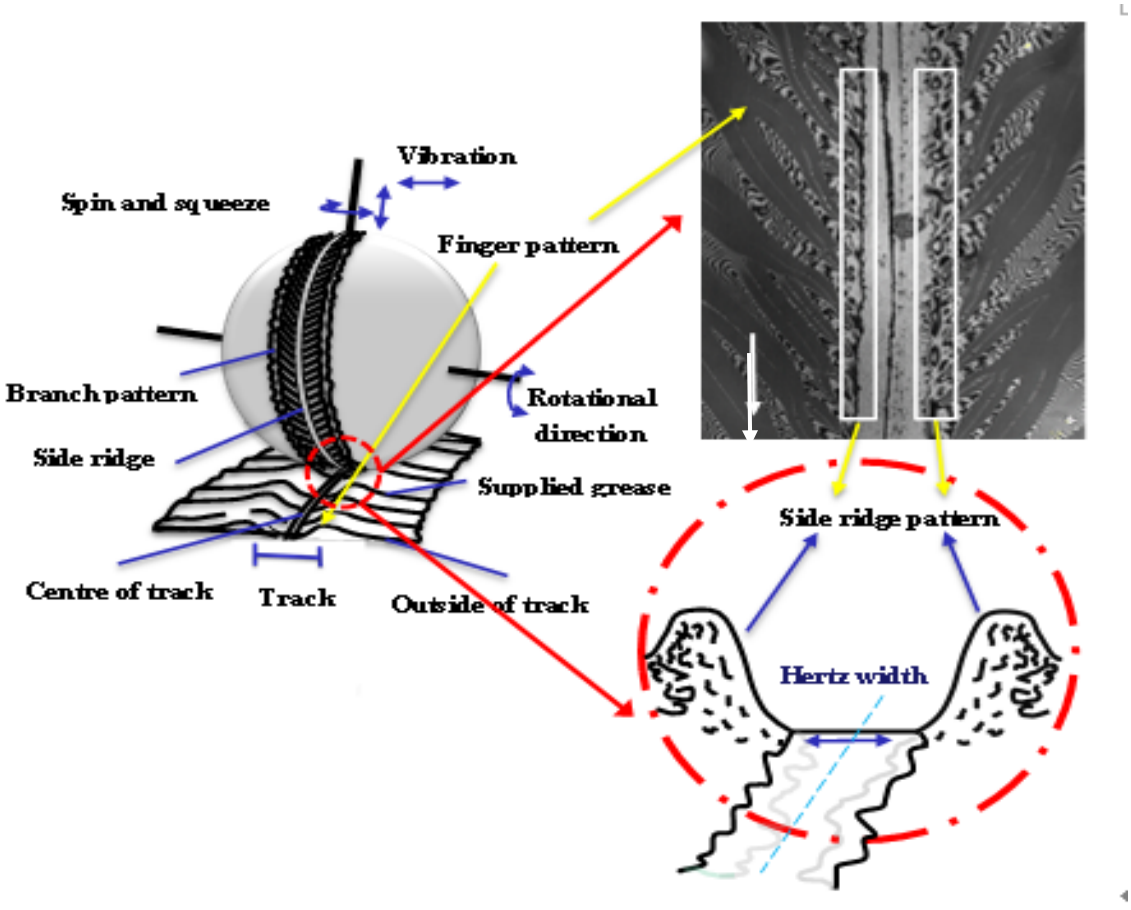

Figure 3.5 Schematic representations of the grease distribution around an EHL contact

Upstream Inlet Center Outlet Downstream

100 μm

Figure 3.6 Schematic representations of the grease patterns taken at different positions after test stop

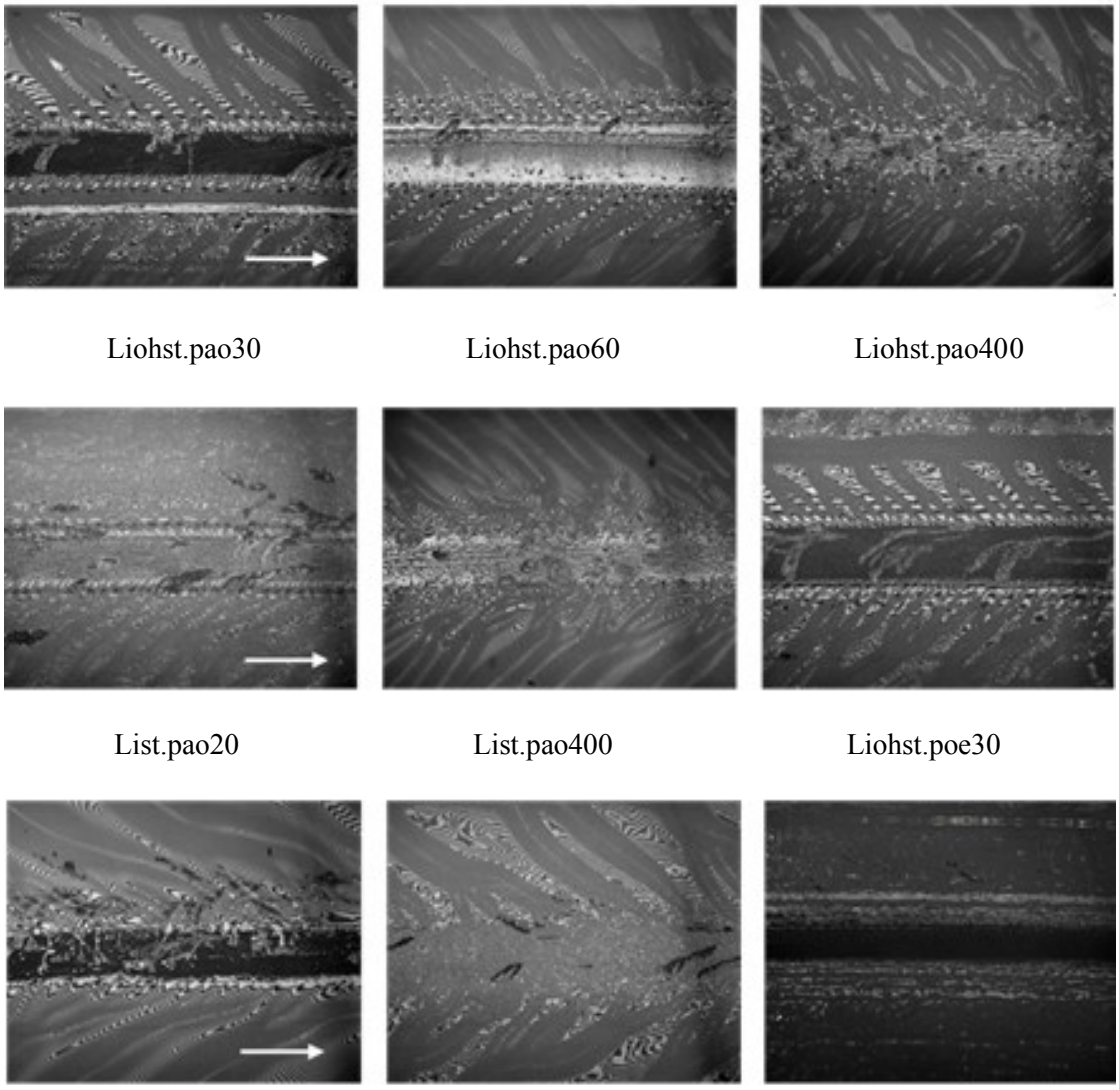

Figure 3.7 Upstream patterns for the test greases with 10 minutes test duration at entrainment speed of 47.1 mm/s in pure rolling state

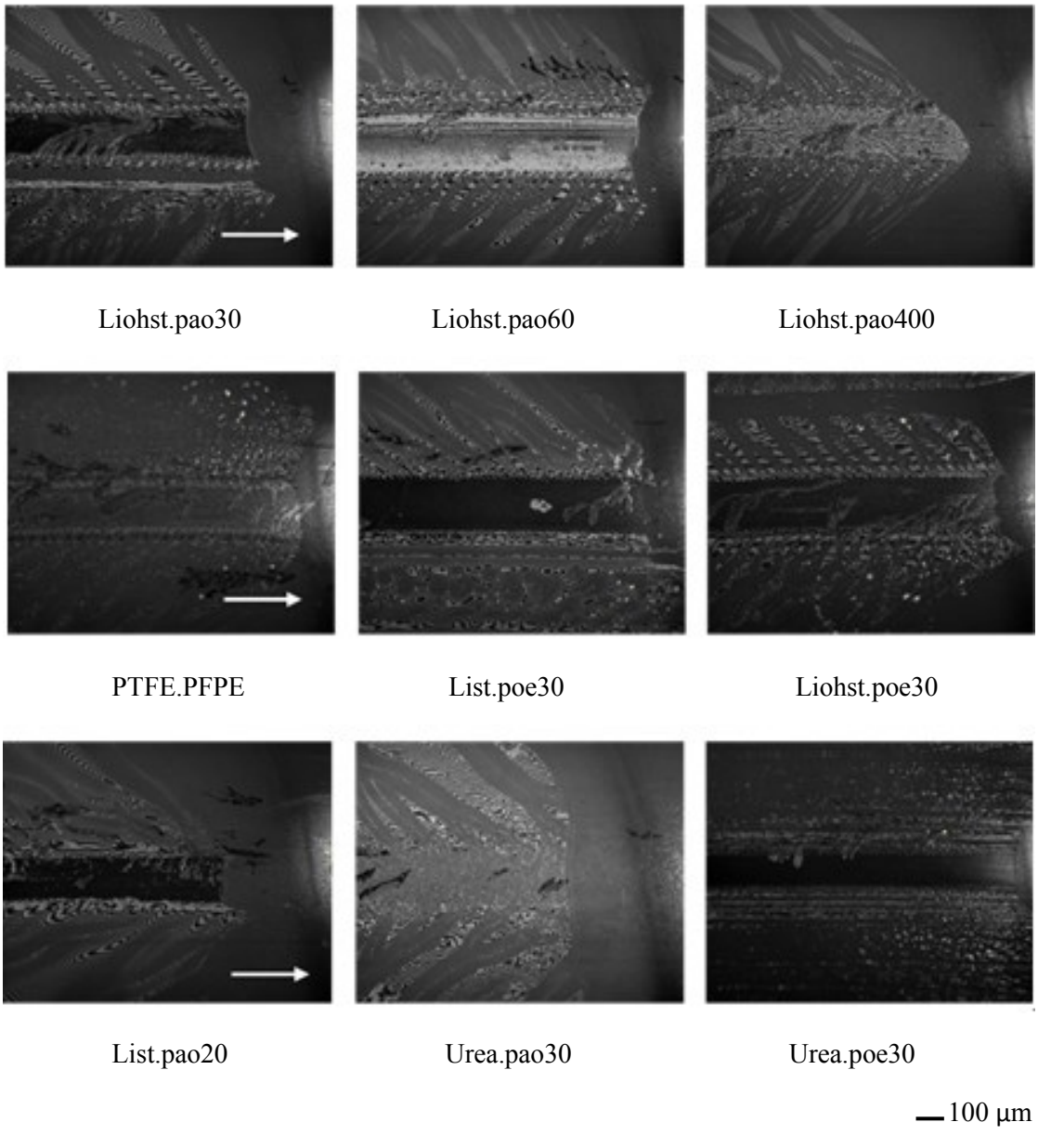

Figure 3.8 Inlet patterns for the test greases with 10 minutes test duration at entrainment speed of 47.1 mm/s in pure rolling state

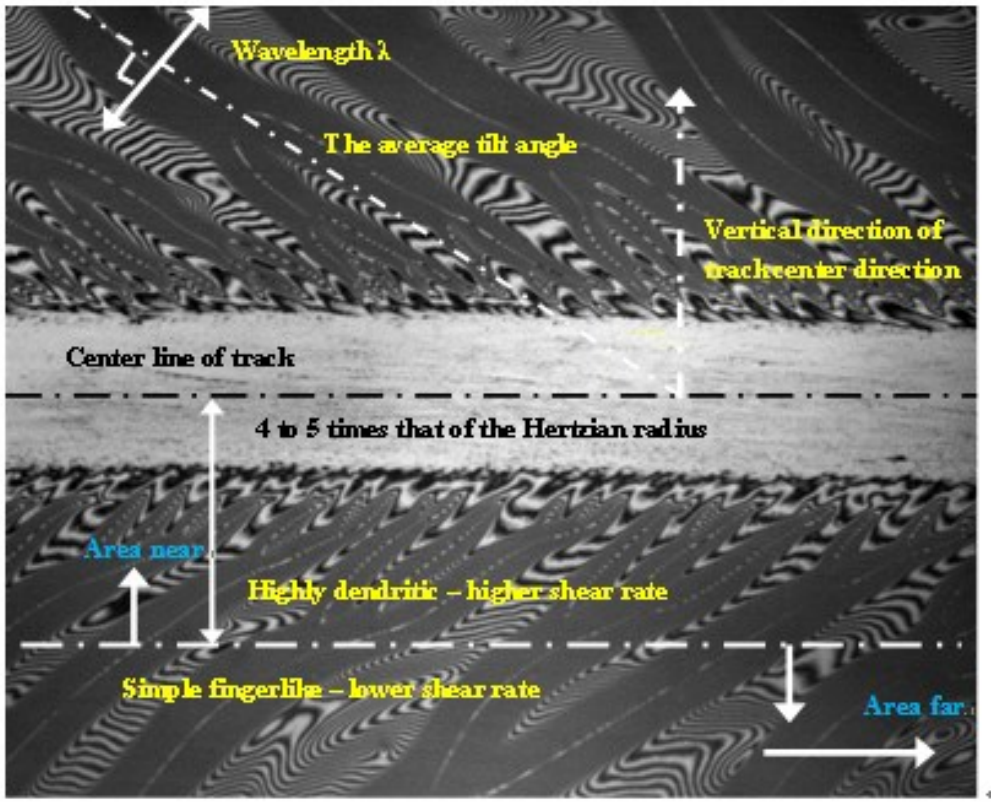

(a) Definition of wavelength λ – the average interval between fingers in area far from the center of track

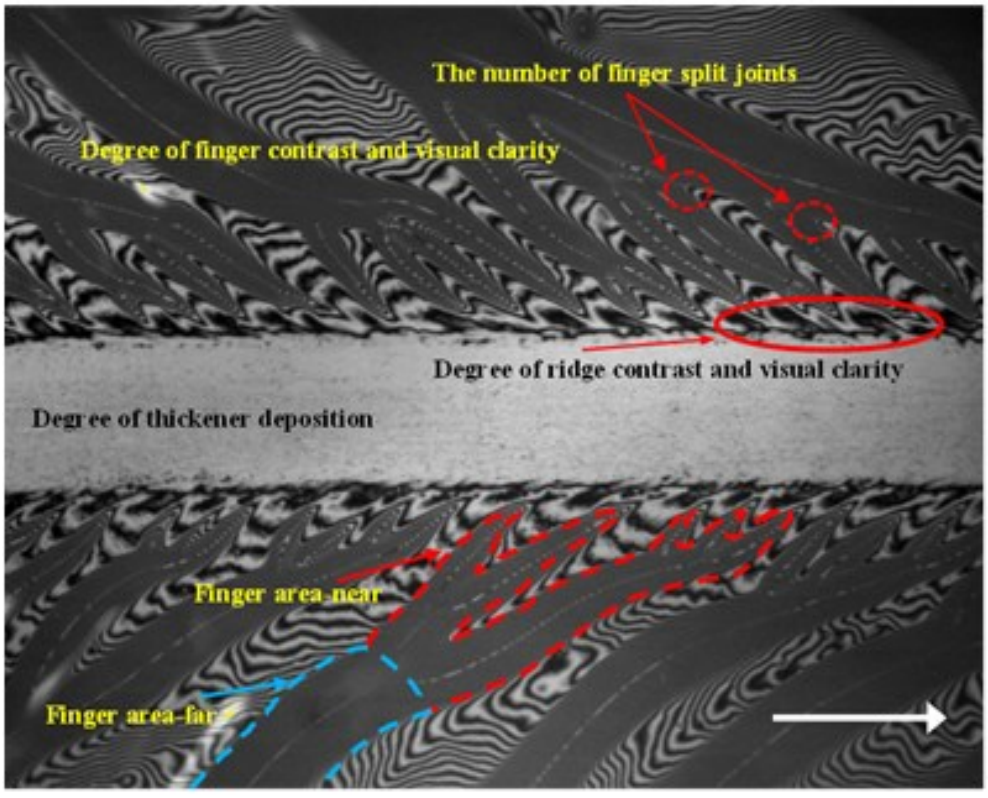

(b) Definition of the degree of thickener deposition, the degree of side ridge contrast and

visual clarity, the degree of finger contrast and visual clarity, the finger area in area near the center of track per disk circle and that of in area far, the number of split joints per disk circle

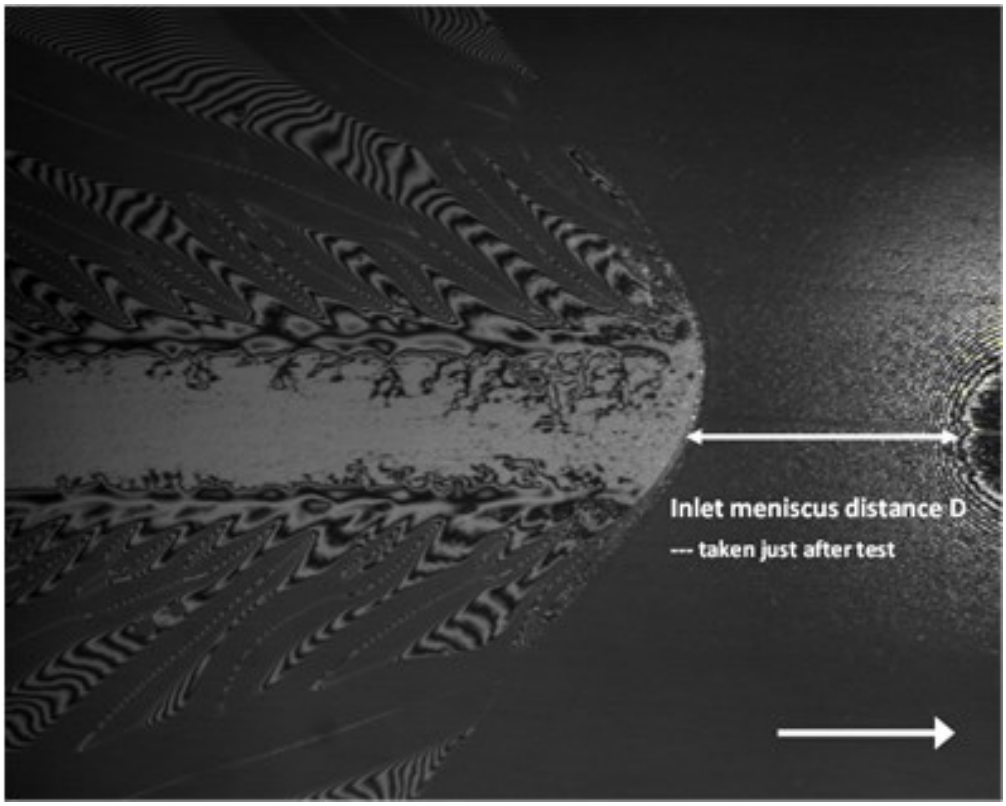

(c) Definition of the inlet meniscus distance

Figure 3.9 Definition of the characteristic parameters of grease track pattern

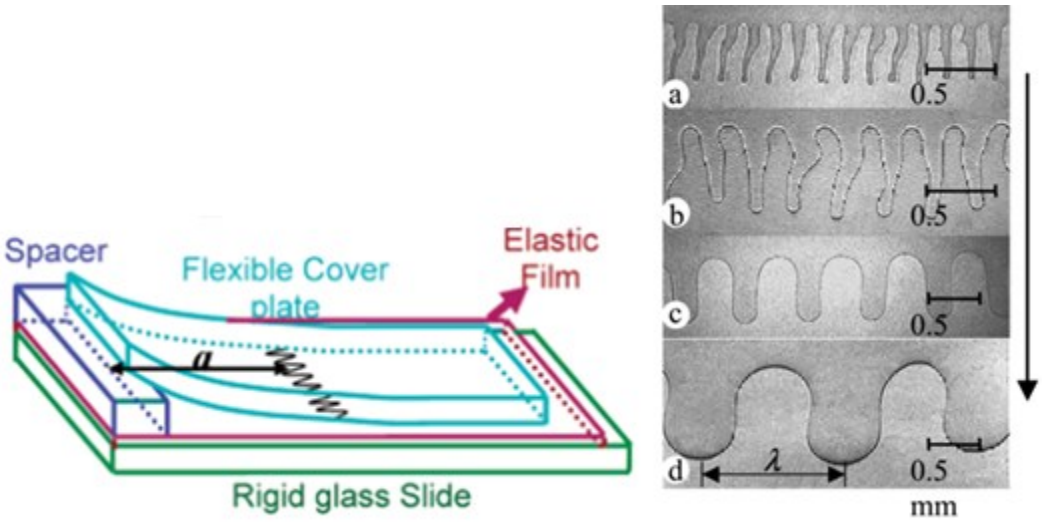

Figure 3.10 Schematic representations of the experiment setup and the corresponding video micrographs [12]

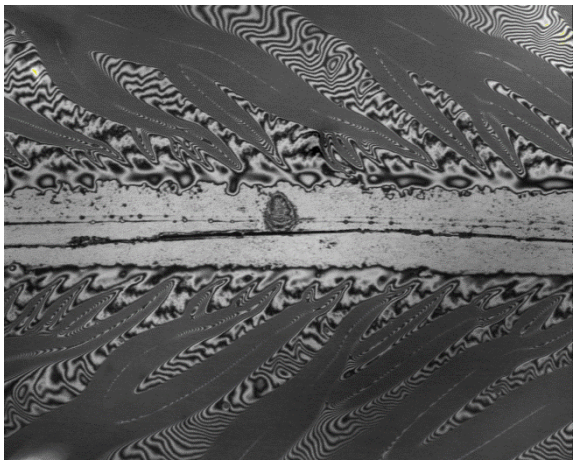

(a) Initial image

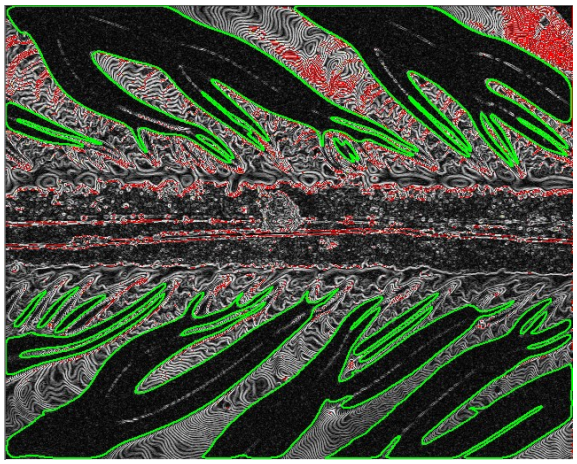

(b) Sobel edge process and object selection image

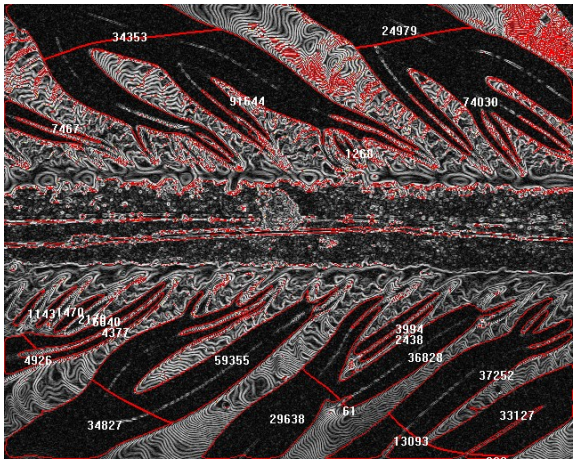

(c) Finger area separation and area calculation image (pixel unit)

Figure 3.11 Process of image treatment

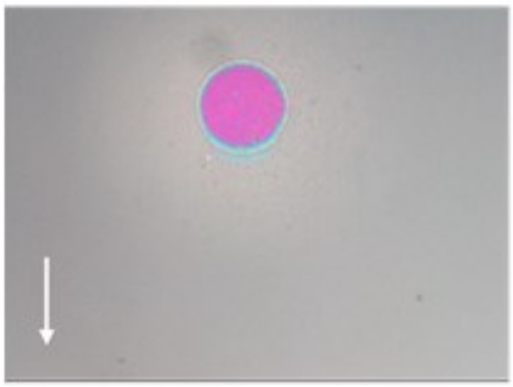
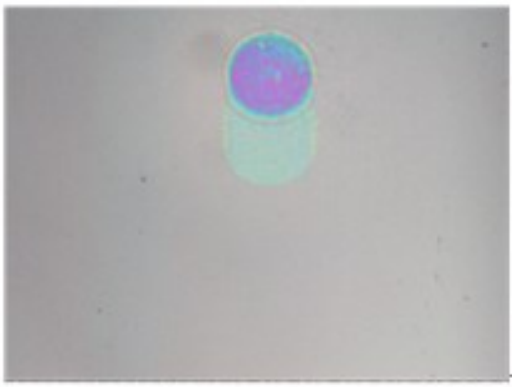

1 mm/s

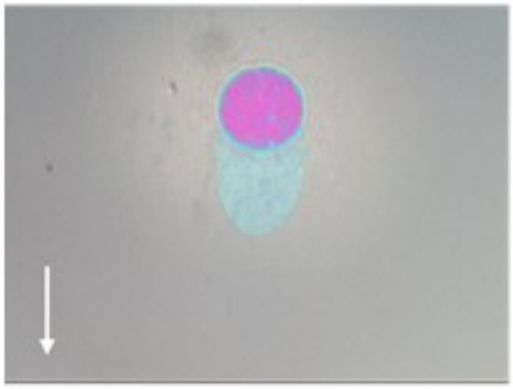
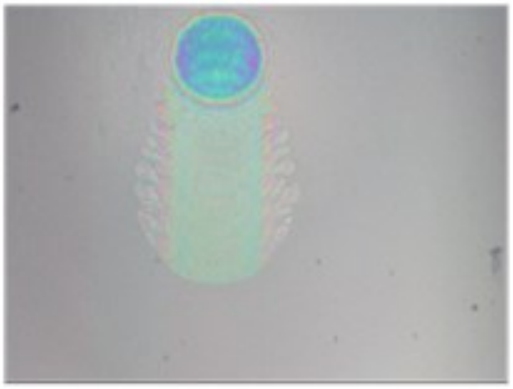

4.2 mm/s

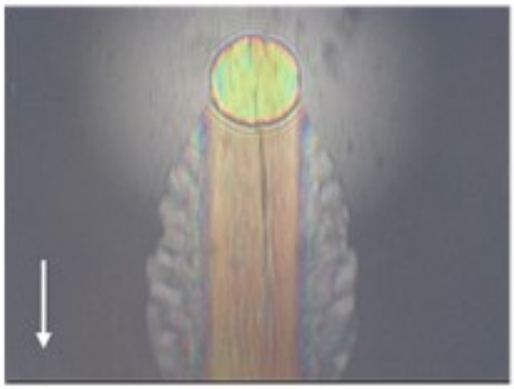
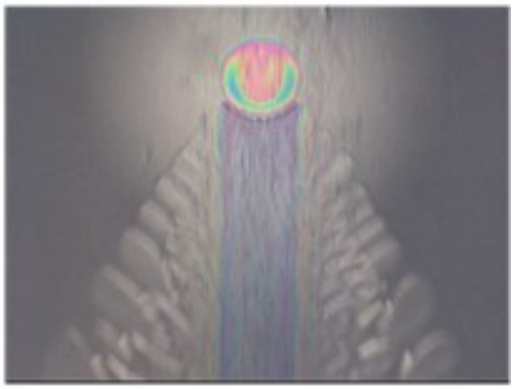

45.8 mm/s

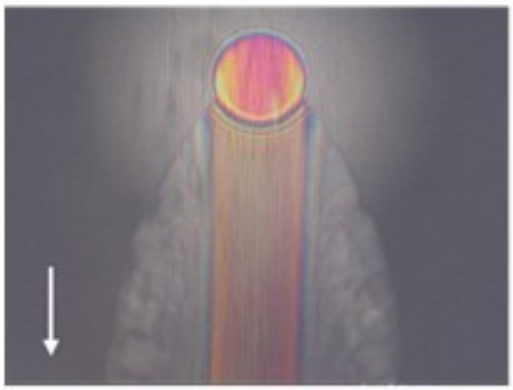
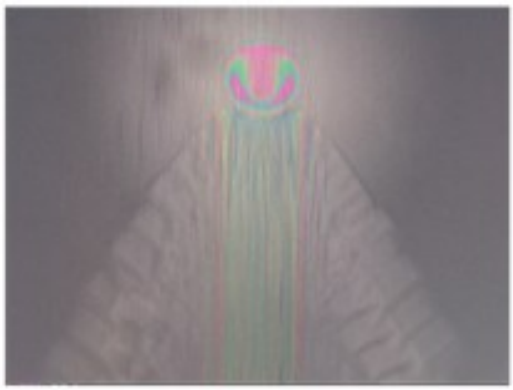

Figure 3.12 Speed evolution of the wake patterns of base oils in pure rolling state

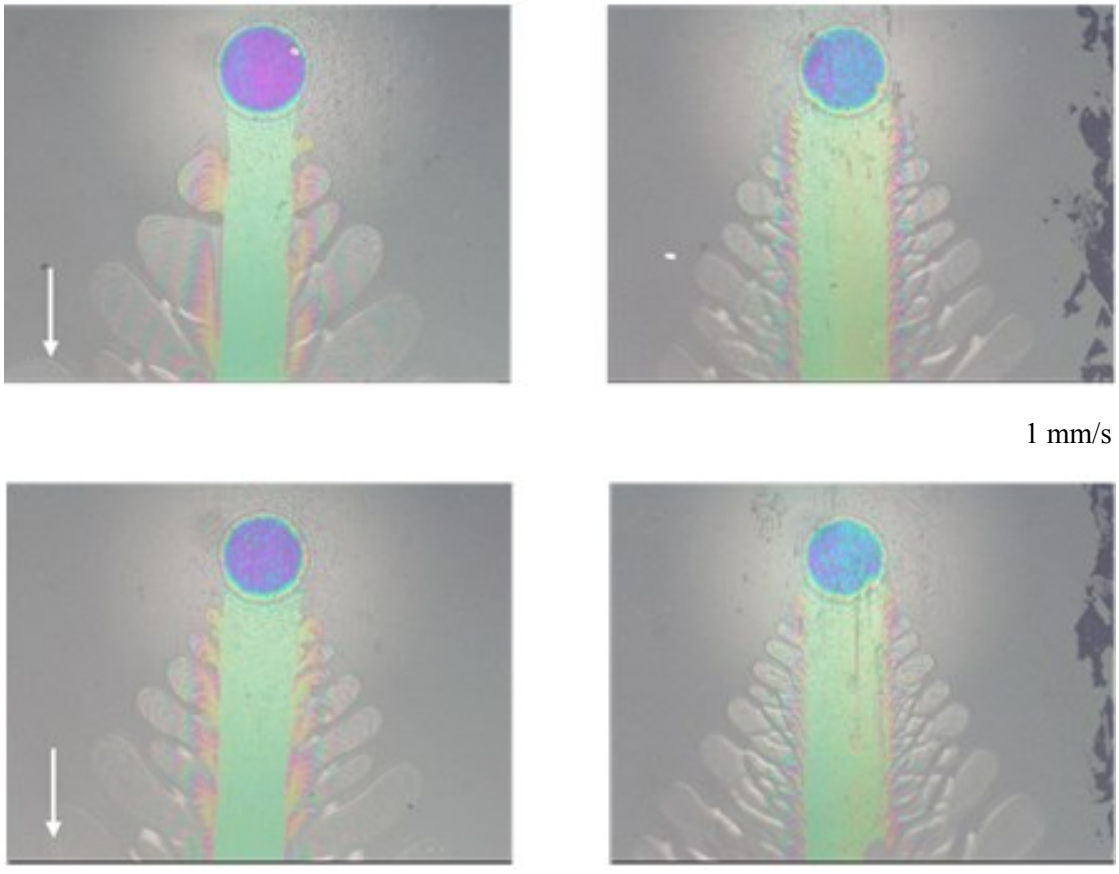

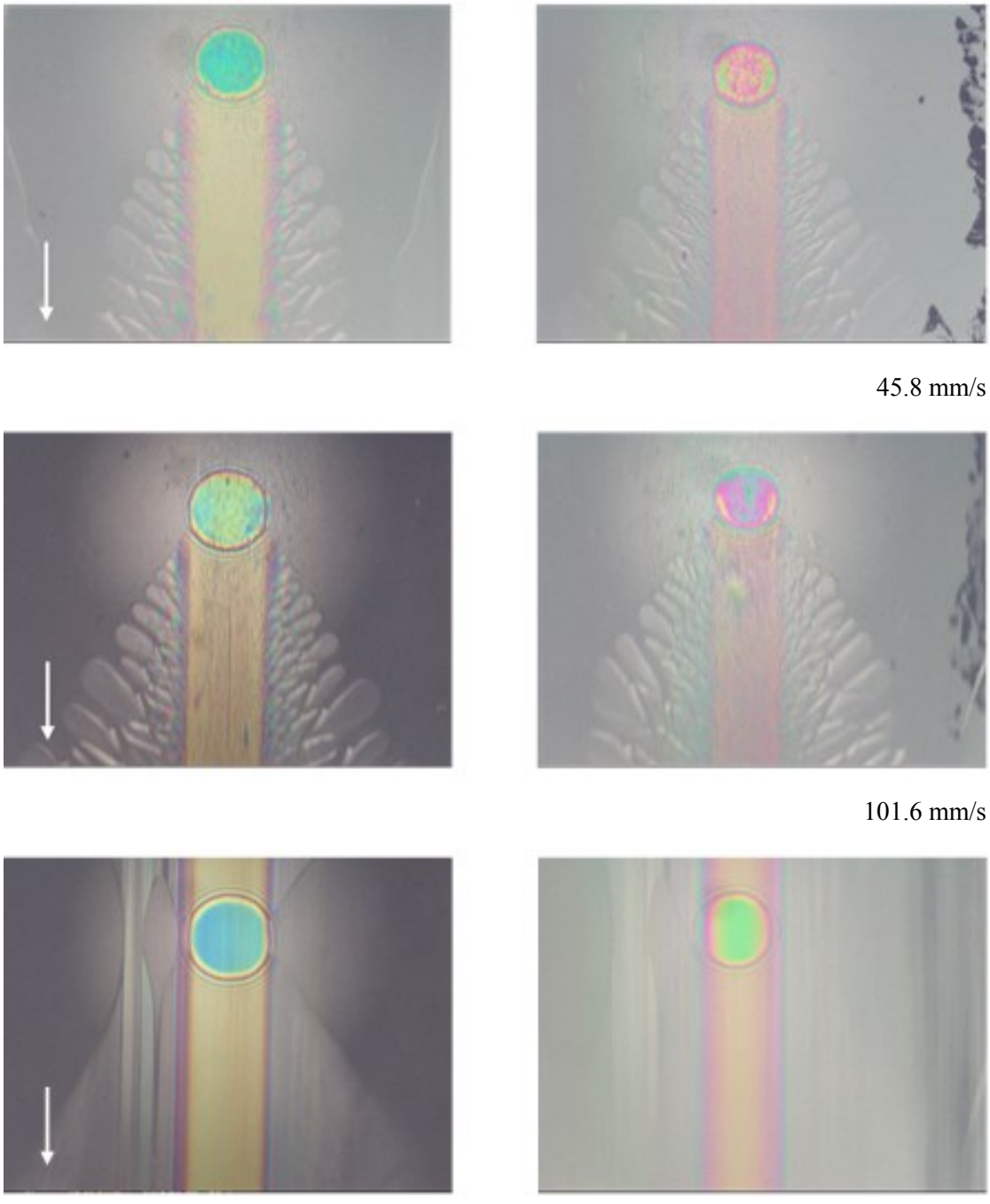

Figure 3.13 Speed evolution of the wake patterns of test greases in pure rolling state

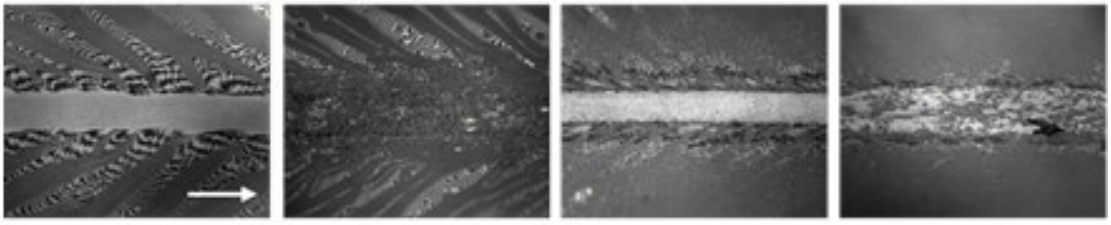

Corresponding Sobel edge images

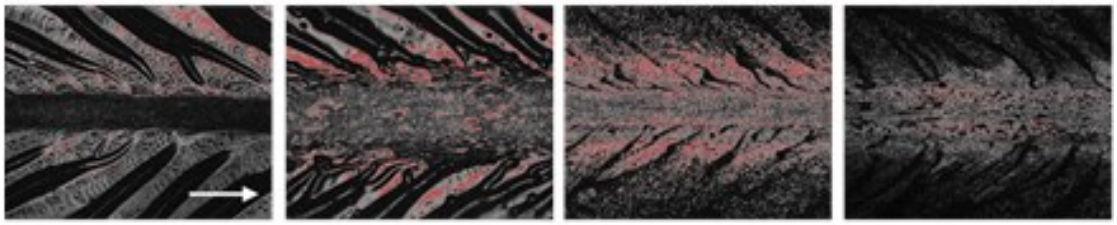

1.9 mm/s

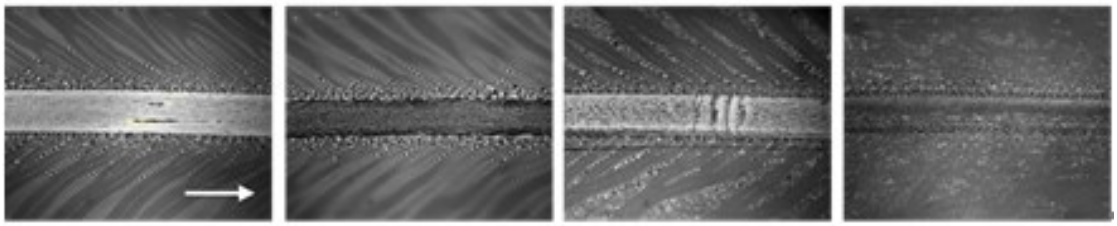

Corresponding Sobel edge images

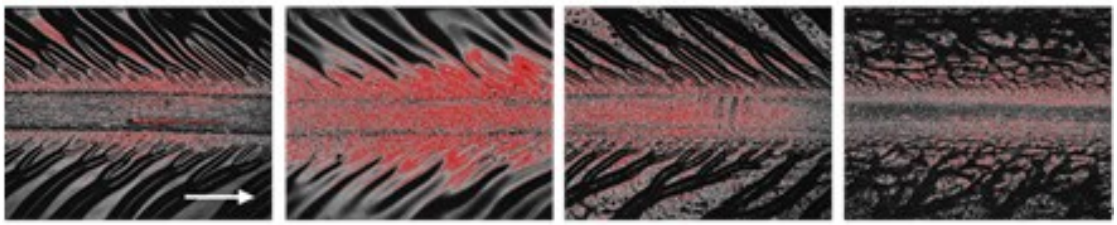

101.6 mm/s

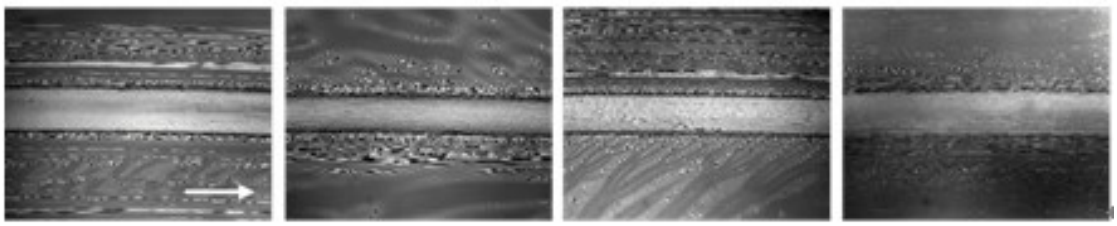

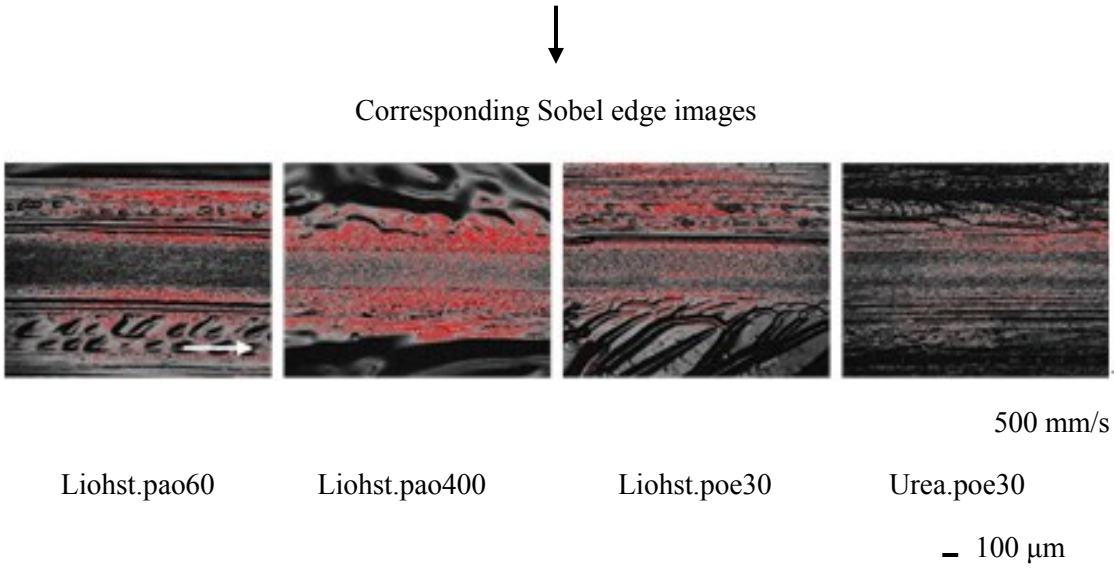

Figure 3.14 Speed evolution of the upstream patterns for slide to roll ratio 0.4

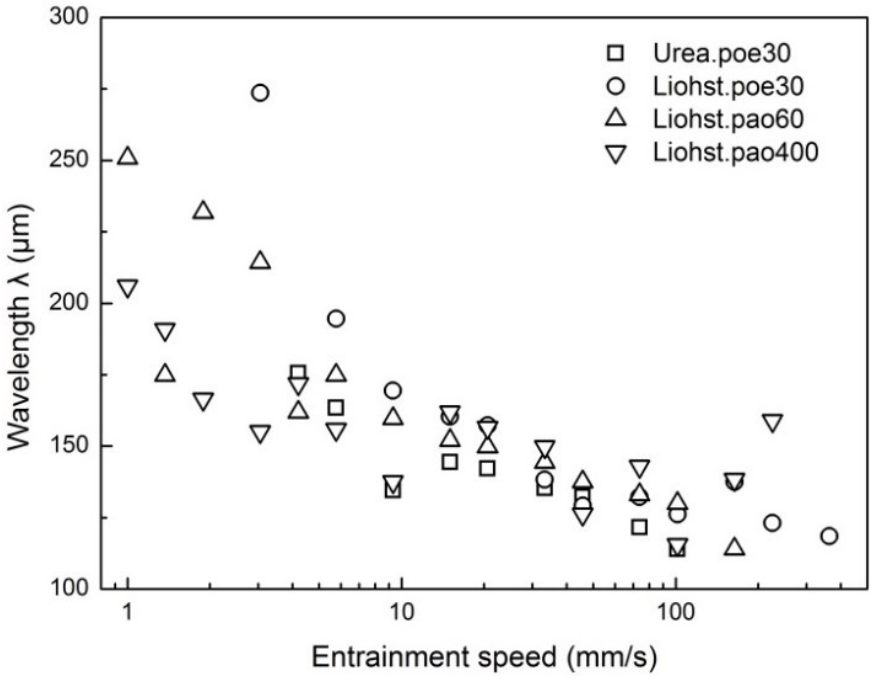

Figure 3.15 Variation of wavelength with entrainment speed

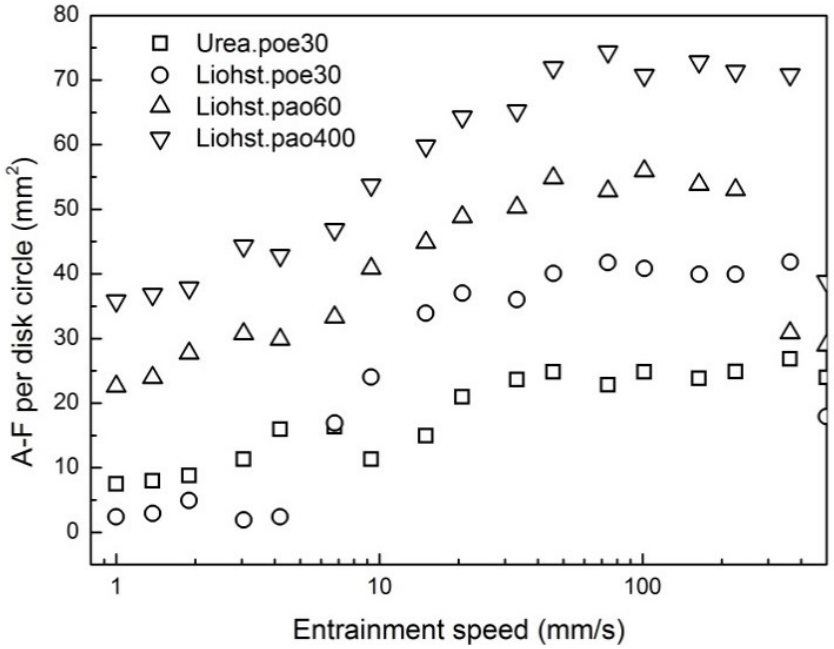

Figure 3.16 Variation of finger area far from the center of track with entrainment speed

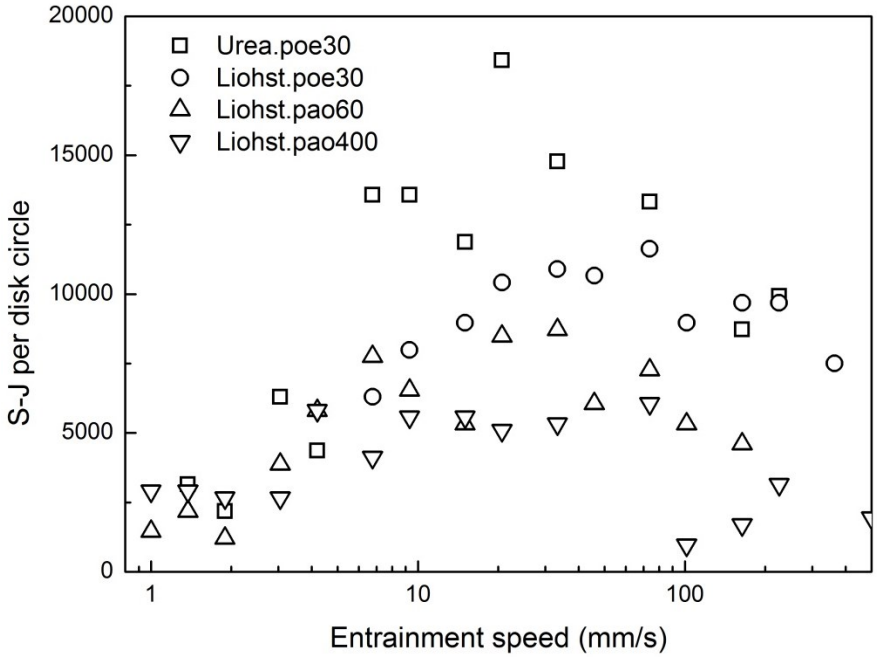

Figure 3.17 Variation of the number of finger split joints with entrainment speed

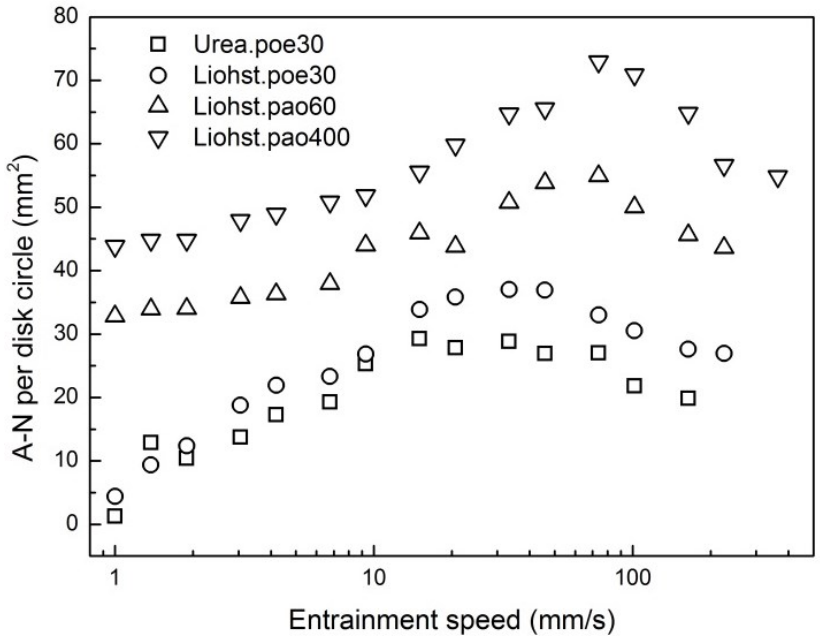

Figure 3.18 Variation of finger area near the center of track with entrainment speed

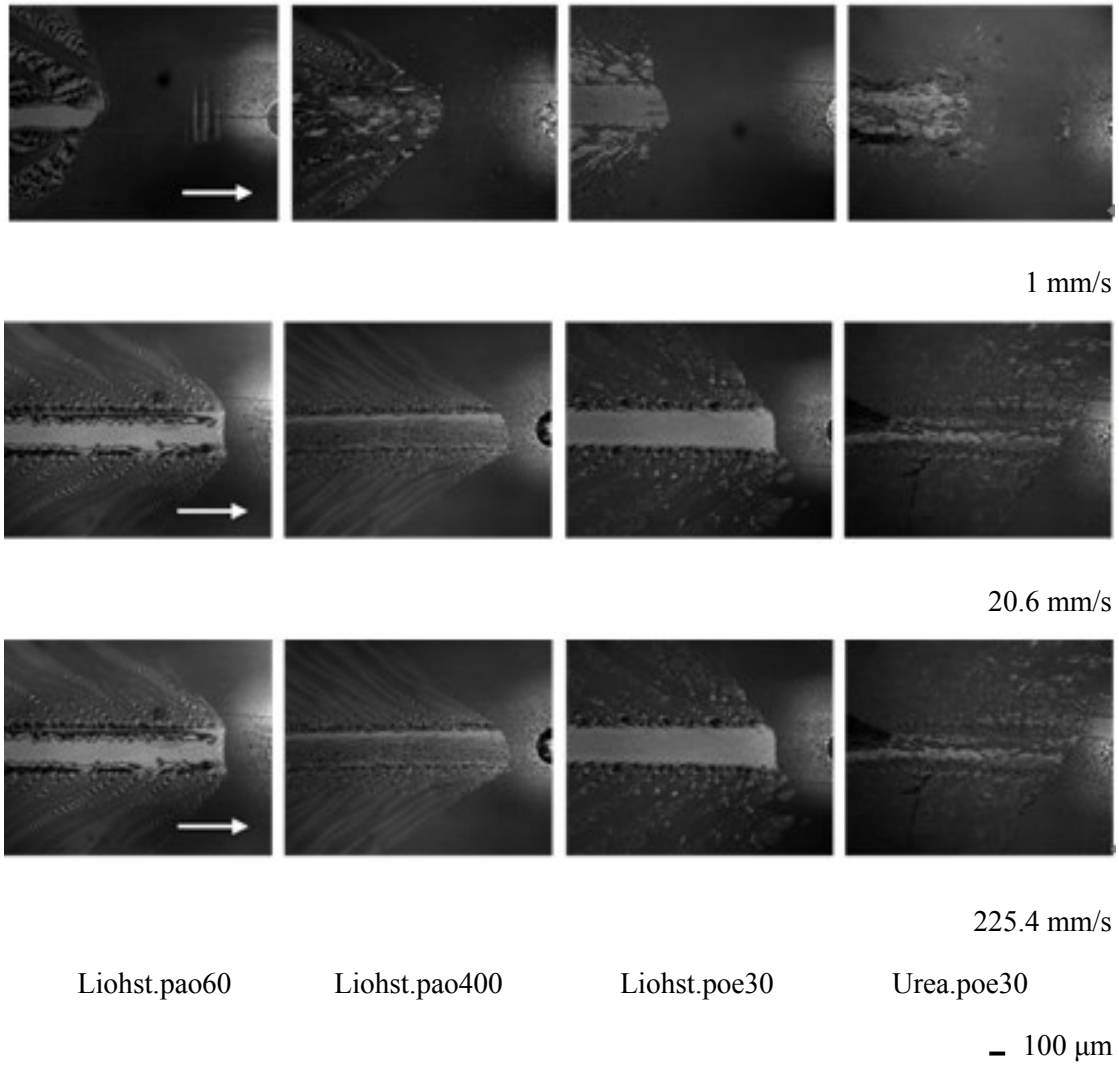

Figure 3.19 Speed evolution of the inlet patterns for slide to roll ratio 0.4

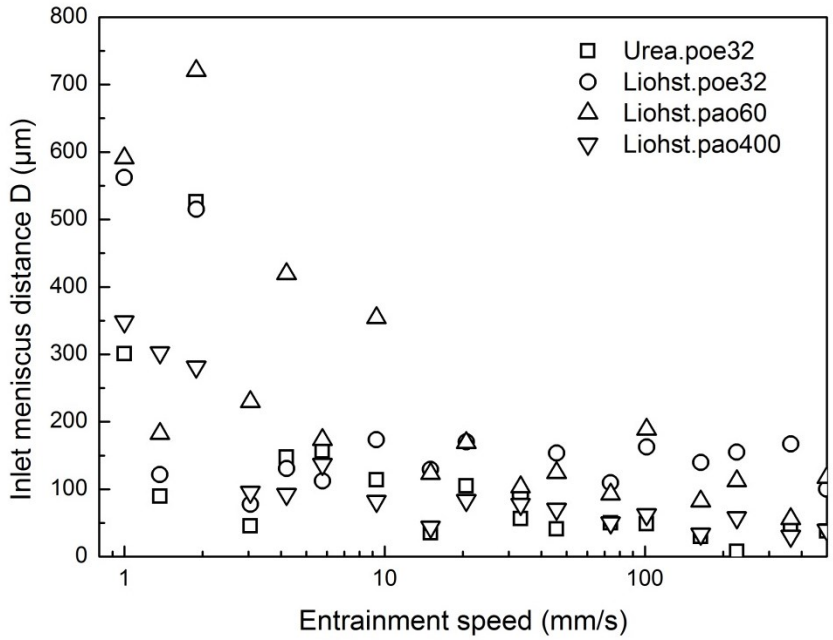

Figure 3.20 Variation of the inlet meniscus distance with entrainment speed

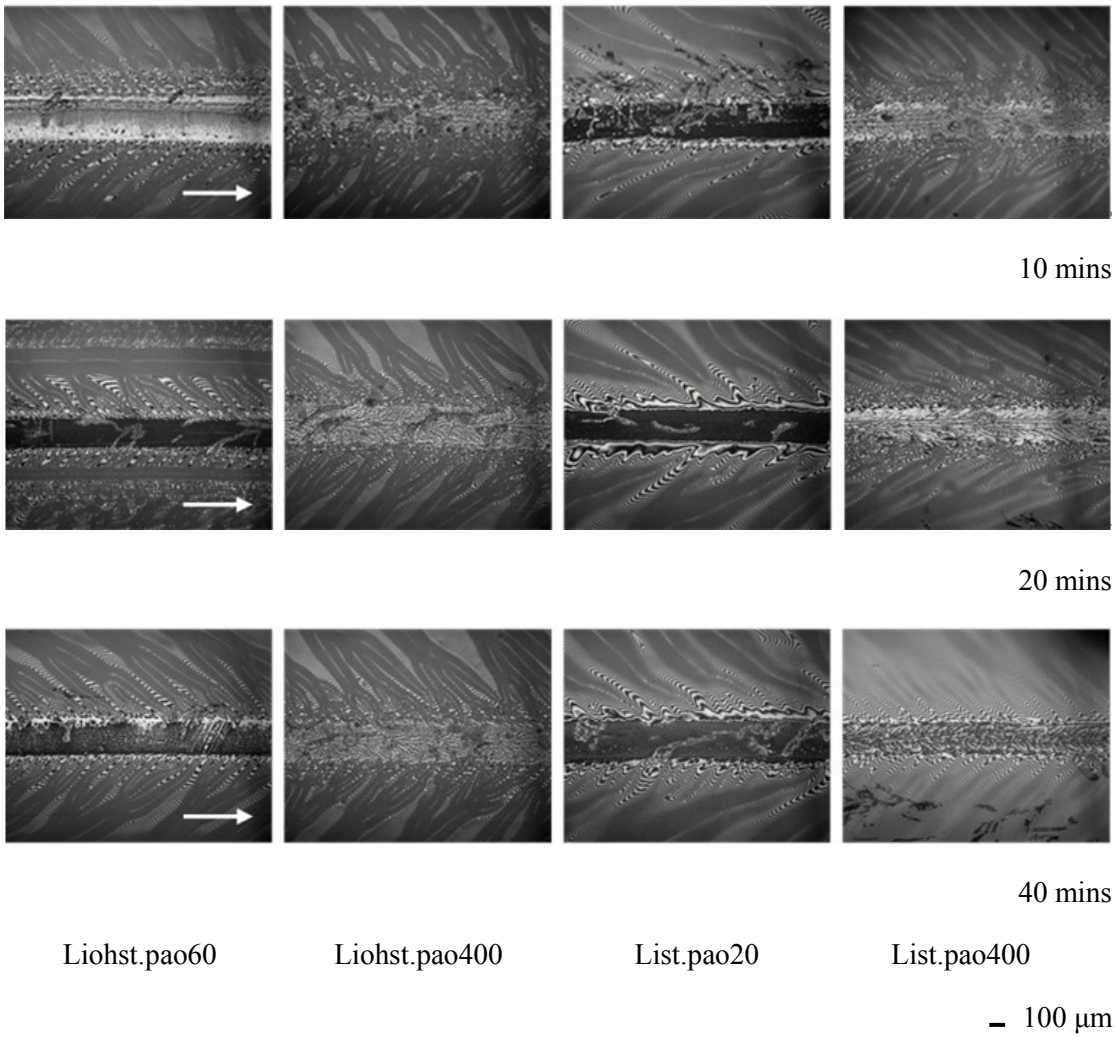

Figure 3.21 Time evolution of the upstream pattern at entrainment speed of 47.1 mm/s in

pure rolling state

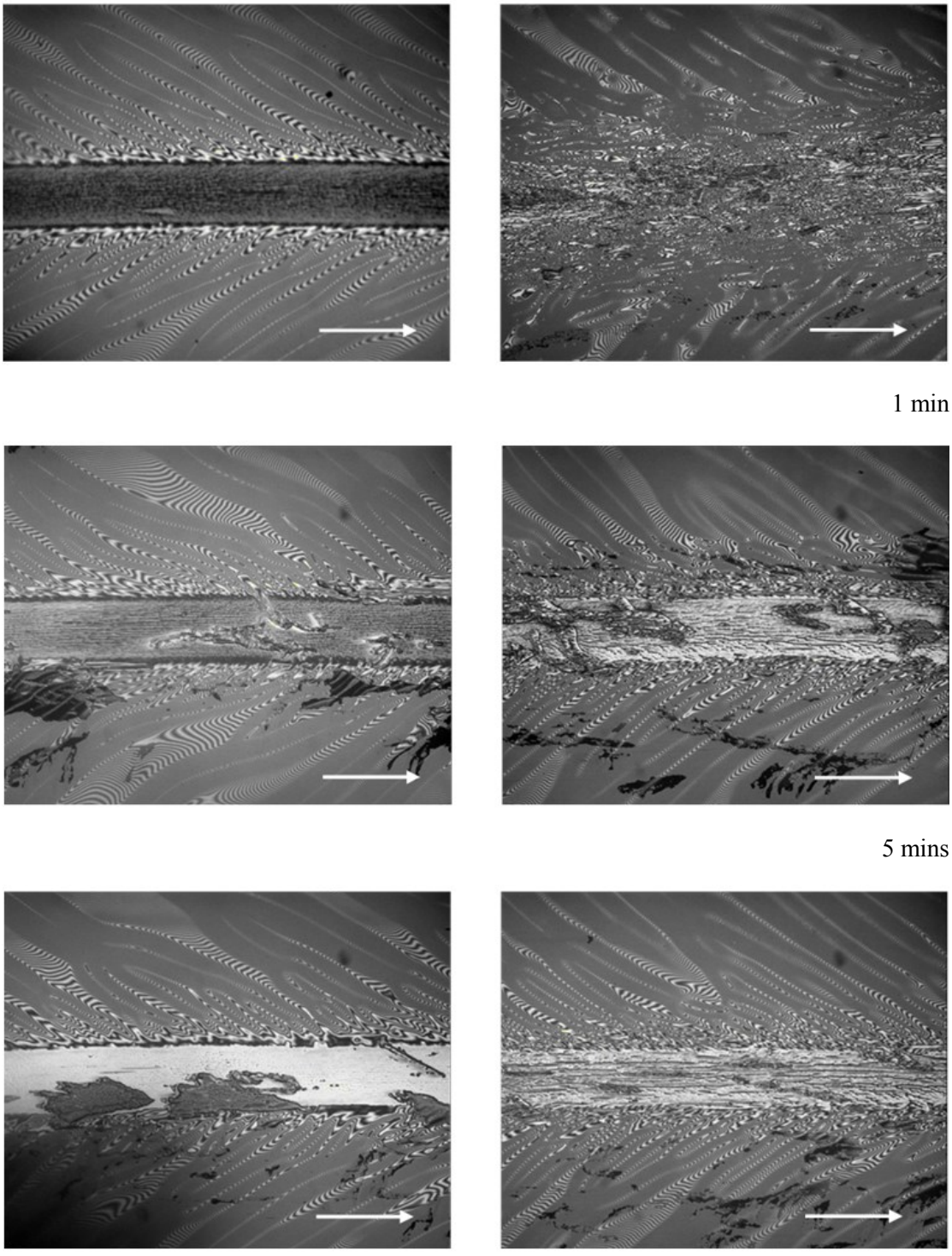

Figure 3.22 Time evolution of the upstream pattern at entrainment speed of 47.1 mm/s for slide to roll ratio 0.6

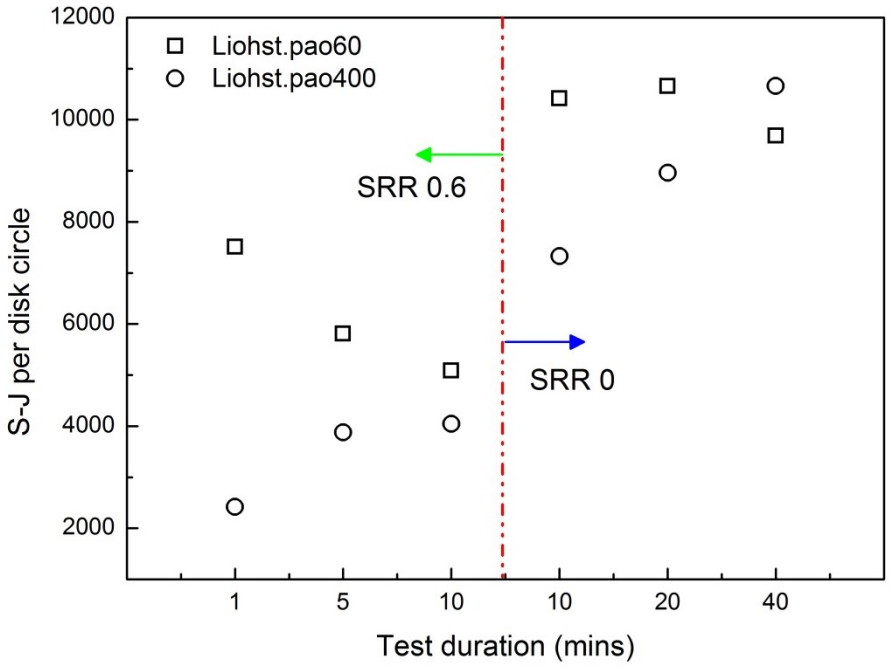

Figure 3.23 Variation of the number of finger split joints with test duration

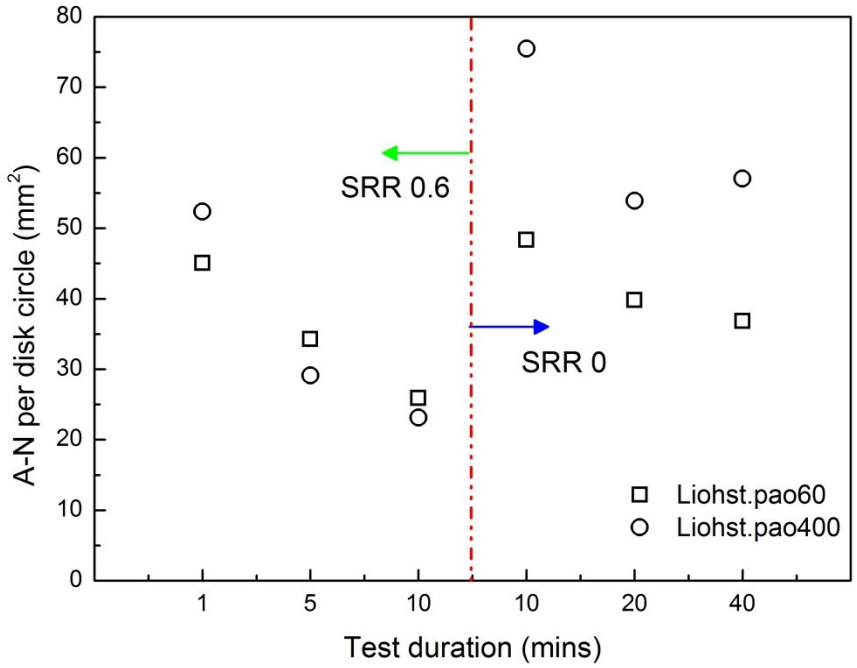

Figure 3.24 Variation of finger area near the center of track with test duration

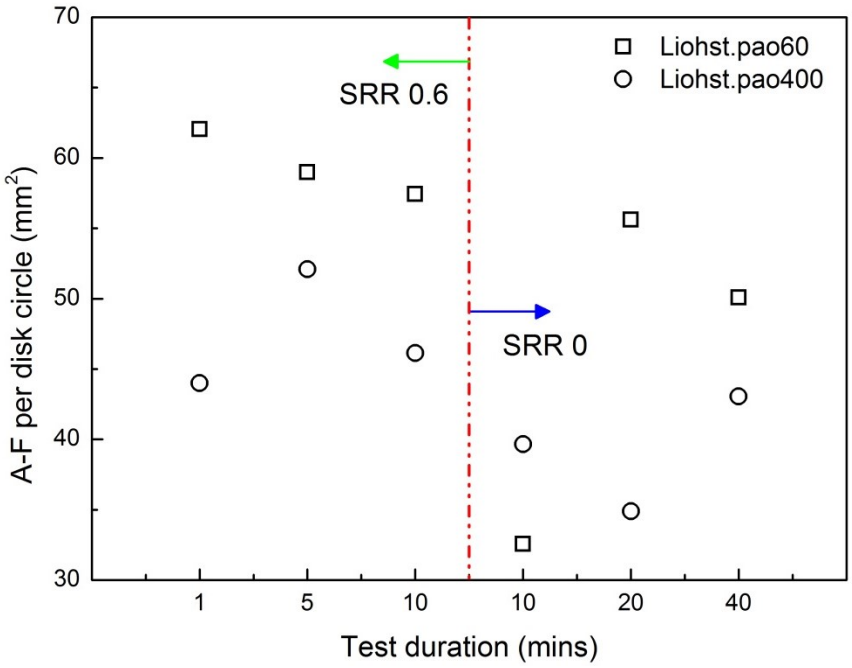

Figure 3.25 Variation of finger area far from the center of track with test duration

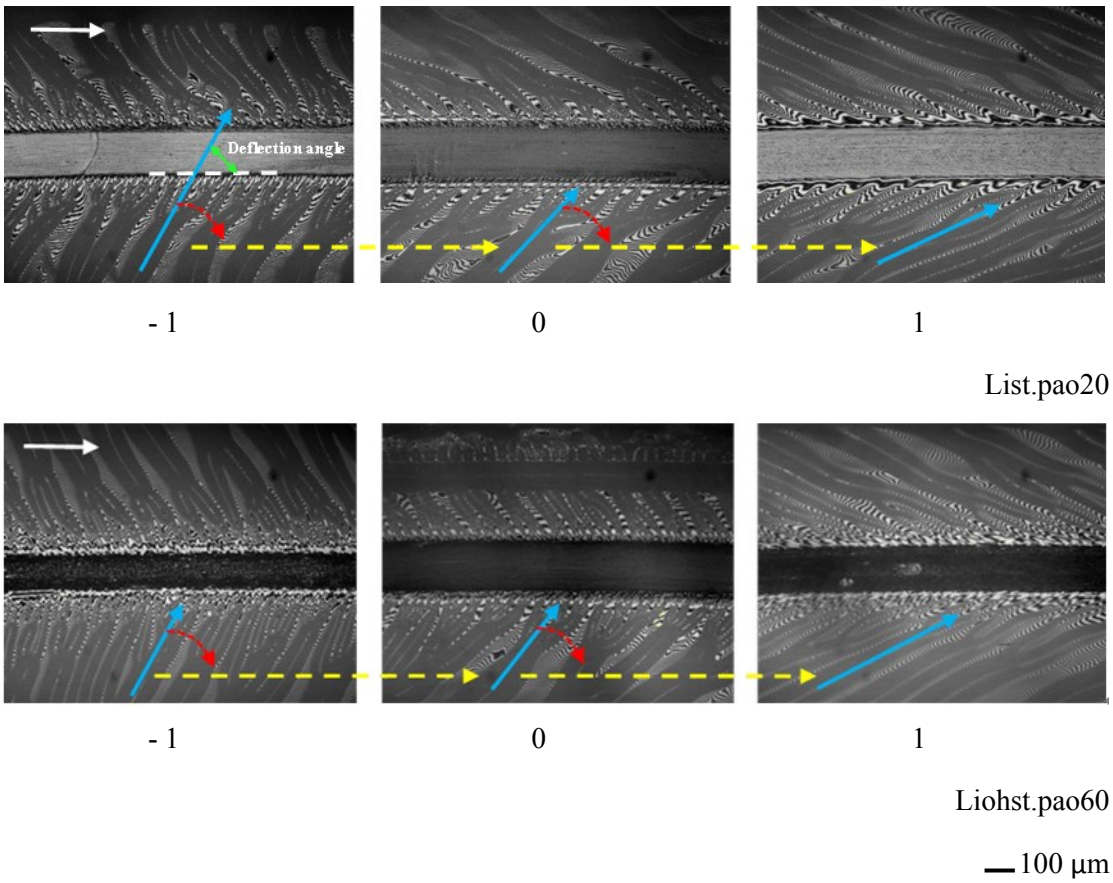

Figure 3.26 Variation of upstream pattern with slide to roll ratios at entrainment speed of 47.1 mm/s

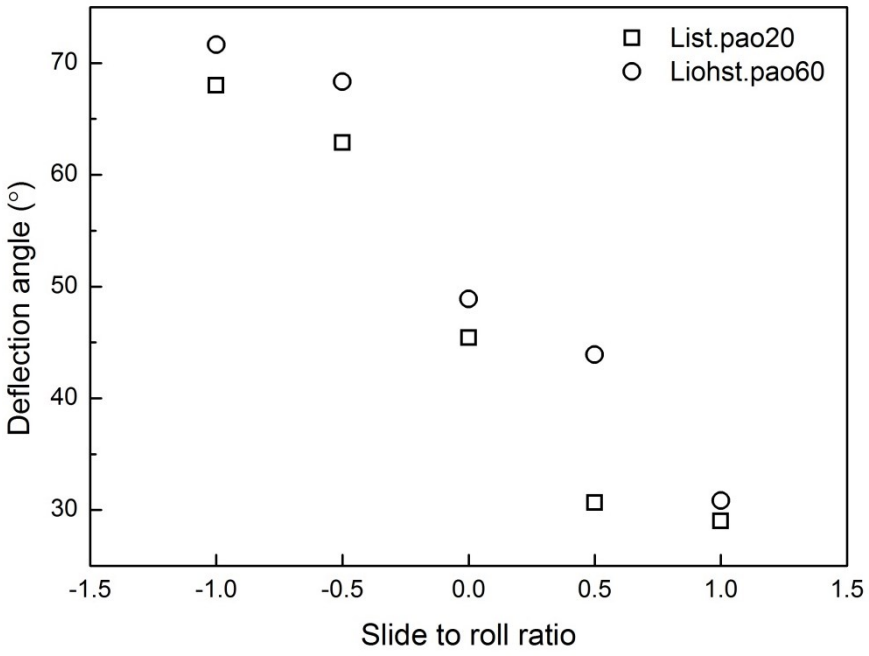

Figure 3.27 Variation of deflection angle with slide to roll ratio

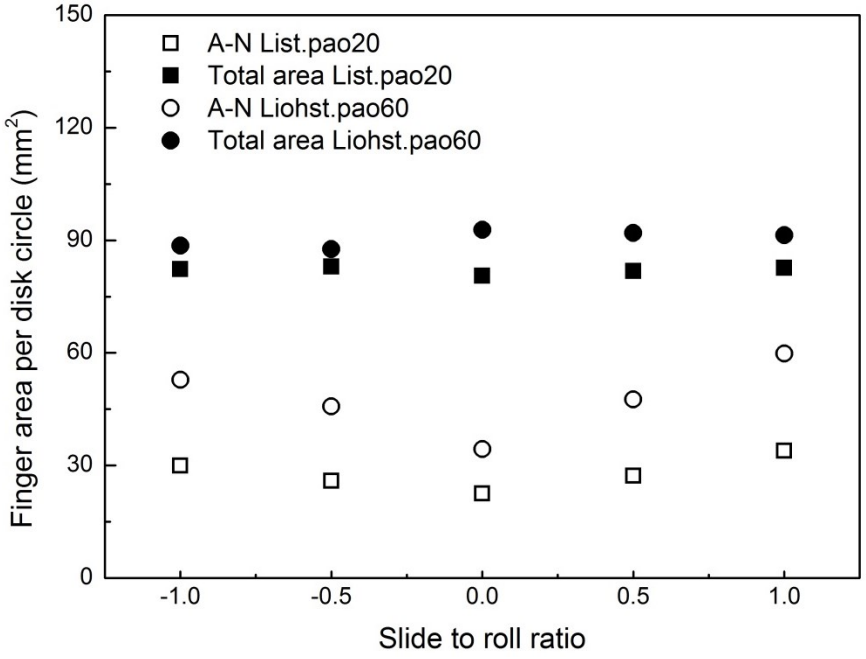

Figure 3.28 Variation of finger area with slide to roll ratio

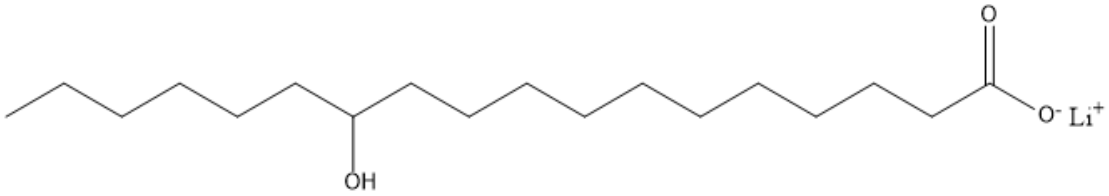

Liohst

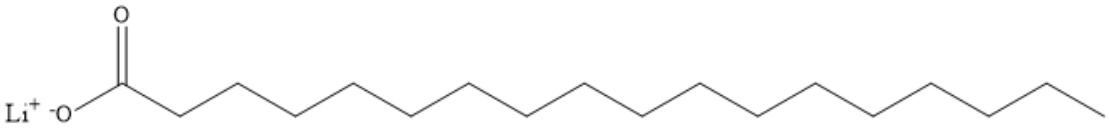

List

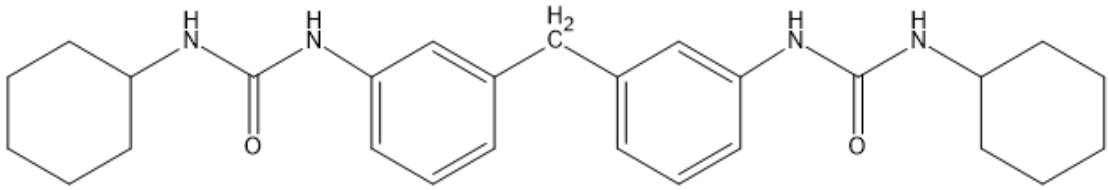

Di-urea

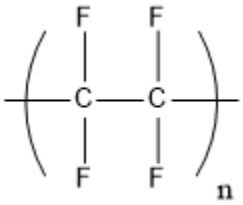

PTFE

Figure 3.29 Chemical structures for greases with different types of thickeners

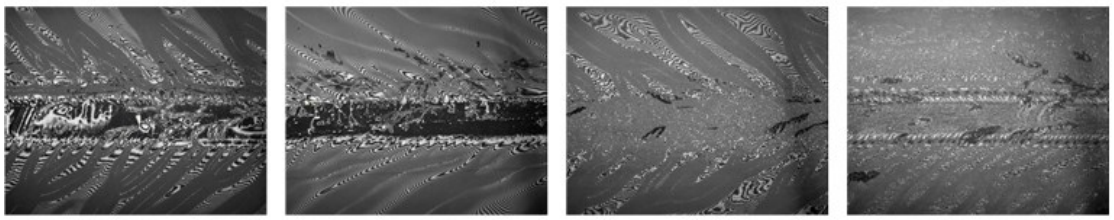

Liohst.pao30 List.pao20 Di-urea.pao30 PTFE.PFPE

100 μm

Figure 3.30 Track patterns for greases with different types of thickeners

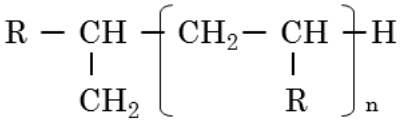

PAO

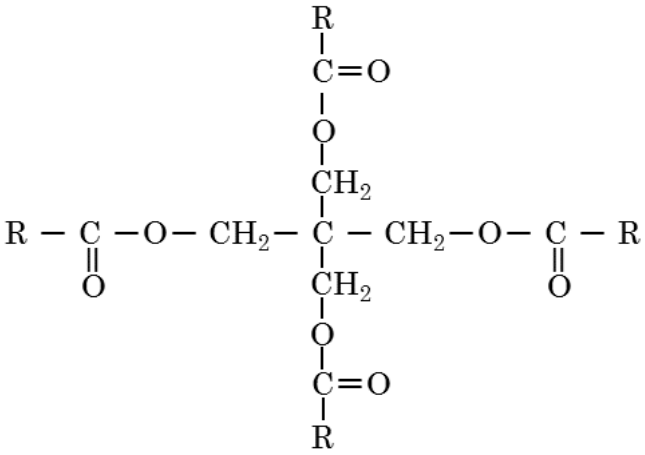

POE

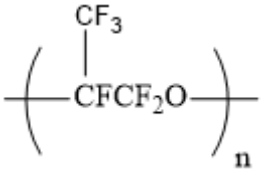

PFPE

Figure 3.31 Chemical structures for greases with different types of base oils

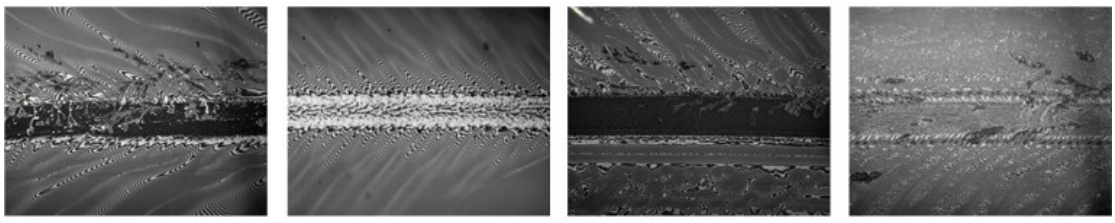

List.pao20 List.pao400 List.poe30 PEFE.PFPE

100 μm

Figure 3.32 Track patterns for greases with different types of base oils

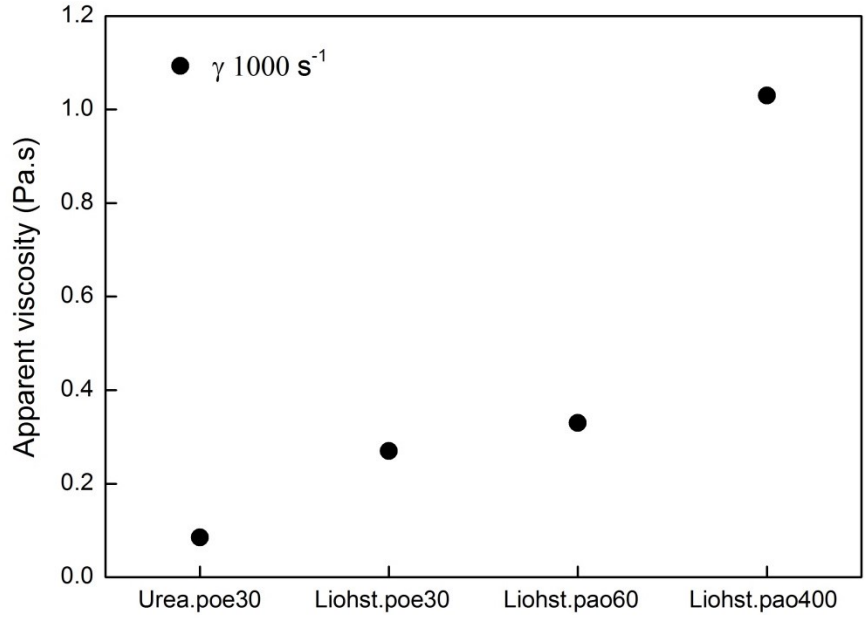

Figure 3.33 Apparent viscosities for test greases at the shear rate of 1000 s^{-1}

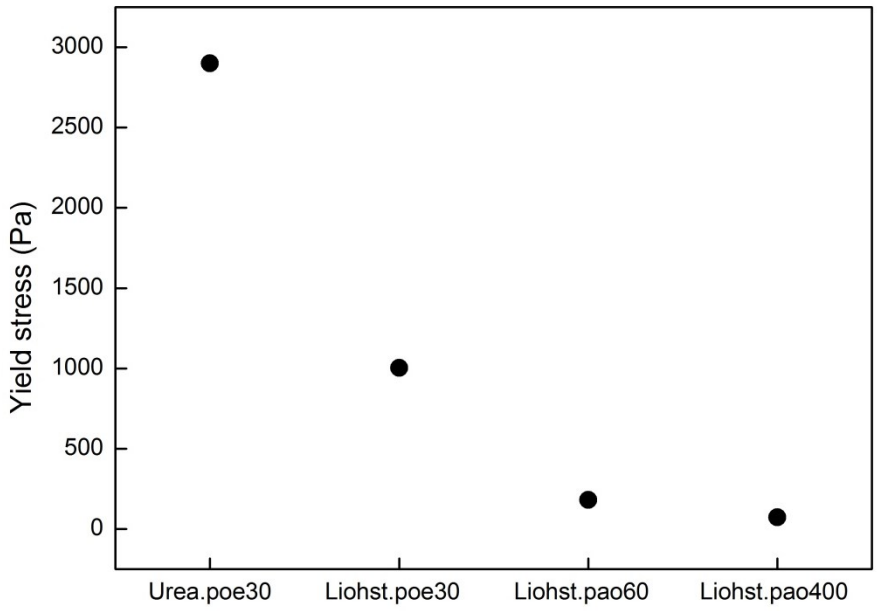

Figure 3.34 Yield stresses for test greases

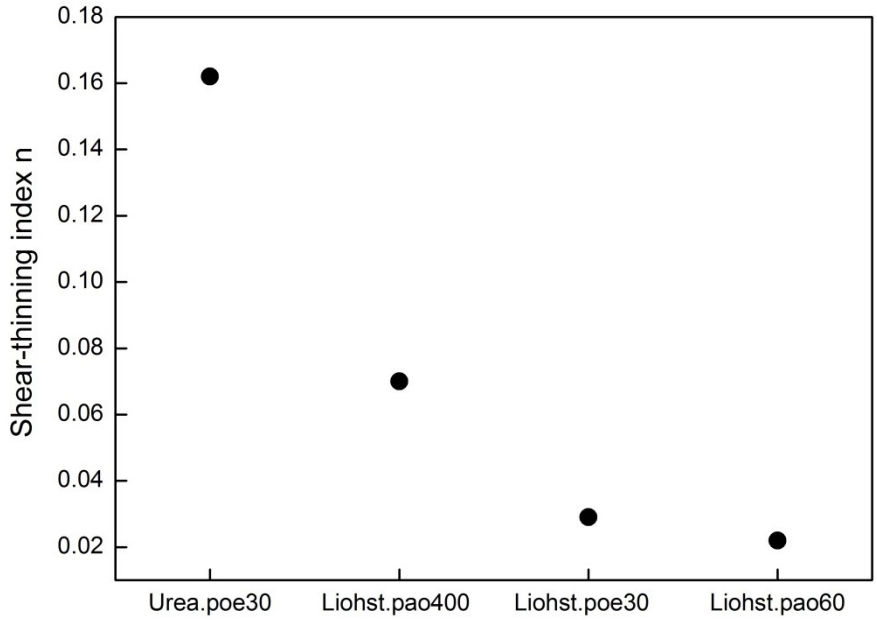

Figure 3.35 Shear-thinning indexes for test greases

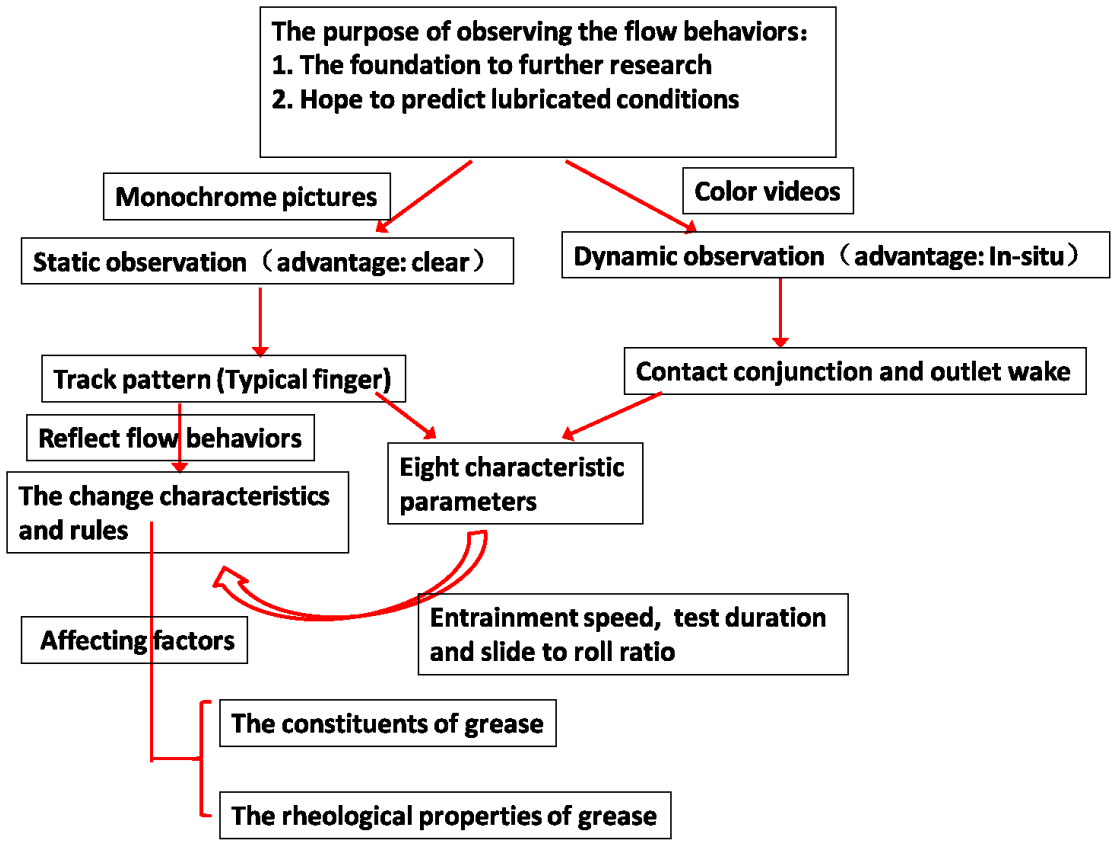

Figure 3.36 The flowchart for chapter 3

CHAPTER 4

The correlation between grease flow behaviors and the corresponding lubricating conditions

Abstract

The optical interferometry is employed to determine grease EHL film thickness in the ball-on-disk test rig. A pair of scoops is also used for artificial replenishment in additional tests in order to understand the changes occurring in lubricant starvation without the artificial replenishment. Through the film thickness data, the relationships between the track patterns and lubrication mechanisms are found. At higher speed, lubricant starvation and finger-loss occur. The starvation speeds are always lower than the finger-loss speeds.

The apparent viscosity of the grease at low shear rate in the inlet zone has a great impact on the resupply of the greases and the starvation speed. The results suggest that the grease finger provides supply to the contact area and the side reservoir, and one part of grease finger that lies near the center of track plays the main role. In addition, the thickener deposition in the center of track plays a positive role in the film formation with some types of greases, especially the Urea greases.

4.1 Introduction

Grease flow has influence on every aspect in lubrication. The most important function of a lubricating grease in machine components is to form a film separating the interacting surfaces such that excessive friction and overheating do not occur which lead to failure and damage. Certainly, the life of real machine component is related with its structure and the operation environment, etc.

Many factors can lead to the degradation of it, such as the persistent high friction coefficient can lead to overheating and unnecessary energy consumption. However, improper lubrication will cause more harm. Especially in grease lubrication, once the grease is pushed aside by the passage of a rolling element during the initial phase of operation, the low mobility of grease prevents it from turning back to the contact point easily. Thus starvation occurs easily.

At present, there is no consensus on the mechanisms of film formation process in the starved regime, and on the influence of the behaviors of lubricants in the space surrounding the contact from which the lubricant is supplied on lubrication performance. The grease distribution on the track directly affect the amount of lubricant can enter the contact area, and also reflects the state of the lubricating contact.

Single point contact using optical interference is widely applied in grease researches. Although its structure is different from real machine component, its basic process and the visual in-situ flow information are both very important for in-depth studies. The lubrication mechanisms in starved regime are complicated.

The rate at which lubricant is entrained and the rate at which it is lost around the contact, *i.e*. the feed and loss rates have been deemed as the determining factors for the degree of starvation in grease lubrication [1]. Starvation occurs when the rate of loss higher than that of feed. It is generally believed that both the thickener and the base oil participate in film formation. Wedeven *et al.* [2] showed that film thickness in starved elastohydrodynamic contact could be predicted using the inlet distance S which was defined as the distance from the position of the inlet meniscus boundary to the edge of the contact.

In oil lubrication, several authors [3-5] model the feed mechanism by assuming that the interacting surface is covered by a uniform layer of lubricant, and that the ball contact produces a depressed oil layer shape, two adjacent side oil ridge lie beside the ball. Surface tension and viscosity [3], Van der Waals forces [4] and centrifugal forces [5] are assumed to be the driving forces to draw adjacent oil back to contact zone.

In grease lubrication, things are more complex due to the participation of the thickener. Kaneta *et al.* [6] studied the effect of thickener structure of Di-urea greases on the formation of non-uniform EHL film. Kimura *et al.* [7] controlled the thickness of the thickener fibers through the optimization of the heating-cooling conditions in its manufacturing process. Yokouchi *et al.* [8] and Oikawa *et al.* [9] studied the effect of fiber length, and showed that the grease with longer soap fibers was more easily entrained into the contact and showed favorable lubrication with low friction coefficient. So far, there has been little research on the track pattern. The purpose of this chapter is to understand the relation between grease flow and lubricating conditions in the starved regime.

4.2 Experimental methodology

In order to observe the grease flow behavior and get the corresponding lubrication conditions. The optical interferometry technique is used to measure film thickness, so the information about the lubricating conditions can be acquired. The experimental methodology and other details for this chapter are listed in the following contents. For the basic experimental procedures, please refer to section 3.2 of Chapter 3.

4.2.1 Film thickness measurements

The measurement of film thickness has great implications for the evaluation of the lubrication conditions. The ratio of its value to the composite surface roughness of two contact surfaces is direct relation to the lubrication regime of the contact conjunction [10]. The lubrication mechanisms for different lubrication regimes vary greatly. Therefore, the first step is to get the accurate value of film thickness.

The EHL film thickness used in this chapter is experimentally acquired by two methods which are all variants of the optical interferometry technique. In Chapter 3, we have adopted a series of video observation experiments and these of static. The video tests use a white light source, the obtained data are color videos, the in-situ flow behaviors around the contact zone can be observed. The static tests use a green light source, the obtained data are monochrome pictures, the detail track pattern leaved by the grease flow can be observed. Two methods are done to know the film thickness of these two series of experiments, respectively.

The first method is called spacer layer imaging method (SLIM), its calibration translate the RGB (Red, Green and Blue) values into Hue values. This translation can make the film thickness to be obtained without being influenced by the variation of the light intensity. Its measurement is based on the color picture cut from the video tests.

Another method is called relative optical interference intensity (ROII), its calibration needs to measure the maximum interference intensity and that of the minimum for each different interference orders. This measurement is based on the monochrome picture during the test which with the experimental setup of static tests.

Therefore, the in-situ film thickness can be acquired for these two series of tests when two measurement methods are adopted. The errors come from the different tests thereby are

removed. The fundamentals of optical interferometry and the application of the optical interferometry to the measurement of the film thickness of the EHD contacts are described in these papers [11-16]. The following contents will mainly illustrate the calibration procedures in practical use.

4.2.1.1 Spacer layer imaging method

Figure 4.1 shows the color image of the interference of the static contact. As can be seen from this picture, the colors of its rings are distributed evenly. The RGB values of the line AB are translated into Hue values [17]. Figure 4.2 plots the Hue values of the line AB versus the distance from the center. The relative stable Hue values at the center correspond to the contact center, *i.e.*, zero film thickness. The sharp increase of Hue values around the positive and the negative 100 μm correspond to the gap distance between two surfaces. Figure 4.3 shows the relationship between Hue values and the gap distances. The calculation of gap distance is provided by Hertz theory [18].

Every unidirectional variation of Hue values starts from the zero gap distance correspond to the color rings as shown in Figure 4.1. These rings outward from the center are called first order, second order…, respectively. Figure 4.4 shows the calibration curve for 1st order. Not all pictures can get the film thickness. We should choose the picture with a uniform color in the contact zone. This also applies to other film thickness measurement methods.

4.2.1.2 Relative optical interference intensity method

The detail of relative optical interference intensity method can be found in these papers [19, 20]. Figure 4.5 shows the principal schematic of the two-beam optical interference. Equation 4.1 lists the basic expression of optical interference under the vertical incidence condition. Where I is the measured interference intensity, I_1 and I_2 are light intensity values of beam I_1 and beam I_2, respectively, λ is the wavelength of the monochrome light, k is the refractive index of the lubricant and Φ is the phase change caused by the coated layers and the steel ball, h is the film thickness to be measured. The value of λ is 520 nm and k is 1.4 in this study. Therefore, the film thickness can be acquired when I_1, I_2 and Φ are known. As the film thickness is zero, the relative light intensity (equation 4.2) is denoted as $\bar{I}_0$, and Φ can be calculated as equation 4.3. Here, n is defined as the interference order. The film thickness h is

described as equation 4.4.

$$I = I_1 + I_2 + 2\sqrt{I_1 I_2}\, cos(^{4\pi kh}/_{\lambda} + \Phi) \tag{4.1}$$

$$\bar{I} = \frac{2I - (I_{max} + I_{min})}{I_{max} - I_{min}} \tag{4.2}$$

$$\Phi = arccos(\bar{I}_0) \tag{4.3}$$

$$h = \frac{\lambda}{4\pi k}\{n\pi + [arccos(\bar{I}) - arccos(\bar{I}_0)] \cdot cosn\pi\} \tag{4.4}$$

where $n = 0, 1, 2 \ldots \ldots$

An interference image at stationary contact is shown in Figure 4.6. Figure 4.7 shows the light intensity distribution of the line CD along the centerline of the contact region and the corresponding gap distance. As it can be seen that I_{max} and I_{min} are not uniform in the different interference orders outside of the point contact area, and the maximum light intensity value I_{max} becomes smaller and smaller and the minimum light intensity value I_{min} becomes larger and larger with increasing interference order n. The calibration process should be carried out to determine the I_{max} and I_{min} in the contact area for each interference order. Figure 4.8 shows the calculation results and the gap distance provided by Hertz theory. The theoretical results agree well with the measurement results.

4.2.2 Starvation measurements

This chapter will put an emphasis on the issues of starvation and replenishment. Firstly, both the method of artificial replenishment and the definition of the critical state between fully flooded condition and starved condition are introduced in the following contents.

4.2.2.1 Artificial replenishment

The lubrication mechanisms in fully flooded state are much simpler than these in starved state. The knowledge of them in fully flooded state is conducive to exploring and understanding the lubrication mechanisms in starved state. In order to prevent the starvation occur, a pair of scoops are pressed up against the underside of the disk near the inlet contact zone as shown in Figure 4.9. The wedge-shaped structure will help to channel grease back to the contact zone, and thus provides enough grease to maintain the lubricating film.

4.2.2.2 Define starvation

Two methods are adopted to define the initiation of starvation in this study. The first one is

shown in Figure 4.10. The film thickness of Liohst.pao60 as a function of entrainment speed and that of the corresponding base oil predicted by Hamrock-Dowson [21] are plotted. The film thickness of grease starts to approach the predicted line with the increase of speed. In the higher speed regime, the entrainment speed which corresponding the film thickness of grease reduces obviously is deemed as the starvation speed.

However, the film thickness of grease could not be predicted in many test conditions, such as, the extension of test duration. In these situations, a new method is needed to evaluate it. A dimensionless parameter $m*$ is used to define the critical state between fully flooded state and starved state. The calculation method is shown as equation 4.5 [21]. R_1 and a are the radii of the ball and the contact, respectively. The central film thickness divided by the radius of the ball is expressed as $H = h_c / R_1$. The inlet distance S is defined as the distance between the contact radius and the lubrication meniscus during test, and it is shown in Figure 4.11. If $S + a \geq a \cdot m^*$, the contact is fully flooded; if $S + a < a \cdot m^*$, the contact is starved.

$$m^* = 1 + 3.06 \times ((R_1/a)^2 \times H)^{0.58} \quad (4.5)$$

4.2.3 Friction coefficient

The separating gap between surfaces can be known directly by film thickness, whereas the friction coefficient can reflects the in-situ rheological properties of lubricant in the contact zone. The value of friction coefficient is proportional to the energy consumption in the contact. For the life of machine elements, the study of the energy consumption by friction has practical meaning. The definition of friction coefficient μ is listed in equation 4.6. It is the ratio of traction force F divided by the load W [10]. F is the sum of shear stress τ in the contact area A, it can be obtained by the sensor underneath the ball carriage. W is the sum of load p in the contact area A. The value of load W keeps a constant 10 N in this study.

$$\mu = \frac{F}{W} = \frac{\int\int_A \tau dxdy}{\int\int_A p dxdy} \quad (4.6)$$

As known that traction force measurement is very sensitive compared to the measurement of the steady state film thickness. The value of it will continuously change as the test progresses. Thereby, the disk revolution is regarded as the unit, the acquired data is the average value for one disk revolution. The final used F is the average value for at least 20 revolutions for most cases. Through this process, a reliable data can be obtained.

4.3 Artificial replenishment

4.3.1 Entrainment speed dependence of film thickness

4.3.1.1 Film thickness and its corresponding flow behaviors

Figure 4.12 shows the entrainment speed dependence of film thickness for four test greases in fully flooded state, and the dashed lines are the film thickness of their corresponding base oil which predicted by EHL theory. At the low speed range, in our tests is lower than 10 mm/s, their curves show a V-shape and their values are much higher than these of the base oils, the grease film thickness first decreases then increases with the increase of entrainment speed.

As the entrainment speed increases, the film thickness for most of greases will approaches to the predicted line of the base oil, and always keeps higher than it. The film thickness of Urea.poe30 and that of Liohst.pao400 are much higher than that of other two greases. Among four test greases, only the film thickness of Urea.poe30 is much higher than the predicted line of base oil throughout the speed range. The track center on the right side of contact zone for Urea.poe30 is also blurred. It is obviously looks different from the others. It is speculated that this is influenced by the thickener. The details on the observation are listed as follows.

Figure 4.13 shows the speed evolution of the contact center for test greases in fully flooded state. In general, it is frequently observed that some thickeners pass through the contact center for Liohst.pao400 and Urea.poe30. This is particularly evident in the low speed range. As it shows in the pictures at the entrainment speed of 1 mm/s and 4.2 mm/s, Liohst.pao400 can often find the stripe-like or dot-like object with black edge pass the contact zone, whereas the contact center of Urea.poe30 always keep irregular ripple shape.

The case for Urea.poe30 seems different from that for Liohst.pao400. It is more likely that the thickener of Urea.poe30 are deposited or adsorbed on the surface of disk rather than pass through the center of contact zone as the others. A model proposed by Cann *et al.*[21] is that the grease-lubricated contacts are layered by a shear degraded residual thickener layer and an oil layer formed by hydrodynamic action.

In our tests, Urea.poe30 conforms to this model, this is perhaps the reason its film thickness behaviors different from that of the others. Besides, from 1 mm/s to 4.2 mm/s, the film thickness of test greases decreases as shown in these pictures, after then gradually increases.

They are consistent with the film thickness results. As the entrainment speed increase, both Liohst.pao60 and Urea.poe30 can see the characteristic horseshoe shape in the contact center.

Figure 4.14 shows the speed evolution of the track pattern for test greases in fully flooded state. In lower speed regime, the basic features of their track pattern are not much difference with these in the entrainment speed series tests in Chapter 3. However, in the high speed range, the completeness of the track pattern can be maintained at high speed, the complexity of track pattern slight increases in the test with artificial replenishment. These are in contrast to the entrainment speed series tests in Chapter 3. It confirms the speculation that the integrality of finger pattern is dependent on the state of the lubricating contact. Because there is no any artificial replenishment method adopted in Chapter 3, it is natural that starvation occur especially when the entrainment speed is high.

Another difference is the thickener deposition in the center of track. With artificial replenishment, the thickener deposition in the center of track will not decline and disappear. On the contrary, as the entrainment speed increase, there are some thickener deposition appear gradually in the center of track for Liohst.poe30 and Liohst.pao60. Their track centers are covered with many tiny needle-like objects and all toward the direction of motion of the specimen surfaces.

The deposition of Urea.poe30 and that of Liohst.pao400 also become smoother and more orderly compared to these at low speed. The thickener suffered repeated shear action will become tiny fragment, thus easier flow with their base oils. In general, except the finger can be retained, the role of thickener in the film formation process could not be diminished. The film thickness of grease, hence, always higher than the film thickness predicted line of the base oil.

Figure 4.15 shows the speed evolution of the contact center for test greases in fully flooded state in video series tests. The overall color of Urea.poe30 and that of Liohst.pao400 are darker than these of other greases, and their contact centers show irregular ripples. The thickener depositions for them are also obvious. At high speed, all greases can maintain the complete wake.

4.3.1.2 The transition speed

The transition speed refers to the entrainment speed which corresponds to the lowest point in V-shape curve as it shows in Figure 4.12. Their details are listed in Table 4.1, all within 10 mm/s. The greases with the same thickener but different base oils like Liohst.pao60 and Liohst.poe30, the greases with the same base oil but different thickeners like Liohst.poe30 and Urea.poe30, the difference of the transition speed in these two groups all varies small.

However, the difference between the transition speed of Liohst.pao60 and that of Liohst.pao400 is large. It thus infers the factor that may affect the value of transition speed is viscosity. Recently, the experiment results of Hui cen *et al*. [22] shows that the transition speed can be postponed with the increment of temperature. It is generally believed that the increment of temperature stands for the decrease of grease viscosity, therefore their experiment results provides support for our viewpoint.

Table 4.1 The transition speed for test greases

	Liohst.pao60	Liohst.poe32	Urea.poe30	Liohst.pao400
Transition speed (mm/s)	3.05	4.2	5.77	6.77

The significance of the transition speed is that it distinguishes two different lubrication regimes. In general: Lower than the transition speed, the film thickness is decrease with the entrainment speed. In this regime, the film thickness mainly consists of thickener, chemical aging is primary [23]. Whereas higher than the transition speed, the film thickness is increase with the entrainment speed; in this regime, the film thickness mainly consists of base oil, physical aging is primary [23]. In different regimes, the lubrication mechanisms are different, thus they need be treated differently.

4.3.2 Revolution dependence of film thickness

4.3.2.1 Film thickness and its corresponding flow behaviors

Figure 4.17 shows the revolution dependence of film thickness for Liohst.pao60 under different SRRs. The entrainment speed keeps constant as 47.1 mm/s. As shown in this figure, the film thickness will decrease sharply in the first few revolutions, and then the film thickness almost does not change. This kind of phenomenon is very common for grease lubrication especially in lab test.

The first thing to consider is that the film thickness of grease applied to the surface of disk

before test (usually millimeter) is much thicker than the hydrodynamic film (usually nanometer). Another reason is that the thickener sucked into the contact zone or the thickener on the center of track can also raise the thickness.

However, as the test continues, the excess greases are pushed to both sides of the contact center. Due to the adhesiveness property of grease, the amount of grease flow back into the contact track center becomes limited, thus the film thickness is gradually stabilized. The pictures and the data selected in this section are all in steady state after at least five revolutions.

Table 4.2 The lubrication conditions under different SRR

SRR	$(S+a)-a\cdot m^*$	Lubrication condition
-1	64.85	Fully flooded
-0.5	76.93	Fully flooded
0	67.39	Fully flooded
0.5	60.91	Fully flooded
1	73.93	Fully flooded

Figure 4.17 shows the inlet area and the track pattern. Table 4.2 shows the value of $(S+a)-a\cdot m^*$, as explained in experimental methodology, if $S+a \geq a\cdot m^*$, the contact is fully flooded. Therefore, all the contact points in different SRRs are in fully flooded conditions. As we have known, the change of SRR will bring profound changes on the deflection angle. The deposition when SRR = 0 is lighter than that when SRR $\neq$ 0.

Moreover, Table 4.3 summarizes some parameters from SRR -1 to SRR 1 for Liohst.pao60. The total finger area for track pattern almost not change, whereas the lowest point for the near finger area (A-N) corresponds to SRR 0, and it continues to increase when the absolute value of SRR changes from 0 to 1. The film thickness is different for different SRR. It is the highest when SRR = 0. This is because the shear action is inevitable under slide-roll condition.

When SRR = $\pm$1, the shear rate is around 100000. When SRR = $\pm$0.5, the shear rate is around 50000. The difference is significant between slide-roll condition and pure rolling condition. It makes the viscosity when SRR $\neq$ 0 always lower than that when SRR = 0. Therefore, the film thickness is the highest when SRR = 0.

Table 4.3 A summary of parameters for Liohst.pao60 under different slide to roll ratios

SRR	-1	-0.5	0	0.5	1
A-N (mm^2)	52.83	45.73	34.34	47.62	59.81
A-Total (mm^2)	88.6	87.64	92.87	91.98	91.38
Film thickness (nm)	46.84	51.23	65.82	57.41	54.28
Shear rate (s^{-1})	106746	48799	0	43546	92115

It is noticed that the film thickness of positive SRR h_{SRR+} is always higher than that of negative SRR h_{SRR-}. The temperature–viscosity wedge effect is deemed as the reason for this phenomenon [24]. If two contacted surfaces move with different speeds, the faster the surface with higher thermal conductivity moves, the lower central film thickness it will form.

4.3.2.2 The initial of wake formation

Figure 4.18 shows the wake pattern formations with time for Liohst.pao60 in different SRR. The open time for the enclosed cavity will be delayed while the contact under slide-roll condition. The enclosed cavity will totally open and forms a fan shape wake around 100 ms. Among them, the open speed for negative SRR is slower than that for positive SRR.

However, there is no obvious difference between them can be seen from these video images after 100 ms. Whether this instantaneous difference has the long-term effects on the lubricating function, actually it could not be concluded. However, there is no similar phenomenon is published until now.

4.3.3 Friction coefficient

Figure 4.19 shows the average friction coefficient values for test greases at the entrainment speed 47.1 mm/s, SRR 0.4, test duration 40 mins. According to the data, the friction coefficient for test greases is almost a constant during 40 mins test, thus these data can be used to represent the whole process. In general, the main influencing factor on the friction coefficient is the type of thickener. In addition, the viscosity of the base oil will also lead to a change in the friction coefficient.

As it shows, three Liohst-based greases: The friction coefficient of Liohst.pao400 and that of Liohst.poe30 are very close to each other, and that of Liohst.pao60 rises almost a third on that of Liohst.pao400. This illustrates for the greases with the same thickener type, the

viscosity of the base oil has a greater impact on the friction coefficient than the type of base oil. Moreover, there are obvious differences among List.poe30, Urea.poe30 and Liohst-based grease. It indicates that the thickener type has a great impact on the friction coefficient.

Figure 4.20 shows the track patterns for test greases which correspond to Figure 4.19. The track pattern of Urea.poe30 is quite different with other four greases. The contrast between the finger part and the interferences between fingers is not obvious. Liohst.pao400 has heavy deposition in the center of track. In general, there is no obvious connection between the track pattern and the friction coefficient can be found.

Figure 4.22 shows the entrainment speed dependence of friction coefficient for test greases, SRR 0.4. As it shows, the friction coefficients are rather scattered within 5 mm/s, especially for Urea.poe30 and Liohst.pao400. The transition speed in the V-curve (the entrainment speed dependence of film thickness) has been discussed in the previous contents. These scattered friction coefficients are all around the transition speed. It means the thickener has great impact on the friction coefficient.

Higher than the transition speed, the friction coefficients for test greases first decrease and then increase. When load keeps constant, the friction coefficient is related with the film thickness and the shear stress in the contact area. However, the dynamic shear stress could not be obtained, thus the yield stress is used to explain the whole process.

The sequence of the relative friction coefficient for four test greases are: Urea.poe30＞Liohst.poe30＞Liohst.pao60＞Liohst.pao400. This is the same with that of yield stress in Table 2.3. Although the sequence of the relative film thickness is different as it shows in Figure 4.12, it is still reasonable when consider the yield stress together.

For Urea.poe30, its film thickness and yield stress are the highest among these greases. Therefore, it is normal that its friction coefficient is also the highest. For Liohst.pao400, its film thickness is high, whereas its yield stress is much smaller than that of others, thus its friction coefficient is the lowest. The difference of film thickness between Liohst.poe30 and Liohst.pao60 is always small, whereas the Liohst.poe30 is 5 times the yield stress of Liohst.pao60. Therefore the friction coefficient of Liohst.poe30 is higher than that of Liohst.pao60. From above analysis, it can be inferred that the friction coefficient is determined by the film thickness and the shear stress in the contact area, and the thickener

should also be considered in some cases.

4.4 Without artificial replenishment

4.4.1 Entrainment speed dependence of film thickness

4.4.1.1 Film thickness and its corresponding flow behaviors

Figure 4.22 shows the entrainment speed dependence of film thickness when there is no artificial replenishment. In the lower speed regime, their curves still show V-curve. As speed increases, the film thickness for four test greases all show sharp decline at some entrainment speed points, *i.e*, the starvation speed. Different types of greases have different starvation speed.

The immediate cause for starvation is the amount of grease in the inlet area is not enough to builds a complete lubricating film. The rate at which lubricant is entrained and the rate at which it is lost around the contact, *i.e*. the feed and loss rates have been deemed as the determining factors for the degree of starvation in grease lubrication [1].

Figure 4.23 shows the speed evolution of the contact zone. There is no much difference between the state without artificial replenishment and that with artificial replenishment when the speed is low. The heavy thickener deposition or the thickener pass through the contact zone both can still be observed for Liohst.pao400 and Urea.poe30. Whether the artificial replenishment is used or not has no effect on the lubricating conditions when there is enough grease in the inlet. The basic features of track pattern almost the same for Figure 4.24 and Figure 4.14 when the speed is low.

As speed increases, the meniscus becomes very close or totally connects to the contact zone. It indicates that the amount of lubricant can be applied to the contact point is limited. Besides the contact zone, the track pattern also show some obvious alterations compared to that with artificial replenishment. In Figure 4.24, the fingers for test greases are more or less destroyed. Some of them can barely see any fingers, such as Liohst.pao60 and Liohst.pao400. Some of them keep part of fingers, such as Liohst.poe30.

The grease distribution on both sides of the center of track seems disorder, whereas the orientation of their streamline is the direction of motion of the specimen surfaces. The clarity of Urea.poe30 first becomes clear but then gets fuzzy with the increasing of entrainment

speed. In addition, the thickener depositions in the center of track are exhausted. However, the thickener deposition can be maintained at high speed in fully flooded state.

4.4.1.2 The starvation speed

Figure 4.25 shows the starvation speed and the apparent viscosity under low and high shear. Data show that both the low viscosity under low shear rate and the high viscosity under high shear rate are helpful to postpone the starvation speed.

Under low shear action, the viscosity is still well above the viscosity under high shear, this relative low viscosity benefits the flow motion. Under high shear action, the viscosity is quite low and close to that of the base oil, the relative high viscosity benefits the formation of lubricating film.

Although it is possible merely a coincidence that the greases with lower base oil viscosity has higher apparent viscosity under low shear rates in this study. Nevertheless, these inferences are possible base on the properties of grease.

Figure 4.26 shows the finger-loss speed and the starvation speed for test greases. We have observed that the track pattern is destroyed when the speed is high. This phenomenon is called finger-loss, and its corresponding speed called finger-loss speed. The finger-loss speed is always higher than the starvation speed. The film thickness at the starvation speed is only smaller than that of fully flooded, but it is not serious enough that it would lead to heavy starvation.

The formation and maintenance of grease finger are dependent on the outlet cavitation. The relative motion between the ball and the disk is cyclical. The grease fingers have been formed gathered and sucked into the inlet area with the movement of disk surface, thus the grease fingers redistribution. At this point, if the outlet cavitation can provide a constant source to form new fingers, the whole disk circle can keeps the finger pattern.

Instead, the finger-loss could not be avoided if the outlet cavitation become weak or disappear. When the starvation becomes worse, the pressure shape will gradually turn into an oval shape, which approaches to that of the Hertzian contact. Therefore the cavitation driven by negative pressure which produced in the outlet area will disappear.

For the rotationally periodic track pattern, the new finger pattern could not be formed, the

previous formed one also be quickly erased. Therefore it is normal that the finger-loss happens after the starvation occurs.

4.4.2 Revolution dependence of film thickness

4.4.2.1 Film thickness and its corresponding flow behaviors

Figure 4.27 shows the evolution of track pattern for Liohst.pao60 at the entrainment speed of 47.1 mm/s, SRR ±1. As it shows, the evolution of track pattern with revolution for different SRR is different at the same entrainment speed. However, there still have several things in common.

First, the clarity of track pattern increases for both SRR +1 and SRR -1. At the revolution of 12, the finger pattern looks blurry. Nevertheless, the finger pattern becomes obvious at the revolution of 60 and 120. Moreover, their depositions in the center of track are reduced gradually. Under slide-roll condition, both of them could not avoid the scratch on the disk. Even so, the selected entrainment speed is low, so not the whole circle of coating is destroyed. So the film thickness could still be measured accurately from those points without scratches. These scratches are distributed on the center of track and grease fingers part. In comparison, the scratches on the center of track are more serious than these on finger part.

The differences of track pattern between SRR +1 and SRR -1 are: The major difference between them is that the track pattern keeps clear and complete finger when SRR is negative, whereas the finger pattern looks disorder at the revolution of 60 and 120 when SRR is positive. As we have observed, the deflection angle decreases gradually when the SRR change from negative 1 to positive 1. Therefore, the deflection angle of SRR -1 is larger than that of SRR +1.

Figure 4.28 shows the film thickness as a function of revolution in Figure 4.27. The solid line is the base oil film thickness predicted by EHL theory, and it represents the lowest limit film thickness in fully flooded state. The film thickness for SRR 1 and that of SRR -1 both continually decrease. Before around 20 revolution, $h_{SRR\ +1} > h_{SRR-1}$. After that, the film thickness of SRR +1 decreases faster, thus $h_{SRR\ +1} < h_{SRR-1}$. Table 4.4 shows, they are in fully flooded state before 10 revolution ((S+a)-a*m > 0 = fully flooded, (S+a)-a*m < 0 = starved). It is easier for SRR +1 enter the starved state.

Table 4.4 The lubrication conditions under different revolutions

(S+a)-a*m	10 revolutions	60 revolutions	100 revolutions
SRR +1	+	-	-
SRR -1	+	+	-

This is reasonable from their track pattern as shown in Figure 4.27. It has been proposed that the formation and maintenance of finger pattern rely on the state of lubricating contact. When starvation occurs, the grease finger will be disturbed by the outlet cavitation which affected by the reduction of film thickness. The film thickness of SRR +1 is lower than that of SRR -1. It can be concluded that the probability of being disturbed for track pattern is higher when SRR is positive.

There are some problems which are worth thinking about. Such as, it is generally believed that $h_{SRR+} > h_{SRR-}$, and this is verified when artificial replenishment is adopted. Nevertheless, $h_{SRR+} < h_{SRR-}$ in starved state. In addition, the track pattern and film thickness when SRR = 0 and these when |SRR| $<$ 1 are not shown in here. This is because: It will take a long time to observe the change of track pattern at lower speed, pure-rolling or when the |SRR| is small. If the speed is too high, the scratches increase the difficulty in measurement.

4.4.2.2 Spread observation

Figure 4.29 shows the evolution of the grease reservoir for Liohst.pao60 at different speed after test. As it shows, the meniscus boundary both at the inlet area and that at the outlet area spread outward after test stop, respectively. It means that there is lubricant flow back to the contact area. The round meniscus surround the contact area is already obvious at 60 s. By measuring the meniscus distance from the edge of inlet area to the center of contact in every pictures, the separation rate per second under the same test conditions is almost constant.

Table 4.5 Separation rates for Liohst.pao60 at different entrainment speed

Entrainment speed	mm/s	1	9.3	101.6	500
Separation rate	μm/s	1.52	4.56	4.56	3.9

Table 4.5 lists the separation rates for Liohst.pao60 at different entrainment speed. The separation rate is 1.52 um/s at the entrainment speed of 1 mm/s. The variation of the separation rate with entrainment speed is not evident after that. At the entrainment speed of

500 mm/s, it drops slightly. In general, the viscosity and consistency of grease will sharply decline under high shear, therefore grease at high speed flow more rapidly. However, the broken fibers and the base oil can potentially form a new uniform solution, its viscosity even increase, *i.e*, flow slower.

Table 4.6 Separation rates for test greases

	Urea.poe30	Liohst.pao400	Liohst.poe30	Liohst.pao60
μm/s	1.52	2.28	3.8	4.3

Figure 4.30 shows the evolution of the grease reservoir for test greases at entrainment speed of 20.6 mm/s after test. The separation rate for different greases is different. Table 4.6 lists the separation rates for test greases. The separation rate of Urea.poe30 and that of Liohst.pao400 are small, and the separation rate of Liohst.poe30 and that of Liohst.pao60 are large. The lubricant replenish rate during the test is impossible to know, whereas the separation rate can also reflect the replenish ability and flow ability to some degree.

4.5 Lubricating conditions and track pattern

4.5.1 Possible mechanisms

Figure 4.31 shows the supply sources of replenishment to the contact in a wider area. As it shows, there are three main ways to supply the lubricant. The first one is the side reservoirs, and it shows a butterfly-shaped with two side bands which located on both sides of contact area. A certain amount of lubricant is gathered above and below the contact zone. The thinnest of side reservoir is the joint between the contact point and 'the butterfly wing', and it gradually spreading outward. There are two side bands stretch out from 'the butterfly wing' on the whole circle of track. The second one is the thickener deposition or bleeding oil left on the center of track. The third one is the grease finger.

Their contribution to the film formation and maintain is different for different grease and different test conditions. The side reservoir and the grease finger are indirect tank, whereas the thickener deposition is directly involved in film formation. However, the effects of thickener deposition are limited. This deposition is physical adsorption in general cases, therefore its stripping easily happened under external force. As we have observed, the thickener deposition significantly reduces under some test conditions, such as long time

duration and high speed. Therefore, the film thickness can be maintained depend on whether they can provide a steady replenishment.

The main ways of replenishment come from the supply of grease finger and that of side reservoirs. It should be remembered that the side reservoir is a dynamic area during test, and it moves with the contact point. Its size can be affected by many factors. Such as: test conditions, the properties of grease, etc. The side reservoir connects directly to the contact point. Nevertheless, the junction between the contact point and the side reservoir is the thinnest part. The scope of area we observed so far as shown in Figure 4.32.

As it shows, the grease finger is another supply source. The finger zone is composed by fingers and black-and-white interference fringes. Two bands which lie between finger zone and the center of track with dense and fine fingers which point to the center of track are called side ridges. These two side ridges are often subjected to shear and squeeze, their bleeding oil will flow into the center of track. In addition, it is possible that the side ridge becomes one part of channel for lubricant flow back through fingers. It is also possible that the side ridge becomes the dam to obstruct flow. Besides, the condition that the fingers connect with the center of track is observed or without obvious side ridge also exists.

Side reservoir

Figure 4.33 shows the side reservoirs replenishment for Liohst.poe30 at the entrainment speed of 119 mm/s. From these can concluded that the side reservoir indeed provides supply, but on condition that it connects with the contact point. Even though the speed is constant, the lubricating condition will not stable unless there is a continual supply. From left to right, the film thickness continues to grow.

In the left picture, the side reservoir can be observed, whereas it does not connect with the contact point. The pictures on the right hand, the side reservoirs can supply lubricant even their inlet distances are almost zero. The junction between the side reservoir and the contact point show obvious change in color. Therefore the film thickness at this position indeed increases, and this increase comes from the replenishment of side reservoir.

Grease finger

The direct evidence that the grease finger provides supply to the contact point is difficult to acquire. From the previous video observation test, it can only be identified when the speed is

low. Even in a stable state at high speed, its wake and the trajectory features of flow are just as in Figure 4.31, only the contour of flow can be seen. Although the grease finger indeed exists, as can be seen from the static observation after test stop.

The film thickness could not be maintained if rely exclusively on the supply of deposition and side reservoir. In reality, lubricating greases keep their performance without resupply or replacement for a long period of time under proper conditions. Thus the inner self-supply should exist. There are three ways that the grease finger associates with the contact point. Firstly, the bleeding oil flow through the finger back to the center of track. Secondly, the grease finger on the disk returns to the inlet area with the periodic rotating of disk. Thirdly, the grease finger provides supply to the side reservoir, thus replenish the contact point indirectly.

According to the practice, the first one is possible. However, the latter two cases are more important for most of greases if without external force exerted on it. The latter two cases are certainly present. Since the fingers on the track is the only source. The grease finger on the track, side reservoir and the amount of lubricant in the inlet area are a dynamic combination. We should take into consideration all aspects of the problems when they are discussed.

Certainly, the ability for the grease finger to supply is different for different types of grease. It is proposed that the influence of the thickener on it is larger than that of the base oil. This is because the thickener is the solid constituent that obstructs grease flow. Suppose the return ability of the base oil is one hundred percent. This ability will decreases with the increasing of the thickener. It means the grease has strong flow ability or the grease which its thickener will be easily destroyed under shear has better finger supply ability. Such as: the resupply ability of the finger for Liohst-based grease is better than that of Urea-based grease.

4.5.2 Grease finger

It is assumed that the finger area is proportional to the amount of grease. As known, the amount of grease which stays at the inlet area determines the film thickness in the starved state. Three ways that the finger associates with the contact point are discussed in previous section. Obviously, the amount of grease which the finger carried and the distribution position of the finger are all related to the replenishment for the inlet area and side reservoir. There are

many problems remain, such as whether the influences of greases which are located in different positions exert on the contact point is consistent. The density of grease finger and the height of grease finger on the disk surface should be known if the amount of grease is required.

However, this is difficult for grease lubrication. The density of grease is determined by the proportion between the thickener and the base oil. Due to shear action, this proportion in grease finger on the track is different for different location. The apparent viscosity of grease declines with the increase of shear rate. The base oil determines the apparent viscosity of grease under high shear. That is to say, the density of grease which really enters the contact zone is almost constant, nearly base oil viscosity.

The height of grease finger on the disk surface is considered half of the gap height where the fingers stop separating [25]. As it shows in Figure 4.31, the finger trunks grow from the side bands. These two side bands are far away from the center of track. Their formation is more affected by the relative motion between the ball and the disk. If this suggestion is correct, there will no major changes in the height of grease finger. Therefore, to simplify this problem, it is assumed that the finger area is proportional to the amount of grease.

Figure 4.34 shows the revolution dependence of film thickness and finger area for Liohst.pao60 without artificial replenishment at the entrainment speed of 47.1 mm/s. Within 10 revolution, the film thickness, finger area-near and finger area-far decline rapidly. After 10 revolution, the film thickness and finger area-near show slightly drop, whereas the finger area-far does not change much. In the previous observation, it is noticeable that the varying tendency of the finger near-area and the film thickness are always the same. Therefore, it is proposed that the grease finger provides supply to the contact area, and the near-finger plays a major role. The far-finger may be influenced by the adhesion property, thus its fluidity is no better than the near-finger.

4.6 Summary

In this chapter, the change features of track pattern and film thickness with test conditions are observed, respectively. The experiment is divided into two sets: with artificial replenishment and without artificial replenishment. The scoops are adopted so that the contact

point keeps in a fully flooded state. In the tests without artificial replenishment, it is normal that starvation occur especially when the entrainment speed is high and the test duration is long.

The entrainment speed dependence of film thickness show a V-curve in the low speed regime. As long as the amount of grease in the inlet area is enough to builds a complete lubricating film. There is no much difference between without artificial replenishment and with artificial replenishment both on the film thickness and track pattern. Lower than the transition speed, the film thickness mainly consists of thickener. It infers the factor that may affect the value of transition speed is viscosity.

As the entrainment speed increases, the film thickness for all test greases all show sharp decline at certain entrainment speed without artificial replenishment. This entrainment speed is called the starvation speed. The track pattern is destroyed when the speed is high, the finger-loss and the thickener deposition is removed. However, not only the integrality of track pattern can be conserved but also the thickener deposition in the center of track will not decline at the same test conditions with artificial replenishment. Moreover, the low viscosity under low shear and the high viscosity under high shear are contributed to postpone the starvation speed. The finger-loss speed is always lower than the starvation speed.

The revolution dependence of film thickness curve shows a decline at the first few revolutions with artificial replenishment, and then the film thickness almost not change. The film thickness is the highest when SRR = 0, and the film thickness of positive SRR h_{SRR+} always higher than that of negative SRR h_{SRR-}. The total finger area for track pattern almost not change, whereas the lowest point for the near finger area (A-N) corresponds to SRR 0, and it continues to increase when the absolute value of SRR change from 0 to 1. In particular, the open time for the enclosed cavity will be delayed while the contact under slide-roll condition in the initial of wake formation.

The film thickness as a function of revolution curve continually decreases without artificial replenishment. In addition, the separation rate per second under the same test conditions is almost constant. It can reflects the replenish ability and flow ability to some degree. The grease which lies near the center of track plays a main role in the replenishment of contact area.

4.7 Conclusions

The main conclusions for this chapter are listed as follows:

1. The features of track pattern are different for different lubricating conditions.
2. The thickener deposition in the center of track plays a positive role in the film formation.
3. Starvation and finger-loss occur at higher entrainment speeds with all the tested greases. The starvation speeds are lower than the finger-loss speeds.
4. The apparent viscosity of the grease at low shear rate in the inlet zone has a great impact on the resupply of the greases and the starvation speed.
5. The grease finger provides supply to the contact area and the side reservoir. One part of grease finger which lies near the center of track plays the main role.

References

[1] Wikström, V. and Jacobson, B., Loss of lubricant from oil-lubricated near-starved spherical roller bearings, Journal of Engineering Tribology, 211, 1, 1997, 51-66.

[2] Wedeven LD, Evans D, Cameron A, Optical Analysis of Ball Bearing Starvation, Journal of Lubrication Technology, 1970; 3: 349-361.

[3] Chiu, Y.P., "An Analysis and Prediction of Lubricant Film Starvation in Rolling Contact Systems," ASLE Transactions, 17, 1, 1974, 37–41.

[4] Jacod, B., Pubilier, F., Cann, P.M. and Lubrecht, A.A., "An Analysis of Track Replenishment Mechanisms in the Starved Regime," Lubrication at the Frontier, Tribology Series, 36, D. Dowson et al eds., Elsevier, 1999, 483-492.

[5] Gershuni, L., Larson, M.G. and Lugt, P.M., "Lubricant Replenishment in Rolling Bearing Contacts," Tribology Transactions, 51, 5, 2008, 643-651.

[6] Kaneta, M., Ogawa, T., Takubo, Y. and Naka, M., "Effects of a thickener structure on grease elastohydrodynamic lubrication films," Proc. IMechE, Pt. J, Journal of Engineering Tribology, 214, 2000, 327-336.

[7] Kimura, H., Imai, Y. and Yamamoto, Y., "Study on Fiber Length Control for Ester-Based Lithium Soap Grease," Tribology Transactions, 44, 3, 2001, 405-410.

[8] Yokouchi, A., Hokao, M. and Sugimura, J., "Effects of Soap Fiber Structure on Boundary Lubrication of Lithium Soap Greases," Tribology Online, 6, 4, 2011, 219–225.

[9] Oikawa, E., Inami, N., Hokao, M., Yokouchi, A. and Sugimura, J., "Bearing torque characteristics of lithium soap greases with some synthetic base oils," Proc. IMechE, Pt. J., Journal of Engineering Tribology, 226, 6, 2012, 575-583.

[10] T. E. Tallian, On Competing Failure Modes in Rolling Contact, ASLE Transactions, 1967; 10: 418-439.

[11] M. Françon, Optical Interferometry, Academic Press, 1966.

[12] G. J. Jonhston, R. Wayte and H. A. Spikes, The Measurement and Study of Very Thin Lubricant Films in Concentrated Contacts, Tribology Transactions, 34, 187- 194, 1991.

[13] R. Gohar and A. Cameron, Optical Measurement of Oil Film Thickness Under Elastohydrodynamic Lubrication, Nature, 200, 458-459, 1963.

[14] R. Gohar and A. Cameron, The Mapping of Elastohydrodynamic Contacts, ASME Transactions, 10, 215-225, 1967.

[15] H. A. Spikes and P. M. Cann, The Development and Application of the Spacer Layer Imaging Method for Measuring Lubricant Film Thickness, Proceedings of the Institution of Mechanical Engineers, Part J, 215, 261-277, 2001.

[16] A. Cameron and R. Gohar, Theoretical and Experimental Studies of the Oil Film in Lubricated Point Contact, Proceedings of the Royal Society, Series A, 291, 520- 536, 1966.

[17] R. Haydn, G. W. Dalke, J. Henkel and J. E. Bare, Application of the HIS Color Transform to the Processing of Multisensor Data and Image Enhancement, Proceedings of the International Symposium on Remote Sensing of Arid and Semi arid Lands, 599-616, 1982.

[18] D. E. Jones and G. A. Schott (Editors), Miscellaneous Papers by Heinrich Hertz, Macmillan, 1896.

[19] Jianbin Luo, Shizhu Wen, Ping Huang, Thin film lubrication. Part I. Study on the transition between EHL and thin film lubrication using a relative optical interference intensity technique, Wear,194, 107-115, 1996.

[20] Liran Ma, Chenhui Zhang, Discussion on the Technique of Relative OpticaInterference Intensity for the Measurement of Lubricant Film Thickness, Tribology Letters, 36, 239-245, 2009.

[21] B. J. Hamrock and D. Dowson, Ball Bearing Lubrication: Elastohydrodynamics of Elliptical Contacts, John Wiley & Sons Inc., 1981.

[22] Cann PM, Starvation and Reflow in a Grease-Lubricated Elastohydrodynamic Contact, Tribology Transactions, 1996; 39: 698-704.

[23] Cen H, Lugt PM, Morales-Espejel G, On the film thickness of grease lubricated contacts at low speeds, Tribol Trans, 2014: 668-678.

[24] H Ito, M Tomaru, T Suzuki, Physical and chemical aspects of grease deterioration in sealed ball bearings, Lubrication engineering, 1988; 44: 872-879.

[25] Kaneta, M., Yang, P.: Effects of thermal conductivity of con- tacting surfaces on point EHL contacts. J. Tribol. 125, 731–738, 2003.

[26] Larrson,P-O. Lubricant replenishment in the vicinity of an EHD contact. PHD thesis, Lulea University of Technology, Sweden, 1996.

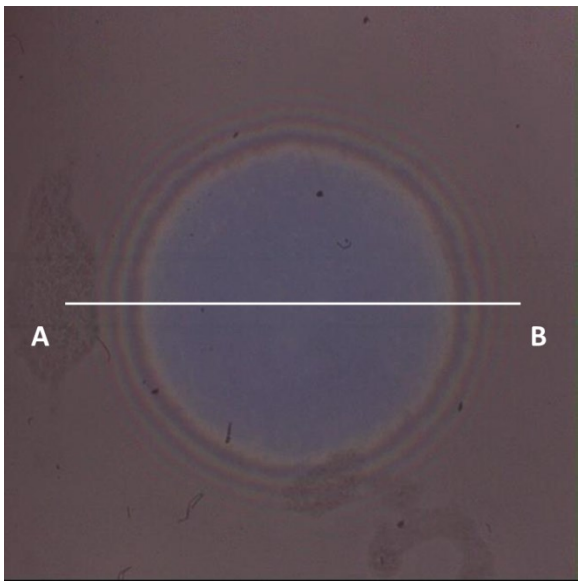

Figure 4.1 Interference image of a static contact

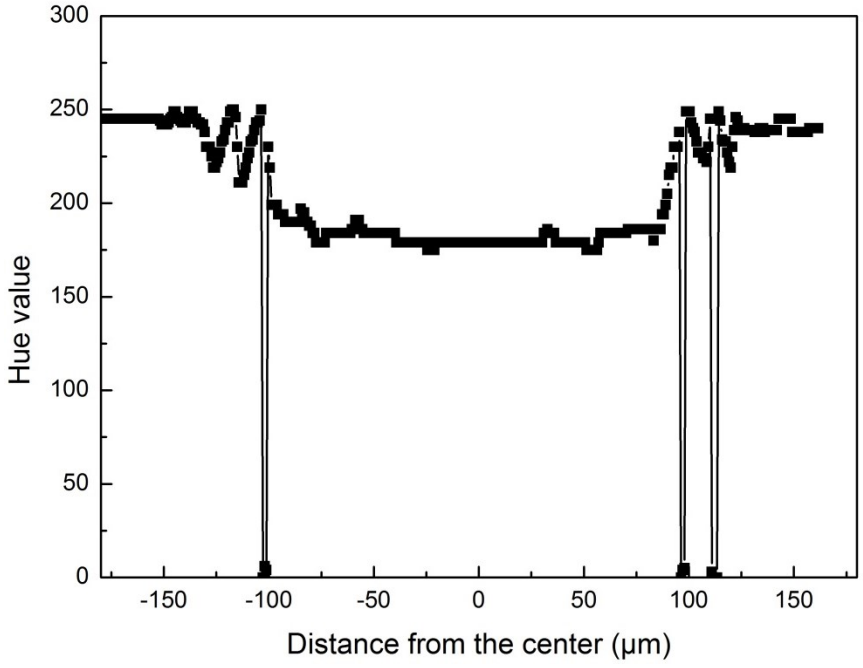

Figure 4.2 Hue values at the cross section AB in Figure 4.1

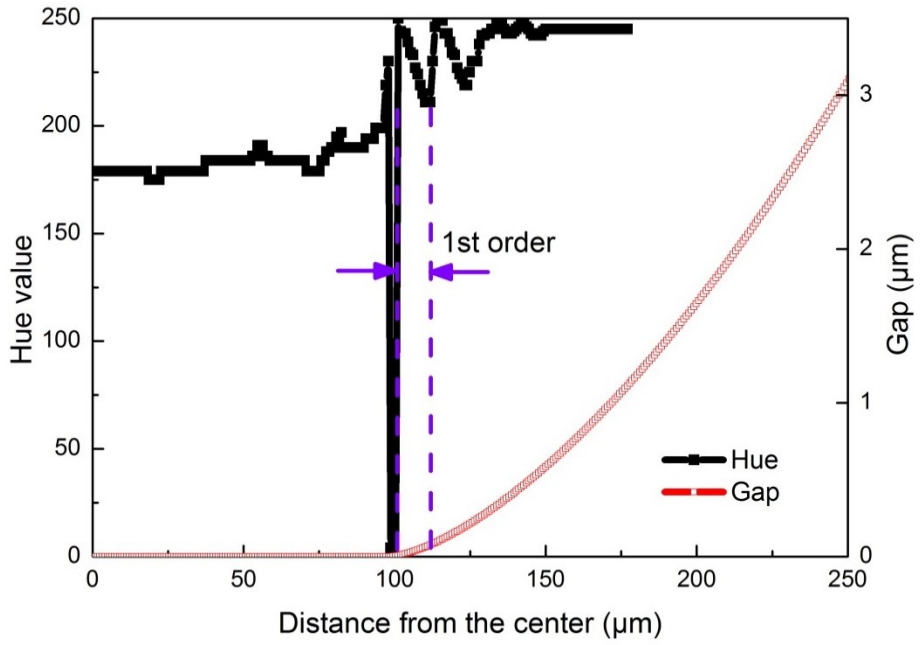

Figure 4.3 Relationship between Hue values and gap distances

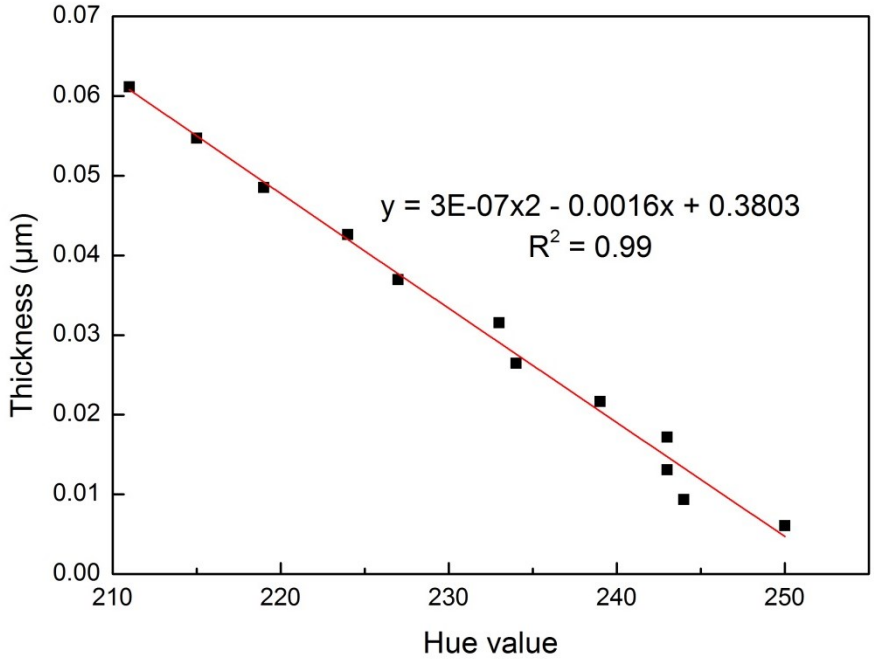

Figure 4.4 Film thickness as a function of Hue value for 1st order in Figure 4.3

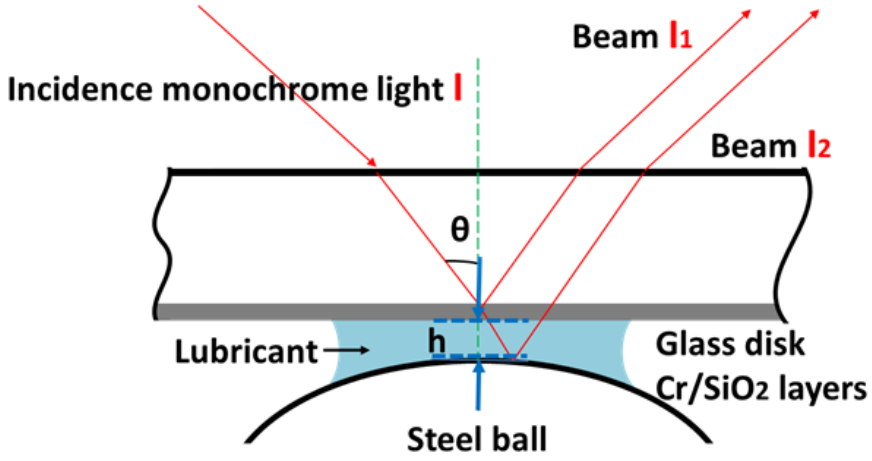

Figure 4.5 Principal schematic of the two-beam optical interference

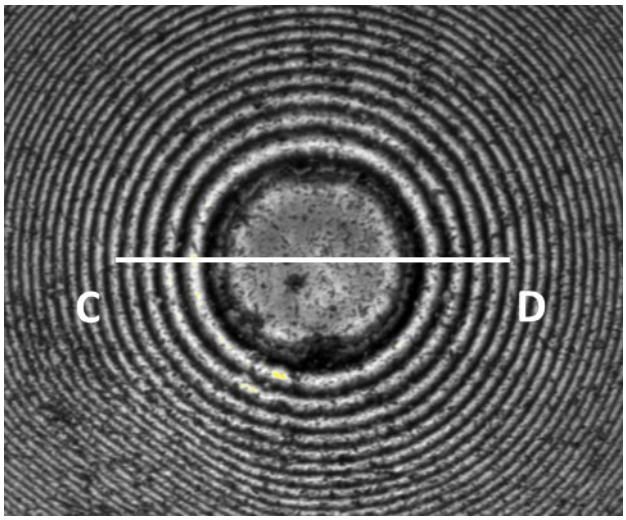

Figure 4.6 The interference image at stationary contact

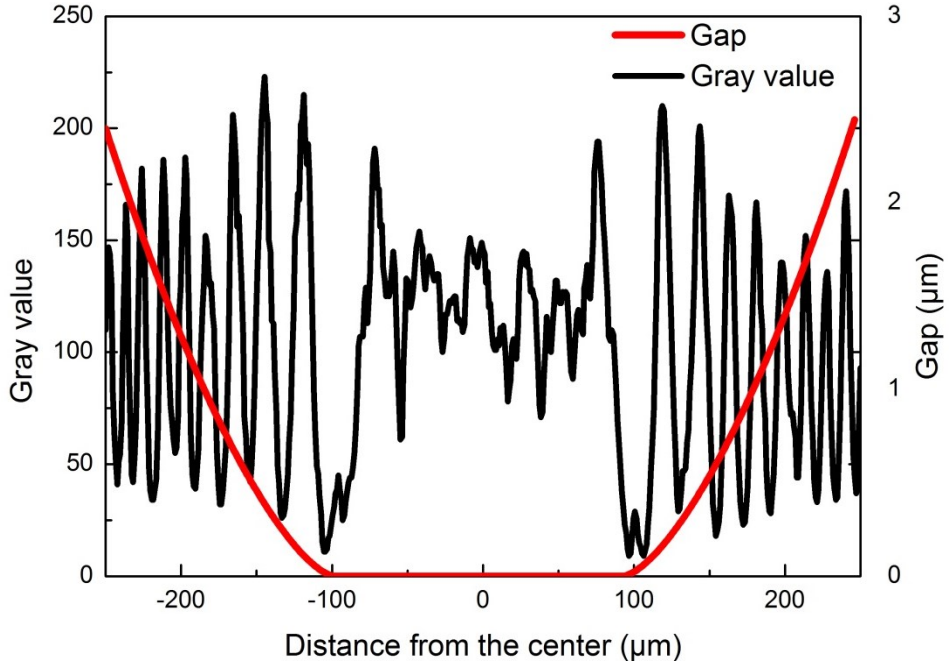

Figure 4.7 The light distribution along the CD centerline and the corresponding gap distance

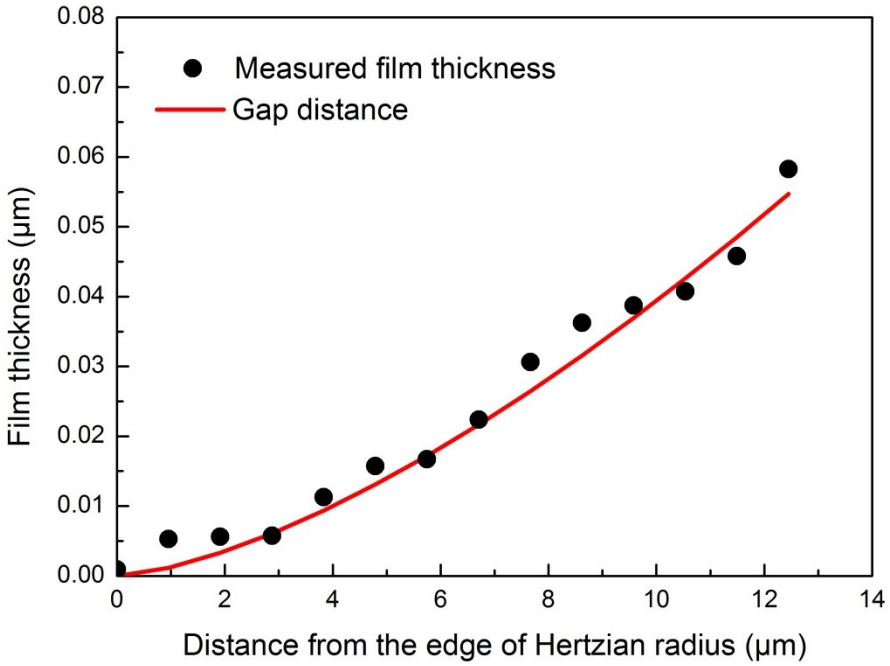

Figure 4.8 The film thickness under stationary contact measured by the ROII method and the gap distance

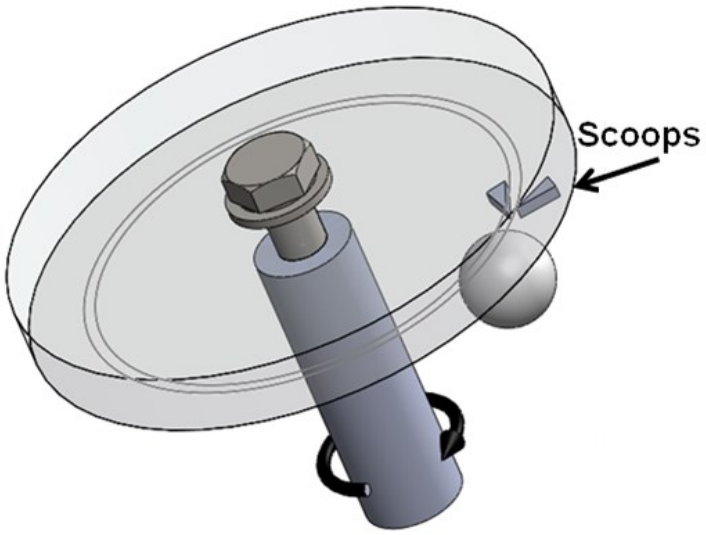

Figure 4.9 Ball-on-disk configuration with scoops

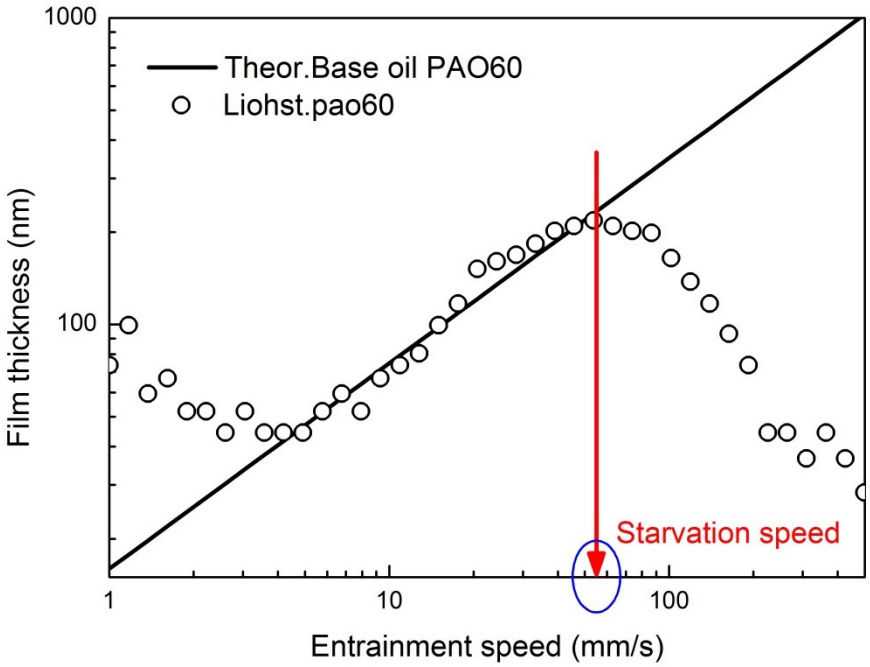

Figure 4.10 The definition of starvation speed as the entrainment speed changes

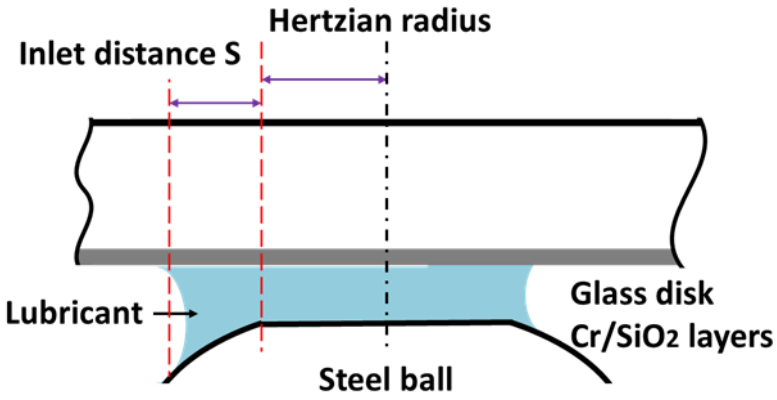

Figure 4.11 The definition of inlet distance S

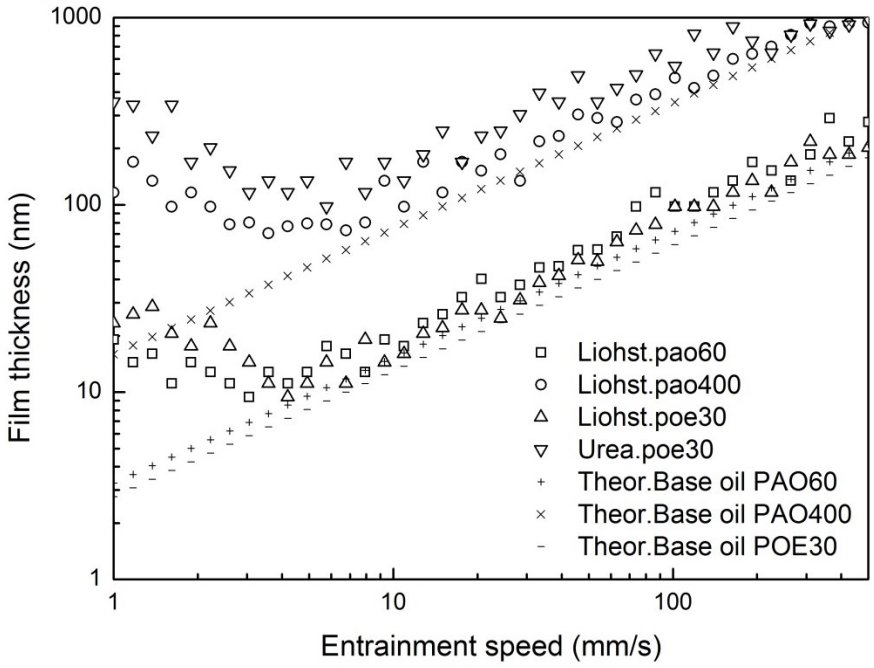

Figure 4.12 Entrainment speed dependence of film thickness in fully flooded condition

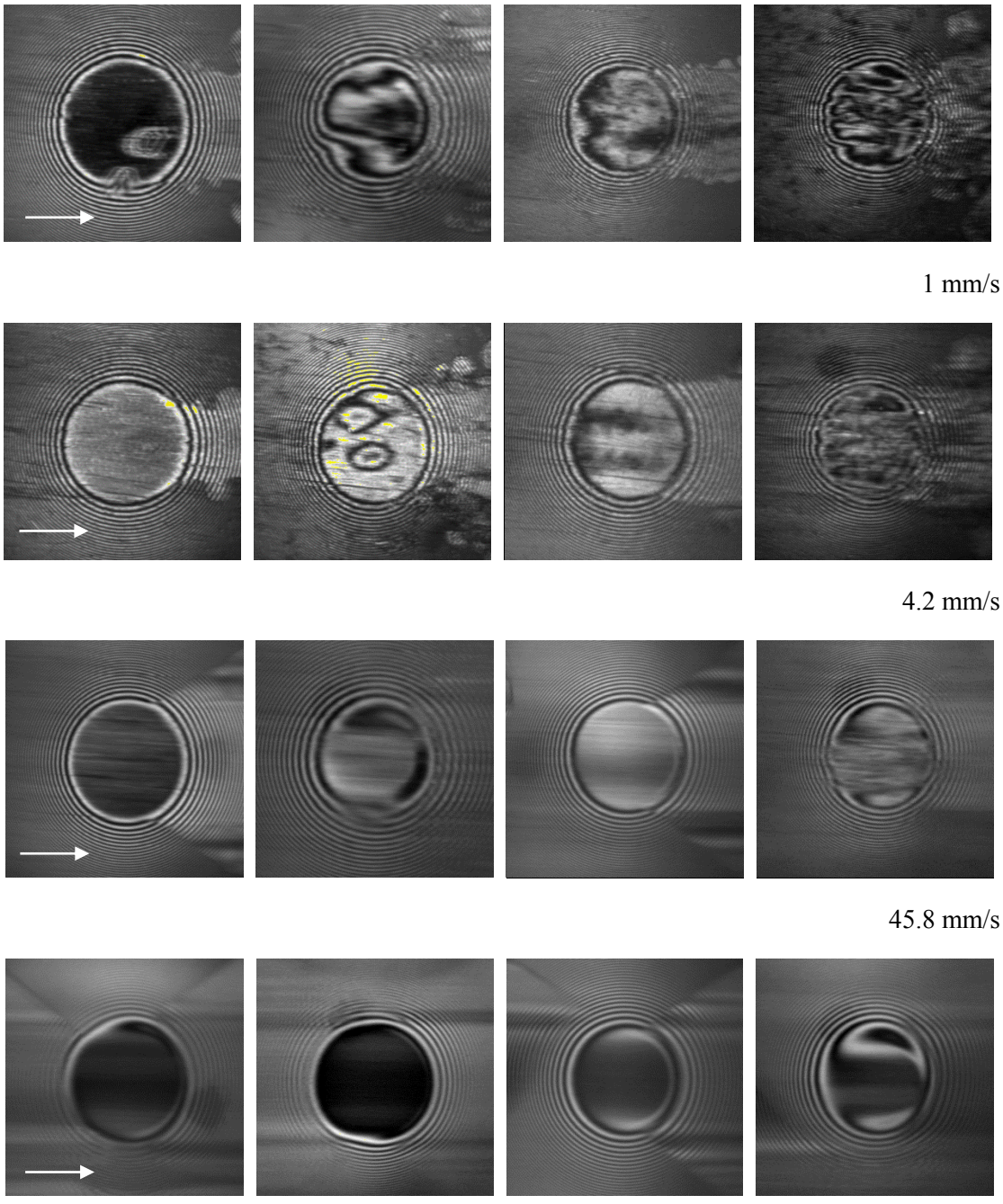

Figure 4.13 Speed evolution of the contact center of test greases in fully flooded state-monochrome images

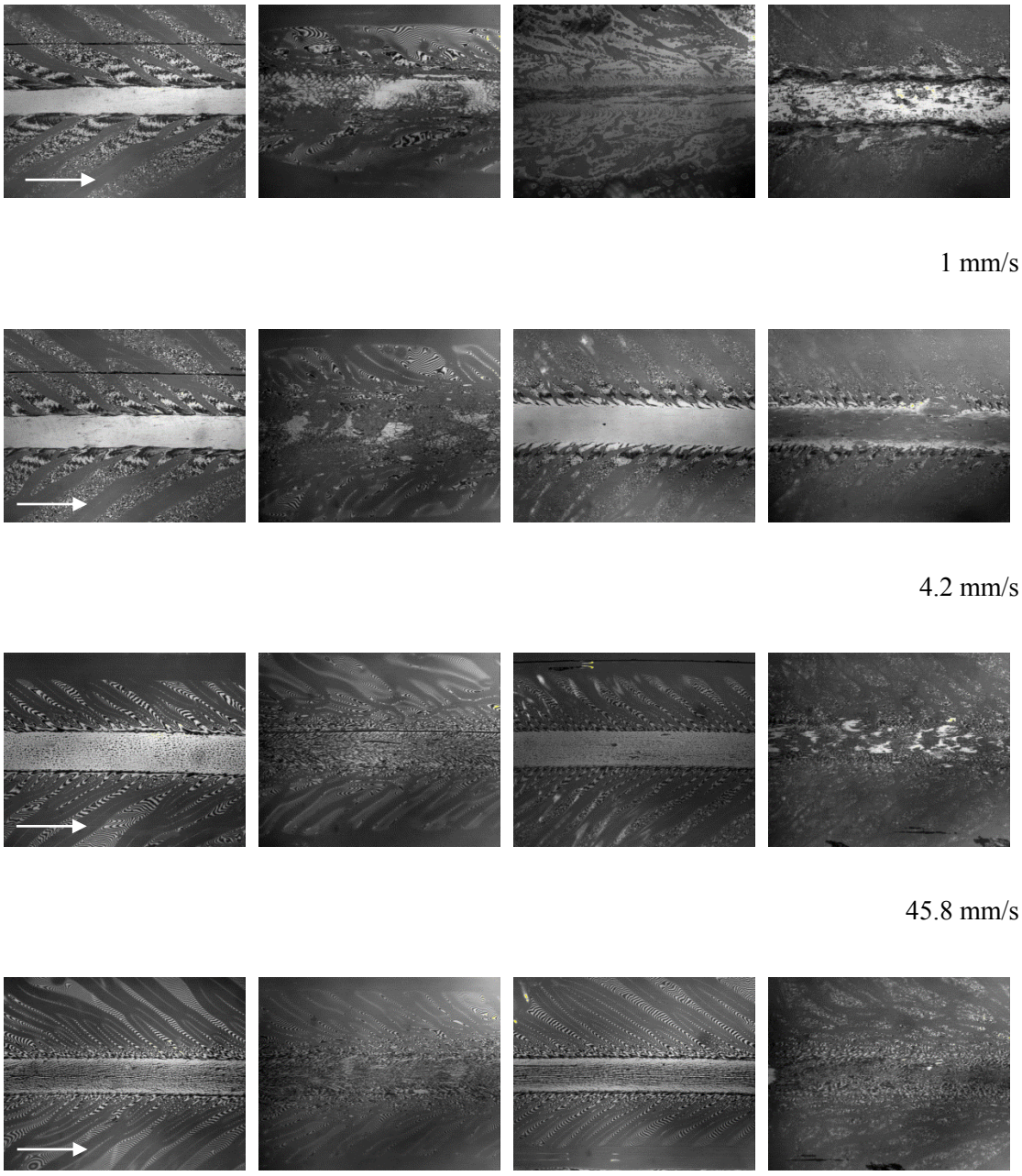

Figure 4.14 Speed evolution of the track pattern of test greases in fully flooded state-monochrome images

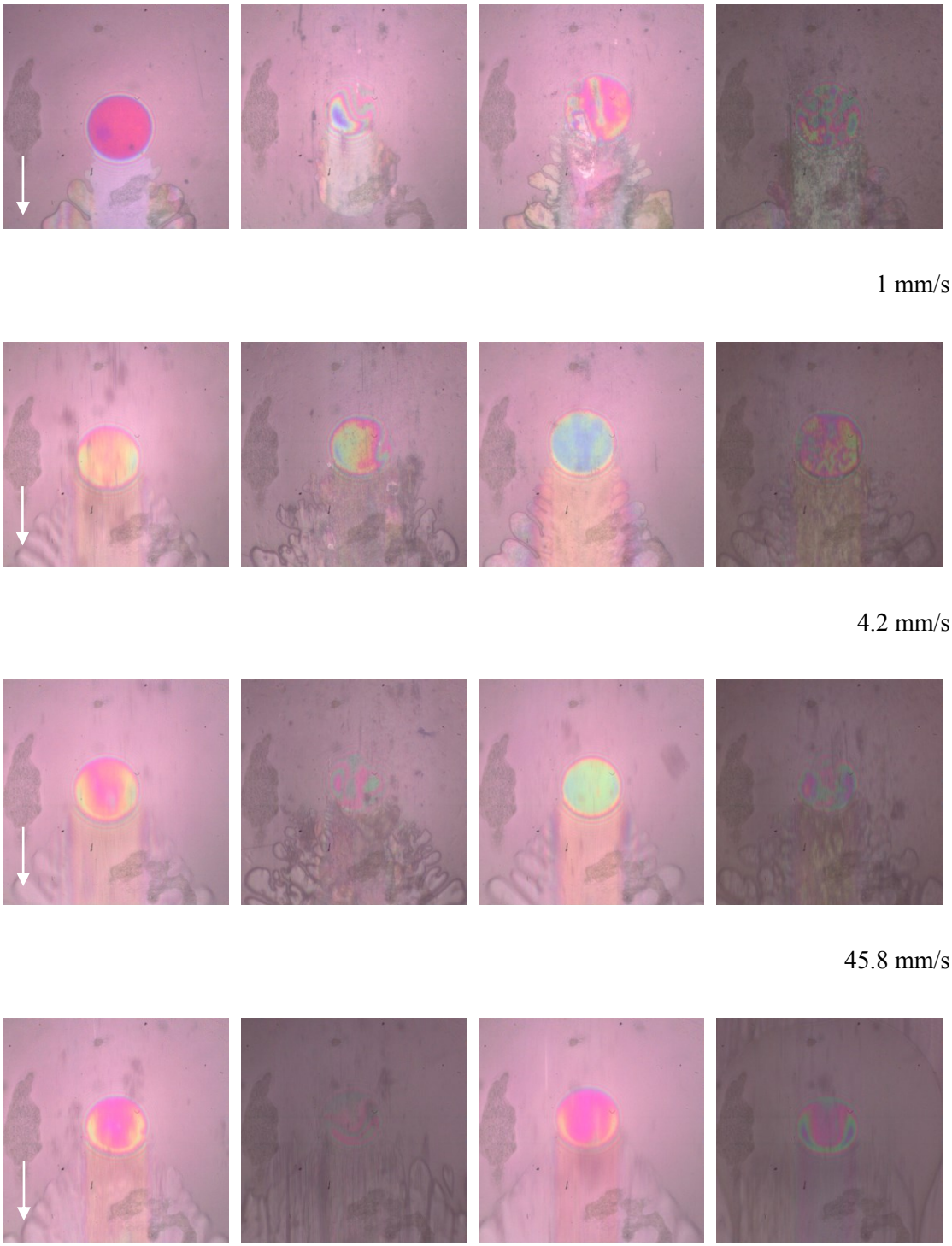

Figure 4.15 Speed evolution of the contact center of test greases in fully flooded state-color images

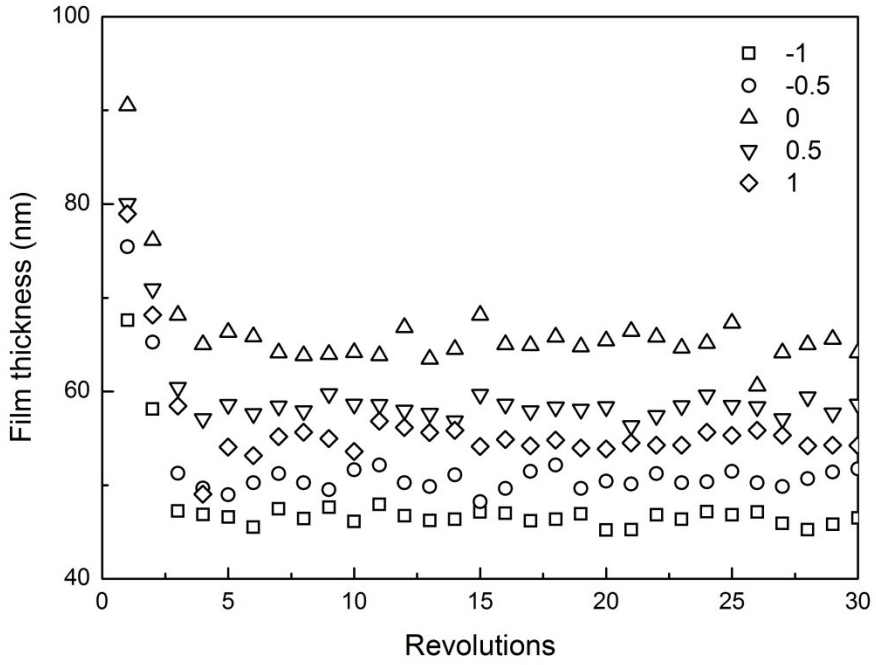

Figure 4.16 Revolution dependence of film thickness for Liohst.pao60 with artificial replenishment at the entrainment speed of 47.1 mm/s

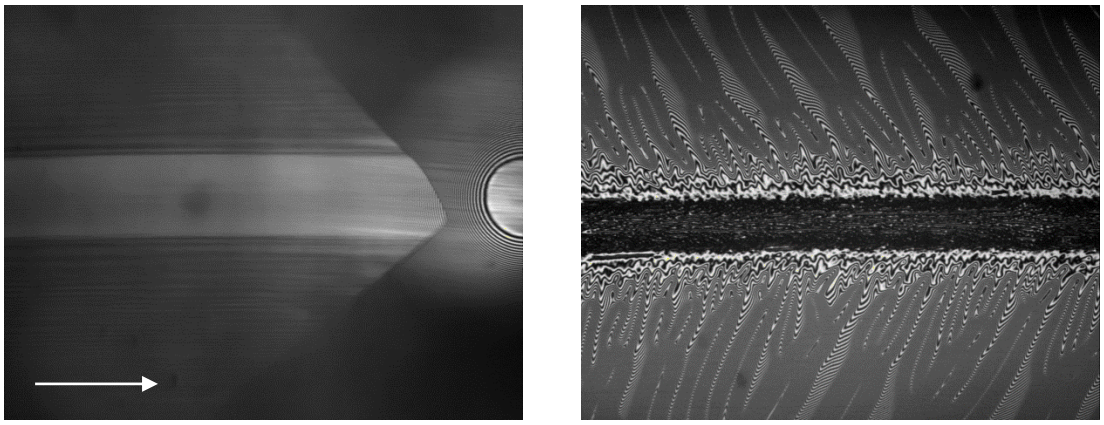

SRR -1, revolution 30

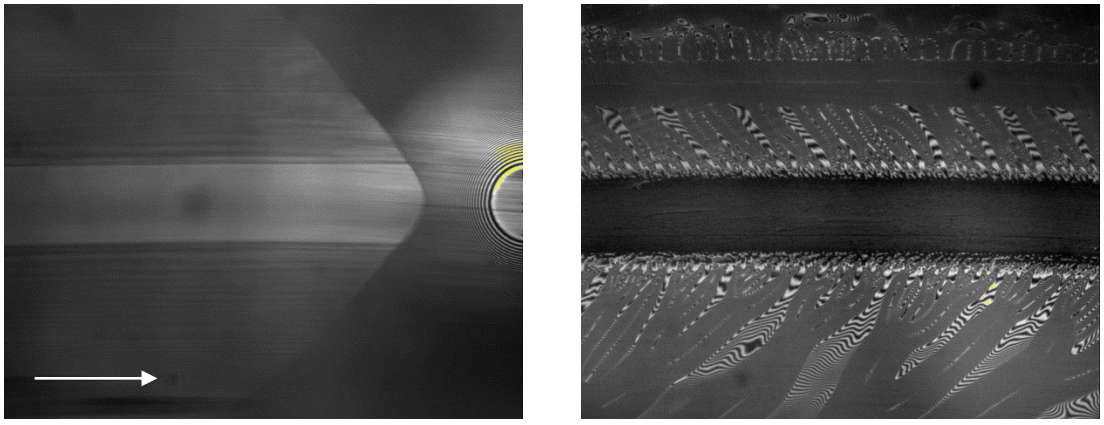

SRR 0, revolution 30

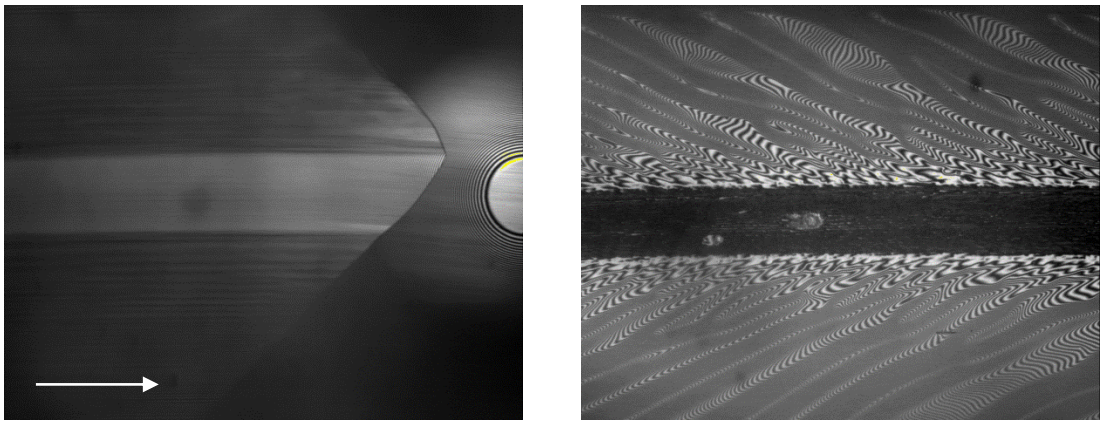

SRR 1, revolution 30

100 μm

Figure 4.17 The inlet and track pattern with artificial replenishment

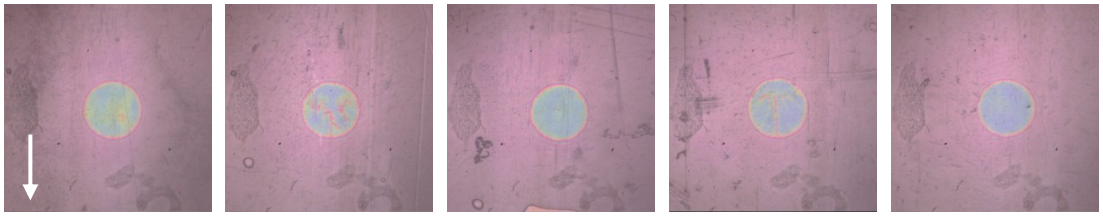

(i) Before test start

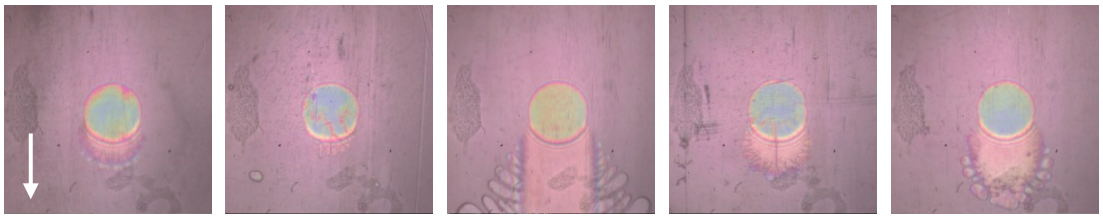

(ii) 10 ms

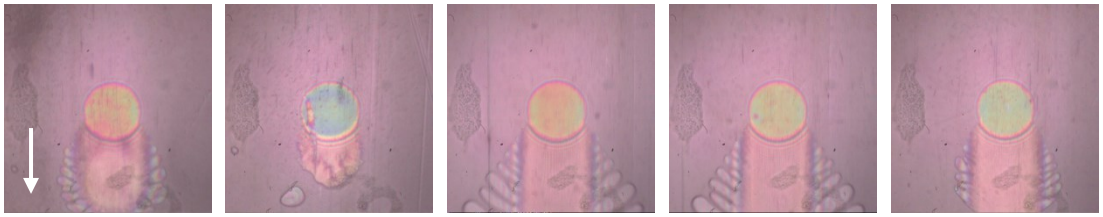

(iii) 50 ms

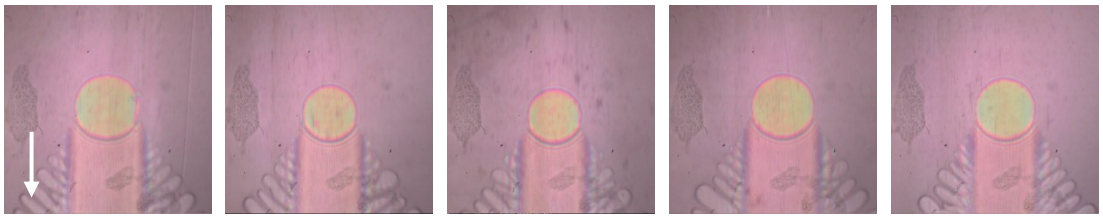

(iv) 100 ms

-0.4 -0.2 0 0.2 0.4

100 μm

Figure 4.18 Wake pattern formations with time for Liohst.pao60 in different slide to roll ratios

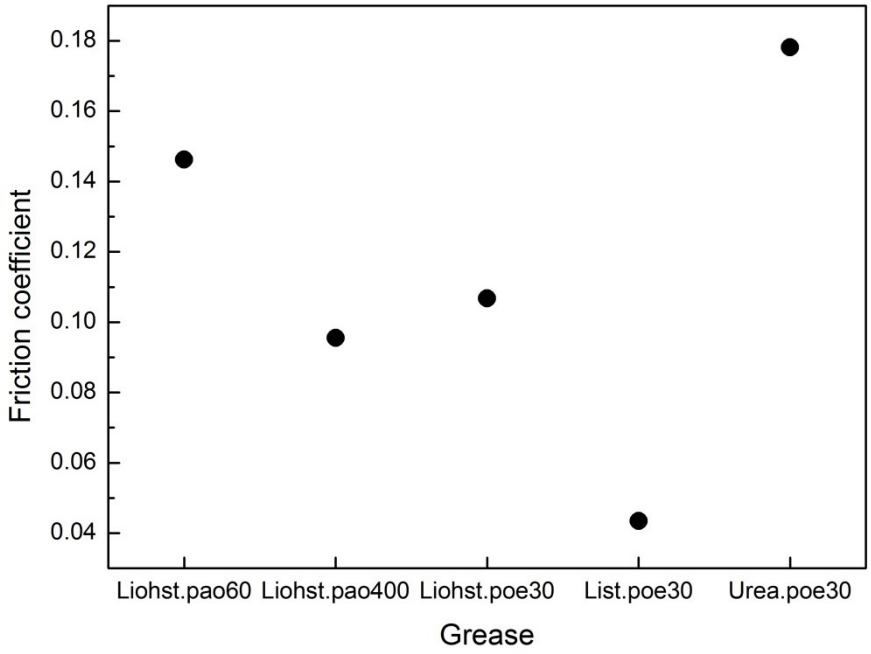

Figure 4.19 Friction coefficients for test greases in 40 mins, entrainment speed 47.1 mm/s, slide to roll 0.4

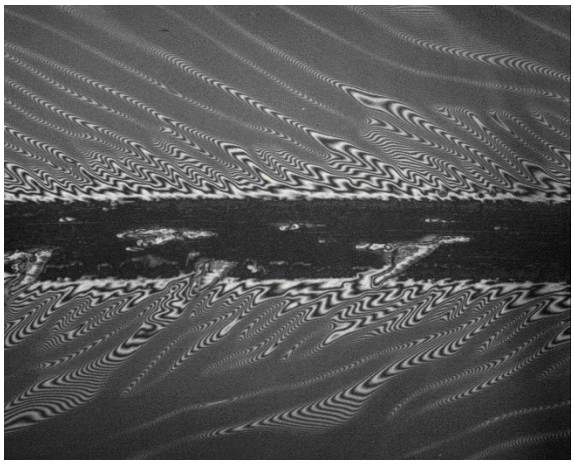

Liohst.pao60

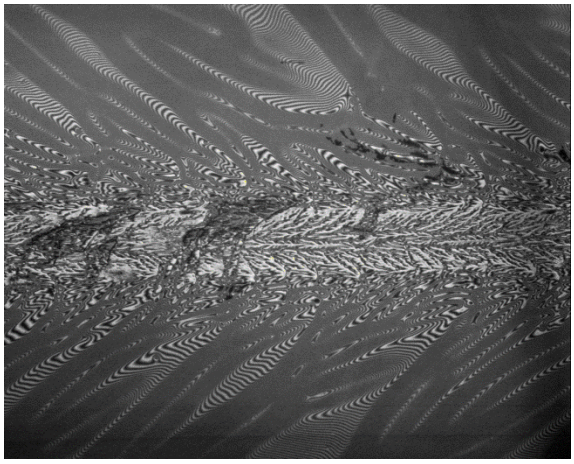

Liohst.pao400

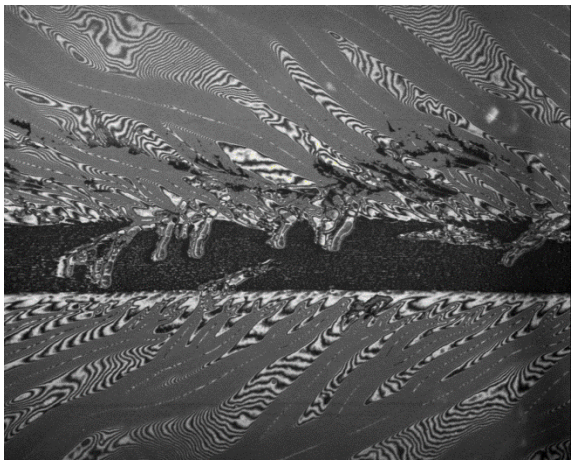

Liohst.poe30

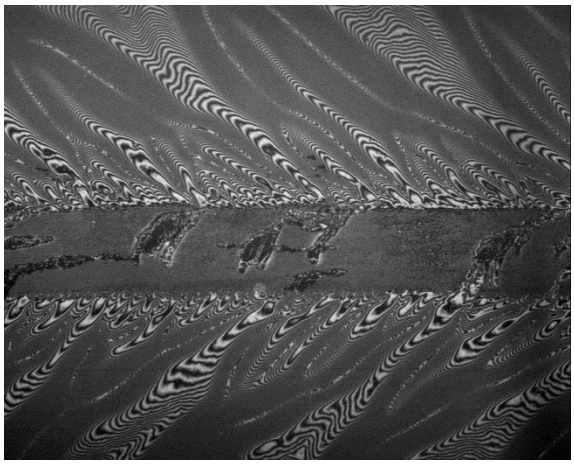

List.poe30

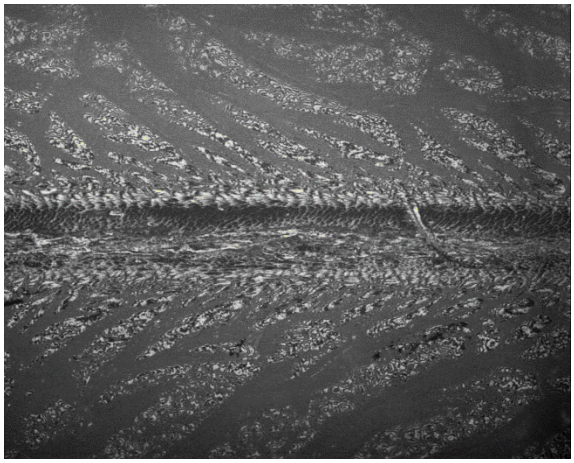

Urea.poe30

100 μm

Figure 4.20 Upstream patterns for test greases in 40 mins, entrainment speed 47.1 mm/s, slide to roll 0.4

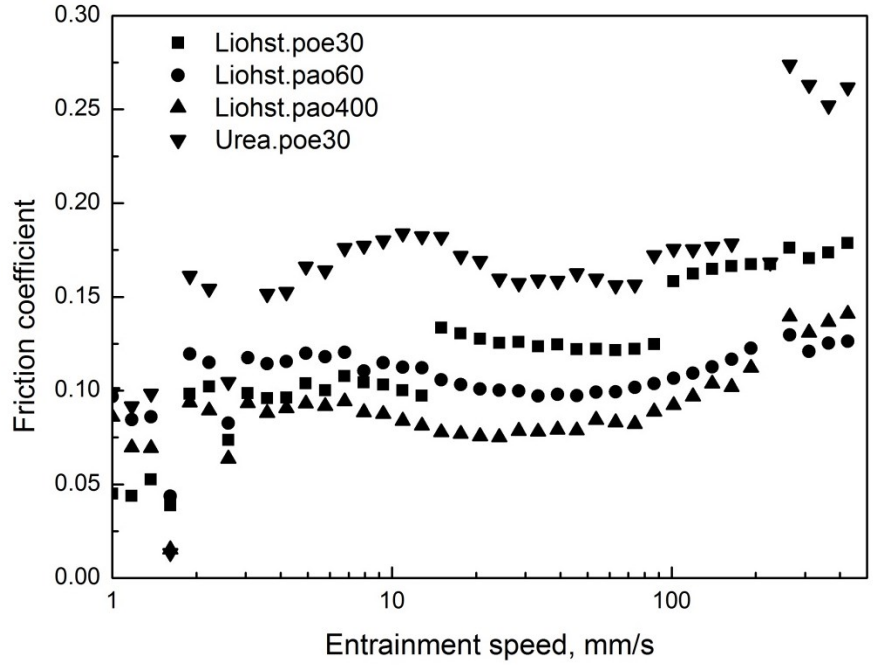

Figure 4.21 Entrainment speed dependence of film thickness for test greases, slide to roll 0.4

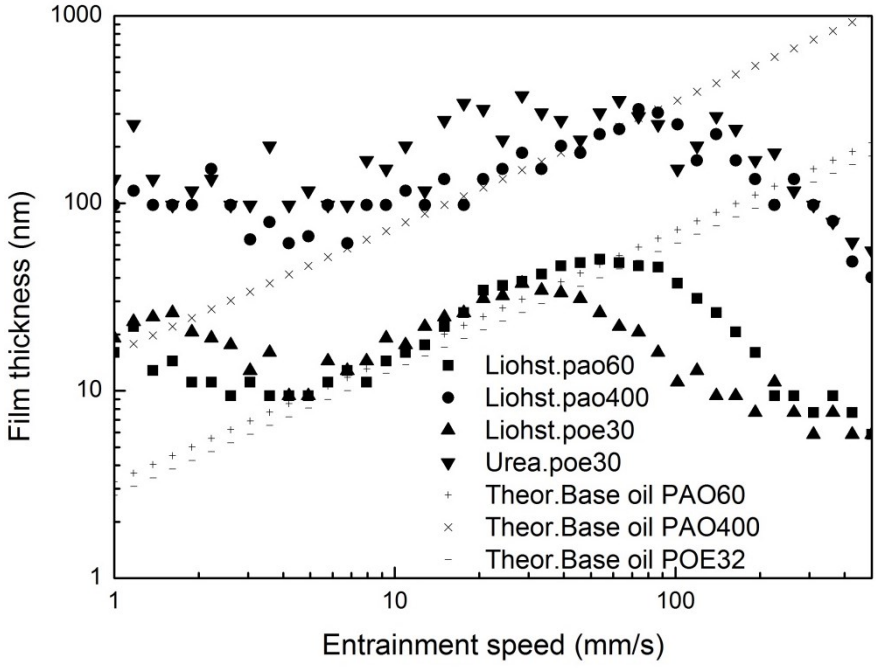

Figure 4.22 Entrainment speed dependence of film thickness in starved state

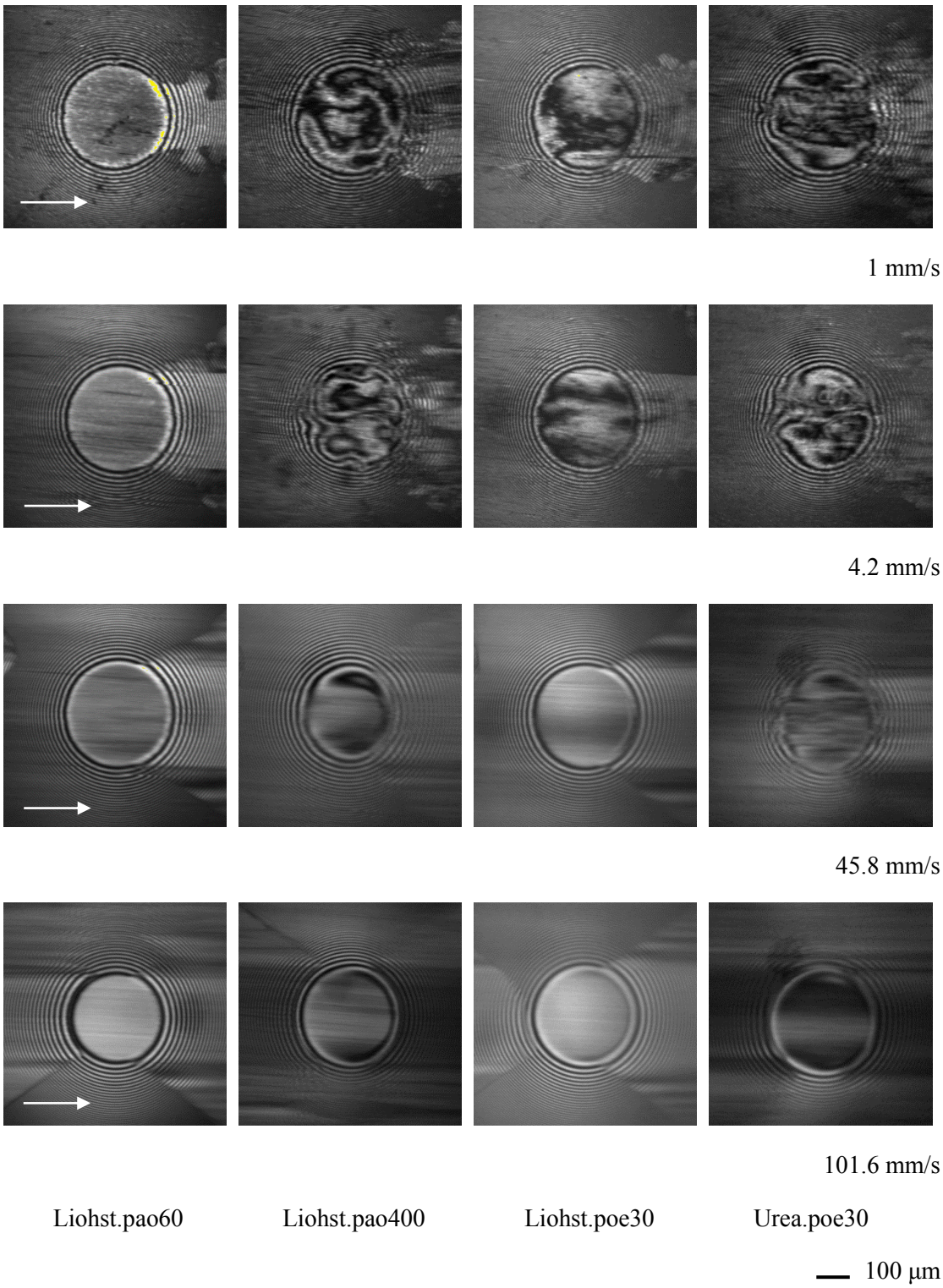

Figure 4.23 Speed evolution of the contact center of test greases in starved state

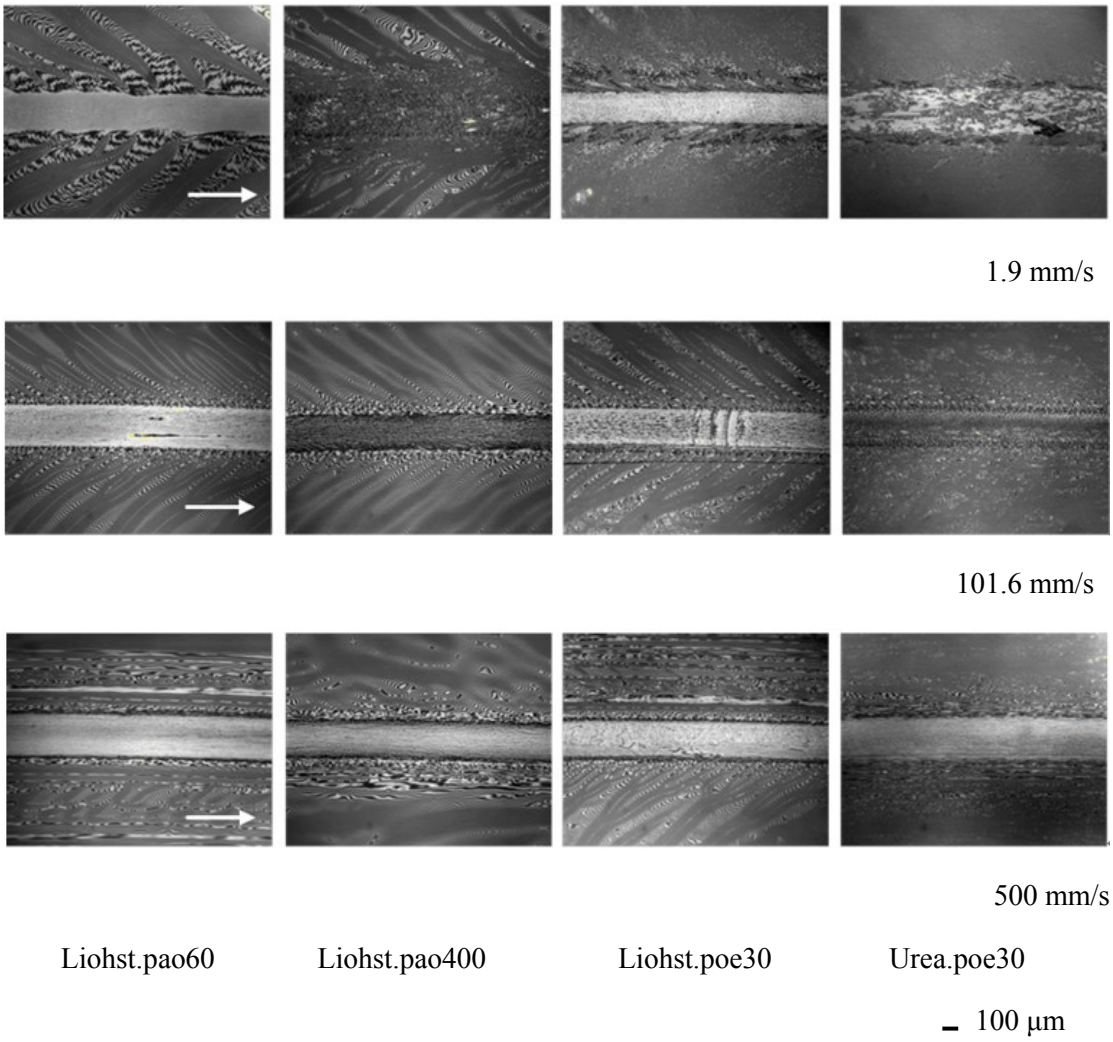

Figure 4.24 Speed evolution of the upstream patterns for slide to roll ratio 0.4

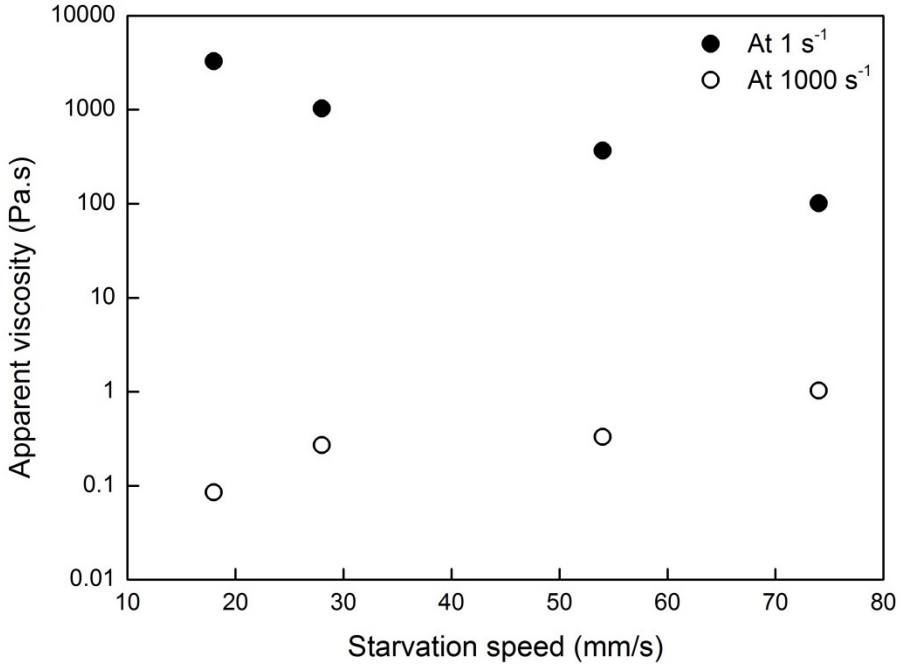

Figure 4.25 The starvation speed dependence of apparent viscosity

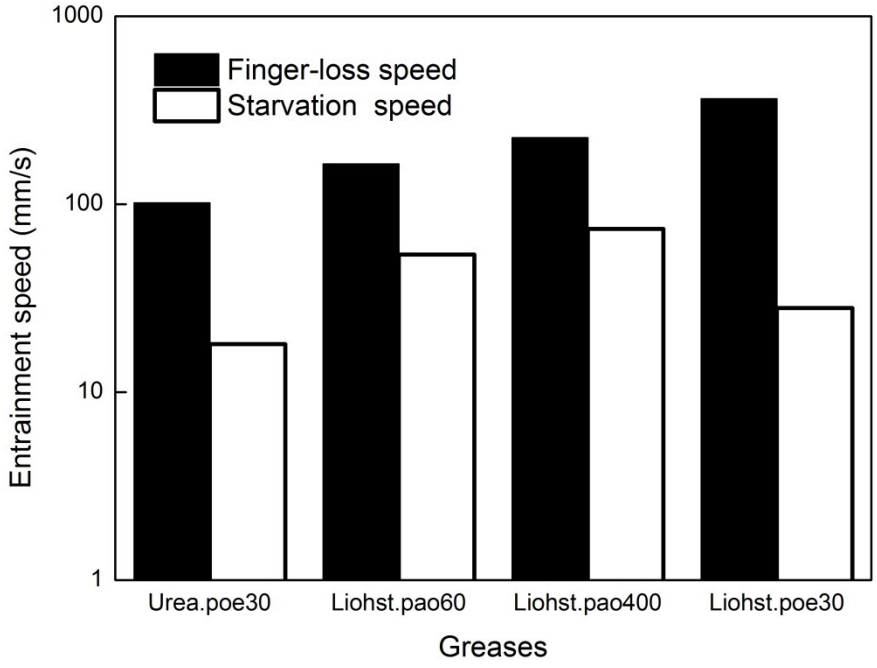

Figure 4.26 Finger-loss speed and starvation speed for test greases

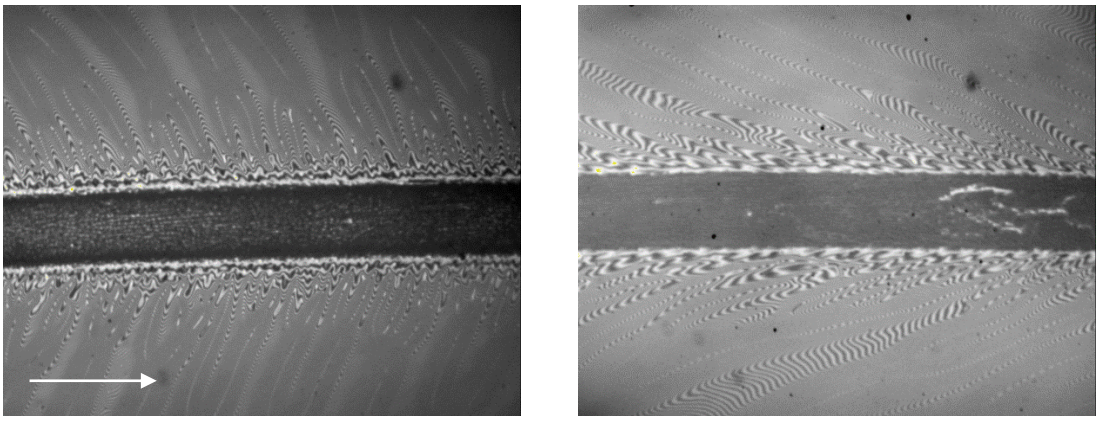

Revolution 12

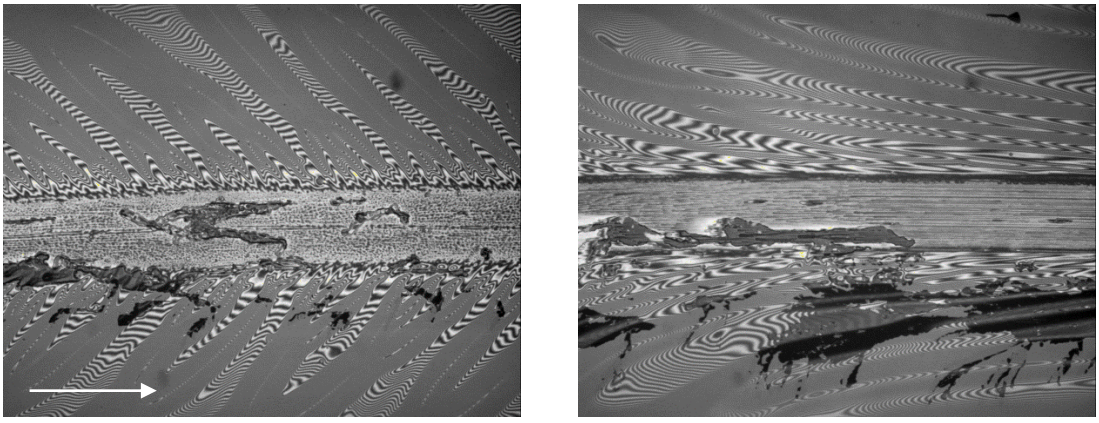

Revolution 60

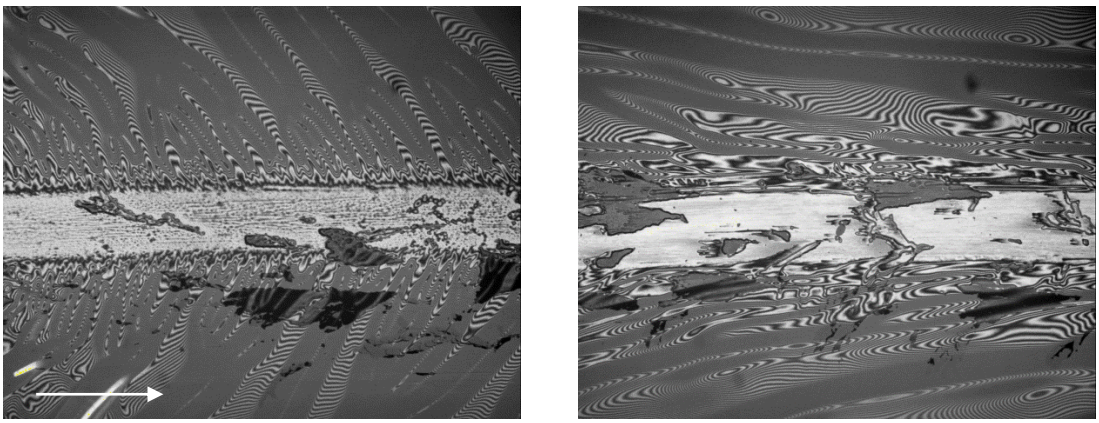

Revolution 120

SRR -1 SRR 1

Liohst.pao60 100 µm

Figure 4.27 The track pattern without artificial replenishment at the entrainment speed of 47.1 mm/s

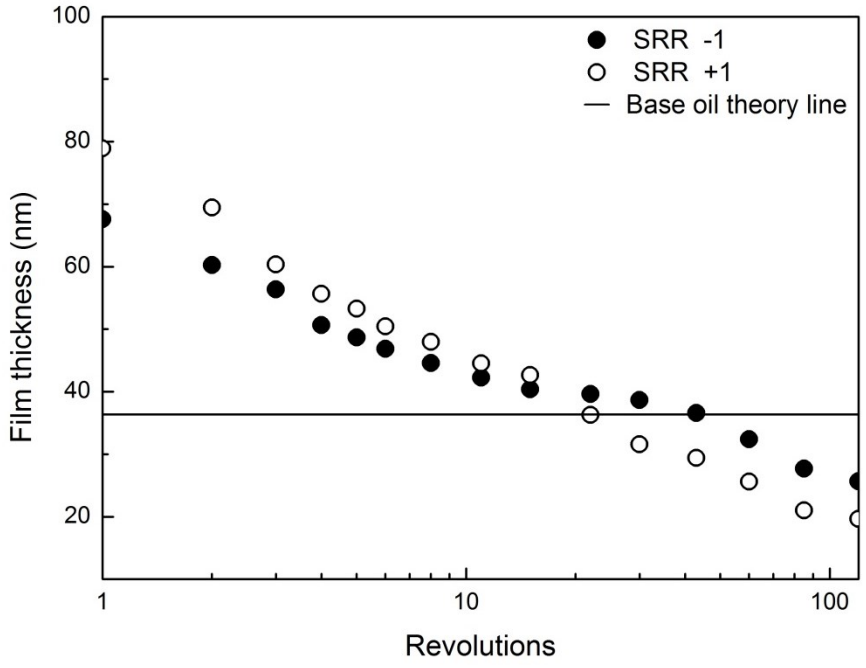

Figure 4.28 Revolution dependence of film thickness for Liohst.pao60 without artificial replenishment at the entrainment speed of 47.1 mm/s

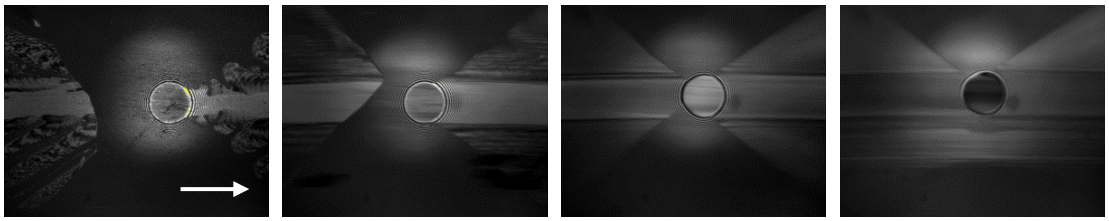

(i) Before test stop

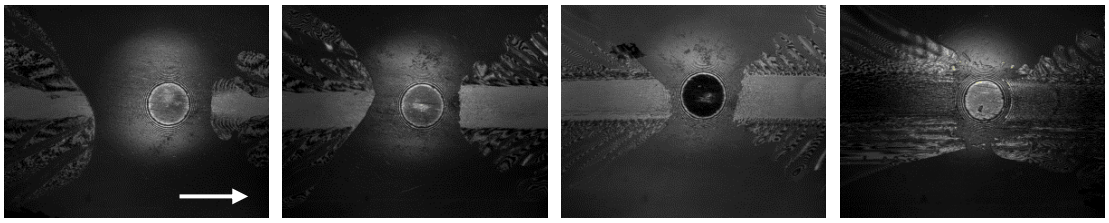

(ii) 1 s after test

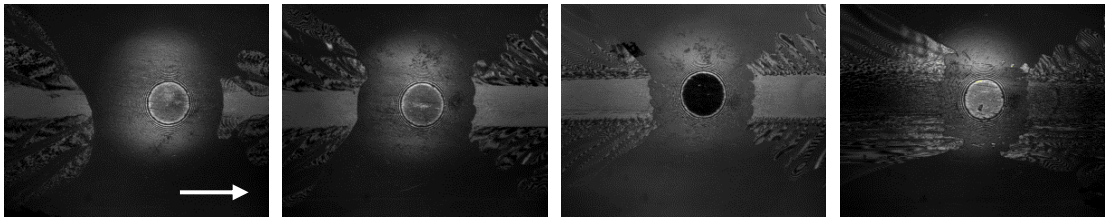

(iii) 5 s after test

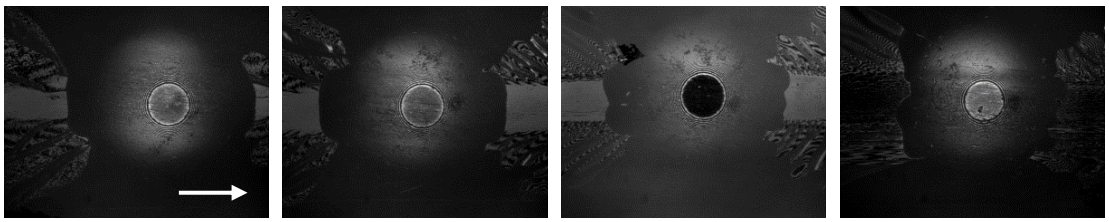

(iv) 60 s after test

1 mm/s 9.3 mm/s 101.6 mm/s 500 mm/s

100 μm

Figure 4.29 Evolution of the grease reservoir for Liohst.pao60 at different speed after test

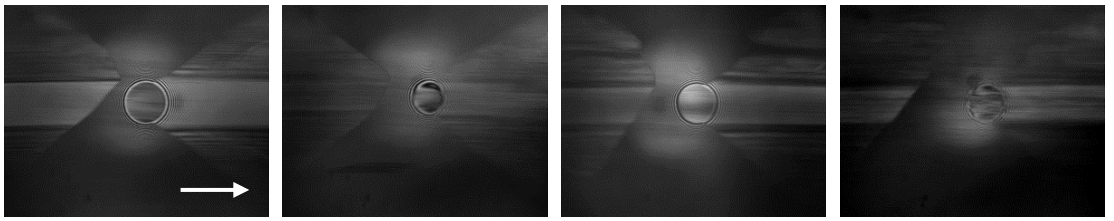

(i) Before test stop

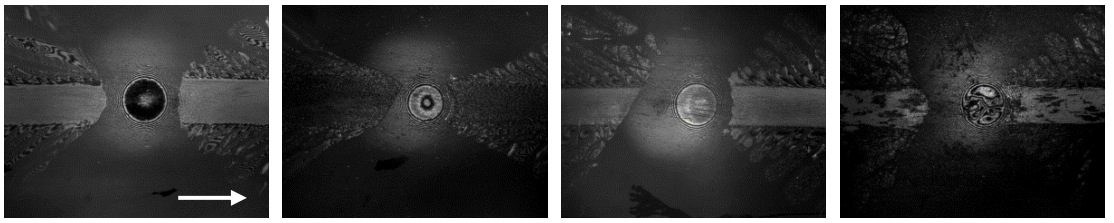

(ii) 1 s after test

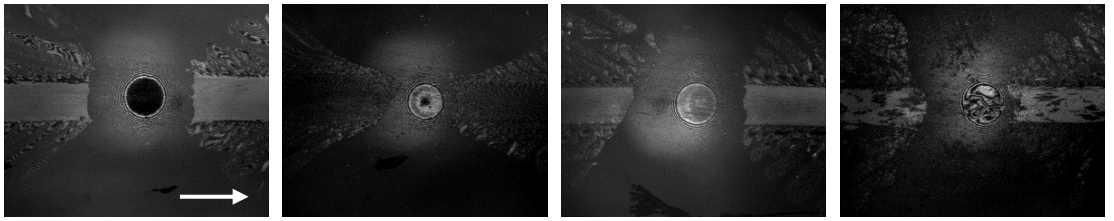

(iii) 5 s after test

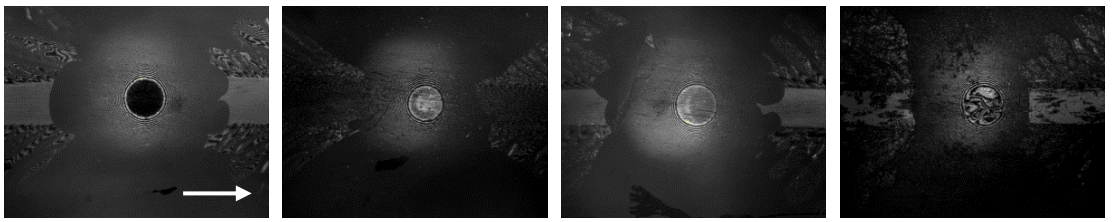

(iv) 60 s after test

Liohst.pao60 Liohst.pao400 Liohst.poe32 Urea.poe32

100 μm

Figure 4.30 Evolution of the grease reservoir for test greases at speed of 20.6 mm/s after test

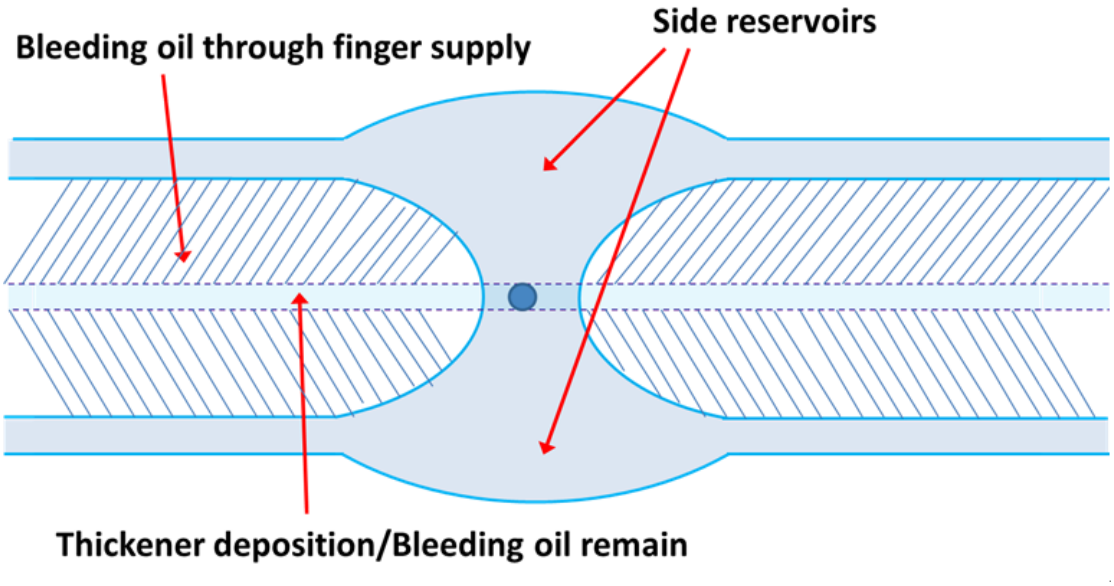

Figure 4.31 Supply sources of replenishment in a wider area

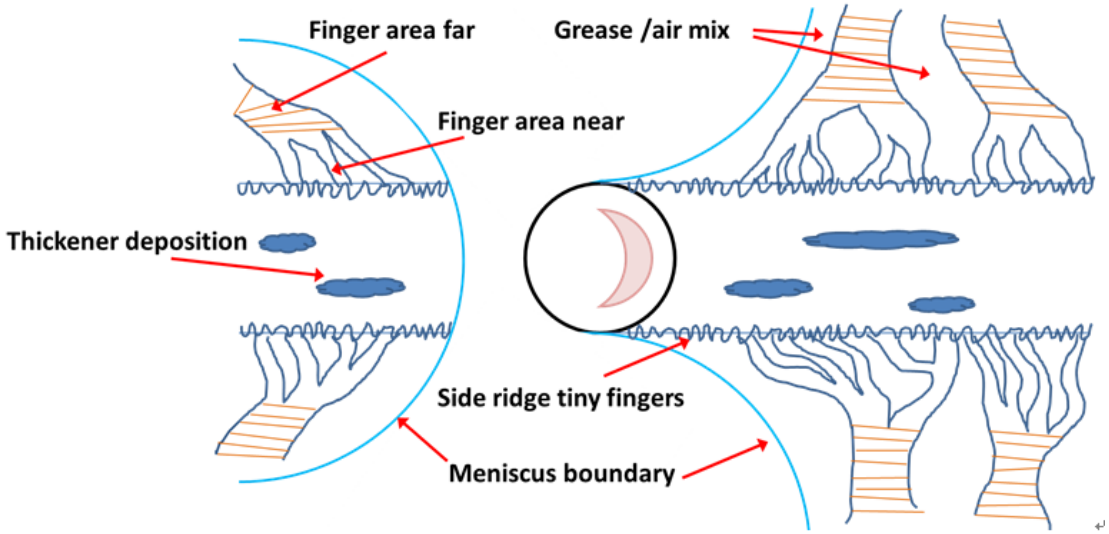

Figure 4.32 Supply sources of replenishment around the contact

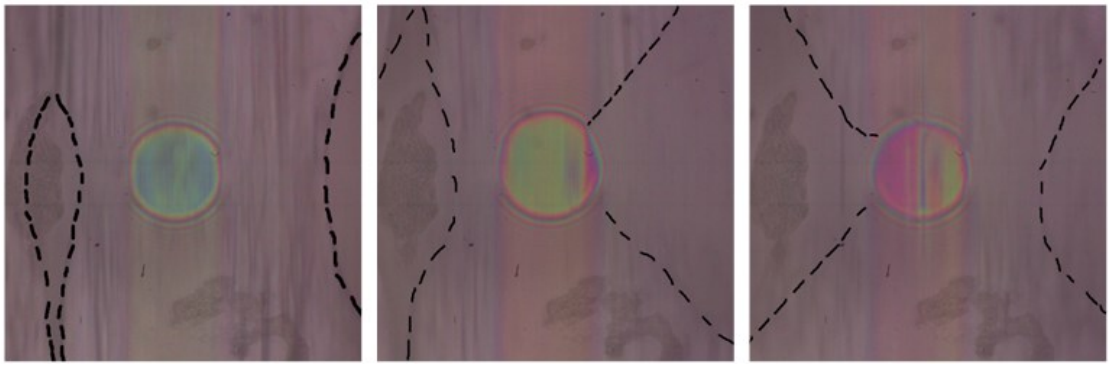

Figure 4.33 Side reservoirs replenishment for Liohst.poe30 at the entrainment speed of 119 mm/s

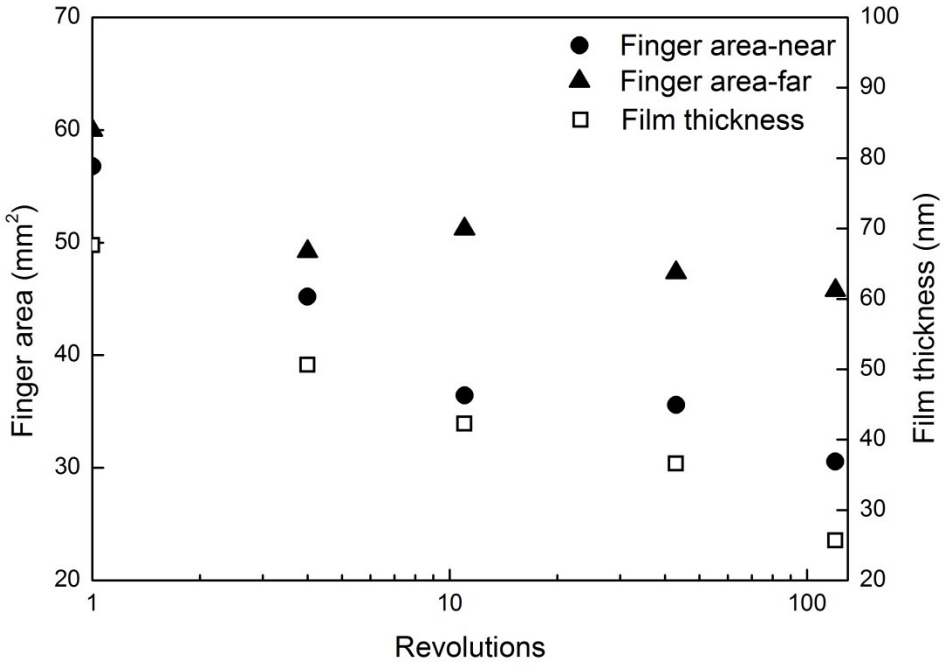

Figure 4.34 Revolution dependence of film thickness and finger area for Liohst.pao60 without artificial replenishment at the entrainment speed of 47.1 mm/s.

CHAPTER 5

Covariance analysis and principal component analysis

On the basis of the results in Chapters 3 and 4, covariance analysis is conducted to find out whether there exists correlation among all these factors including characteristic parameters, operating conditions, rheological parameters and film formation. In addition, principal component analysis is conducted to find the most representative parameters that represent the change in the features of grease flow when the entrainment speed, test duration and slide-to-roll ratio change. The covariance analysis shows that the eight characteristic parameters are more or less correlated with each other, and the principal component analysis suggests that some of them are strongly related and some are not in terms of their relationships with operating conditions, rheological parameters and film formation. The near finger area, the degree of contrast of ridges and the wavelength contain similar information regarding lubricating conditions. Each of the degree of finger contrast, the number of finger split joints, and the degree of thickener deposition separately reflects other characteristics including grease properties. These quantitative relations clearly represent the relationships found in Chapters 3 and 4.

5.1 Introduction

From the observation and analysis in Chapter 3 and 4, as it shows in Figure 5.1 that the features of track pattern changes with test conditions, rheological parameters and lubricating conditions. Although different types of greases have different features, in general, common changes exist in different greases and relate with other factors. Covariance analysis is a statistical method can find the correlation relationship between random variables. It is conducted to find out whether there exists correlation among all these factors.

Eight characteristic parameters are defined to describe the features of track pattern in Chapter 3. However, not all parameters show obvious distinctions or change regularly when test conditions change. Some parameters show prominent changes and others not. Principal component analysis is a method to simplify the datasets, and it can keep the most important parts. The aim of principal component analysis is to select the most appropriate parameters which can represent the change of track morphology when the entrainment speed, test duration and slide to roll ratio change, respectively.

5.2 The principle and procedure

5.2.1 Test greases

Table 5.1 shows the test greases. Five greases with different thickener, base oil and its viscosity are chosen for analysis. The thickener types are: Liohst, List and Di-urea. The base oil types are: Pao and Poe. Their detail information please refers to Table 2.2.

Table 5.1 Grease samples

Grease X_i	X_1	X_2	X_3	X_4	X_5
	Liohst.pao60	Liohst.pao400	List.poe30	List.pao20	Di-urea.pao30

5.2.2 Covariance analysis

These factors such as characteristic parameters, test conditions, rheological properties and film thickness, inevitably they have correlations among each other. It is hoped to know the whole system and find out some useful information. The thing to remember is the covariance analysis can only find out whether there is a linear relationship exists between two factors and the strength of this relationship, it does not tell the entire story. There could be other relationships exist.

Table 5.2 lists the data for the covariance analysis. As it shows, the variables are eight parameters; entrainment speed, SRR and test duration; the apparent viscosity under the shear rate of 1, 100 and 1000 s^{-1} (Please refers to Chapter 2); film thickness and the lubricating conditions. The definition of lubricating condition is listed in the bottom of this table: 1 is fully flooded, 0 is starved condition.

Table 5.2 Test data

	Parameters	Entrainment speed	SRR	Test duration	Apparent viscosity	Film thickness	Lubricating condition
Grease X_i	λ to D-T	1 to 500 mm/s	-1 to 1	1 to 40 mins	Constant for X_i at 1,100 and 1000 s^{-1}	h (X_i, test conditions)	1 or 0

Lubricating conditions 1 is fully flooded, 0 is starved condition

In the covariance analysis between multiple variables, the measurement value between two variables is called correlation coefficient, *i.e.*, r_{ij}. Two variables, the change of one will raises that of another, the change of another variable as a percentage of total variation is the correlation coefficient. Therefore, the correlation coefficient can give an explicit explanation on the relationship between two variables.

Set variables: $x_1, \ldots, x_m$. Their sample points are $(x_{1i}, \ldots, x_{mi})$ $i = 1, \ldots, n$. The formula of correlation coefficient between x_i and x_j is:

$$r_{ij} = \frac{SP_{ij}}{\sqrt{SS_i SS_j}} \quad i, j = 1, 2, \ldots, m.$$

where $SP_{ij} = \sum(x_i - \bar{x}_i)(x_j - \bar{x}_j)$, $SS_i = \sum(x_i - \bar{x}_i)^2$, $SS_j = \sum\left(x_j - \bar{x}_j\right)^2$.

The properties of correlation coefficient:

When $-1 \leq r_{ij} \leq 1$, r_{ij} is dimensionless and $|r_{ij}| \to 1$, the linear relationship between x_i and x_j is strong. When $|r_{ij}| \to 0$, the linear relationship between x_i and x_j is weak or not exist.

Moreover, t-test is adopted to validate that whether the linear relationship is significant or not. The formula is:

$$t = \frac{r_{ij}}{\sqrt{\left(1-r^2{}_{ij}\right)/(n-2)}},$$

Significant $Sig. = p$, if $p \leq 0.05$, the linear relationship between x_i and x_j is significant. If $p \leq 0.01$, the linear relationship between x_i and x_j is highly significant. If $p > 0.05$, the linear relationship between x_i and x_j is very weak or not exist.

5.2.3 Principal component analysis

In statistics, the principal component analysis (PCA) is a technology to simplify the datasets. It is a linear transform can transfer the data to a new coordinate system. This transform makes the largest variance of the data projection on the first coordinate system (the first principal component), the second largest variance of it on the second coordinate system (the second principal component), etc. The procedures of PCA used in our study are as follows:

(1). An original multiple track pattern characteristic matrix is defined as:

$$X = \begin{bmatrix} x_1(1) & \cdots & x_{1l}(n) \\ \vdots & \ddots & \vdots \\ x_m(1) & \cdots & x_{ml}(n) \end{bmatrix}, \quad i = 1, 2, \ldots, m; j = 1, 2, \ldots, n; k = 1, 2, \ldots, l$$

where m is the number of grease types, n is the number of the morphology parameters, and l is the test conditions, such as entrainment speed, test duration and slide-to-roll ratio. $x_{ik}(j)$ is the jth morphology parameter of ith grease under certain test conditions，such as the S-J, A-N, D, λ and A-F.

(2). The corresponding correlation coefficient matrix is calculated as:

$$R_{ij} = \left(\frac{Cov(x_i(j), x_i(l))}{\sigma_{x_i}(j)\sigma_{x_i}(l)}\right), j = 1, 2, \ldots, n; l = 1, 2, \ldots, n,$$

where $\mathrm{cov}(x_i(j), x_i(l))$ is the covariance of sequences $x_i(j)$ and $x_i(l)$, $\sigma_{x_i}(j)$ is the standard deviation of sequence $x_i(j)$ and $\sigma_{x_i}(l)$ is the standard deviation of sequence $x_i(l)$.

(3). The eigenvalues and eigenvectors are determined from the correlation coefficient matrix:

$(R - \lambda_k I_m)V_{ik} = 0$,

where the eigenvalue: $\lambda_k (k = 1, 2, \ldots, n)$, $\lambda_1 \geqslant \lambda_2 \geqslant \ldots \geqslant \lambda_n \geqslant 0$ and the eigenvectors $V_{ik} = [a_{k1} a_{k2} \ldots a_{kn}]^T$ correspond to the eigenvalue λ_k.

(4). The contribution rate of each component is determined by:

$b_k = \frac{\lambda_k}{\sum_{j=1}^{n} \lambda_j}$ ($k = 1, 2, \ldots, n$),

$CR = \sum_{k=1}^{m} b_k$,

where b_k is the contribution rate of each component and *CR* is cumulative contribution rate.

(5). Lastly, the principal components are obtained from:

$Z_{mk} = \sum_{i=1}^{n} x_m(i) \cdot V_{ik}$,

where Z_{m1} is the first principal component, Z_{m2} is the second principal component, etc. The principal components are aligned in descending order with respect to the contribution rate. Therefore, the first component Z_{m1} accounts for most of the contribution rate in the data.

5.3 Covariance analysis

Table 5.3 lists the results of covariance analysis. It is the matrix of the correlation coefficients and the t-test values. * means significant, and ** means highly significant, the data without mark means non-significant. The data used in the rest of content have ignored the pair of variables which non-significant. When the correlation value is positive, this pair of variables is positive correlation, *i.e.*, one of them increases with the increasing of another. When the correlation value is negative, this pair of variables is negative correlation, *i.e.*, one of them decreases with the increasing of another.

Table 5.3 Covariance analysis results

		λ	S-J	A-N	A-F	D	D-F	D-R	D-T	Entrainment speed	SRR	Test duration	1 s^{-1} (Pa.s)	100 s^{-1} (Pa.s)	1000 s^{-1} (Pa.s)	Film thicknes	Lubricating conditions
λ	Correlation coefficient	1	-.366**	-.580**	-0.1300363	.690**	-0.1413514	-.340**	0.0434057	0.021231726	.295*	-.251*	-0.02805994	0.042234104	0.076881445	-0.12175734	-.261*
	Sig.(2-tailed)		0.00123375	4.9832E-08	0.26615442	7.2042E-12	0.22640808	0.0028457	0.71155757	0.856521275	0.0102065	0.029992569	0.811127508	0.719015089	0.512080714	0.29805346	0.023965353
S-J	Correlation coefficient		1	.453**	.237*	-.497**	0.02900238	.240*	-0.1554732	.247*	-0.193687	0.126705211	.357**	-.337**	-.247*	0.21119511	-0.12702486
	Sig.(2-tailed)			4.5185E-05	0.04075675	5.8702E-06	0.80490722	0.03824459	0.18288065	0.032836703	0.0959098	0.27870101	0.001650325	0.003133332	0.032964655	0.06893299	0.277480256
A-N	Correlation coefficient			1	0.07734487	-.412**	-.236*	-0.1176342	-0.0973302	0.033154572	-.292*	-0.19434509	-0.017001513	-0.039441578	-0.095460457	0.09180882	0.176694412
	Sig.(2-tailed)				0.50953308	0.00024106	0.04161689	0.31483612	0.4061309	0.777650555	0.011154	0.094765029	0.884888632	0.736895148	0.4152502	0.43339816	0.12939894
A-F	Correlation coefficient				1	-0.1634692	0.05844313	0.11574379	-0.1424963	0.000652735	-0.042059	-0.00380179	0.143228289	-0.1421641	-0.138013572	0.20089454	0.044690705
	Sig.(2-tailed)					0.16110851	0.61844353	0.32273003	0.22263119	0.995565454	0.7201334	0.97417571	0.220239384	0.223722439	0.237674943	0.08394463	0.703409103
D	Correlation coefficient					1	-0.1375711	-.465**	0.1252722	-.262*	0.1948208	-0.21951441	-0.06546178	0.10808675	-0.134839635	-.246*	0.093251715
	Sig.(2-tailed)						0.23919711	2.6181E-05	0.28421769	0.023130781	0.0939439	0.058454882	0.576849286	0.355983895	0.248742697	0.03308331	0.426174142
D-F	Correlation coefficient						1	.427**	-0.1806111	0.144560055	0.0628971	.349**	-6.24734E-18	0	0	-0.05031706	-0.05143445
	Sig.(2-tailed)							0.00013336	0.12098578	0.215934462	0.5918983	0.002154779	1	1	1	0.66813334	0.661209293
D-R	Correlation coefficient							1	-.274*	.382**	0.0426606	.385**	0.015054429	-0.037166139	0.005980839	0.0169098	-.403**
	Sig.(2-tailed)								0.01732811	0.000721601	0.7162973	0.00064474	0.897996525	0.751568744	0.959384428	0.88550539	0.000343695
D-T	Correlation coefficient								1	-0.157029307	-0.002805	0.21491287	-0.003773698	0.009316447	-0.001499219	-0.07444759	.262*
	Sig.(2-tailed)									0.178484373	0.9809457	0.064077562	0.974366482	0.936770656	0.989814843	0.52556675	0.023070623
Entrainment speed	Correlation coefficient									1	0.1333376	-0.07925224	-1.94655E-17	7.49037E-18	-1.84242E-18	-0.19584385	-.679**
	Sig.(2-tailed)										0.2541015	0.49911618	1	1	1	0.09219715	2.07481E-11
SRR	Correlation coefficient										1	-0.1045051	-9.82349E-18	-1.20964E-17	-1.48768E-17	-0.07841015	-.259*
	Sig.(2-tailed)											0.37223948	1	1	1	0.50370146	0.024959471
Test duration	Correlation coefficient											1	-1.0616E-17	2.8759E-17	2.1436E-17	0.00803379	0.153827349
	Sig.(2-tailed)												1	1	1	0.94546152	0.187615249
1 s^{-1} (Pa.s)	Correlation coefficient												1	-.944**	-.485**	.594**	-0.05494488
	Sig.(2-tailed)													8.05408E-37	1.01697E-05	1.9442E-08	0.639642689
100 s^{-1} (Pa.s)	Correlation coefficient													1	.353**	-.668**	0.063348643
	Sig.(2-tailed)														0.001904018	5.9927E-11	0.589235902
1000 s^{-1} (Pa.s)	Correlation coefficient														1	.265*	0.051413921
	Sig.(2-tailed)															0.02178932	0.66133625
Film thickness	Correlation coefficient															1	0.057158708
	Sig.(2-tailed)																0.626192193
Lubricating conditions	Correlation coefficient																1
	Sig.(2-tailed)																

5.3.1 Track pattern

Table 5.4 Track pattern

A-N & S-J	A-N & λ	A-N & D-F	
D-R & S-J	D-R & D-F	D-R & λ	D-R & D-T
D &S-J	D & λ	D & A-N	D & D-R
S-J & λ	S-J & A-F		

Table 5.4 shows the correlation between characteristic parameters. They are from Table 5.3. Although different characteristic parameters describe different locations of the track pattern and their features are also different, the grease flow is an entire process, cannot be separated. Therefore there are many characteristic parameters related with each other exist.

These correlation pairs can be described as an evolution of track pattern, regardless of the type of grease. When the inlet meniscus distance D gradually decrease, the average interval between finger trunks, *i.e*, λ also decrease. However, the near-finger area A-N will increase with the finger split joints S-J, the track pattern become more complex. The degree of track pattern contrast and visual clarity also changes, such as the degree increase at side ridge D-R and finger D-F position. The deposition in the center of track D-T will decrease in this process.

These parameters are related with each other, from the change of one parameter can reflect the situations of others. Therefore in actual researches, the specific parameters adopted depending on specific conditions and their physical meanings. Except the inlet distance D and the wavelength λ have been used in some articles [1-2], other parameters have not been used to study the grease flow behaviors.

5.3.2 Test conditions

Table 5.5 Test conditions

Speed & S-J	Speed & D	Speed & D-R
Test duration & D-F	Test duration & λ	Test duration & D-R
SRR & A-N	SRR & λ	

Table 5.5 shows the track pattern characteristic parameters and test conditions. They are from Table 5.3. As can be seen, there are some characteristic parameters have linear relationship with the test conditions. These include:

When there only the entrainment speed changes, the inlet meniscus distance D will decreases and the finger split joints S-J and the degree of finger contrast and visual clarity D-F will increase. They almost coincide with the result of observation in the entrainment

speed series test in Chapter 3. The change trend of S-J is obvious. It can be seen in Figure 3.14. However, the degree of finger contrast and visual clarity D-F is not the case. Some greases like Liohst.poe30, its clarity looks obscure at first but then becomes clear. Whereas Liohst.pao60 can keeps clarity all the time. Therefore, when considering the correlation between finger clarity D-F and entrainment speed, it is possible that the situation is not obvious, though does not violate this relationship.

With the increasing of SRR, the covariance analysis results show that the wavelength λ will gradually increases and the near-finger area A-N will gradually decreases. As we have observed, the A-N changes with SRR, but not the linear relationship. The correlation coefficient is not high in this case. This is probably the reason for this result.

When there only the test duration changes, the degree of finger contrast and visual clarity D-F and the degree of ridge contrast and visual clarity D-R increase with the increasing of test duration. The wavelength λ will decreases. These changes may come from the changes of the distribution of viscoelasticity, which due to the rolling action for long periods [3]. These changes will happen whether SRR is zero or not, the shear action can only contribute to the change of track features under slide-roll conditions.

From the above analysis, the variation of the parameterized track pattern can represent the grease flow behaviors. Although different track pattern has its own unique features, the characteristic parameters can show the same change trend under some conditions. So it has universality to a certain extent. Certainly, the grease lubrication mechanisms behind these features are more important. It proves that use these parameters to study grease flow behaviors is not only feasible, but also very meaningful.

5.3.3 Apparent viscosity

Table 5.6 Apparent viscosity

1000 s^{-1} & 100 s^{-1}	1000 s^{-1} & 1 s^{-1}	100 s^{-1} & 1 s^{-1}
1 s^{-1} & S-J	100 s^{-1} & S-J	1000 s^{-1} & S-J

Table 5.6 lists the correlation between characteristic parameters and apparent viscosity. As it shows, apparent viscosity has no relationship with the test conditions. This result is not true, but reasonable. There is no better way to know the rheological properties of grease except using the rheometer. Either the geometry of rheometer or the range of shear rate is different from these in an EHL contact. It is very difficult to connect each other. Therefore, the rheological data from rheometer is usually used to discuss the difference between different types of grease, not the same grease under different test conditions.

In the data table for covariance analysis, the apparent viscosity is the same for the same type of grease, so it is natural that the result shows they have no relationship. However, we

should know that the rheological properties will change under different test conditions, this relationship could not be discussed since there is no way to know it.

The characteristic parameter related to the apparent viscosity is only finger split joints S-J. As mentioned above, the grease with higher viscosity under low shear will drop more with the increasing of shear rate. Therefore they are not in conflict. The finger split joints S-J will increase with the increasing of entrainment speed. Naturally, when SRR is not zero, the viscosity will decline obviously. This means the decline of viscosity probably the main reason for the increasing of S-J. This is consistent with the covariance analysis results.

The relationship between the apparent viscosities under different shear rate, from these results, it can be explained that: As the shear rate increases, the grease with higher viscosity under low shear will drop more. The viscosity of the base oil: Pao60 is 0.11 Pa.s, Pao400 is 0.88 Pa.s. The viscosity of grease: Liohst.pao60 is 0.33 Pa.s at the shear rate of 1000 s^{-1}, Liohst.pao400 is 1.03 Pa.s at the shear rate of 1000 s^{-1}. In real EHL contact, the shear rate will far excess 1000 s^{-1}. Thus the viscosity of grease will be more approximate to that of base oil. As can be seen, the whole range of viscosity for grease under high shear is quite low. However, the viscosity of grease under low shear like 1 s^{-1} can range from several hundred to several thousand. From these variations, the covariance analysis result is true.

5.3.4 Film thickness and lubricating conditions

Table 5.7 Film thickness

h & 1 s^{-1}	h & 1000 s^{-1}	h & 100 s^{-1}
h & D		

Table 5.7 shows the variables related to the film thickness. From these results, the apparent viscosity and the inlet distance related to the film thickness. This is in line with the general case. The inlet meniscus distance D is proportional to the amount of lubricant in the inlet area [2]. The amount of lubricant in the inlet area determines the film thickness [3]. The higher the apparent viscosity, the higher the film thickness can be obtained at the same conditions [4].

Table 5.8 Lubricating conditions

Lubri & D-T	Lubri & D-R	Lubri & λ
Lubri & SRR	Lubri & Entrainment speed	

Table 5.8 shows the variables related to the lubricating conditions. The characteristic parameters related with the lubricating conditions are: The degree of thickener deposition D-T, the degree of ridge contrast and visual clarity D-R and the wavelength λ. The positive role that the thickener deposition in the center of track plays in the lubrication is confirmed in chapter 4. A model proposed by Cann *et al*. [5] is that the grease-lubricated contacts are layered by a shear degraded residual thickener layer and an oil layer formed by hydrodynamic

action. From the actual observation, this model is correct when the contact conjunction is under low shear or in a fully flooded state.

The degree of ridge contrast and visual clarity D-R is visual definition. The higher the D-R, the ridge more sharp, *i.e*, it contains more grease. There are many models about this ridge [6-8]. As the rolling elements rotate, it produces a depressed oil layer shape in the center of track. Two adjacent oil ridges are formed due to the push of rolling elements.

Chiu [8] is the first one simulates the replenishment process of two side ridges towards the track. He assumes the surface is fed by a uniform layer of oil, and the trigger forces are surface tension and viscosity. Later Van der Waals force [7] and centrifugal forces [8] are also considered. Side ridge is preserved from this dynamic process.

It is possible that the side ridge becomes one part of channel for lubricant flow back through fingers. However, it is also possible that the side ridge becomes the dam to obstruct flow. It depends on the interaction between the thickener and base oil.

The wavelength λ represents the density of the number of fingers. It is mainly determined by the entrainment speed [1]. The correlation between lubricating conditions and the wavelength λ is overlap with the correlation between lubricating conditions and entrainment speed.

The effect of entrainment speed to lubricating conditions is obvious. According to the Hamrock-Dowson equation [4], the increase of entrainment speed can increase the film thickness. Other test condition which related with lubricating conditions is SRR, and the main reason is the change of rheological properties due to the shear action under slide-roll condition.

5.4 Principal component analysis

5.4.1 Entrainment speed

The total variance explained is listed in Table 5.9. In this table, the column of initial eigenvalues gives an ordered sequence of principal component score, the numeric equivalent of the eigenvalues of the correlation coefficient matrix. Therefore, the percentage of variance for every principal component can be calculated based on the eigenvalues.

Since the sum of all eigenvalues equals to the number of variables, that is $m = \sum \lambda = 8$. The percentage of variance for the first eigenvalue is λ_1/m = 4.45/8 = 55.63, and so on. Then the percentage of variance cumulative can be calculated. The column of extraction sums of squared loadings, it shows the information of two principal components from the left-hand column. The selection principle is $\lambda > 1$.

Table 5.9 Total variance explained

Component	Initial Eigenvalues			Extraction Sums of Squared Loadings		
	Total	% of variance	Cumulative %	Total	% of variance	Cumulative %
1	4.45	55.63	55.63	4.45	55.63	55.63
2	1.12	14.01	69.64	1.12	14.01	69.64
3	0.9	11.29	80.94			
4	0.7	8.8	89.74			
5	0.38	4.74	94.48			
6	0.24	3	97.49			
7	0.13	1.67	99.15			
8	0.068	0.85	100			

Table 5.10 shows the component matrix, the correlation coefficients between each variable and the corresponding principal component are listed in each column. As an example, in the first column, -0.93 is the correlation coefficient between λ and the first principal component. From this table, λ, A-N and D-R relate more to the first principal component.

Table 5.10 Component matrix

	Component	
	1	2
λ	-0.93	-0.054
S-J	0.74	0.024
A-N	0.89	-0.049
A-F	0.45	-0.46
D	-0.8	0.27
D-F	0.25	0.86
D-R	0.91	0.028
D-T	-0.64	-0.27

As shown in Table 5.11, the compositions for the first principal component are λ, A-N and D-R, the composition for the second principal component is D-F. According to the previous analysis results, λ, A-N and D-R are related with each other. It means one of these three can

be selected and represent the other two. When we describe the features of track pattern in the entrainment speed series test, it is enough to have one of λ, A-N and D-R, D-F. As for λ, A-N and D-R, the choice depends on the type of grease, etc.

Table 5.11 Analysis results for entrainment speed

	Constitutes
The first principal component	λ, A-N, D-R
The second principal component	D-F

From the observation results in Chapter 3, the change of λ, A-N with entrainment speed are very evident. As for D-R, it is also evident for Liohst.poe30 in Figure 3.14. Therefore, the results of principal component analysis for entrainment speed series test can be found in real observation, and these results are credible.

5.4.2 Test duration

Table 5.12 Analysis results for test duration

	Constitutes
The first principal component	D, D-R
The second principal component	A-F
The third principal component	S-J

The steps of analysis performed are the same as the entrainment speed part. Table 5.12 shows the summary on the principal component analysis results for test greases. Besides the first component and the second one, the third principal component is needed to meet the require information amount.

D and D-R are the compositions for the first principal component, and the second one is A-F, the third principal component is S-J. The same as the previous analysis for entrainment speed test. D and D-R are correlated with each other. It means that enough information can be obtained when one of them is selected. Therefore, any one of D and D-R, A-F and S-J can represent the change of track features in the test duration series test.

5.4.3 Slide to roll ratio

Table 5.13 Analysis results for slide to roll ratio

	Constitutes
The first principal component	A-N, D-F, D-R
The second principal component	D
The third principal component	λ

Table 5.13 shows the summary on the principal component analysis results for test greases. There are three principal components for test greases. A-N, D-F, D-R appear in the first principal component, and the second one is D, the third principal component is λ. A-N, D-F and D-R are related with each other. On the same principle, the results show that any one of A-N, D-F and D-R, D and λ can represent the change of track features in the slide to roll ratio series test. In the SRR observation part, we have observed that A-N changes regularly with SRR, this is consistent with the analysis of PCA.

5.5 Conclusions

The main conclusions for this chapter are listed as follows:

1. Many characteristic parameters are related with each other, regardless of the type of grease
2. Some characteristic parameters have linear relationship with the test conditions.
3. The apparent viscosity is related with the finger split joints.
4. The apparent viscosity and the inlet distance related to the film thickness.
5. The first principal component includes: one of λ, A-N, D-R and D-F for entrainment speed test. One of D, D-R; A-F and S-J for test duration test. One of A-N, D-F, D-R; D and λ for slide-to-roll ratio test.

References

[1] Jing Chen, Hiroyoshi Tanaka, Joichi Sugimura. Experimental Study of Starvation and Flow Behavior in Grease-Lubricated EHD Contact. Tribology Online, 2015; 10: 48-55.

[2] Wedeven LD, Evans D, Cameron A, Optical Analysis of Ball Bearing Starvation, Journal of Lubrication Technology, 1970; 3: 349-361.

[3] Bikerman, J.J. The rheology of adhesion. In Rheology Theory and Applications (Ed. F. Eirich), 1960, 3, 479-503.

[4] B. J. Hamrock and D. Dowson, Ball Bearing Lubrication: Elastohydrodynamics of Elliptical Contacts, John Wiley & Sons Inc., 1981.

[5] Cann PM, Starvation and Reflow in a Grease-Lubricated Elastohydrodynamic Contact, Tribology Transactions, 1996; 39: 698-704.

[6] Chiu YP. An Analysis and Prediction of Lubricant Film Starvation in Rolling Contact Systems, ASLE Transactions, 1974; 17: 22-35.

[7] B. Jacod, F. Pubilier, P.M.E. Cann, A.A. Lubrecht, An Analysis of Track Replenishment Mechanisms in the Starved Regime, Tribology Series, 1999; 36: 483-492.

[8] J.Yin, K.I. Eissa, R.Gohar, P.M.E. Cann, Rebounding lubricant layers, Lubrication Science, 1999; 12: 1-30.

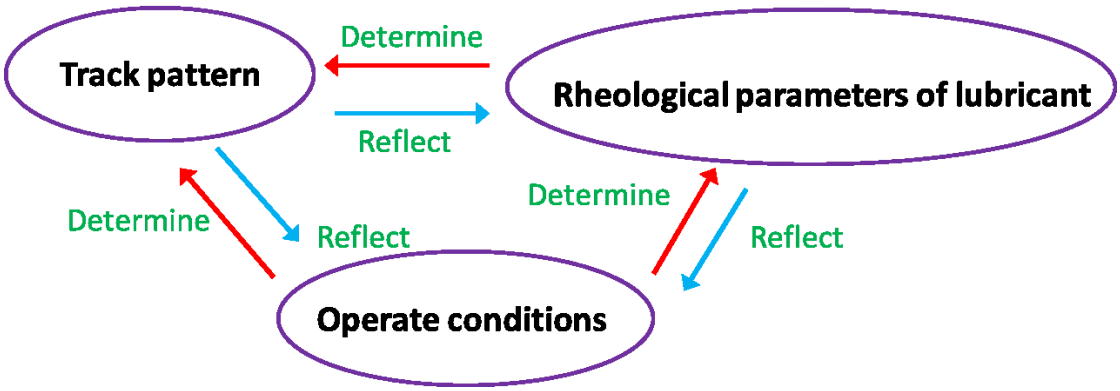

Figure 5.1 Schematic representation of the relationships among track pattern, operate conditions and rheological parameters of lubricant

CHAPTER 6

Observation on the flow behaviors of side reservoirs

An attempt is made to observe in-situ the behaviors of greases with a wider observation range by using a fluorescence technique. It is shown that the technique is capable of studying the replenishment of grease by the grease from the side reservoir merging with grease left in the form of the fingers at sides of the track. It is also shown with fluorescence that, in the case with di-urea grease, EHL film thickness first decreases with time due to weak supply of the grease and subsequently increases due to thickener deposition on the track.

6.1 Introduction

The primary reason for the decision to adopt the fluorescence measurements is still to observe the grease flow behaviors. Despite two groups of tests are conducted in chapter 3, these tests can only show the details of track pattern leaved by grease flow while the test stop. And this static observation can only be applied under the stable conditions, such as the condition that flow behaviors which change a lot with test duration is not included. Fluorescence technique is a good way to know the in-situ flow behaviors. Moreover, it can provide a wider observation range.

6.2 Fluorescence measurements

Two types of fluorescence images are used in this chapter. In summary, the monochrome image is suitable for the observation of small contact zone, and the color image is suitable for that of wider area. The experimental methodology and other details for this chapter are listed in the following contents. The test greases are Urea.pao30 and List.pao30. For the basic experimental procedures, please refer to 3.2 section of chapter 3.

A fluorescent substance can absorb light at one wavelength, and then subsequently emit light of another wavelength. The wavelengths and intensities at which fluorophores absorb and emit are determined by their electrochemical structure. The fluorescence technique can be used in the measurement of film thickness, as long as it emits fluorescent light with sufficient intensity [1].

In order to increase the emission intensity and to be able to select the desired excitation and

emission wavelengths, the pyrene which dissolves well in the oils is used as a dye in this study. The concentration of it in grease is 2.0 %. According to a hand book of fluorescence [2], pyrene has an absorption peak wavelength of 336 nm, and an eximer emission peak wavelength of 480 nm at high solute concentration in cyclohexane.

However, another main constituent of grease is thickener. The pyrene does not dissolve in thickener. In addition to the thickener type that contain molecular features such as double bonds which allow for absorption in the ultra-violet and re-emission in the visible [1], in our study is Di-urea. Hence, the fluorescence images shown in this study mainly indicate the distribution of base oils. Overall, the fluorescence measurement provides the possibility of observing the base oil flow around the contact zone. This is impossible in ordinary optical interferometry measurement.

The experimental setup for fluorescence measurements is almost the same as the static test in 3.2 section of chapter 3. The only difference is the selection of the filters [3]. The test greases as shown in Table 2.2, the pyrene are added to them. Lower concentration of pyrene will not affect the rheological properties of grease.

6.2.1 Monochrome images

The benefit of using CCD monochrome camera is the in-situ information can be recorded with the aid of software. Figure 6.1 is the fluorescence image with an objective lens of a magnification of 4 (4X), the red circle shows the contact zone, the fan shape with black color is cavity, the light intensities of other areas are proportional to the distribution of the amount of base oils if the assumption that a constant concentration of pyrene is meet. The influences of cavities and sensitivity of the CCD camera make the film thickness measurement could not be obtained very accurate [4].

Figure 6.2 is the fluorescence image with an objective lens of an objective lens of a magnification of 10 (10X), the valid film thickness could not be got due to the low intensity. In this chapter, the monochrome fluorescence images used are 4X. These images are used to observe the flow behaviors relative near the contact zone.

6.2.2 Color images

In addition, in order to observe a wider area around the contact zone which includes the

side reservoirs as shown in Figure 4.28, a separate camera is used to get the color image like Figure 6.3. As it shows in this picture, the trend of base oils can be clearly seen. Unfortunately, the photographic method is merely manual operations, not the same as that of CCD camera which has the aid of software. It has constrained the application range of the color fluorescence images.

For instance, the tests use the revolution as the unit, if the speed is low, the operation time maybe enough to get the corresponding picture; if the speed is high, it is not allowed to get one. The operation time includes manual operation time and the exposure time. Therefore, it is difficult to reduce too much. As shown, the contact zone is quite small, this image also not favorable to be used to measure the film thickness. Despite all these unfavorable factors, it is clearly a step forward to know the conditions in a wider area.

6.3 Results and discussion

6.3.1 Effects of entrainment speed

Figure 6.4 shows the reflection picture and the fluorescence picture for Urea.pao30 at static state. In these pictures, the Hertz contact area is marked with red dotted line. The reflection picture can only show the position of contact area, whereas the fluorescence picture can reflect the distribution trend of lubricant.

In the fluorescence picture, the intensity is proportional to the amount of lubricant. That means the portion with bright blue color has a large quantity of lubricant, contrary to the dark color in the contact center. On the right side of the fluorescence picture, the clear oil boundary can also be seen. All these phenomena could not be observed in the reflection picture.

Figure 6.5 shows the fluorescence pictures at different entrainment speed, these pictures are taken at stable state. They show a speed evolution process of side reservoirs. There is full of lubricant in the inlet area, and the cavity starts to form at the entrainment speed of 1 mm/s. After that, the amount of lubricant in the inlet area show a gradual decline, the meniscus boundary gradually moves closer to the contact point, i.e, the inlet distance S decreases.

At the entrainment speed of 2.8 mm/s and 4.6 mm/s, there are two bands, which derived from the junction between side reservoirs and the contact area. The purple colors in the center of contact tracks are more obvious than that of other speed. The thickener of Urea can emits

fluorescent light, it shows purple color. As can be seen from these fluorescence pictures, there are more or less purple deposition in the center of track, this color becomes light with entrainment speed. This is consistent with the previous observation.

As the entrainment speed increases, these two bands disappear, the contact zone direct connects with the side reservoirs. At the entrainment speed of 7.7 mm/s, the distribution boundary of grease flow becomes more indistinct than that of lower speed. Some possible reasons include: First is the increase of speed. Moreover, the quantity of grease fingers increase. From the previous observation, the finger area will increases with entrainment speed. However, compare with side reservoirs, the quantity of grease included in fingers is still very small. Therefore, there is only the indistinct boundary rather than grease fingers can be seen in these in-situ fluorescence pictures.

Figure 6.6 shows the variation of mean intensity of the EHL contact center with entrainment speed in Figure 6.5. The mean intensity is affected by the intensity of surrounding area, and not always proportional to the film thickness. This means the film thickness is possible first decreases and then increases if the intensity of surrounding area is insufficient to change the sequence. This decrease may from the consumption of thickener deposition. As it shows in Figure 6.5, the purple color is indeed more obvious when the speed is lower than 7.7 mm/s.

Figure 6.7 shows the variation of track pattern with entrainment speed. From these pictures, the fingers grow from two bands of the side reservoirs and extend into the center of track. At the entrainment speed of 7.7 mm/s and 12.9 mm/s, the purple thickener deposition can be seen on the center of track. However, these purple depositions become gradually weaken. The grease fingers become more complex with Entrainment speed as the previous observation.

Figure 6.8 shows the contact center just before test stop and after test stop for List.pao20 with the increasing of entrainment speed. The boundary of wake becomes clear after test stop. In addition, the wake is messy and obscure when the speed is low. The wake is gradually open and the clear finger pattern can be seen after test stop with the increasing of entrainment speed. These are consistent with the observation results in Chapter 3.

6.3.2 Effects of test duration

Figure 6.9 shows the reflection picture and the fluorescence picture for Urea.pao30 at static state. The black-and-white fluorescence picture reduces the shooting area, but can record the time-variation process. As can be seen, the intensity of contact area is still weak, the darkest color spread outward to light grey. The intensity of the center line should fits with the deformation of the ball gap.

Figure 6.10 shows the variation of fluorescence images with test duration for Urea.pao30 at the entrainment speed of 2.8 mm/s. They show a replenish process for the side reservoirs. As time progresses, the black cavity on the right side of contact point gradually exhibits. At 100 ms, the outlet cavity grows into fan shape. Sometimes there is a relative movement between the disk and the ball, thus the contact point moves down.

From 150 ms, a gap emerges between the contact zone and the side reservoirs. Figure 6.11 is the mean intensity points in Figure 6.10. As it shows, the mean intensity at fourth and fifth points fall sharply. That is, the separation between the contact zone and side reservoirs may causes a significant decline in film thickness. At 250 ms and 300 ms, the contact area reconnects to the side reservoirs. The corresponding mean intensity increases correspondingly as shown in Figure 6.10. This proves that it is possible the replenishment of side reservoirs makes the film thickness of contact point increases again.

Figure 6.12 shows the fluorescence images in the stop process. The first picture is the reflection picture, the fluorescence pictures are start from the second one. The difference between the reflection picture and the second fluorescence picture is not obvious, the test conditions is stable. During the same test, it can be changed from fluorescence picture to reflection picture by the change of filters. The third picture is the fluorescence picture after test. It can be seen that there are fingers grow from the meniscus boundary and toward to the center of track.

The last one is the fluorescence picture of track pattern. Compare with the previous color fluorescence picture, it can clearly show the finger split. As mentioned earlier, the interferometric fringe between fingers is composed by air and grease. From this fluorescence picture, it is no doubt that the finger is composed by grease, the clear finger contour can be obtained in the fluorescence picture. However, it is not the same case for interferometric

fringes. Therefore, the assumption that these fringes are air is basically correct. The fluorescence intensity of fringes is very small compared with that of fingers.

6.4 Conclusions

Using the fluorescence measurements to observe the flow behaviors of side reservoir is an attempt. Although the further research needs to overcome some practical difficulties, such as the concentration of dye in grease and the emission intensity, it is still a step forward. The simple observation on the speed-variation and time-variation of grease flow are made. The color fluorescence pictures show that it is possible to see the movement of thickener and base oil at the same time. The black-and-white fluorescence pictures show that the side reservoirs indeed provide replenishment for the contact point.

References

[1] Smart, A.E., Ford, R.A.J.: Measurement of thin liquid films by a fluorescence technique. Wear 29, 41-47, 1974.

[2] Berlman, I.B., Handbook of Fluorescence Spectra of Aromatic Molecules, Academic Press, 383-385, 1971.

[3] Sugimura, J., Yoshimuzu, I., Yamamoto, Y.: Study of elastohydrodynamic contacts with fluorescence microscope. In: Dow-Symposium on Tribology. Thinning Films and Tribological Interfaces, pp. 609-617. Elsevier, Amsterdam (2000).

[4] Sugimura, J., Akiyama, M: Study of non-state grease lubrication with fluorescence microscope, Tribology Series, 39, 285-294, 2001.

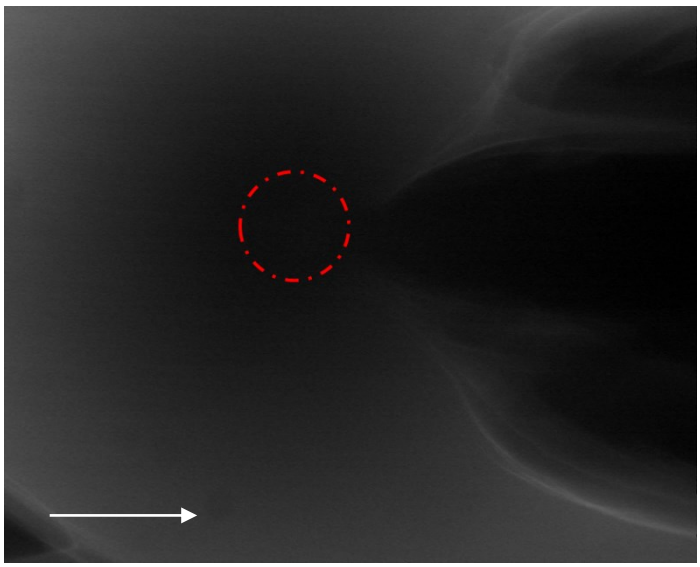

Figure 6.1 Fluorescence image with an objective lens of magnification of 4

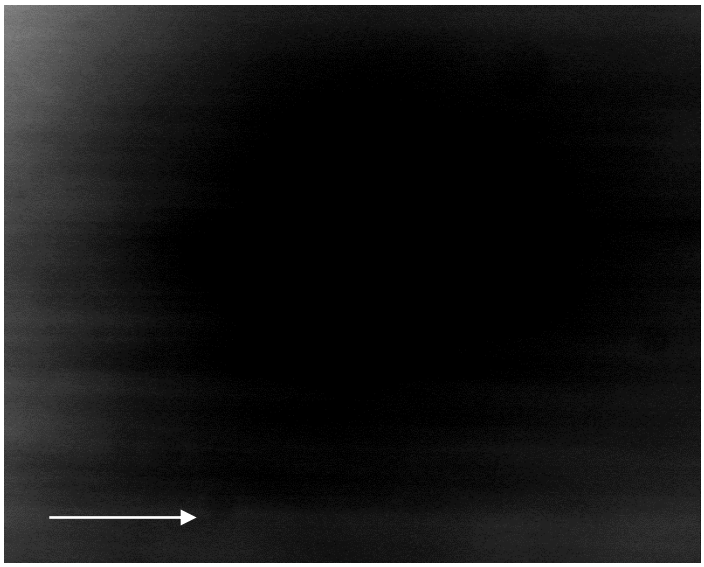

Figure 6.2 Fluorescence image with an objective lens of magnification of 10

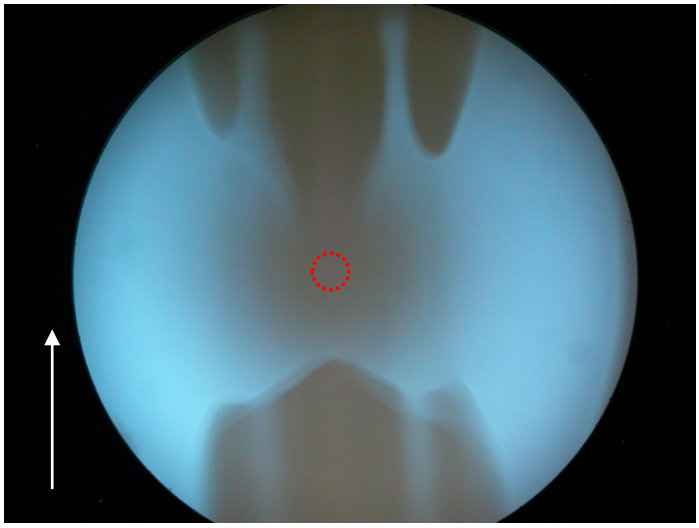

Figure 6.3 Fluorescence image with a separate camera

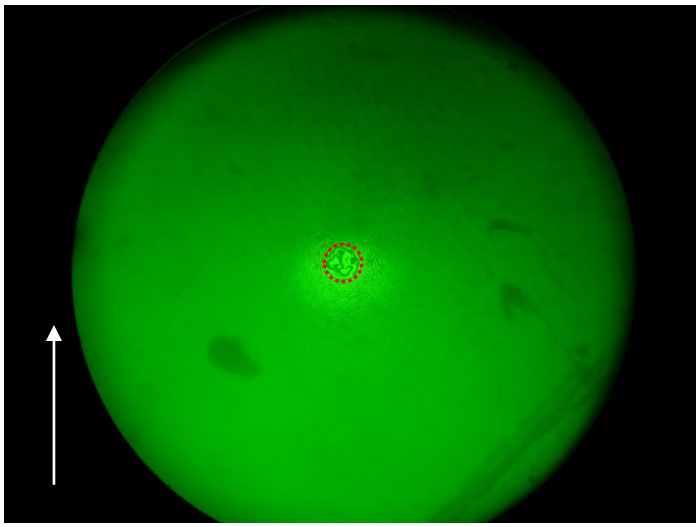

(a) Reflection image

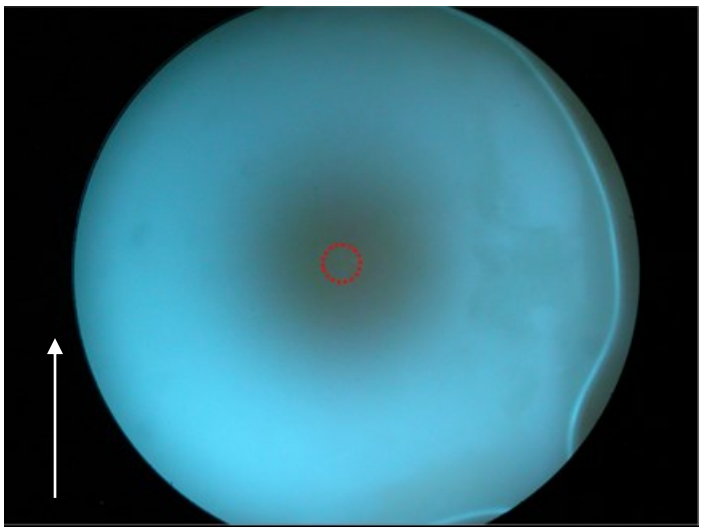

(b) Fluorescence image

100 µm

Figure 6.4 Images of a contact point before test, load 10 N, Urea.pao30 + 2 mass% pyrene

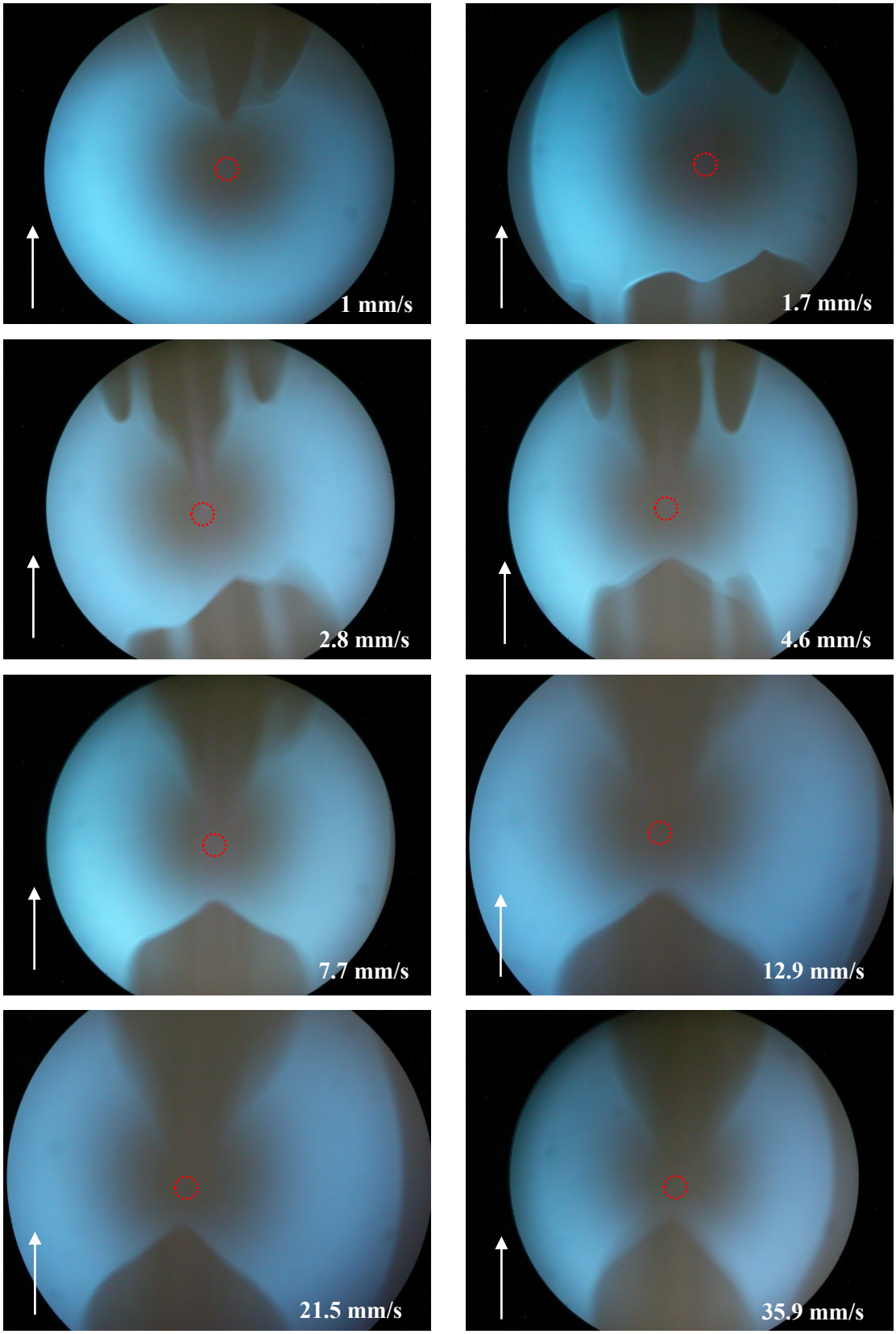

100 µm

Figure 6.5 Fluorescence images with entrainment speed change, SRR 0.5, load 10 N, Urea.pao30 + 2 mass％ pyrene

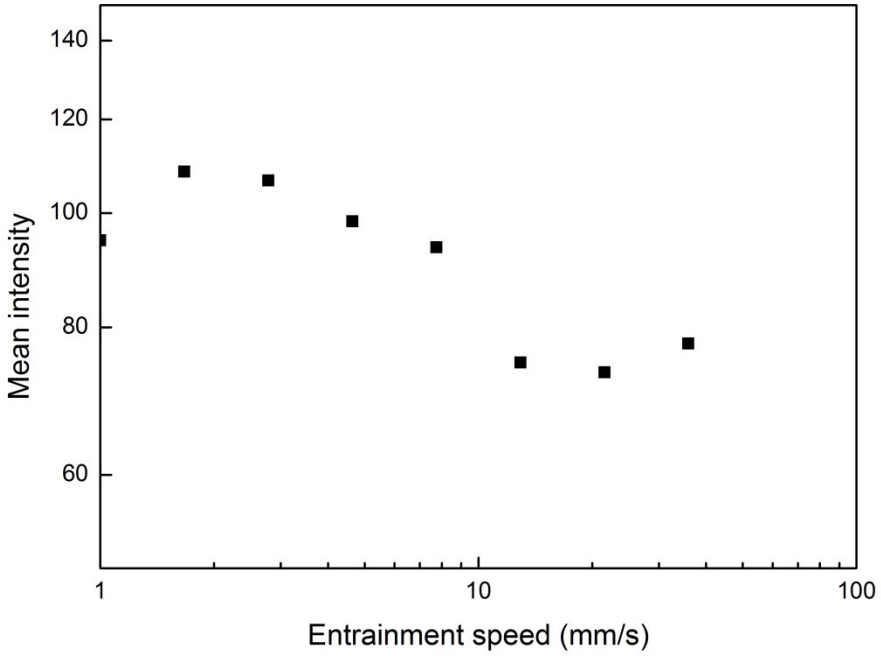

Figure 6.6 Variation of the intensity of the EHL contact center with entrainment speed

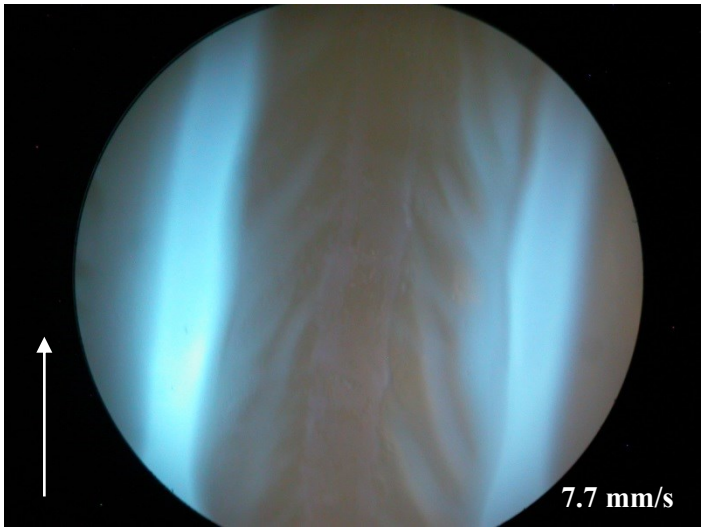

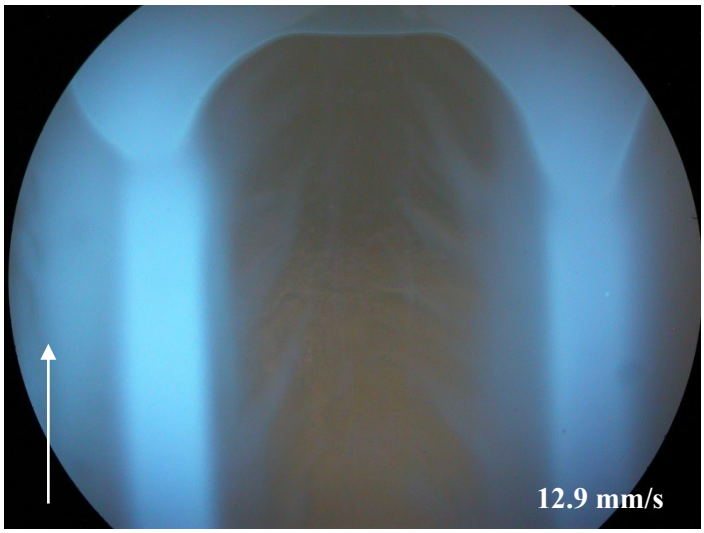
12.9 mm/s

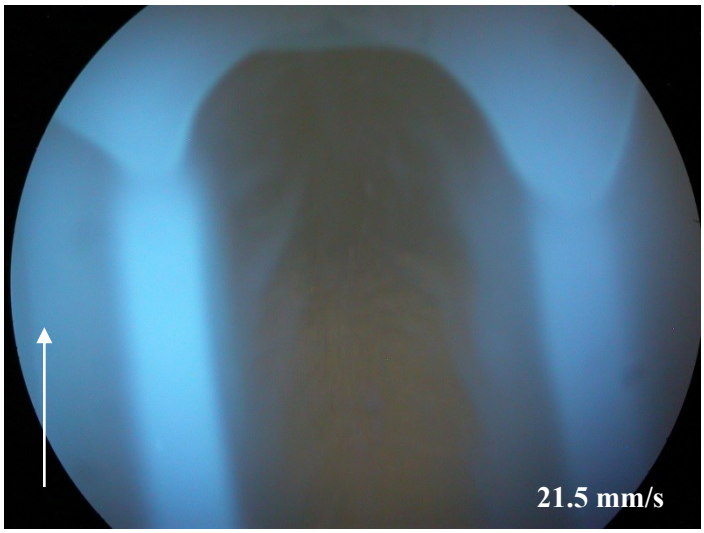
21.5 mm/s

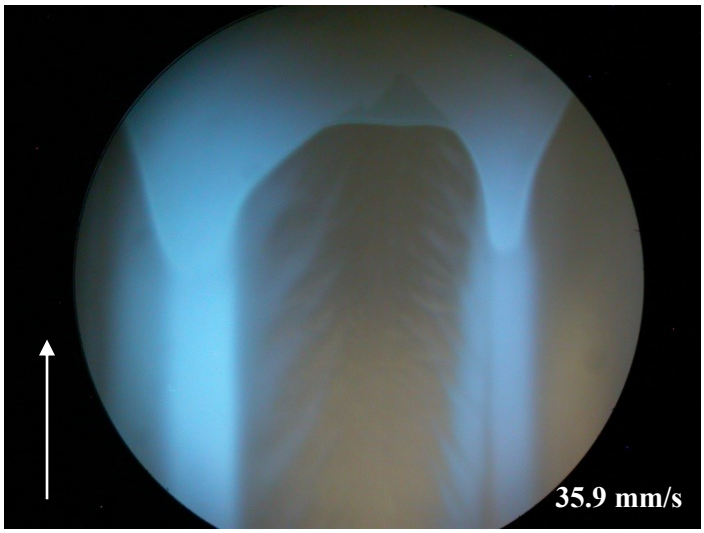
35.9 mm/s

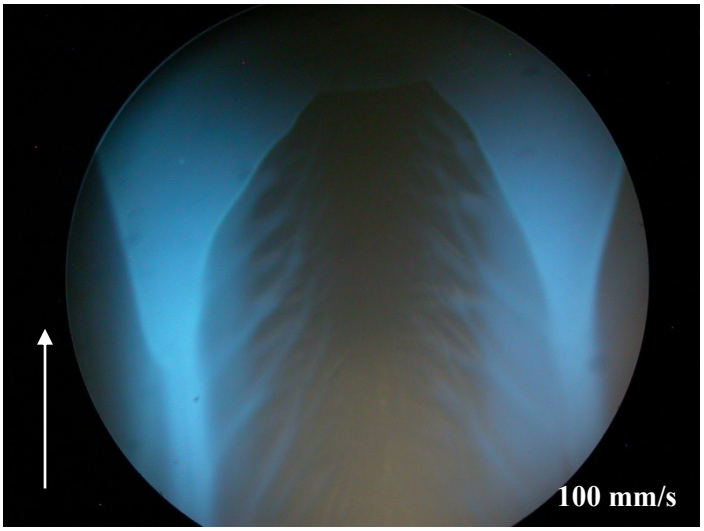

Figure 6.7 Variation of track pattern with entrainment speed

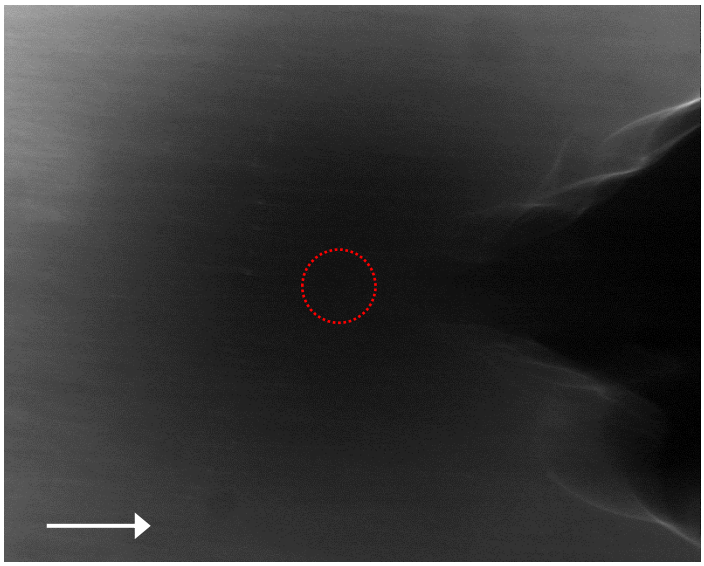

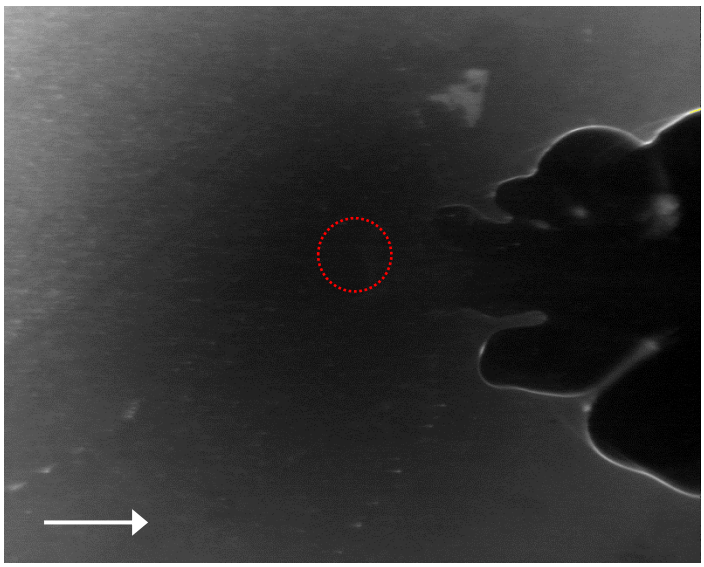

(a) Just before test stop and after test stop at the entrainment speed of 1.17 mm/s

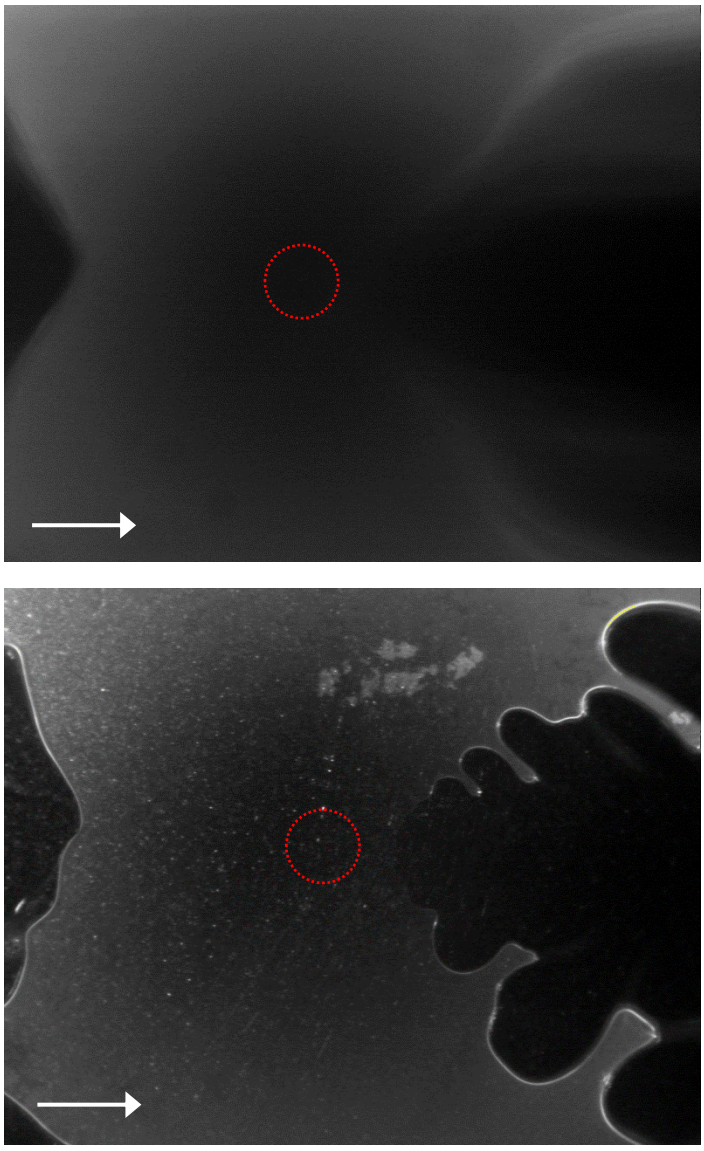

(b) Just before test stop and after test stop at the entrainment speed of 4.20 mm/s

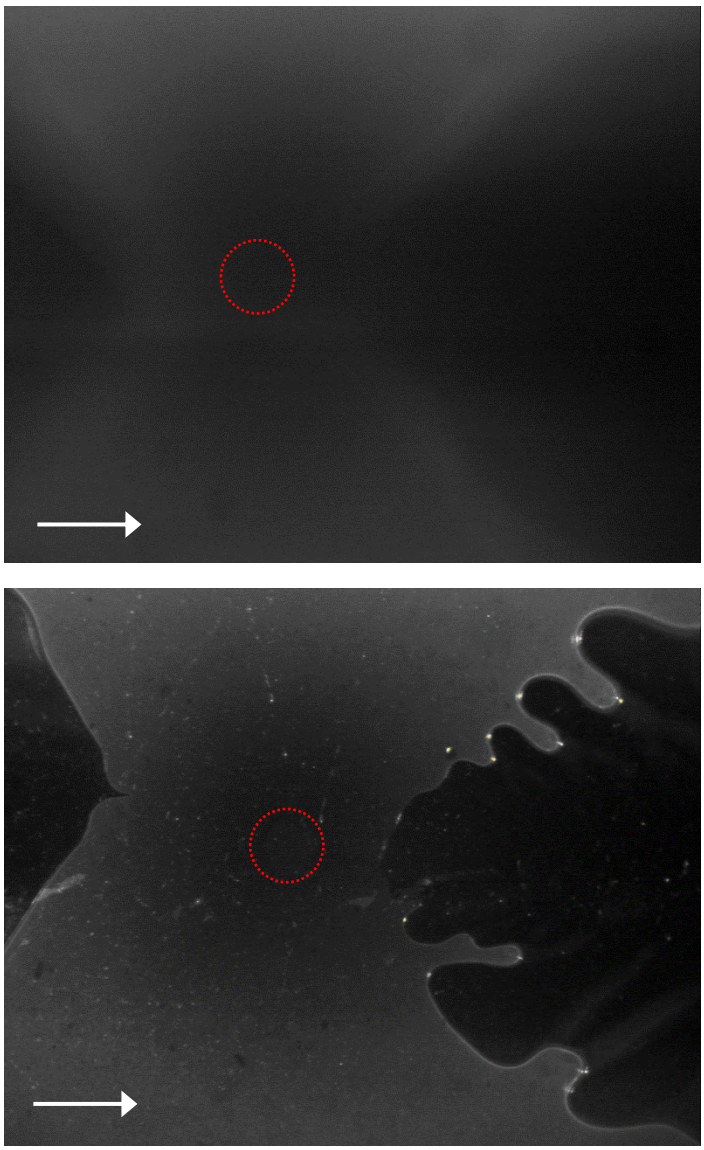

(c) Just before test stop and after test stop at the entrainment speed of 20.65 mm/s

100 µm

Figure 6.8 Variation of fluorescence images with entrainment speed, SRR 0.5, load 10 N, List.pao30 + 2 mass％ pyrene

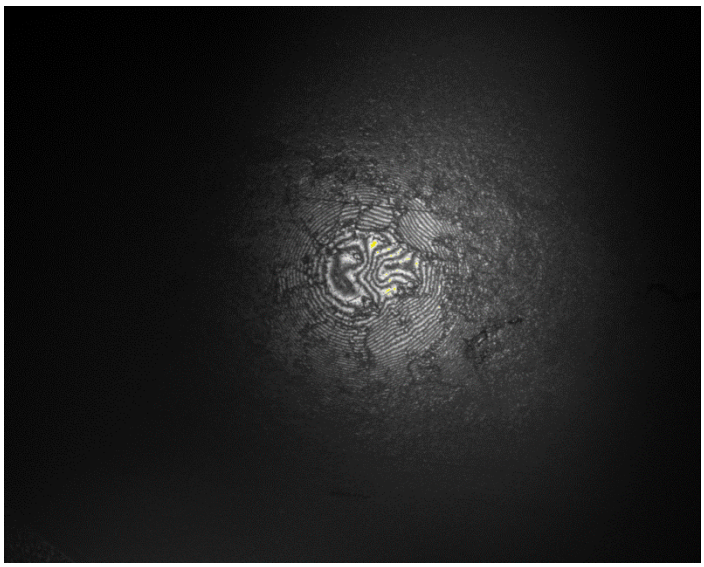

(a) Reflection image

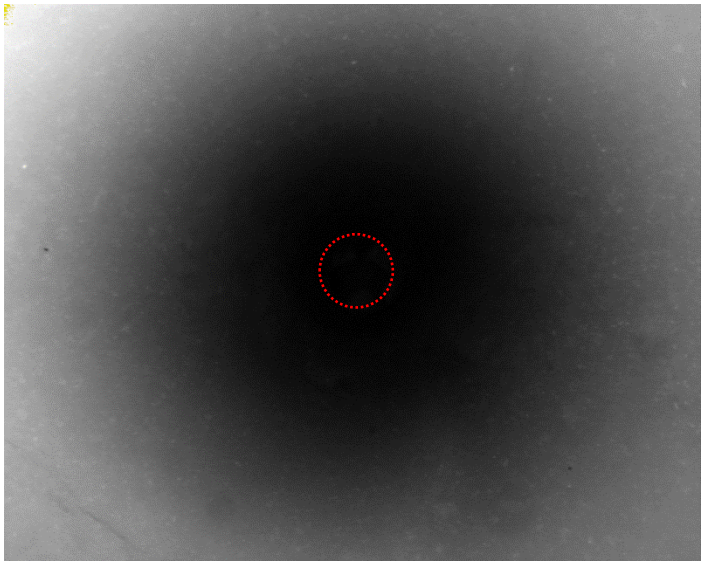

(b) Fluorescence image

100 μm

Figure 6.9 Images of a contact point before test, load 10 N, Urea.pao30 + 2 mass％ pyrene

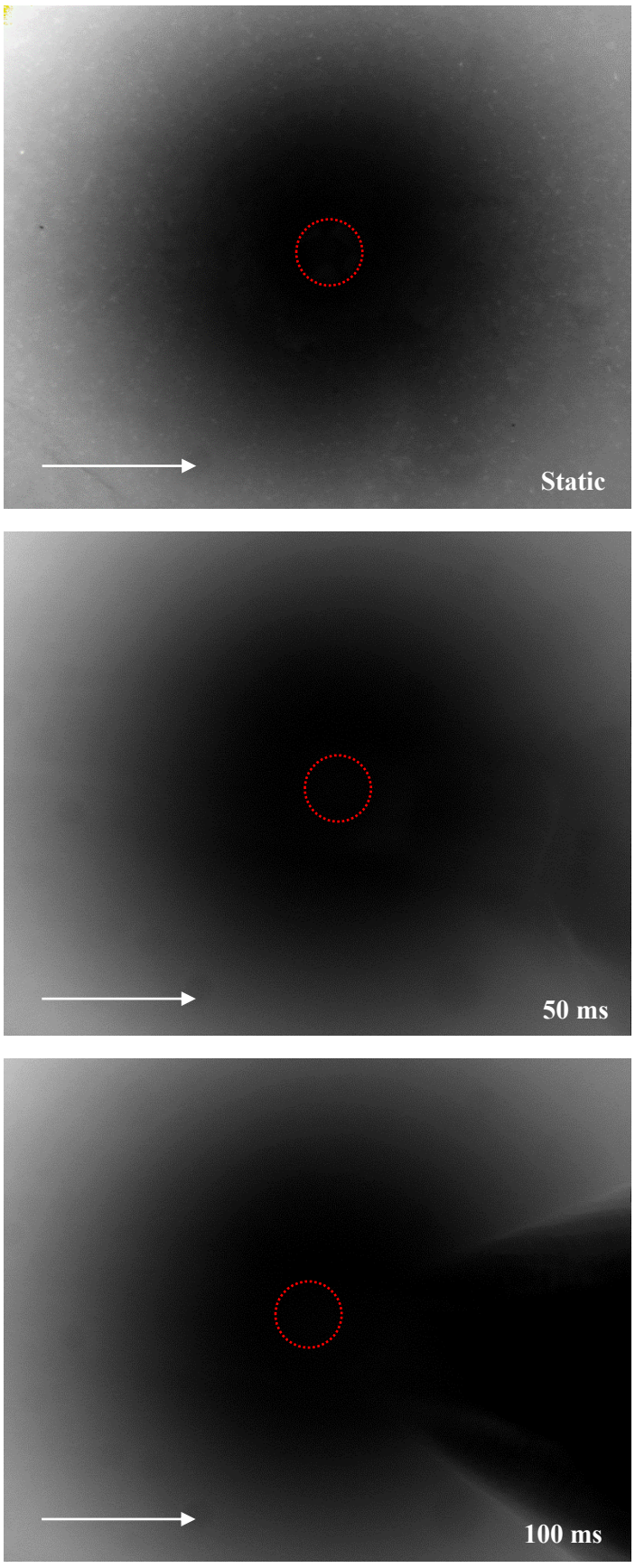
Static
50 ms
100 ms

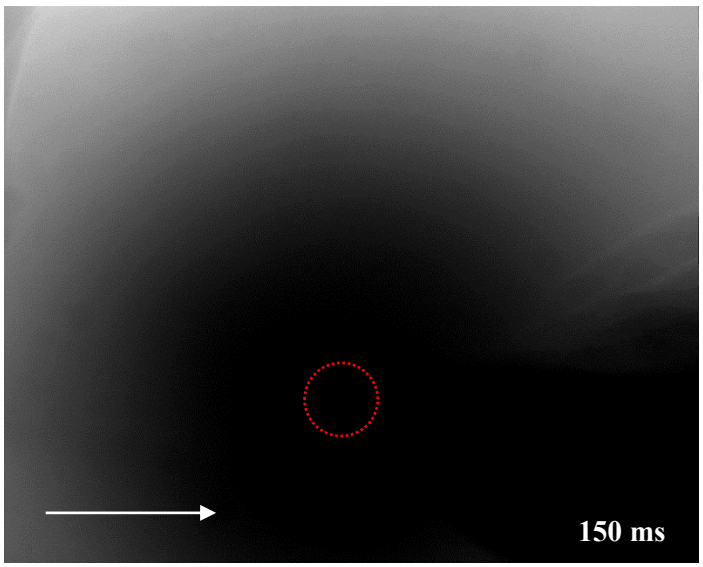
150 ms

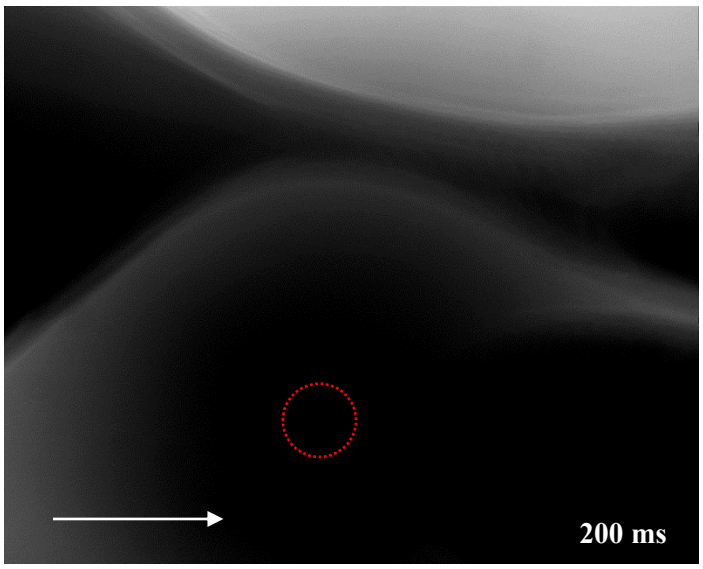
200 ms

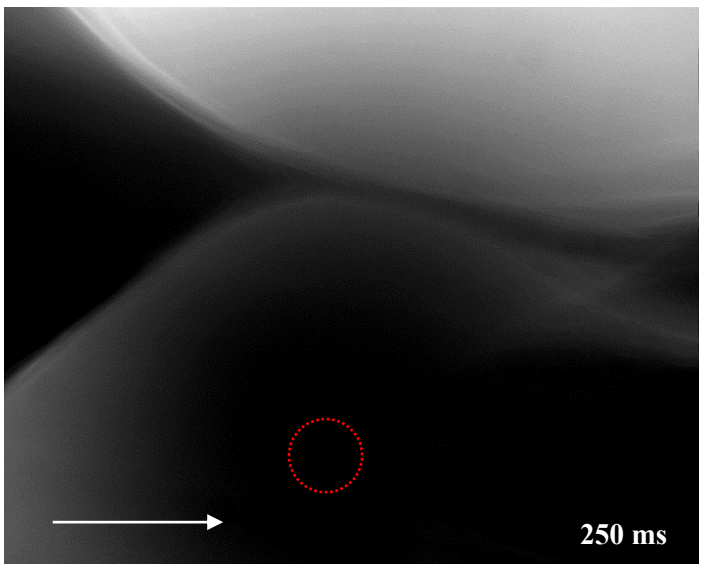
250 ms

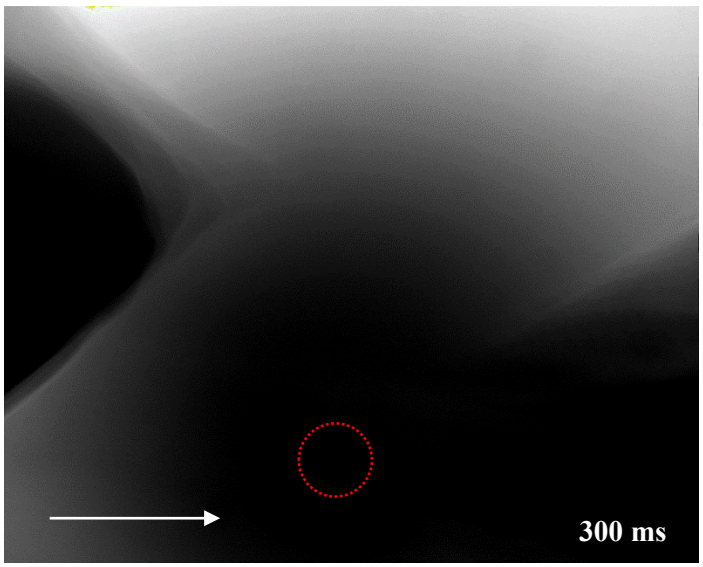

Figure 6.10 Variation of fluorescence images with test duration, SRR 0.5, load 10 N, 2.8 mm/s, Urea.pao30 + 2 mass% pyrene

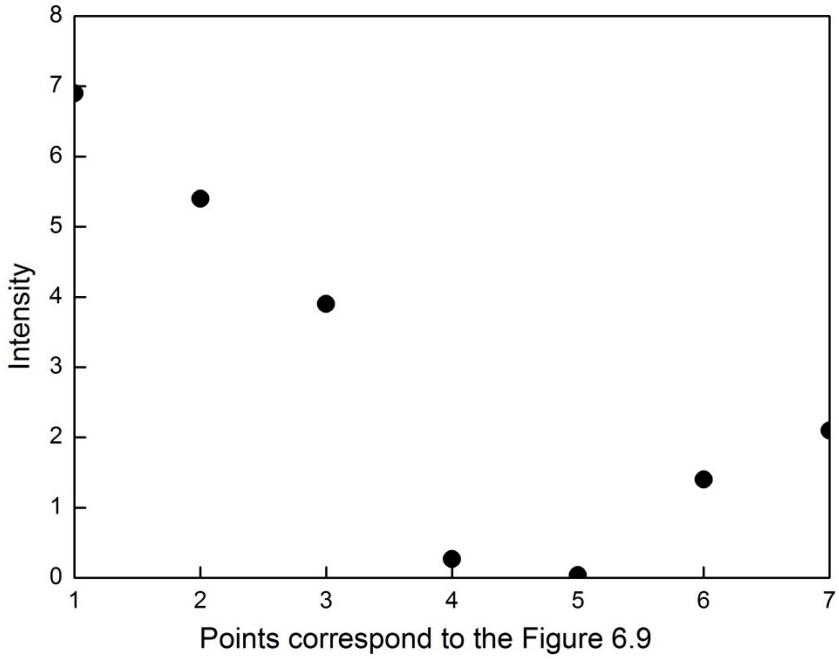

Figure 6.11 Variation of the intensity at the EHL contact center in Figure 6.9

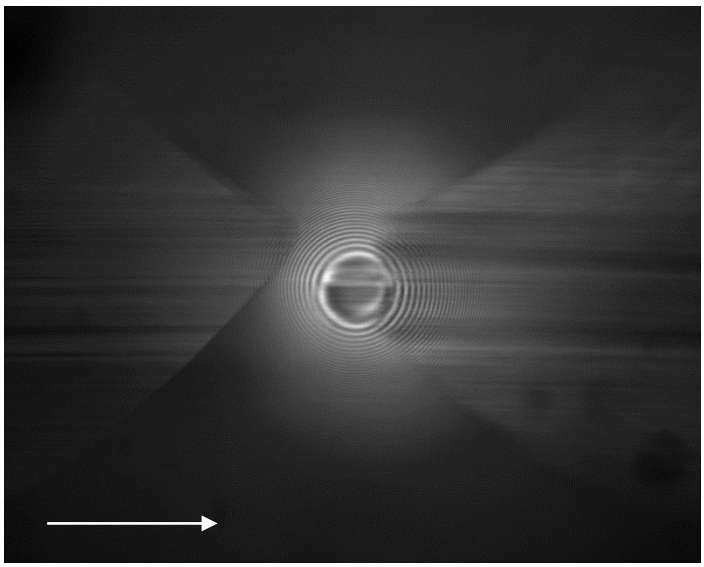

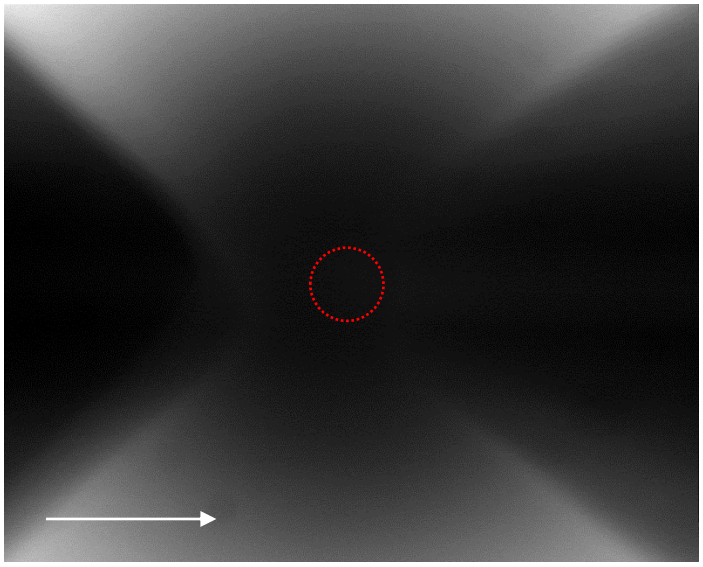

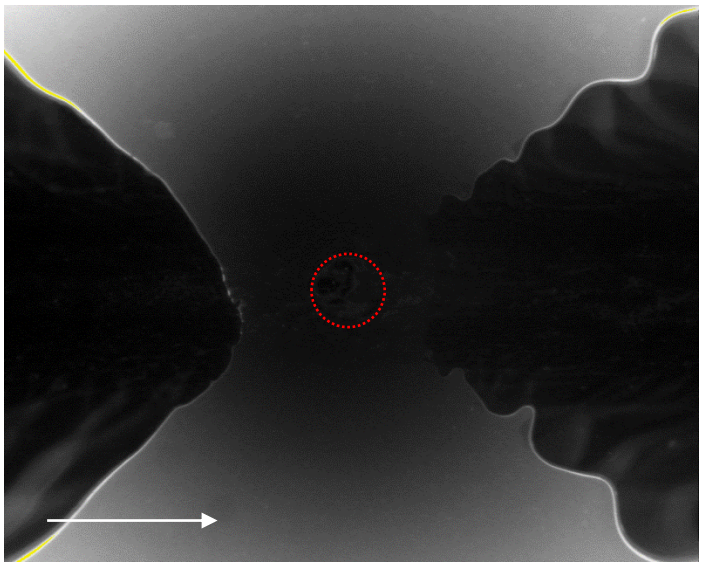

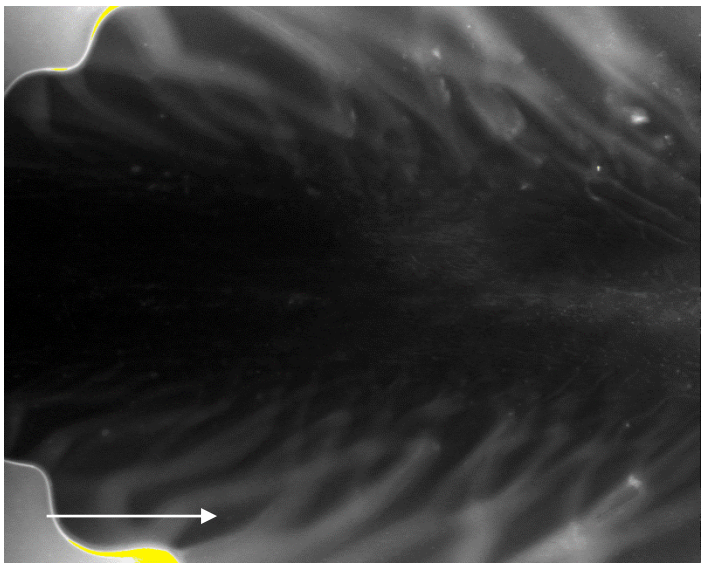

100 μm

Figure 6.12 Observation on the track pattern after test stop, SRR 0.5, load 10 N, 100 mm/s, Urea.pao30 + 2 mass％ pyrene

CHAPTER 7

Conclusions and further works

The grease flow behaviors in point contact have been studied. In summary, this study develops a new method to describe visual characteristics of flow and tracks around the contact in rolling/sliding point contact EHL with greases, finds dependence of the flow characteristics parameters on various factors including operating conditions, rheological properties of greases and the state of fluid film formation, and proposes mechanisms of grease supply to the contact which depend on these factors. The main conclusions are summarized in this chapter and some further works are given.

7.1 Conclusions

In the past few decades, some researches have involved the flow pattern. However, research has mainly been focused on some concrete problems, such as the lubricating conditions in the contact conjunction, the physical and chemical properties of lubricant, etc. There is few research mainly related to the issue of grease flow pattern at present.

Due to the semi-solid composition and the complex rheological properties, the features of grease flow are different for different grease types and different conditions. This unique flow pattern contains a lot of important information: the interaction between the thickener and the base oil, the lubricating conditions, the rheological properties and the mechanisms of redistribution and transportation, etc. There are few reports on their relationships.

In the work presented in this thesis, the focus is on the grease flow behaviors in point contact. It includes the features of flow pattern surround the contact point and the lubricating conditions of the contact point. The purpose of this study is to find the information behind the flow pattern as mentioned above through systematic observation on the features of grease flow.

The main conclusions are summarized as follows:

1. The features of track pattern are different for different grease types and different operating conditions.
2. The variation of the pattern parameters represents the grease flow behaviors, regardless of

the type of grease.

3. It is found that Lithium-12-hydroxy stearate grease shows clear track patterns, whereas Di-urea grease shows obscure track pattern and heavy thickener deposition in the center of the track.
4. The thickener type and base oil viscosity are more important than base oil among the factors that affect the area of grease fingers at the sides of the tracks.
5. The changes in rheological properties produce changes in the patterns. For example, the grease with smaller yield stress and higher viscosity tends to have larger finger area. The grease with better flow ability at low shear rates tends to have a clearer finger pattern.
6. It is proposed that the formation and maintenance of grease fingers in the track pattern are dependent on the state of lubrication.
7. At higher speed, lubricant starvation and finger-loss occur. The starvation speeds are always lower than the finger-loss speeds.
8. The apparent viscosity of the grease at low shear rate in the inlet zone has a great impact on the resupply of the greases and the starvation speed.
9. It is suggest that the grease finger provides supply to the contact area and the side reservoir, and one part of grease finger that lies near the center of track plays the main role.
10. The thickener deposition in the center of track plays a positive role in the film formation with some types of greases, especially the Di-urea greases.
11. The covariance analysis shows that the eight characteristic parameters are more or less correlated with each other.
12. The principal component analysis suggests that some of them are strongly related and some are not in terms of their relationships with operating conditions, rheological parameters and film formation.
13. The fluorescence technique is capable of studying the replenishment of grease by the grease from the side reservoir merging with grease left in the form of the fingers at sides of the track.

7.2 Further works

Some further works are shown as follows:

1. The rheological properties of grease are very important for track features and grease lubrication. If there is new technique can be used to know the information under EHL conditions, it should be attempted.
2. The physical and chemical changes of grease finger can be tested for different test conditions in starved state.
3. The microstructure of grease can be achieved by AFM or SEM. Therefore the network of thickener can be known and related with different track patterns.
4. The fluorescence measurements can be extended by varies test greases and test conditions.

ACKNOWLEDGMENTS

In the past five and half years, it is a pleasure to do doctoral research. I am greatly thanks to my two supervisors Professor Sugimura Joichi and Mr. Tanaka Hiroyoshi. Professor Sugimura gives valuable opinions and guidance, no matter on the study or the life. Especially in the final year, I could not able to concentrate properly on the research without his financial assistance and detailed guidance.

Thanks Mr Tanaka Hiroyoshi, he spent vast time to my research, from selection of the topic, experimental design. His patient and kindness help me to gain the knowledge. It is great pleasure to be a student of them.

Thanks to Professor Sawae Yoshinori, Professor Yagi Kazuyuki and Professor Ito Kohei for serving as reviewers and examiners of this research. Their valuable comments contributed to improve the quality of this research.

Thanks Kurono Yoshie, she kindly provides help for my life. And all the staff members and students at Kyushu University Tribology Laboratory, this research could not be conducted smoothly without their support.

Thanks to my motherland china for providing the scholarship. Thanks the supports from my parents.